UC San Diego
UC San Diego Electronic Theses and Dissertations

Title
Dissecting the allosteric regulation of PKA-I alpha activation

Permalink
https://escholarship.org/uc/item/3c2453zt

Author
Cheng, Cecilia Yuen-Man

Publication Date
2009

Peer reviewed|Thesis/dissertation

eScholarship.org Powered by the California Digital Library
University of California

UNIVERSITY OF CALIFORNIA, SAN DIEGO

Dissecting the Allosteric Regulation of PKA-I alpha Activation

A Dissertation submitted in partial satisfaction of the Requirements for the degree Doctor of Philosophy

in

Chemistry

by

Cecilia Yuen-Man Cheng

Committee in charge:

Professor Susan S. Taylor, Chair
Professor Timothy Baker
Professor Tracy M. Handel
Professor Simpson Joseph
Professor Michael Sailor

2009

Copyright

Cecilia Yuen-Man Cheng, 2009

All rights reserved

The Dissertation of Cecilia Yuen-Man Cheng is approved, and it is acceptable in quality and form for publication on microfilm and electronically:

_____

_____

_____

_____

_____

Chair

University of California, San Diego

2009

For my parents

TABLE OF CONTENTS

TABLE OF CONTENTS v
LIST OF ABBREVIATIONS x
LIST OF FIGURES xii
LIST OF TABLES xv
ACKNOWLEDGMENTS xvi
VITA xix
ABSTRACT OF THE DISSERTATION xxi
Chapter 1 1
Introduction 1
1.1. Signal transduction 1
1.2. Protein kinases 3
1.3. cAMP dependent kinase (Protein Kinase A, PKA) 7
1.3.1. The Catalytic Subunit 11
1.3.2. The Regulatory Subunits 15
1.3.3. Inhibition Mechanism of PKA Holoenzymes 20
1.4. Relevance of PKA in Disease 22
1.5. Major outstanding questions regarding the allosteric regulation of PKA activation 24
Chapter 2 27
PKA-Iα Holoenzyme Structure: Dynamic Conformational Change of RIα Reveals Mechanism for cAMP-dependent Activation 27
2.1. Introduction 27
2.2. Experimental Methods 30
2.3.1 Molecular Cloning 30
2.3.2 Protein Preparation 31
2.3.3 Holoenzyme Formation for Crystallography 31
2.3.4 Crystallization and Data Collection 32
2.3.5 Structure Determination and Refinement 32

2.3.6 cAMP Activation of PKA by Fluorescence Polarization 33
2.3.7 Holoenzyme Formation Assay 34
2.3.8 cAMP Activation of PKA using a Catalytic Coupled Assay 34
2.3. Results and Discussion 35
2.4.1 Rationale for crystallization of the RIα(91-379:R333K) mutant 35
2.4.2 Structural Overview of the RIα(91-379):C Complex 36
2.4.3 Domain B of the Regulatory Subunit Provides an Additional Docking Surface for the Activation Loop and Presents a Novel Interaction Site on the Catalytic Subunit 40
2.4.4 Major Conformational Changes Occur in RIα Upon Binding the Catalytic Subunit 44
2.4.5 αB/αC helix flexibility is important for PKA activation by cAMP 52
2.4.6 Residues Required for Stabilizing cAMP in the Regulatory Subunit are Trapped at a Remote Site in the Holoenzyme Structure 54
2.4.7 The Glu261-Arg366 Salt Bridge Functions to Trap the Two cAMP Capping Residues. 55
2.4.8 Model of PKA Activation by cAMP 60
2.4. Conclusions 63
Chapter 3 65
Small Angle X-ray Scattering and Site-Directed Mutagenesis Uncovers a Dynamic RIα Domain B in PKA-RIα Complexes 65
3.1. Introduction 65
3.1.1. Small angle X-ray scattering 67
3.2. Experimental Methods 75
3.2.1. Protein preparation 75
3.2.2. SAXS Data collection 76
3.2.3. Data analysis 76
3.3. Results 77
3.3.1. RIα heterodimers 78
3.3.2. Effect of deleting Domain B 78
3.3.3. Effect of R333K on RIα heterodimer 81

3.3.4. Effect of R209K on RIα heterodimers 83
3.3.5. Effect of K285P mutation on RIα heterodimers 84
3.3.6. Biochemical analysis of PKA-Iα heterodimers 89
3.4. Discussion 89
3.5. Conclusions 99
Chapter 4 101
Dissecting the Regulatory Subunit Inhibitor Sequences as Binding Motifs for the Catalytic Subunit 101
4.1 Introduction 101
4.2 Experimental Methods 106
4.2.1. Protein Preparation 106
4.2.2. Peptide Array 107
4.2.3. Peptide Blot Regeneration 108
4.2.4. Crystallography 110
4.3 Results 110
4.3.1. RI peptides 110
4.3.2. RIIα peptides 113
4.3.3. RIIβ peptides 117
4.3.4. Effect of phosphorylation site mimics 119
4.3.5. PKI 121
4.3.6. Co-crystallization of RII Inhibitor Peptides and C-subunit 124
4.4 Discussion 126
4.4.1. Binding determinants for RII inhibitor sequences 128
4.4.2. Comparison between RI and RII peptides 131
4.4.3. Binding determinants of PKI 132
4.4.4. Proposed mechanism for allosteric regulation 133
4.5 Conclusions 135
Chapter 5 137
Biochemical and Structural Characterization of Phospholamban-PKA Complex: Implications Towards Heart Disease 137
5.1. Introduction 137

5.2. Experimental Methods 143
5.2.1. Materials 143
5.2.2. Peptide array 144
5.2.3. Crystallography 145
5.2.4. Data processing and refinement 146
5.2.5. Fluorescence polarization 147
5.3. Results 150
5.3.1. Peptide Array identifies phospholamban residues important for C-subunit recognition 150
5.3.2. Structural Overview of the PKA C-subunit:PLN:AMPPNP Complex 152
5.3.3. Detailed interactions at the active site cleft 156
5.3.4. Biochemical analysis of Glu203 on phospholamban binding 159
5.3.5. Effect of phospholamban peptide length on C-subunit complex formation 159
5.3.6. Effect of phospholamban ΔR14 and R9C mutations on C-subunit interactions 161
5.4. Discussion 163
5.4.1. AMPPNP traps phospholamban within the C-subunit active site 163
5.4.2. Comparison of the PLN:C-subunit complex with other PKA structures 165
5.4.3. Redefining PKA substrate classification 169
5.4.4. Physiological relevance of Glu203-Arg9 ion pair 169
5.5. Conclusions 173
Chapter 6 174
cAMP Analog Specificity of PKA Isoforms 174
6.1. Introduction 174
6.2. Experimental Methods 178
6.2.1. Protein preparation 178
6.2.2. HE-33 Crystallization, Data Processing, and Refinement 178
6.2.3. 8-CPT Crystallization 179
6.3. Results 181
6.3.1. Progress $RI\alpha_{AB}$:8-CPT Co-Crystallization 181
6.3.2. Crystal structure of $RI\alpha$ bound to HE-33 181

6.4. Discussion 187
6.5. Conclusions 192
Chapter 7 193
Conclusions 193
7.1. Future Work 198
REFERENCES 200

LIST OF ABBREVIATIONS

Å. Angstrom

AKAP. A-kinase anchoring protein

ATP. adenosine triphosphate

cAMP. adenosine 3',5'-cyclic monophosphate.

C-subunit. The Catalytic Subunit of PKA.

CNB. Cyclic nucleotide binding.

C-terminus. Carboxy-terminus.

D/D. Dimerization Docking domain.

D-AKAP2. Dual A-kinase anchoring protein-2.

DNA. Deoxyribonucleic Acid.

DTT. Dithiothreitol.

E. coli. *Escherichia coli*

EDTA. Ethylenediaminetetraacetic acid.

EGTA. [ethylenebis(oxyethylenenitrilo)] tetraacetic acid

IP20. Residues 5-24 of PKI.

kDa. Kilodaltons.

MALDI. Matrix-Assisted Laser Desorption/Ionization

MES. 2-(N-morpholino) ethanesulfonic acid

mg. milligram

μl. microliter

$MgCl_2$. Magnesium chloride.

mM. millimoles/liter

MOPS. 3-(N-morpholino) propanesulfonic acid.

mRNA. Messenger ribonucleic acid.

NaCl. Sodium chloride

N-terminus. Amino-terminus.

PAGE. Polyacrylamide gel electrophoresis.

PBS. Phosphate buffered solution.

PDB. Protein data bank.

PKA. Protein Kinase A or cyclic-AMP Dependent Protein Kinase

PKI. Protein kinase A inhibitor.

R-subunit. The Regulatory Subunit of PKA.

SDS-PAGE. Sodium dodecyl sulfate

TCEP. Tris(2-Carboxyethyl) phosphine Hydrochloride

TBS. Tris-Buffered Saline

Tris. Tris Hydroxymethylaminoethane.

WT. Wild type.

LIST OF FIGURES

Figure 1. Structure of the PKA catalytic subunit. 5

Figure 2. Structural conservation of the protein kinase fold. 6

Figure 3. The Human Kinome. 8

Figure 4. Major structural elements within the PKA C-subunit. 13

Figure 5. Domain organization of the PKA regulatory subunits. 16

Figure 6. Crystal structure of a PKA complex between the C-subunit and RIα containing only one of the two cAMP binding domains. 21

Figure 7. Overview of the PKA RIα(91-379):C Holoenzyme Complex. 37

Figure 8. A stereoview of the phosphate binding cassette in Domain B. 38

Figure 9. Peptide Recognition Site. 41

Figure 10. The αG helix and P+1 loop of the catalytic subunit bound to the phosphate binding cassette (yellow) and N3A motif (cyan) of the regulatory subunit. 42

Figure 11. The Regulatory Subunit Provides a Large Docking Surface that Shields the Catalytic Machinery of the C-subunit. 43

Figure 12. RIα Undergoes Dramatic Conformational Changes Upon Binding the Catalytic Subunit. 46

Figure 13. Conformational Changes in the Regulatory Subunit is a Result of Structural Rearrangements in the Helical Regions. 47

Figure 14. Schematic Diagram of the Structural Motifs in the Regulatory Subunit. 49

Figure 15. The global organization of the αB/C helix relative to the two N3A motifs in RIα and the activation loop and P+1 loop in the C-subunit. 50

Figure 16. Binding of the Catalytic Subunit Reorganizes Two Regulatory Subunit Structural Motifs (the N3A motif and the Phosphate Binding Cassette) to Create a Contiguous Hydrophobic Interface. 51

Figure 17. Effects of Gly235 mutants on inhibition and cAMP activation. 53

Figure 18. Association of mutant regulatory subunits with catalytic subunits measured by the catalytic Cook Coupled assay. 57

Figure 19. A Novel RIα Electrostatic Interaction in the Holoenzyme Conformation Functions as a “Capping Residue Trap” Important for PKA Activation. 58

Figure 20. Activation of PKA with cAMP monitored by the catalytic Cook Coupled assay. 59

Figure 21. SAXS experimental setup. 68

Figure 22. Simulated P(r) functions of particles with different shapes. 74

Figure 23. SAXS profiles of RIα(91-379) heterdimers. 79

Figure 24. SAXS profiles of RIα(91-244) heterodimers. 80

Figure 25. SAXS profiles of R333K heterodimers. 82

Figure 26. SAXS profiles of R209K heterdimers. 85

Figure 27. Comparison of R-subunit Domain B interactions in PKA-Iα and PKA-IIα Structures. 86

Figure 28. AGC insert. 87

Figure 29. Inhibition of C-subunit with RIα mutants. 92

Figure 30. Model of Domain B motion of PKA-Iα. 96

Figure 31. Simulations of Domain B motion of PKA-Iα. 98

Figure 32. Crystal structures of C-subunit complexes to date. 104

Figure 33. Sequence alignment of R-subunit inhibitor sequences. 105

Figure 34. Schematic of Peptide Array. 109

Figure 35. Peptide blots of RIα and RIβ inhibitor sequences. 112

Figure 36. Peptide blots of RIIα inhibitor sequences. 114

Figure 37. Amino acid substitution of RIIα peptides. 116

Figure 38. Peptide blots of RIIβ inhibitor sequences. 118

Figure 39. Amino acid substitution of RIIβ peptides. 120

Figure 40. Summary of inhibitor sequence peptides and mutation of phosphorylation sites. 122

Figure 41. Peptide blots of PKI. 123

Figure 42. Amino acid substitution of PKI peptides..... 125

Figure 43. Co-crystallization of R-subunit inhibitor peptides, C-subunit, and ATPγS. ... 127

Figure 44. Detailed interactions of RIIα:C and RIIβ:C inhibitor sequences..... 129

Figure 45. Calcium cycling in cardiac myocytes regulates cellular contraction and relaxation. 138

Figure 46. Activation of SERCA. 140

Figure 47. Phospholamban domain organization..... 142

Figure 48. Peptide array of phospholamban peptides. 151

Figure 49. Structure of PKA C-subunit bound to Phospholamban$_{1-19}$. 154

Figure 50. Hydrogen bond interactions between C-subunit and phospholamban. 157

Figure 51. Effect of AMP-PNP on f-PLN binding to wild-type and E203Q C-subunit. ... 160

Figure 52. Effect of phospholamban peptide length and AMP-PNP on binding to the C-subunit. 162

Figure 53. Effect of phospholamban mutations ΔR14 and R9C on binding to wild-type C-subunit. 164

Figure 54. N-terminal Arginine and Glu203^{C} Interaction is Conserved. 167

Figure 55. Role of Glu203 in C-subunit Substrate/Inhibitor Recognition. 168

Figure 56. Alignment of PKA substrate phosphorylation sites. 170

Figure 57. Alignment of PKA substrate phosphorylation sites. 171

Figure 58. Summary of cAMP analog substitutions. 177

Figure 59. Co-crystallization of RIα and 8-CPT. 182

Figure 60. Structural overview of HE-33 bound to RIα..... 185

Figure 61. Structural alignment of RIα bound to cAMP and HE-33. 186

Figure 62. Structural comparison of Domain A nucleotide binding pockets between RIα and RIIβ. 189

Figure 63. Structural comparison of Domain B nucleotide binding pockets between RIα and RIIβ. 190

LIST OF TABLES

Table 1. Data and refinement statistics of the RIα_{AB}:C:AMPPNP:Mn^{2+} complex. 39

Table 2. Comparison of R_g and D_{max} of PKA-Iα heterodimers. 90

Table 3. Association and dissociation rates of PKA-Iα and PKA-IIβ complexes (BIACORE). 91

Table 4. Data and refinement statistics for the phospholamban$_{1-19}$:C-subunit:AMPPNP:Mg^{2+} complex. 153

Table 5. Crystallographic data reduction and refinement statistics for the RIα:HE-33_2 complex. 183

ACKNOWLEDGMENTS

First and foremost I would like to thank my parents for their enduring support and encouragement in all my personal and professional endeavors. They never discouraged me from my pursuits. They have always pushed me to strive to do my best and to not give up even when things were tough. They instilled in me a work ethic, drive, commitment, and curiosity that helped push me through graduate school to bring me here to where I am today.

I would like to thank my advisor Susan Taylor for her continuous support in all research directions I pursued. From the start, she was always quick to point me in the right direction of help, whether it be discussions or use of equipment or reagents. I am grateful for all the opportunities she has given me throughout the years and I always appreciate her good intentions. She has been there for moral support and I truly appreciate her kindness and sensitivity.

Don Blumenthal has served as a second mentor to me, both professionally and personally, throughout my graduate career. He has always strived to help me through the endless nights I spent both at the synchotron and at the University of Utah collecting data. He has an uncanny ability to simplify complicated problems and always gave me sound advise on experiments. I also greatly appreciate all the time and effort he spent teaching me the ins and outs of SAXS, as well as helping me collect data countless of times.

I would also like to acknowledge my undergraduate mentor Martin Stone. Without him, I would not have gone to graduate school. I started as a music major in undergrad

and shortly after I decided to pursue science, I joined Martin's lab. I loved it immediately and stuck with it. My experiences in his lab taught me how to think scientifically, think critically, be efficient, and how to do experiments. These skill sets gave me the experience I needed in order to survive in a big lab. He also showed me that one can strive for balance between excelling professionally and having a rewarding outside life. Without this balance, I would not have enjoyed my graduate school career.

I also want to thank my committee members for their help over the years, Dr. Timothy Baker, Dr. Tracy Handel, Dr. Simpson Joseph, and Dr. Michael Sailor. Although we only met a handful of times over the years, I always came away with new insights and good ideas for future experiments.

I am also indebted to everyone in the Taylor lab over the years who made the experience fun and rewarding. Simon Brown was always there to help me out with anything, be it about research ideas, experimental problems, advice on good backpacking trips, or always being up for a much-needed beer. He was also a great friend and travel buddy throughout the years. Adrian Saldana taught me how to design experiments and how to write effectively. Mike Deal was always there to help me with any technical issues with equipment, gave me endless supplies of protein, and gave me countless moments of entertainment whether it be lab stories, funny videos, or simple lab banter. CJ Allison was always helpful and prepared for lab emergencies from telling me where all the secret reagent stashes were, to getting any piece of equipment fixed, to helping me get the best prices for anything. Jie Yang always took the time out to help me discuss experimental methods and results. Ganesh Anand was there in the beginning to help enlighten me on the field of PKA as well as guide me on experiments. Choel Kim taught me crystallography when I first joined the lab. Sarma was always available to help

me with pressing crystallography issues and I am indebted to his insights. My bay mates Manjula and Jon were always there to help with experiments and were always there to support my coffee addiction. Eric was always there to help with things when I didn't have enough time. Teaching and mentoring an undergraduate in the lab, Shelley Phoun, has also been a valuable experience. It has been a joy and pleasure working with Shelley in my last year, for she was always there to help me out when I needed it most and it's been fun watching her grow as a scientist. And to all the other present and former Taylor Lab members who have been there throughout my graduate career.

I am also grateful for all my friends that I have met while in San Diego. The people who have crossed my path have supplied me with endless moments of fun and support, whether it be from rock climbing, backpacking, surfing, adventures in the desert, fundraising events, or simply enjoying nice home cooked meals, I am truly grateful to have them in my life.

I also want to thank Jon Clemens for his unending love and support. He's given me a different perspective on life and has been with me through countless fun adventures outside of lab in the last four years that made my time here truly memorable.

Chapter 2, in full, is a reprint of the material as it appears in Kim C*, Cheng CY*, Saldana A, and Taylor SS. "PKA-Iα Holoenzyme Structure Reveals Mechanism for cAMP-dependent Activation." Cell. 2007. Sep 21:130(6):1032-43. I was the primary investigator and author of this paper. (* denotes co-authorship)

VITA

Education

2009 Ph.D., Chemistry
University of California, San Diego

2006 M.S., Chemistry
University of California, San Diego

2002 B.S., Biology
Indiana University

Publications (* Co-first author)

Cheng, C.Y. and Taylor, S.S. Crystal structure of the PKA and phospholamban complex. *Manuscript in preparation*.

Cheng, C.Y. and Taylor, S.S. Structural Recognition Motifs for PKA_C. *Manuscript in preparation*.

Cheng, C.Y., Blumenthal, D.K., and Taylor, S.S. Small angle X-ray scattering and site directed mutagenesis uncovers a dynamic RIα Domain B in PKA-RIalpha complexes. *Manuscript in preparation.*

Brown SHJ, **Cheng CY**, Saldahna A, Taylor SS. Protein Kinase A Isozyme Assay Reveal True Selectivity of cAMP Derivatives. *Manuscript in preparation*.

Taylor SS, Kim C, **Cheng CY**, Brown SHJ, Wu J, and Kannan N. Signaling through cAMP and cAMP-dependent protein kinase: Diverse strategies for drug design. *Biochim Biophys Acta*. Oct 12 2007.

Kim C, **Cheng CY***, Saldana A, and Taylor SS. PKA-Iα Holoenzyme Structure Reveals Mechanism for cAMP-dependent Activation. *Cell*. 2007. Sep 21:130(6):1032-43.

Cheng CY, Jarymowycz VA, Cortajarena AL, Regan L, and Stone MJ. Repeat motions and backbone flexibility in designed proteins with different numbers of identical consensus tetratricopeptide repeats. *Biochemistry*. 2006. Oct 3; 45(39): 12175-83.

ABSTRACT OF THE DISSERTATION

Dissecting the Allosteric Regulation of PKA-I alpha Activation

by

Cecilia Yuen-Man Cheng

Doctor of Philosophy in Chemistry

University of California, San Diego, 2009

Professor Susan S. Taylor, Chair

Cyclic adenosine monophosphate (cAMP) signaling through cAMP-dependent protein kinase (PKA) is a ubiquitous mammalian signaling pathway involved in metabolism, cell proliferation, and cell death. While the PKA catalytic (C) subunit has served as a prototype for the protein kinase superfamily, the regulatory (R) subunit defines the mechanism whereby cAMP translates an extracellular signal into an intracellular biological response.

This dissertation investigates three major areas of PKA research: 1) defining the molecular features that govern RIα:C complex formation as a means to understand the allosteric regulation of cAMP-induced PKA activation; 2) elucidating the molecular rules that govern substrate recognition; and 3) understanding the molecular basis for isoform-specific activation by cAMP derivatives.

A structure of a PKA RIα:C holoenzyme was solved with a RIα deletion mutant that contains both cAMP binding domains. This structure revealed the extraordinary conformational range that the R-subunit can adopt as it toggles between binding the C-subunit and cAMP. Mutational analysis explains how Domain B is a "gate-keeper" for Domain A. A critical salt bridge links the two hydrophobic capping residues that stack against cAMP (for Domains A and B), such that binding of cAMP to Domain B can release the capping residue for Domain A. Small angle X-ray analysis of various mutant RIα-subunits revealed that Domain B is also highly dynamic. Dissection of the inhibitor sites from both cAMP binding domains shows that binding is only preserved for RII subunits. The differences observed between the RI and RII subunits suggest why the RII subunits, but not RI, can bind to the C-subunit in the absence of ATP.

A crystal structure of a complex between PKA and a specific substrate, phospholamban, was solved, revealing an overall common docking mode as the protein inhibitors at this site. Peptide array methods, site-directed mutagenesis, and biochemical analysis combined defines a unique consensus substrate recognition motif for PKA substrates as R-X_y-R-R-X-S/T-φ, where y is 0-4 residues.

Finally, the crystal structure of RIα bound to a cAMP analog, HE-33, was solved, revealing the structural basis of how cAMP analogs result in selective activation of Type Iα versus Type IIβ isoforms.

Chapter 1

Introduction

1.1. Signal transduction

A cell is the basic unit of living organisms. One of the most important problems in biology is to understand how the numerous cells in an organism communicate with each other to create functional tissues and organs and to produce physiological responses that bring about changes in heart rate, pain, and inflammation, to name a few.

The fundamental aspect of life is a cell's remarkable responsiveness to chemical or environmental stimuli, such as hormones, growth factors, and nutritional stress. Transmission and amplification of signals throughout a cell is responsible for a host of cellular functions that affect memory, inflammation, growth, differentiation, gene expression, metabolism, development, and cell death. Between a cell's exposure to stimuli and its subsequent physiological response is a complex signaling system that brings together both convergent and divergent networks of protein, lipid, and small molecule interactions. Some extracellular signals detected by membrane receptors are broadcasted into a cell through low molecular weight compounds called second

messengers. Some of the principal second messengers are phosphatidyl inositol derivatives, Ca^{2+}, diacylglycerol, cyclic guanidine phosphate (cGMP), and cyclic adenosine phosphate (cAMP). These messengers continue to amplify the signaling cascade by binding to and/or modifying their subsequent cellular targets. The epicenter of information transfer from molecule to molecule is often times in the form of chemical modifications including phosphorylation, sulfonation, palmytolation, myristilation, and small molecule modifications, to name a few. These modifications are sometimes reversible.

Protein phosphorylation, or the addition of a phosphate (PO_4) group, is one of the most simple yet also one of the most important modifications that regulate protein function in living cells and is precisely controlled by the action of protein kinases. Kinases catalyze the transfer of the ATP γ-phosphate to serine, threonine, or tyrosine amino acids on eukaryotic peptide or protein substrates. In prokaryotes, phosphorylation occurs on histidine, arginine, and lysine side chains. Transfer of the phosphate moiety acts as molecular switch that converts proteins from one state to another, or an “off” (inactive) and an “on” (active) switch. This simple modification can produce profound effects such as conformational changes, modulation of binding affinities between interacting proteins, offer docking sites for other proteins, stabilize an active or inactive state, and affect activity and cellular targeting. Substrates are sometimes phosphorylated by many different kinases in succession, and the substrates can even be the kinases themselves. Phosphorylation is a reversible process carried out by enzymes called phosphatases. Kinases and phosphatases are typically co-localized in multimeric complexes so that phosphorylation or dephosphorylation events can be rapidly controlled.

Just as kinases are central to cell survival and communication, aberrant regulation of protein phosphorylation is detriment to human health leading to problems ranging from cancers, cardiovascular disease, endocrinological disorders, immune diseases, and diabetes. Because of these issues, kinases are attractive drug targets in today's pharmaceutical industry and many efforts among today's scientists are focused on generating either agonists or antagonists to protein kinases for disease therapeutics. Both small molecules (such as Gleevac that target Src, a tyrosine kinase) and anti-sense oligonucleotides have been already developed for a few kinases. In order to generate rationally designed therapeutics, several steps are first needed. If we think of protein kinases as molecular machines, we must first determine what these molecules look like (or how atoms are arranged within these molecules), second understand how they work (how the catalytic machinery functions), and third understand how they are regulated. This knowledge can then be used to devise molecules that counteract deviant kinases that give rise to disease.

1.2. Protein kinases

Protein kinases were discovered nearly 60 years ago with the recognition that glycogen phosphorylase activity was regulated by reversible phosphorylation (Fischer and Krebs, 1955; Sutherland and Wosilait, 1955). Today, completion of the human genome sequence reveals that kinases are one of the largest protein families and account for 2% of the human genome, encoding for more than 500 proteins. Each kinase recognizes a barcode on their target substrates in the form of specific amino acid combinations encompassing the phosphorylation site (or P-site). These sequences are

diverse and even overlap between kinases. While some substrates are only phosphorylated by a single kinase, other substrates can be phosphorylated at the same amino acid by multiple kinases, enabling crosstalk between signaling networks.

It was recognized early on that kinases share a considerable amount of sequence homology, and it was predicted that they also share many common features such as their catalytic mechanism and overall structural core (Hanks and Hunter, 1995; Hanks et al., 1988). The first high-resolution protein kinase structure was solved in 1991 for cAMP dependent kinase (Knighton et al., 1991b), providing the first glimpse of a kinase at the atomic level. This kinase has a pac-man shape, with two domains (a small N-terminal lobe and a large stable C-terminal lobe) that together coordinates and positions the γ-phosphate from ATP for transfer to its substrate (Figure 1). Residues from both lobes form the catalytic center. In fact, the most conserved residues across all kinases center around the ATP binding site. Today, over 100 unique crystal structures of protein kinases have been solved and they all share the same overall topology. Despite the similarities in structural organization, all kinases have extremely diverse substrate specificities. Substrate selectivity, in turn, arises from conformational differences within the catalytic pocket, proximal and distal substrate docking sites, and surface charge characteristics (Figure 2). Apart from the catalytic core, kinases differ immensely in that some contain linked (or unlinked) regulatory domains, differ in their activation mechanism, and vary immensely in their sub-cellular localization.

Eukaryotic protein kinases have been classified into families based on sequence alignment of the catalytic domain. The modern classification system identifies nine distinct families. One of the most well understood classes is the AGC family kinases.

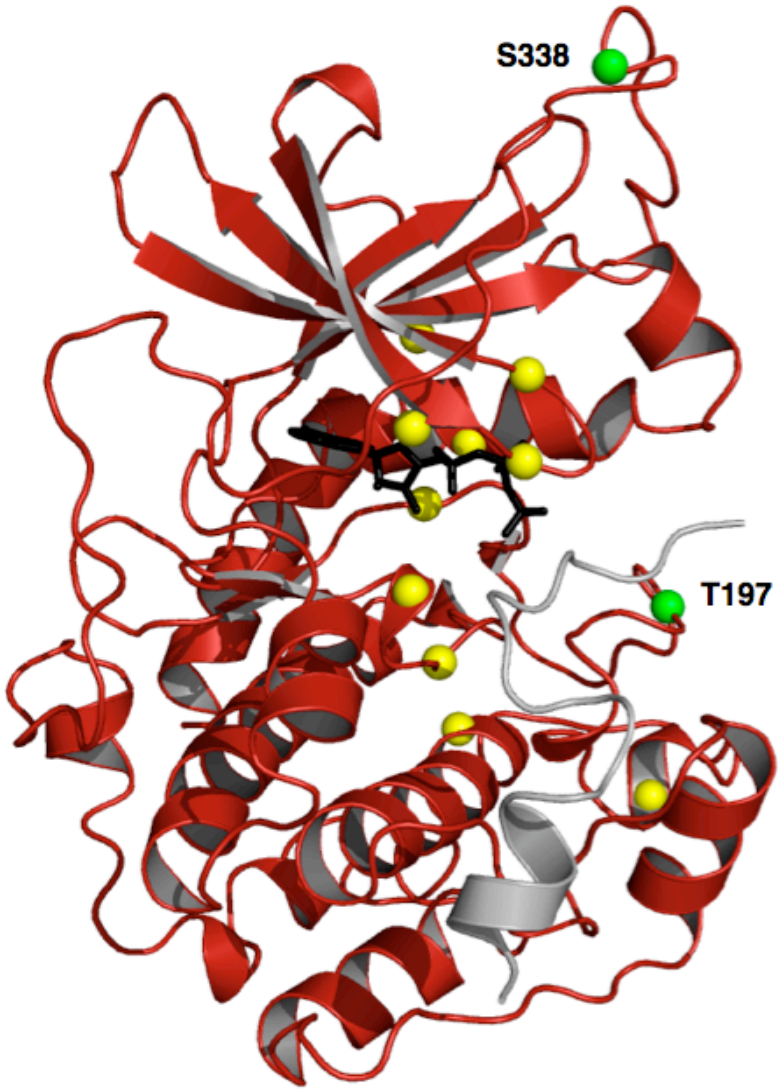

Figure 1. Structure of the PKA catalytic subunit.

A ribbon diagram of the C-subunit (C:ATP:PKI_{5-24}, [pdb:1atp]) showing conserved residues (yellow), phosphorylation sites (T197 and S338, green), ATP in the active site (black sticks), and the inhibitor peptide PKI_{5-24} (gray).

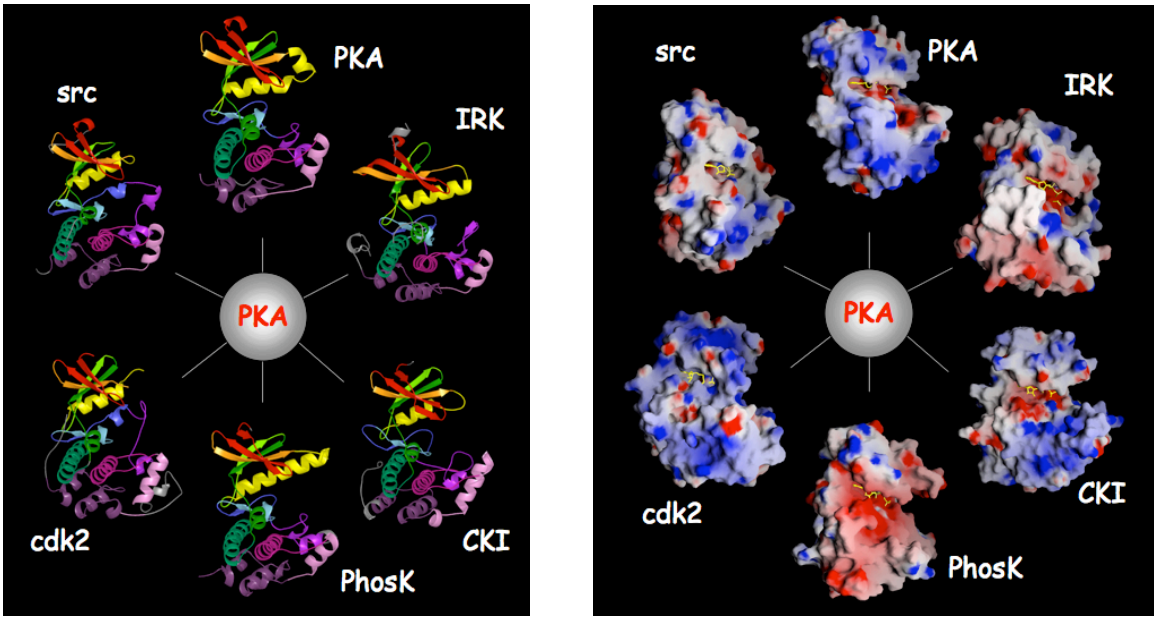

Figure 2. Structural conservation of the protein kinase fold.

Comparison between several kinases (PKA (Knighton et al., 1991b), cdk2 (De Bondt et al., 1993), src (Xu et al., 1999), phosphorylase kinase (Owen et al., 1995), casein kinase I (Xu et al., 1995), and IRK (Hubbard, 1997)) show that all share a common structural fold (left) but are highly diverse in their electrostatic surface (right). Ribbons on left are color coded according to subdomains defined by Hanks and Hunter (Hanks and Hunter, 1995).

The AGC family of kinases is named after PKA (Protein Kinase A or cAMP dependent kinase), PKG (Protein Kinase G), and PKC (Protein Kinase C) (Figure 3). AGC kinases share a high degree of sequence similarities within their catalytic domain, but differ in their regulatory organization. While the catalytic and regulatory domains for both PKG and PKC are connected in a contiguous protein sequence, these domains are on separate protein sequences for PKA. This distinction makes PKA a unique and simple system in which the catalytic and regulatory domains can each be studied separately. Over the last 30 years, a wealth of knowledge has been amassed for PKA, contributing to our overall understanding of kinases in general. The following sections review our current understanding of PKA.

1.3. cAMP dependent kinase (Protein Kinase A, PKA)

PKA is a Ser/Thr kinase first characterized in 1968 (Walsh et al., 1968). It has a long-standing place in history: it was one of the first kinases to be discovered (Walsh et al., 1968), the first to be sequenced (Shoji et al., 1981), and the first kinase structure to be solved (Knighton et al., 1991b). It has scores of substrates and phosphorylation of these substrates (and their consequent downstream events) engages diverse functional results including glycogen (Krebs and Beavo, 1979; Roesler et al., 1988) and lipid metabolism, gene regulation (Roesler et al., 1988), memory (Arnsten et al., 2005), cell division and cell death (Chen et al., 1998).

PKA is the primary receptor for the second messenger cAMP. Upon cell stimulation, hormones bind to G-protein coupled receptors. These receptors release G_s-proteins, activating adenlyate cyclase (AC) to catalyze the conversion of ATP to cAMP.

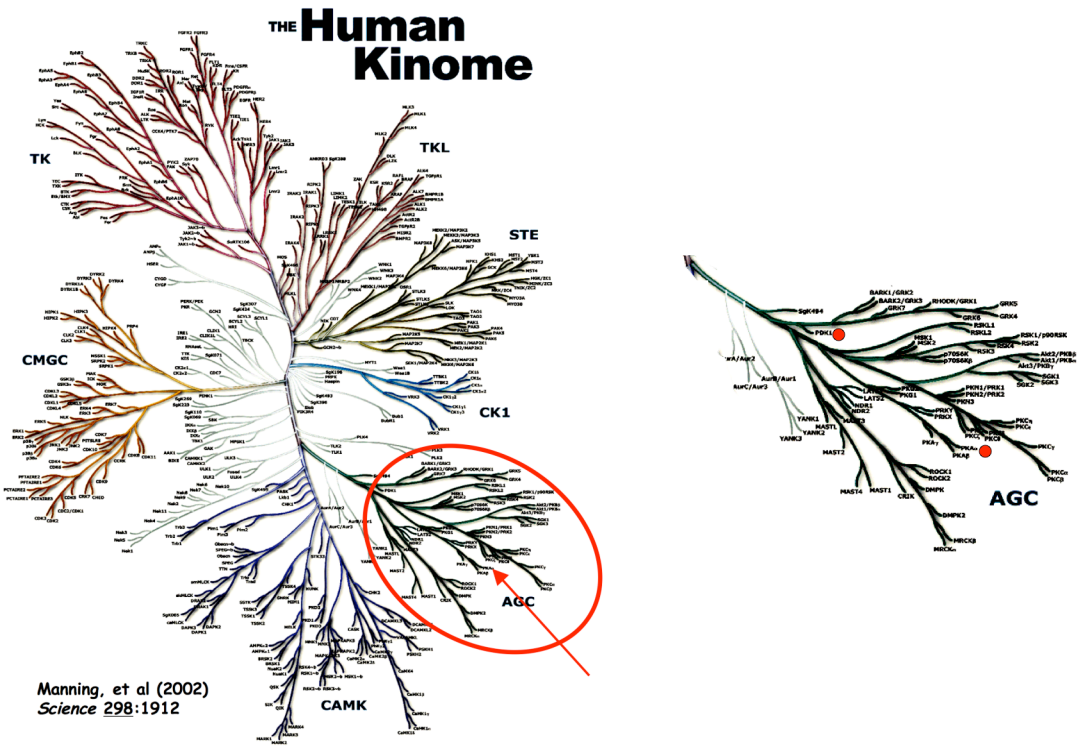

Figure 3. The Human Kinome.

Left, the Human Kinome, demonstrating kinase diversity. Right, the AGC branch of the Human Kinome showing the kinases that belong to the subfamily. Highlighted are PKA as well as PDK1, which is the major activator for most of the AGC kinases.

In the absence of cAMP, PKA holoenzyme exists as an inactive tetramer comprised of two catalytic subunits bound to two regulatory subunits. The two subunits form a high affinity complex (K_D = 0.2 nM) (Herberg et al., 1996a) where the R-subunit masks the catalytic machinery by blocking access of substrates to the active site (Kim et al., 2005). Activation of PKA relies on the binding of two cAMP molecules to each of the R-subunits. This action reduces the affinity between the R- and C-subunits (Anand et al., 2007a), leading to dissociation of the holoenzyme into a dimer of R-subunits, and two free catalytically active C-subunits.

The C-subunit is also regulated by a non-cAMP responsive mechanism through the heat stable Protein Kinase Inhibitor (PKI). PKI is a small helical 77 amino acid protein that is widely expressed in many tissue types. It is highly specific for PKA and is an extremely potent competitive inhibitor of the C-subunit (K_i = 0.5 - 2 nM) (Demaille et al., 1977; Whitehouse and Walsh, 1983). Like the R-subunits, a portion of PKI binds to the active site of the C-subunit, obstructing access of substrates to the catalytic pocket. A 20 amino acid fragment (residues 5-24) alone is highly specific for PKA (K_i = 2.3 nM) (Scott et al., 1986). Structural analysis shows that five amino acids at the N-terminus (residues 5-10) dock to a complementary groove on the C-subunit through hydrophobic interactions. Unlike the R-subunits, PKI contains a nuclear export signal that actively transports the C-subunit from the nucleus to the cytosol (Wen et al., 1994; Wen et al., 1995).

PKA is also regulated by sub-cellular localization through another class of scaffolding proteins called A Kinase Anchoring Proteins (AKAP). Given that PKA has such a broad range of substrates, AKAPs function to target PKA to large signaling complexes near its substrates rather than floating freely inside the cell. Sequestering

PKA to a specific sub-cellular location not only ensures that the enzyme is near its appropriate targets, but also prevents indiscriminate phosphorylation of other substrates. These protein scaffold complexes also bring together other proteins necessary for enzyme regulation, such as membrane channels, phosphatases, and phosphodiesterases, to name a few. Thus, AKAPs are means to unite divergent signaling pathways to facilitate the precision of intracellular signaling events. There are over 50 proteins identified in this family in mammals and lower organisms (Wong and Scott, 2004). For PKA, AKAPs bind to the N-terminal helical region of the R-subunits. Many AKAPs are associated with membranes (therefore targeting PKA to membranes as well), but a few AKAPs are also cytosolic. AKAPs target PKA to a wide range of cellular distributions including the mitochondria (Newhall et al., 2006), the nucleus (Coghlan et al., 1994), the sarcoplasmic reticulum in the heart (Robinson et al., 1996), and Ca^{2+} channels (Hulme et al., 2003).

Given the promiscuity of PKA, its activity must be tightly controlled. In summary, the four main factors that contribute to PKA regulation are: 1) cAMP; 2) inhibitor proteins; 3) ATP; and 4) sub-cellular localization. The alteration of any of these factors in the cell creates profound biological consequences that can lead to defects in cellular function and human disease. Research in the PKA field over the last three decades has focused on understanding how the C-subunit catalytic machinery works, as well as how cAMP binds to the regulatory subunits. The following two sections are a general overview of our current understanding of the catalytic and regulatory subunits of PKA.

1.3.1. The Catalytic Subunit

General Features

There are four isoforms of the catalytic subunit, α, β, γ, and PRXXY. Each of these isoforms are differentially expressed in tissues and multiple splice variants exists for the α and β isoforms.

The catalytic subunit is a dynamic bi-lobal protein that has the same conserved structural core shared by all Ser/Thr and Tyr kinases. The kinase core is approximately 250 amino acids in length with a small N-terminal domain (comprised of 5 anti-parallel β-sheets and two α-helices), a flexible linker, and a large C-terminal domain (solely comprised of α-helices). On either side of the central core is a 39-residue N-terminal tail and a 50-residue C-terminal tail.

The N-terminal tail is important for localization of the C-subunit to various cellular targets by either covalent modifications or through interaction partners. At the N-terminus is a glycine residue that is readily myristylated. PKA was in fact the first protein shown to be myristylated, which may help target the C-subunit to membranes (Carr et al., 1982). Ser10 is phosphorylated and mutants of this residue showed decreased activity and produced mostly insoluble material (Yonemoto et al., 1997). Asn2 can be deamidated, which leads to the buildup of C-subunit in the nucleus (Kinzel et al., 2000; Pepperkok et al., 2000). The N-terminal helical region also binds to A Kinase Interacting Protein (AKIP), which brings the C-subunit into the nucleus (Sastri et al., 2005). The first exon also exhibits many alternative splice sites. The N-terminus is the most diverse region among all the C-subunit isoforms, and this variation is likely to be important for biological function.

The C-terminal tail, unlike the N-terminal tail, is a conserved structural feature of AGC kinases (Kannan et al., 2007a). In one section, the tail is anchored to the large lobe, and contains many crucial elements important for kinase activity. In a different section, the tail has a dynamic acidic region and presumably a docking site for other proteins (such as PDK1, unpublished). The C-terminal tail is also a protein docking site for other AGC kinases, where SH3 domains bind to AKT (Jiang and Qiu, 2003) and HSP90 and Cdc37 bind to PKC (Gould et al., 2009).

Main Structural Elements of the Kinase Core

Over the years, crystal structures for various conformational states of the catalytic subunit have been solved: the closed conformation was crystallized in the presence of ATP, Mg^{2+}, and PKI inhibitor (Knighton et al., 1991c); the dynamic apo conformation is the most open state that does not contain either nucleotide or peptide (Akamine et al., 2003); and a transition-state mimic was crystallized in the presence of aluminum fluoride, ADP, Mg^{2+}, and PKI (Madhusudan et al., 2002). These structures demonstrate how dynamic the C-subunit is. Individually, each lobe in the C-subunit is rather rigid. Instead, the motions stem from movement of loops and a linker region *between* the two lobes. These structures provided insights into key elements of the C-subunit necessary for proper function of the catalytic machinery. Several reviews offer an in-depth treatment of all the structural elements, but the following simply outlines the major features and their roles (Figure 4).

Glycine rich loop - This loop resides in the N-terminal lobe (GTGSFG, residues 50-55) and is the most flexible fragment of the kinase, evident by high B-factors in the crystal structures. It is required for anchoring ATP in the active site cleft, as well as

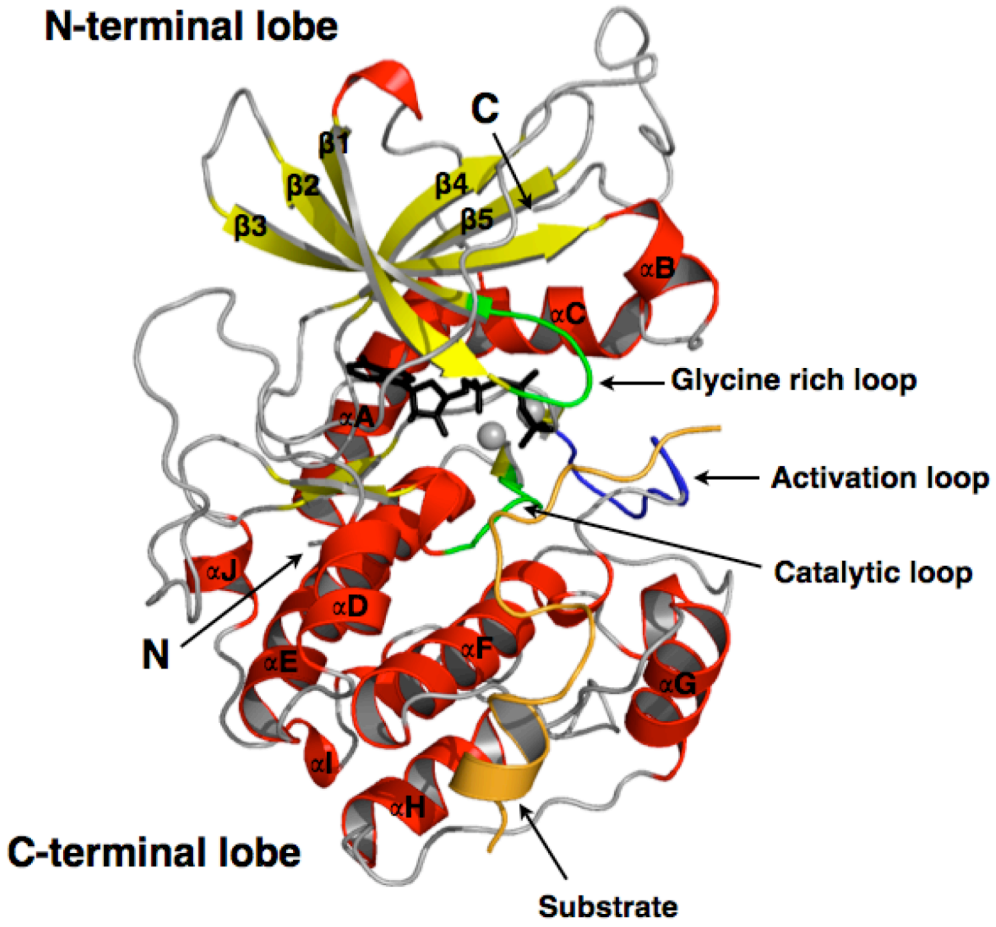

Figure 4. Major structural elements within the PKA C-subunit.

Alpha helices are in red, beta sheets are in yellow, PKI inhibitor peptide is in orange, ATP is in black, and magnesium ions are depicted as grey spheres.

positioning the γ-phosphate in the correct orientation for phosphoryl transfer. Both structural and biochemical data show the importance of Ser53 and Gly55 for interacting with and positioning the γ-phosphate of ATP. This glycine loop is actually found in many kinases, presumably due to its innate plasticity to facilitate nucleotide binding in the kinase pocket.

Catalytic loop – This loop contains one of the catalytic residues that mediates the phosphoryl transfer from ATP to a substrate. Asp166 is thought to be the catalytic base that orients the P-site serine or threonine for catalysis.

αC-helix of the N-terminal lobe – In many kinases, movement of the αC helix is imperative for positioning key amino acids in the active kinase. In PKA, this helix contains a glutamic acid residue (Glu91) that interacts with Arg165 adjacent to the catalytic residue Arg166 that carries out the phosphoryl transfer. In the inactive state of many kinases (such as src (Xu et al., 1999), hck (Sicheri et al., 1997), cdk2 (De Bondt et al., 1993; Jeffrey et al., 1995; Russo et al., 1996), and insulin receptor (Hubbard, 1997; Hubbard et al., 1994)), this αC helix is rotated such that their Glu91 equivalent residue faces solvent. Lysine 72 directly interacts with ATP (Iyer et al., 2005). Mutation of this lysine completely abolishes any catalytic activity.

Activation segment – This region spans residues 184-208 and is important for all protein kinases (Johnson et al., 1996). In PKA, this loop contains a critical threonine residue (Thr197) whose phosphorylation is responsible for organizing the catalytic residues so that optimal substrate docking and subsequent phosphorylation can occur (Yonemoto et al., 1997). Mutation of this threonine abolishes kinase activity. This threonine is embedded in the PKA consensus sequence and is presumably auto-phosphorylated by the C-subunit in *e. coli*. Thr197 can also be phosphorylated *in vitro* by

PDK1. In general, many protein kinases (but not all) have a Ser, Thr, or Tyr in the activation loop whose phosphorylation (hence change in conformational state) controls the activity of the kinase. Furthermore, this loop contains a conserved aspartate residue (Asp184) that stabilizes a Mg^{2+} ion in the catalytic pocket, essential for neutralizing the charged phosphate moieties of ATP.

1.3.2. The Regulatory Subunits

Distinguishing Features Between the Four Isoforms

There are two major classes of R-subunits, RI and RII, that are functionally non-redundant, and within these classes are α and β subtypes (RIα, RIβ, RIIα, RIIβ). The two different isozymes, Type I and II, were first identified based on their elution profiles from DEAE-cellulose columns (Corbin et al., 1975; Reimann et al., 1971). Although all isoforms share the same domain organization (Figure 5), they differ in sequence, sub-cellular localization, tissue-specific expression, biochemical properties, and ability to be phosphorylated by the C-subunit.

Functional studies of knockout mice deficient in specific R-subunit genes clearly show that the isoforms are inexchangeable, where only deletion of RIα (and not other isoforms) is embryonically lethal as a result of mesoderm-dependent cardiovascular development failure. On the flip side, deletion of RIIβ in mice is not detrimental, but is instead compensated by increased levels of RIα. These mice, however, have smaller fat cells and are resistant to obesity (Cummings et al., 1996).

On a cellular level, RI isoforms are predominantly found in the cytosol while the RII isoforms are localized to plasma membranes. The targeting of RII subunits is a

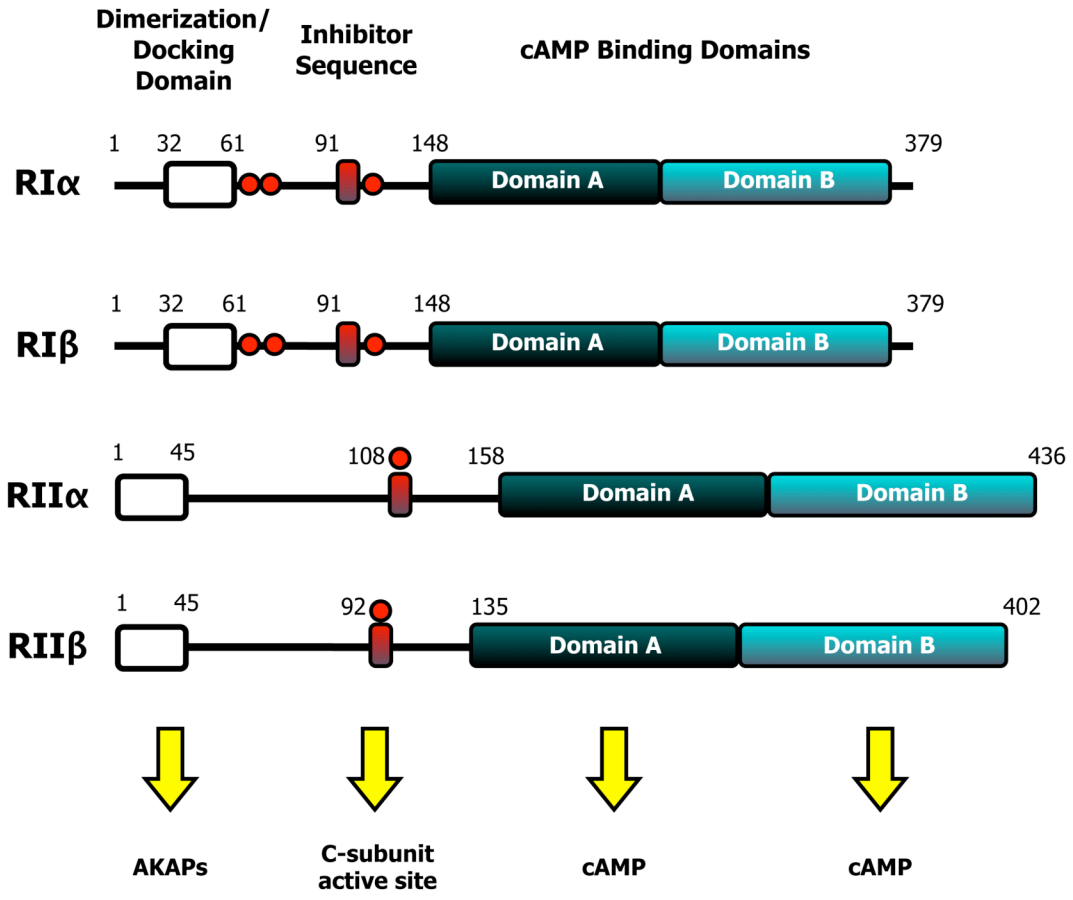

Figure 5. Domain organization of the PKA regulatory subunits.

consequence of interactions with AKAPs. These AKAP proteins bring together other proteins critical for kinase regulation at a central hub, including phosphatases and phosphodiesterases.

On a biochemical level, the most significant difference between RI and RII subunits is that only Type II R-subunits can be phosphorylated by C-subunits, thus making the RII subunits both substrates *and* inhibitors of the C-subunit. Type II subunits contain a serine at the P-site, while Type I subunits are pseudo-substrates in that they contain an alanine or glycine at the P-site. The physiological relevance of this phosphorylation has not been well studied, but presumed to add yet another layer of regulation to precisely mediate a cell's response to stimuli. In other words, Type II holoenzymes are not only sensitive to cAMP, but also to ATP. In situations where high levels of ATP are present (such as in the mitochondria), PKA can be readily activated upon the changing needs of a cell. Along those lines, the Type I isoforms can only form holoenzymes with the C-subunit in the presence of magnesium and ATP, whereas the Type II isoforms can readily form a high affinity complex without ions or nucleotides (Herberg and Taylor, 1993).

General Architecture of the Regulatory Subunits

Despite the many biological and biochemical differences between the four R-subunit isoforms, all share the same general domain organization. In contrast to the C-subunit, the R-subunits are highly modular, flexible, and dynamic. All contain an N-terminal dimerization domain that bind to AKAPs, a flexible linker, an inhibitor sequence that binds to the active site cleft of the C-subunit, and two tandem cAMP binding domains (Figure 5).

The dimerization domain is an anti-parallel four-helix bundle that interacts with AKAPs. Two helices from each monomer come together to form a groove in which a single AKAP helix can fit. This short 20 amino acid domain is all that is required to dimerize and bind AKAPs. Both crystallographic and NMR structures were solved for a several R-subunits bound to an assortment of AKAP peptides and illustrated the distinguishing features between RI and RII isoforms. The RIα dimerization domains are charged, whereas the RIIα and RIIβ surfaces are rather hydrophobic. Mutational studies of these regions explain how the binding specificities of AKAPs to their respective R-subunits is achieved (Banky et al., 1998; Banky et al., 2000; Banky et al., 2003; Kinderman et al., 2006).

The following linker region is the most variable region among the four isoforms. The linkers differ in both sequence and in length. Solution studies propose that this linker is responsible for the differences in the overall shape of the R-subunits (Vigil et al., 2004). Furthermore, this region is a potential docking surface for other proteins. The sequence of the linker region contains a poly-proline region and a phosphorylatable serine (Ser81), making this region a prime site for Grb (Tortora et al., 1997) and 14-3-3 binding (unpublished). Much is still unknown about the linker regions.

The inhibitor sequence is varied across the four isoforms, but all carry the consensus PKA sequence R-R-X-S/T-ψ. Crystal structures of the RIα:C, RIIα:C, and RIIβ:C complexes reveal that each isoform binds to the active site cleft in a similar manner, occluding the space where substrates would dock. Despite those similarities, the Type I and Type II isoforms differ somewhat. While the RII subunits have a serine at the P-site, the RI subunits have either a glycine or alanine, making them pseudosubstrates.

The C-terminal cAMP binding domains are presumably the result of a gene duplication event and is made up of a highly rigid β-sandwich fold and a flexible α-helical subdomain. Each domain is comprised of roughly 120 amino acids. Crystal structures of of both RIα (Su et al., 1995b) and RIIβ (Diller et al., 2001) bound to cAMP show that the β-sandwiches of these two domains are superimposable and the differences arise from the α-helical domain. Each domain contains a structurally conserved helix-loop called the phosphate binding cassette (PBC) that binds to cAMP. Within the PBC is a conserved glutamic acid residue (Glu200) that interacts with the ribose 2'-hydroxyl of cAMP and a conserved arginine that binds to the exocyclic oxygen. cAMP is further stabilized by a distal hydrophobic interaction against the adenine ring. Mutagenesis shows that each of these three residues is vital for binding to cAMP. Details of these interactions will be discussed later in Chapter 2.

Other cAMP Binding Proteins

The cyclic nucleotide-binding module evolved as sensors of the second messenger cAMP, and is conserved from primitive bacteria to humans. Other than the PKA regulatory subunits, several proteins contain cAMP binding domains including the prokaryotic transcription regulator catabolite activator protein (CAP), and the eukaryotic proteins hyperpolarization-activated cyclic nucleotide-modulated channels (HCN) (DiFrancesco and Tortora, 1991; Gauss et al., 1998; Nakamura and Gold, 1987), and guanine nucleotide exchange factors (exchanging protein directly activated by cAMP, EPAC) (de Rooij et al., 1998; Kawasaki et al., 1998). A recent analysis of genomic sequences from the National Center for Biotechnology Information's non-redundant amino acid database and Global Ocean Sampling database identified over 7,000

proteins (both prokaryotes and eukaryotes) containing cyclic nucleotide binding domains (Kannan et al., 2007b). Many of these domains were fused to other functional domains within the same protein, suggesting that they evolved as scaffolds to respond to a variety of signals.

Crystal structures have been determined for many of these proteins and together provide a general mechanism for how cAMP binds to these domains. All of these proteins share a similar cAMP binding module that consists of the conserved eight-stranded β-sandwich and the PBC described above (Berman et al., 2005). They all also contain α-helical elements, but unlike the β-sandwhich, are not as universally conserved.

1.3.3. Inhibition Mechanism of PKA Holoenzymes

The first glimpse of how PKA was inhibited by the regulatory subunit came to light when the structure of a small piece of RIα was solved in complex with the C-subunit (Figure 6) (Kim et al., 2005). This small piece of RIα consisted of residues 91-244 that included the inhibitor sequence and only one of the two cAMP binding domains. This fragment is the smallest piece of the RIα subunit that still bound to both the C-subunit and cAMP with high affinity. This structure revealed an extended interface between the two proteins as well as a view of how the inhibitor sequence became ordered and bound to the active site cleft of the C-subunit (the inhibitor site is not observed in other R-subunit structures). The structure also hinted at the extreme flexibility that must exist within the R-subunits as a major conformational change occurred in the C-terminal-most portion of the RIα fragment. It was hypothesized that the second domain moves with the helix, but is only speculative without the crystal structure with an intact Domain B. To

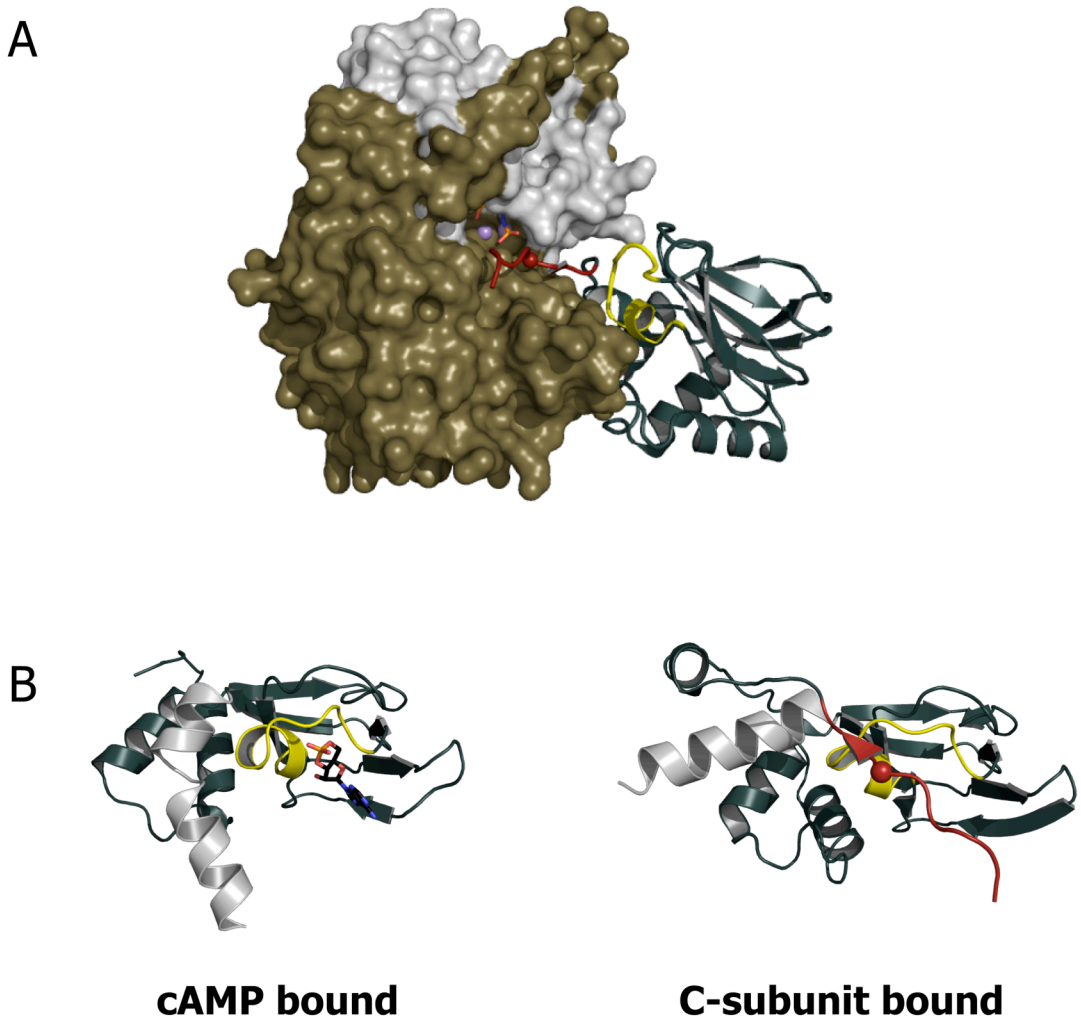

Figure 6. Crystal structure of a PKA complex between the C-subunit and RIα containing only one of the two cAMP binding domains.

(A) Structure of the overall complex. The inhibitor sequence of the R-subunit (red) is bound to the active site cleft with AMPPNP (sticks) and two Mn^{2+} ions (purple). A large interface is formed between the two proteins. (B) Conformational changes associated with the R-subunit upon binding to cAMP (left) and the C-subunit (right). The major structural differences between the two conformations lie in the αC helix (white). The C-subunit is shown in surface rendering with the small lobe in white and the large lobe in tan. The R-subunit is shown as a cartoon in teal with the inhibitor sequence in red (with the P-site shown as a ball) and the phosphate binding cassette in yellow.

truly understand the full extent of the conformational change, the full mode of inhibition, as well as the activation mechanism by which cAMP dissociates the complex, a crystal structure of the full complex (or at least with *both* cAMP binding domains) must be solved.

1.4. Relevance of PKA in Disease

Clearly, each of the four R-subunit isoforms is utilized in a different manner in the cell and are functionally inexchangable. Several reports also indicate that in certain disease states, the relative level of each isoform is altered. This is true for Systemic Lupus Erythematosus (SLE), Carney complex, and a variety of cancers.

SLE is an autoimmune disease characterized by aberrant T lymphocyte effector function creating altered immune responses to autoantigens (Dayal and Kammer, 1996). Both RIα and RIIβ protein and mRNA levels are drastically reduced (Pepperkok et al., 2000). Diminished PKA-catalyzed protein phosphorylations for the Type-Iα and Type-IIβ in SLE T-cells is also reduced (80% and 40%, respectively) (Kammer et al., 1994). There is also a reduction of RIβ protein levels as the result of a block in protein translation (Khan et al., 2001). Furthermore, cDNA sequence analysis of SLE patients revealed a number of mutations in RIα transcripts including deletions, transitions, and transversions (Laxminarayana and Kammer, 2000; Laxminarayana et al., 2002) and a high prevalence of PKA activity persisting over time (Kammer, 1999).

Carney complex is an autosomal dominant condition that leads to skin hyper-pigmentation, endocrine defects, and in some cases tumors in the heart and skin. The principal cause of this disease is heterogeneous mutations in RIα including

transversions, premature stop trunctations, and deletions leading to nonsense- mediated mRNA decay and overall reduction of RIα protein expression (Bertherat et al., 2009; Groussin et al., 2006; Horvath et al., 2008). The precise mechanism by which these mutations cause aberrant RIα subunits is unclear. It has been hypothesized that these mutations lead to aberrant RIα proteins incapable of properly inhibiting the C-subunit, thus resulting in overactive and unregulated PKA-dependent protein phosphorylation.

Where under-expression of the R-subunit proteins leads to systemic lupus erthematosus, over-expression of RIα is associated with many cancers, tumorogenesis, and tumor growth (such as breast, ovarian, colon, and renal cancers). Evidence from a variety of experimental approaches have also identified that relative levels between RI and RII PKA in cells play a major part in the delicate balance between cell growth and differentiation. Loss of this balance may promote cancer formation and progressions. In fact, the expression of RI proteins in cancer cells is significantly higher than RII proteins (Cheadle et al., 2008; Meoli et al., 2008; Miller, 2002). Moreover, cancer cells that expressed more RIα displayed enhanced growth rates (Cho-Chung, 1990; McDaid et al., 1999). Targeting RIα with anti-sense oligonucleotides for both cancer cell lines and animal models show reductions in cell growth as well as tumor growth, providing a potential target for cancer therapies (Nesterova and Cho-Chung, 2005; Tortora et al., 1991).

1.5. Major outstanding questions regarding the allosteric regulation of PKA activation

Since PKA is such a promiscuous protein, its regulation must be finely tuned and highly responsive to a cell's constantly changing needs. The misregulation of PKA phosphorylation may progress to detrimental health problems such as heart disease and cancers. The four main modes of PKA regulation are through cAMP, inhibition by the regulatory subunits, ATP, and sub-cellular localization. Understanding the chemical and biological mechanisms of how each of these factors function to regulate PKA is paramount in developing drug therapies to counteract PKA-associated diseases. While a considerable body of knowledge has grown over the last few decades concerning the precise mechanism of how each of these factors function, there are still many unanswered questions in the field, including the following:

1. What is the mechanism by which the R-subunit senses cAMP leading to dissociation of the holoenzyme complex? How is the signal of cAMP binding to the R-subunit actually transmitted throughout the protein? And what are the precise conformational changes associated with the R-subunit between C-subunit and cAMP binding?
2. What is the precise role of the inhibitor segment of the regulatory subunits? Can we learn from the endogenous inhibitor sequences to develop peptide inhibitors that are highly specific for PKA?
3. How does the interaction between PKA and substrates compare with the interaction between PKA and known endogenous inhibitors?

4. Can we generate cAMP derivatives that can selectively target one PKA isoform over another as a strategy for drug design? What are the rules that govern cAMP analog binding to specific holoenzyme isoforms?

The focus of this dissertation is to define the molecular features that govern RIα:C complex formation as a means to understand the allosteric regulation of cAMP-induced PKA activation. Each of the questions described above are addressed in the subsequent chapters.

Chapter 2 describes the RIα:C holoenzyme structure solved with a deletion mutant that contains both cAMP binding domains explaining why Domain B is indeed a "gate-keeper" for Domain A.

Chapter 3 focuses on the dynamic properties of mutant RIα heterodimers. Small angle X-ray scattering was utilized to illustrate the dynamic nature of Domain B in RIα.

Chapter 4 investigates the role of the inhibitor site alone (devoid of both cAMP binding domains) in PKA complex formation. Differences observed between the four regulatory subunit isoforms are explained to give rise to isoform-specific mechanisms of cAMP-induced activation.

Chapter 5 describes the crystal structure solved between PKA and a specific substrate, phospholamban, and compares results with endogenous inhibitor complexes. Peptide array methods, site-directed mutagenesis, and biochemical analysis combined defines a unique consensus substrate recognition motif for PKA substrates in general.

Chapter 6 investigates the structural basis of how cAMP analogs results in the selective activation of either Type Iα or Type IIβ isoforms. The crystal structure of RIα

bound to a cAMP analog, HE-33, is described and compared with a structure of RIIβ bound to the same analog.

Chapter 2

PKA-Iα Holoenzyme Structure: Dynamic Conformational Change of RIα Reveals Mechanism for cAMP-dependent Activation

---

2.1. Introduction

Cyclic adenosine monophosphate (cAMP) signaling through cAMP-dependent protein kinase (PKA) is a ubiquitous mammalian signaling pathway that has been conserved in all eukaryotes, with the exception of the plant phyla. While the catalytic (C) subunit has served as a prototype for the protein kinase superfamily, the regulatory (R) subunit defines the mechanism whereby the second messenger, cAMP, translates an extracellular signal into an intracellular biological response. This mechanism of cAMP regulation is conserved from bacteria to man, and the domain that recognizes cAMP is likewise universal.

The crystal structure of the catalytic subunit defined for the first time the conserved structural features of the protein kinase superfamily (Knighton et al., 1991d).

It is a globular bilobal protein with a highly dynamic small lobe that serves as the binding site for ATP, burying the adenine ring in a deep hydrophobic pocket and positioning the γ-phosphate for transfer to a protein substrate. The stable large lobe serves as a framework for the catalytic machinery and also as a docking scaffold for binding to protein partners that act as substrates or inhibitors (Cheng et al., 2001; Johnson et al., 2001; Knighton et al., 1991a; Knighton et al., 1991d). The activation loop is a characteristic motif of the protein kinase family that upon phosphorylation optimizes the catalytic machinery for phosphoryl transfer (Adams et al., 1995; Nolen et al., 2004; Steinberg et al., 1993). In PKA, this loop (residues 191-197, VKGRTWT) also functions as a major binding surface for the R-subunit (Kim et al., 2005).

In contrast, the R-subunit is a highly dynamic and modular protein that serves as one of the major receptors for cAMP in eukaryotic cells. At the N-terminus is a helical dimerization docking (D/D) domain that interacts with scaffold proteins, referred to collectively as **A** **K**inase **A**nchoring **P**roteins (AKAPs) (Kinderman et al., 2006; Newlon et al., 2001). Following this domain is a variable and flexible linker region containing an inhibitor site that docks to the active site cleft of the C-subunit. Two tandem cAMP-binding domains (Domain A and Domain B) lie at the C-terminus. Each cAMP-binding domain consists of a β-sandwich and a non-contiguous helical subdomain. Among the four known protein families that bind cyclic nucleotides (PKA/PKG, CAP, HCN, and EPAC), the most conserved feature of each domain is the phosphate binding cassette, a helix-loop region where cAMP binds. The C-subunit is locked in a dormant state in the absence of cAMP through formation of a holoenzyme inhibitory complex, where the R-subunit dimer binds to two C-subunits. Binding of cAMP to the R-subunit unleashes the catalytic subunit thereby allowing phosphorylation of PKA substrates. There are two

major classes of R-subunits, RI and RII, that are functionally non-redundant, and within these classes are α and β subtypes (RIα, RIβ, RIIα, RIIβ) (Brandon et al., 1997).

While crystal structures for separate catalytic and regulatory subunits of PKA have been known for some time, understanding the molecular features of the universal cAMP signaling pathway requires having a structure of the holoenzyme complex. The recent structure of the C-subunit bound to a deletion mutant of RIα containing only Domain A provided clues to the dramatic conformational switch that the R-subunit must undergo to release the C-subunit and bind cAMP (Kim et al., 2005). This complex, however, lacked the second cAMP-binding domain that is crucial for allosteric activation of PKA by cAMP. Activation of the type I holoenzyme by cAMP is a highly ordered process. In holoenzyme complexes with R-subunits containing both cAMP-binding domains, Domain A is inaccessible until cAMP occupies Domain B (Herberg et al., 1996b; Ogreid and Doskeland, 1981a, b). This obligatory activation pathway led to the designation of Domain B as a “gatekeeper” for Domain A.

Here we report a holoenzyme structure that contains both cAMP-binding domains of RIα (Domain A: residues 123-259 and Domain B: residues 260-379). The complex reveals an extended R/C interface that protects sites in the C-subunit essential for catalysis and substrate binding. It shows an extended interface surrounding the activation loop and defines a novel interaction site between Domain B in RIα and an S-shaped loop (residues 276-286) on the large lobe of the catalytic subunit (subsequently referred to as the αH-αI loop). The structure also shows local conformational changes within the helical regions as well as dramatic global rearrangement of the two cAMP-binding domains as the R-subunit wraps around the large lobe of the catalytic subunit. Finally, this new structure reveals for the first time a highly conserved holoenzyme-

specific salt bridge formed in Domain B involving two residues (Glu261 and Arg366) that are solvent exposed in the cAMP-bound conformation. In the holoenzyme, this salt bridge tethers the two adenine capping residues (Trp260 and Tyr371). The importance of this salt bridge and the two capping residues in facilitating PKA activation are confirmed by mutagenesis. Taken together, the molecular features revealed by this new structure allow understanding of the communication pathway between the two cAMP-binding domains and provides a mechanism for the ordered and cooperative activation of PKA by cAMP.

2.2. Experimental Methods

2.3.1 Molecular Cloning

DNA for RIα mutants were generated by Quikchange mutagenesis according to the Strategene protocol. The oligos used in the reactions were as follows:

W260A-F	5' GAA TCT CTG GAC AAG **GC**G GAG CGT CTC ACG GTA GC
W260A-R	5' GC TAC CGT GAG ACG CTC C**GC** CTT GTC CAG AGA TTC
Y371A-F	5' CGC AAC ATC CAG CAG **GC**C AAC AGC TTC GTG TC
Y371A-R	5' GA CAC GAA GCT GTT G**GC** CTG CTG GAT GTT GCG
E261A-F	5' GAA TCT CTG GAC AAG TGG G**C**G CGT CTC ACG GTA GC
E261A-R	5' GC TAC CGT GAG ACG C**G**C CCA CTT GTC CAG AGA TTC
R366A-F	5' C CGA CAT CCT CAG **GC**C AAC ATC CAG CAG
R366A-R	5' CTG CTG GAT GTT G**GC** CTT GAG GAT GTC GG
G235A-F	5' C AGA AGG ATC CTC ATG G**C**A AGC ACG CTG AGA AAG C
G235A-R	5' G CTT TCT CAG CGT GCT T**G**C CAT GAG GAT CCT TCT G

G235L-F	5' C AGA AGG ATC CTC ATG **CTG** AGC ACG CTG AGA AAG C
G235L-R	5' G CTT TCT CAG CGT GCT **CAG** CAT GAG GAT CCT TCT G
G235P-F	5' C AGA AGG ATC CTC ATG **CCG** AGC ACG CTG AGA AAG C
G235P-R	5' G CTT TCT CAG CGT GCT CGG CAT GAG GAT CCT TCT G
R226A-F	5' GG GGC ATT GAC GCG GAC AGC TAC AG
L233A-F	5' GC TAC AGA AGG ATC **GC**C ATG GGA AGC ACG
L233A-R	5' CGT GCT TCC CAT G**GC** GAT CCT TCT GTA GC 3

2.3.2 Protein Preparation

The catalytic subunit was expressed and purified in *E. coli* as described previously (Gangal et al., 1998). For crystallography, three RIα mutants were generated by Quikchange mutagenesis according to the Strategene protocol (RIα(91-379); RIα(91-379:R209K); and RIα(91-379:R333K)). These mutants lacked the N-terminal dimerization/docking domain (residues 1-90). The essential arginine in the PBC of each cAMP binding domain were also mutated, Arg209 in Domain A and Arg333 in Domain B. Four additional mutants were generated with Quikchange mutagensis for biochemical analysis, RIα(91-379:E261A), RIα(91-379:R366A), RIα(91-379:W260A), and RIα(91-379:Y371A). All RIα mutants were expressed in *E. coli* BL21 (DE3) cells (Novagen) and purified as described in (Su et al., 1995a; Wu et al., 2004).

2.3.3 Holoenzyme Formation for Crystallography

Three RIα mutants (RIα(91-379), RIα(91-379:R209K), and RIα(91-379:R333K)) were mixed with wild-type C-subunit in a 1:1.2 molar ratio and dialyzed by concentration

at 4°C in 10 mM MOPS (pH 7.0), 2 mM $MnCl_2$, 50 mM NaCl, 2 mM EDTA and EGTA, 1 mM TCEP-HCl, 0.2 mM AMP-PNP, and 10% glycerol. Holoenzyme was separated from excess C-subunit by gel filtration chromatography as described (Wu et al., 2004).

2.3.4 Crystallization and Data Collection

The RIα(91-379:R333K):C complex was crystallized at 25°C in hanging drops using the vapor diffusion method in 2.0M $(NH_4)_2SO_4$, 0.1M Citrate, (pH 5.5). These crystals were transferred to a cryoprotectant solution (mother liquor containing 20% glycerol) and flash-cooled in liquid nitrogen. X-ray diffraction data was collected at the SER-CAT insertion-device beamline 19-ID (Advanced Photon Source, National Laboratory, Argonne, IL, USA) on SBC2 3k X 3k CCD (ANL). Diffraction data were processed and scaled using HKL2000. Initial indexing clearly indicated a primitive hexagonal lattice without any ambiguity (distortion index 0.12%). The final data was integrated and scaled in $P3_221$ (a = b = 125.9 Å, c = 141.0 Å) with satisfactory statistics. The statistics of the data processing are in Table 1.

2.3.5 Structure Determination and Refinement

Initial phases of the RIα(91-379:R333K):C complex were generated by molecular replacement using the RIα(91-244):C complex (PDB code 1U7E) (Kim et al., 2005) as a search model using Phaser (Storoni et al., 2004). Although our initial solvent content analysis predicted that two molecules per asymmetric unit is the most probable (V_M=2.2 $Å^3$/Dalton), a phaser run in a single-model mode unambiguously found only one molecule (Z score 24-60) in the asymmetric unit, corresponding to a solvent content of

72.3% (V_M=4.5 Å^3/Dalton). The phases obtained from the phaser run were improved by solvent flattening using DM (Cowtan, 1994). The resulting F_o map calculated from the improved phases showed a well-defined electron density for the B-domain of RIα. Secondary structure of the RIα Domain B was built in manually using XtalView and this was followed by iterative cycles of structure refinement using REFMAC in the CCP4 suite. The final refinement implementing TLS refinement (Winn et al., 2001) for each chain converged to R and R_{free} values of 0.192 and 0.212, respectively with excellent geometry (Table 1). The final model contained residues 13 to 350 for the C-subunit and residues 90 to 379 for the R-subunit. The final model was evaluated using PROCHECK (Table 1) (Laskowski et al., 1993). Water molecules were incorporated using warp (Murshudov et al., 1997) and manually verified. The coordinates have been deposited in the Protein Data Bank under the accession code 2QCS. All figures were made using PyMol (DeLano Scientific)

2.3.6 cAMP Activation of PKA by Fluorescence Polarization

A new fluorescence polarization assay developed for measuring the apparent activation constant of PKA for cAMP (EC_{50}) and was done in parallel with the standard cook assay. FAM-IP20 used in this study was synthesized as described (Saldanha et al., 2006). Holoenzyme was formed *in situ* by incubating 7 nM C-subunit and 8.4 nM R-subunit mutants for 20 minutes in 25 mM HEPES (pH 7.0), 75 mM KCl, 10 mM $MgCl_2$, 2 mM ATP, 2 mM DTT, 0.005% Triton-X. 1.5 nM of FAM-IP20 was then added and incubated for an additional 10 mins. 75μl of this holoenzyme solution was aliquoted into each well in a 384-well solid black Fluotrac-200 plate (Greiner, part no. 781076). In all

cases, 2-fold dilutions of cAMP ranging from 4 to 4096 nM were added to each well and incubated for 60 minutes at 25°C. The assay was performed using a GeniosPro microplate reader (Tecan, Research Triangle Park, NC) where fluorescence polarization readings were with 485 nm excitation (20 nm bandpass) and 535 nm emission (20 nm bandpass) filters. Data were analyzed using Prism 4 software (GraphPad, San Diego, CA). Each protein was tested in quadruplicates.

2.3.7 Holoenzyme Formation Assay

C-subunit (10 nM) was incubated with varying concentrations of R-subunit mutants (0-75 nM) at 25°C in the assay mix according to Cook et. al. (Cook et al., 1982). Reaction mix (155μl) was aliquoted into each well of a 96-well clear bottom untreated Costar plate (Corning, cat no. 3631) using multichannel pipettes. The reaction was initiated by addition of 200μM Kemptide and depletion of NADH was monitored for 2 minutes at 340 nm in a GeniosPro microplate reader (Tecan, Research Triangle Park, NC).

2.3.8 cAMP Activation of PKA using a Catalytic Coupled Assay

All PKA activity assays were performed using a modified protocol of the spectrophotometric method described by Cook et al (Cook et al., 1982). Briefly, holoenzyme was formed *in situ* by incubating 10 nM C-subunit and 12 nM R-subunit mutants for 20 minutes in 25 mM HEPES (pH 7.0), 75 mM KCl, 10 mM $MgCl_2$, 1 mM ATP, 1 mM phosphoenolpyruvate, 15 units/ml lactate dehydrogenase, 7 u/ml pyruvate kinase, and 0.2 mM NADH. 145μl of holoenzyme solution was aliquoted into each well

in a 96-well clear bottom untreated Costar plates (Corning, cat no. 3631) using multichannel pipettes. 2-fold dilutions of cAMP ranging from 4 to 4096 nM were added to each well and incubated for 10 minutes at 25°C. The reaction was initiated by addition of 0.2 mM Kemptide. The activity of free C-subunit was followed spectrophotometrically by monitoring continuous decrease in absorbance at 340 nm due to oxidation of NADH using a GeniosPro microplate reader (Tecan, Research Triangle Park, NC). Data were fit with Prism 4 software (GraphPad, San Diego, CA) to determine the apparent activation constants (EC_{50}). Each data point was measured in quadruplicate.

2.3. Results and Discussion

2.4.1 Rationale for crystallization of the RIα(91-379:R333K) mutant

In an effort to define the unique dynamic behavior of the RIα(91-379) heterodimer compared to RIIα and RIIβ heterodimers, we generated two mutants in RIα that abolished high affinity binding of cAMP in each domain. In these mutants, the essential arginine in the phosphate binding cassette was replaced with lysine, R209K for Domain A and R333K for Domain B. Small angle X-ray scattering showed significant differences between the wild-type, R209K, and R333K heterodimers (see Chapter 3). Since our previous attempts to crystallize the wild-type heterodimer were unsuccessful, we set up all three complexes for crystallization. Although the wild type construct and a comparable mutation in Domain A were set up in parallel for crystallization, the R333K mutant was the only one to yield well-diffracting crystals. We are continuing our small angle X-ray scattering analysis to more comprehensively define the different dynamic features of these three proteins and to elucidate its functional importance.

2.4.2 Structural Overview of the RIα(91-379):C Complex

The holoenzyme crystal structure of a mutant RIα(91-379:R333K) in complex with the C-subunit, AMP-PNP, and two Mn^{2+} ions was solved to 2.3 Å resolution using the RIα(91-244):C complex as a molecular replacement probe (Kim et al., 2005). We attempted to crystallize three deletion mutants of RIα (RIα(91-379), RIα(91-379:R209K), and RIα(91-379:R333K)) in complex with the C-subunit, but only the holoenzyme formed with RIα(91-379:R333K) (subsequently referred to as RIα*) produced crystals that diffracted. The RIα*:C structure was crystallized in a $P3_221$ space group with 73% solvent and shows minimum contact between symmetrically related molecules (Table 1). The surface area on the catalytic subunit that is masked by binding of RIα is approximately 3800 $Å^2$ (Figure 7). As with the previous RIα(91-244) holoenzyme structure, the C-subunit adopts a closed conformation with its active site bound to AMP-PNP, two Mn^{2+} ions, and the inhibitor site of the R-subunit. The previous RIα(91-244):C structure showed major reorganization of Domain A upon binding to the C-subunit. Our new holoenzyme structure defines the full extent of the conformational change in the R-subunit that must occur to accommodate the C-subunit. As RIα adopts an extended dumbbell shape that complements the large lobe of the C-subunit, the two cAMP-binding domains become uncoupled. The largest binding interface lies between the C-subunit and Domain A of the R-subunit, while Domain B extends the interaction surface and makes a novel contact to the αH-αI loop in the C-subunit.

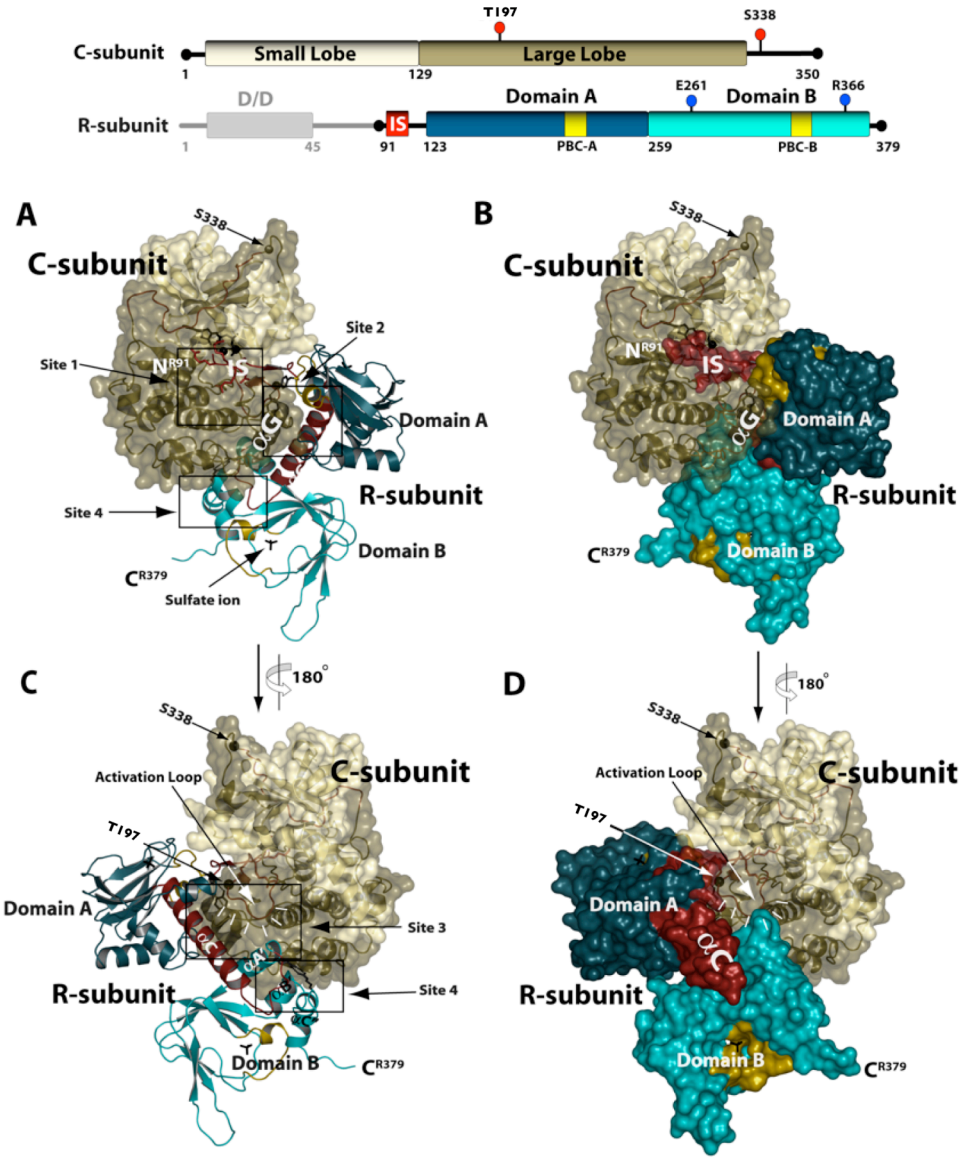

Figure 7. Overview of the PKA RIα(91-379):C Holoenzyme Complex.

Top, Domain organization of the catalytic and regulatory subunits. The two red spheres indicate phosphorylation sites Thr197^{C} and Ser338^{C} in the catalytic subunit. (A) View showing the inhibitor sequence of the regulatory subunit bound to the active site cleft of the catalytic subunit. Boxed regions show interaction sites between the R- and C-subunits at the active site (site 1, left) and the G helix (site 2, right). (C) 180° rotation of the view shown in A. Boxed regions show the interaction site at the activation loop (site 3, top) and H and I loop (site 4, bottom). (B, D) Surface representation of both subunits are in the same view as in A and C, respectively. The catalytic subunit is bound to AMP-PNP (black sticks) and Mn^{2+} (blue spheres) with the small lobe (white) and the large lobe (tan) in surface rendering. The regulatory subunit is shown as a cartoon representation in figures 1A,C with Domain A in dark teal, Domain B in cyan, the PBC in yellow, and the B/C helix and inhibitor site in red.

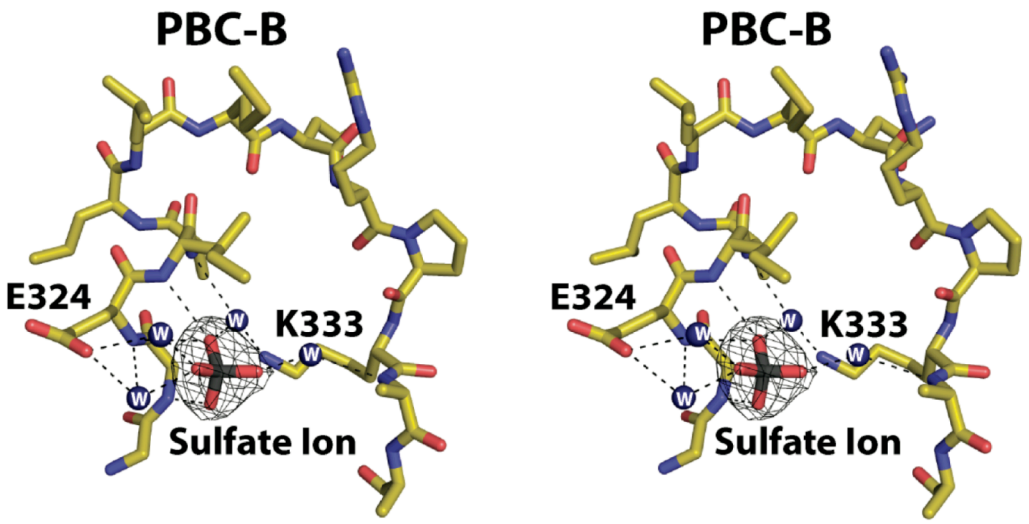

Figure 8. A stereoview of the phosphate binding cassette in Domain B.

A sulfate ion shown with $2F_o$-F_c electron density contoured at 3σ binds to the cyclic phosphate binding site similar to cAMP. In contrast to Domain A, the phosphate binding cassette in Domain B is more exposed and thus primed for binding cAMP.

Table 1. Data and refinement statistics of the RIα$_{AB}$:C:AMPPNP:Mn^{2+} complex.

Data Set	APS Beamline 19ID
Space group	$P3_221$
Cell constants (Å)	a=b=125.8, c=140.9
Number of crystals	1
Wavelength (Å)	0.97934
D_{min} (Å)	2.2
Mosaicity (°)	0.2
Unique reflections	62748
Average redundancy	6.5
R_{sym}[$] (%)	8.7 (49.4)[§]
Completeness (%)	95.3 (69.8)[§]
<I>/<%>	19.2 (1.8)[§]
Resolution range for refinement (Å)	20–2.2
Total reflections used	59193
Number of protein atoms	5023
Number of water molecules	423
Rmsd bond lengths (Å)	0.011
Rmsd bond angles (°)	1.36
R_{work}[‖] (%)	19.2
R_{free}[¶] (%)	21.2
Average *B* factor (Å^2)	43.9

[$]$R_{sym}$ = &$_h$&$_i$|$I(h)$ - $I(h)_i$|I&$_h$&$_i$ $I(h)_i$, where $I(h)$ is the mean intensity after rejections.

[§]Numbers in parentheses correspond to the highest resolution shell of data, which were 2.28 to 2.2 Å.

[‖]R_{work} = &$_h$||$F_{obs}(h)$| -|$F_{calc}(h)$||I&$_h$|$F_{obs}(h)$|; no I/%cutoff was used during refinement.

[¶]5.0% of the truncated data set (3545 refelections) was excluded from refinement to calculate R_{free}.

2.4.3 Domain B of the Regulatory Subunit Provides an Additional Docking Surface for the Activation Loop and Presents a Novel Interaction Site on the Catalytic Subunit

As defined previously (Kim et al., 2005), an extended surface on the C-subunit is utilized for binding to the R-subunit: i) site 1, the predominantly acidic active site (Figure 9); ii) site 2, the substrate binding loop (P+1 loop, residues 198-205) and the hydrophobic αG helix (Figure 10); and iii) site 3, the activation loop (Figure 11b). The new RIα*:C structure reveals expanded interaction surfaces at sites 1 and 3 and defines for the first time a fourth site, the αH-αI loop, that interacts uniquely with Domain B in the R-subunit (Figure 11c), supporting previous hydrogen/deuterium exchange data (Anand et al., 2003). We first discuss new features of site 3 that are revealed by the structure and then describe site 4. Additional information regarding sites 1 and 2 are found in the Supplementary Material.

At site 3, separation of the RIα cAMP-binding domains provides an additional docking surface that fully encloses the activation loop of the C-subunit within the R:C interface (Figure 11a,b). The previous RIα(91-244):C complex lacking Domain B showed a dramatic extension of the αB/C helix in Domain A, which docked against the activation loop and masked the region extending from the P+1 loop to the activation loop (Kim et al., 2005). In the RIα*:C structure, the activation loop is now completely enclosed within the R/C interface and is sandwiched between the two cAMP-binding domains. The additional docking surface arises from complete extension of the αB/C helix from residues 226 to 250 through to the αA helix in Domain B. The entire extension was not observed in the previous structure since the RIα construct terminated at residue 244.

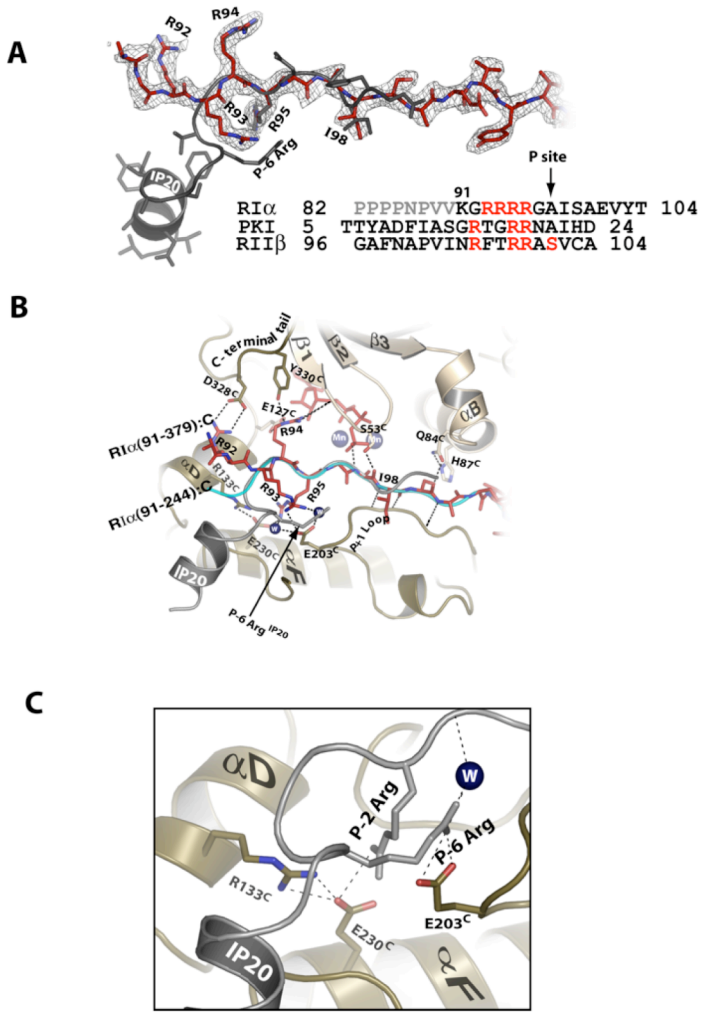

Figure 9. Peptide Recognition Site.

(A) Overlay of the regulatory subunit and the PKI at the inhibitor site. The inhibitor sequence of RIα is shown with $2F_o$-F_c electron density contoured at 1σ. (B) Overlay of three structures (RIα(91-379):C in red, RIα(91-244):C in cyan, and IP20:C in gray) at the activation site. The extended peptide recognition site for PKA is defined in novel ways for the two PKA inhibitors, RI and PKI. Both inhibitors require ATP and two Mg^{2+} ions to form a high affinity complex (<1 nM). The P-2 Arg (through its interactions with $Tyr330^C$) engages the C-terminal tail thereby locking the enzyme into a closed conformation. In this structure $Arg92^R$ also interacts with $Asp328^C$ and further locks the C-terminal tail into place. The P-5 arginine, $Arg93^R$, surprisingly reaches over to $Glu203^C$ in the P+1 loop. (C) P-6 arginine in the IP20:C complex. $Glu203^C$ provides a docking site for the P-6 argnine in PKI similarly to $Arg93^R$ of RI(91-379) although the two arginines approach Glu203 from different directions.

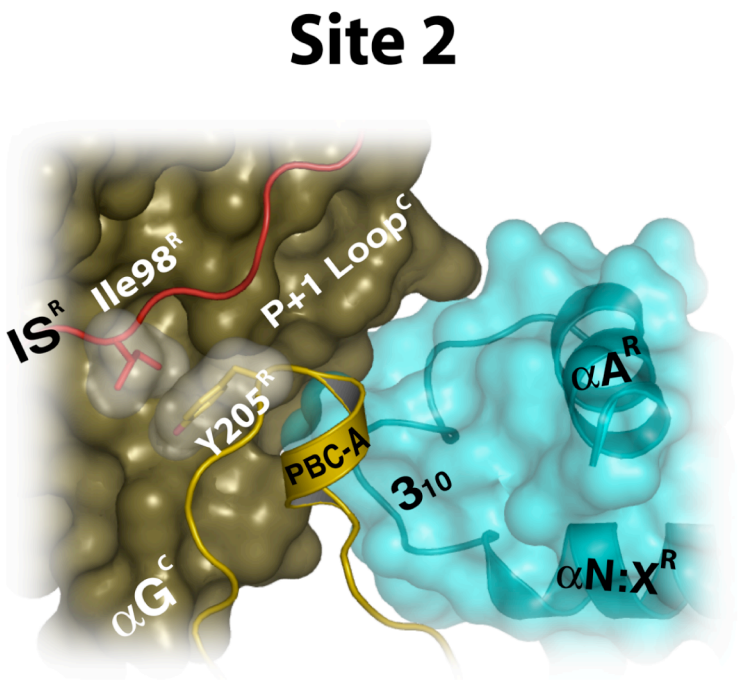

Figure 10. The αG helix and P+1 loop of the catalytic subunit bound to the phosphate binding cassette (yellow) and N3A motif (cyan) of the regulatory subunit.

The αfG helix and P+1 loop forms a large hydrophobic surface that interacts with a complementary surface on the regulatory subunit, which consists of hydrophobic residues in the phosphate binding cassette in Domain A and the 3_{10} loop. The highlight of interactions at this site is a hydrogen bond formed between two tyrosine residues, $Tyr247^C$ and $Tyr205^R$, that directly links the two subunits.

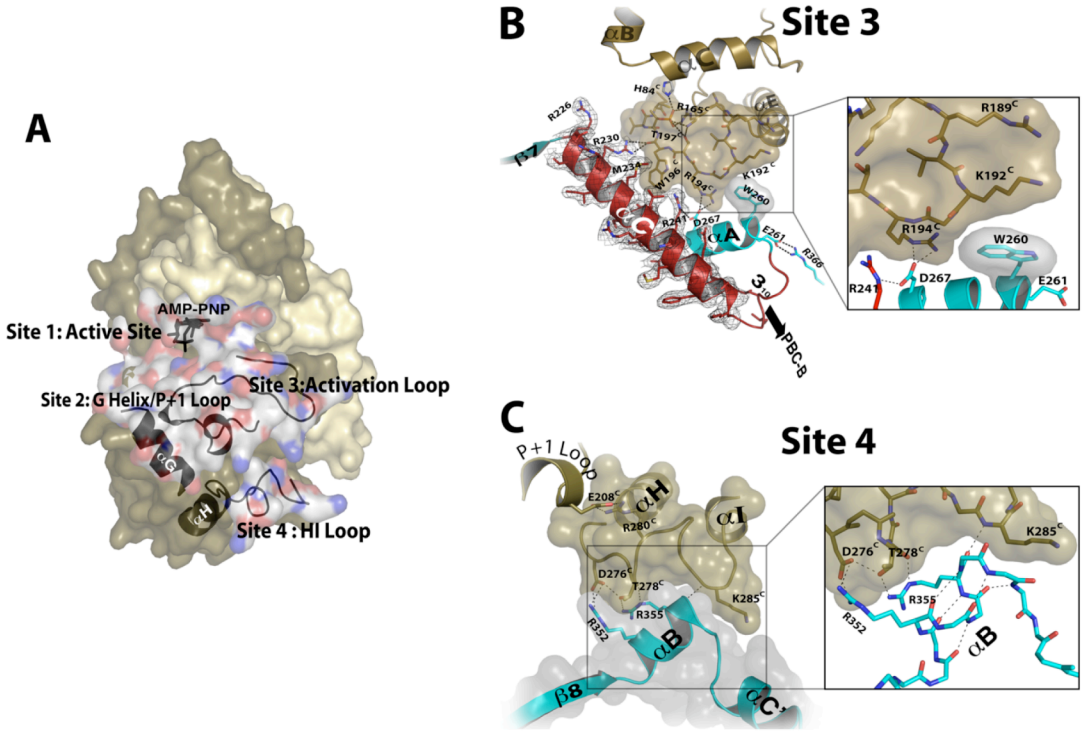

Figure 11. The Regulatory Subunit Provides a Large Docking Surface that Shields the Catalytic Machinery of the C-subunit.

(A) Individual sites are mapped on the catalytic subunit with specific binding regions rendered in cartoon. (B) Site 3: The activation loop in the catalytic subunit (tan) interacts with the B/C helix, 3_{10} loop (red) and A helix (cyan). This region of the regulatory subunit is stabilized by a key salt bridge between Arg241^{R} (in the C helix of Domain A) and Asp267^{R} (in the A helix of Domain B) and is maintained in both the holoenzyme and cAMP-bound conformations. Asp267^{R} also interacts with Arg194^{C}, in effect cementing Domains A and B of the regulatory subunit to the catalytic subunit activation loop. Right, detailed interactions of the Trp260^{R}:Lys285^{C}:Asn283^{C} hydrophobic stack and Arg241^{R}:Asp267^{R}:Arg194^{C} interaction. (C) Site 4: The novel site between the αB helix of Domain B and the αH-I loop of the catalytic subunit (tan), which contains a segment unique to AGC kinases. The right inset shows zoomed view of hydrogen bond network between the αB helix in Domain B (sticks) and the catalytic subunit.

Strikingly, the residue used to cap the cAMP-binding site in Domain A, Trp260^{R}, packs against the N-terminal tip of the activation loop (Figure 11b, right). As described later, binding of the C-subunit causes Trp260^{R} to move nearly 30 Å away from the phosphate binding cassette in Domain A.

In addition to the first three sites that surround the C-subunit active site, the RIα*:C structure reveals a fourth novel distal site formed exclusively between Domain B of the R-subunit and the large lobe of the C-subunit. Site 4 consists of the αH-αI loop on the large lobe of the C-subunit (residues 276-286) that docks to the αB helix of the R-subunit (Figure 11a,c). A short segment within the αH-αI loop (residues 282-286) was found to be an AGC kinase-specific insert (Figure 27) (Kannan et al., 2007a) and mutagenesis studies suggest that this is an allosteric site that is coupled to peptide recognition (Deminoff et al., 2006). Furthermore, Arg355^{R} in the R-subunit αB helix forms multiple interactions with the catalytic subunit and participation of this residue is noteworthy as it is conserved in both RI and RII isoforms and is likely to be a hotspot for protein:protein interactions for cAMP-binding proteins in general.

2.4.4 Major Conformational Changes Occur in RIα Upon Binding the Catalytic Subunit

Global changes

The RIa*:C structure containing both cAMP-binding domains shows the major conformational change in the R-subunit that must occur to enable binding to the catalytic subunit. In the cAMP bound conformation, the two cAMP-binding domains, joined by the kinked αB/C helix in Domain A, form a compact globular structure where the two

domains pack together with a large interface (Su et al., 1995a) (Figure 12a). The αB/C helix is anchored to Domain B through hydrophobic interactions and is directly linked to Trp260^{R}, the capping residue that stacks with cAMP in Domain A. However, upon binding to the C-subunit, the two domains separate and the R-subunit adopts an extended dumbbell shape. The center of Domain B moves over 60 Å away from its position in the cAMP bound structure due to extension of the αB/C helix. The interface shared between the domains in the cAMP bound structure is replaced by the C-subunit in the holoenzyme. This large domain movement is rarely seen in proteins and arises from rotations at three pivot points along the αB/C helix (Figure 12b).

Each cAMP-binding domain is comprised of two subdomains: a non-contiguous α-helical subdomain and a contiguous β-sheet subdomain that contains the phosphate binding cassette. Superposition of the two conformational states of RIα (holoenzyme and cAMP-bound) shows that the conformation of the β-sandwich, with the exception of the phosphate binding cassette, does not change (Figure 13a). Removal of cAMP from the cAMP-bound complex creates a more dynamic structure, but does not stabilize the open and extended conformation of the αB/C helix (Gullingsrud et al., 2006; Vigil et al., 2006b). Instead, the C-subunit induces the major conformational change that RIα undergoes, and these changes are associated primarily with the helical regions (Figure 13b,c). For each domain in the R-subunit this includes, in addition to the major changes in the αB/C helices discussed above, reorganization of the phosphate binding cassette and a conserved structural element that bridges the αX:N and αA helices in Domain A (residues 123-150) and the αC helix of Domain A with the αA helix of Domain B (residues 245-267). We define this structural element as the N3A motif (Figure 14 and

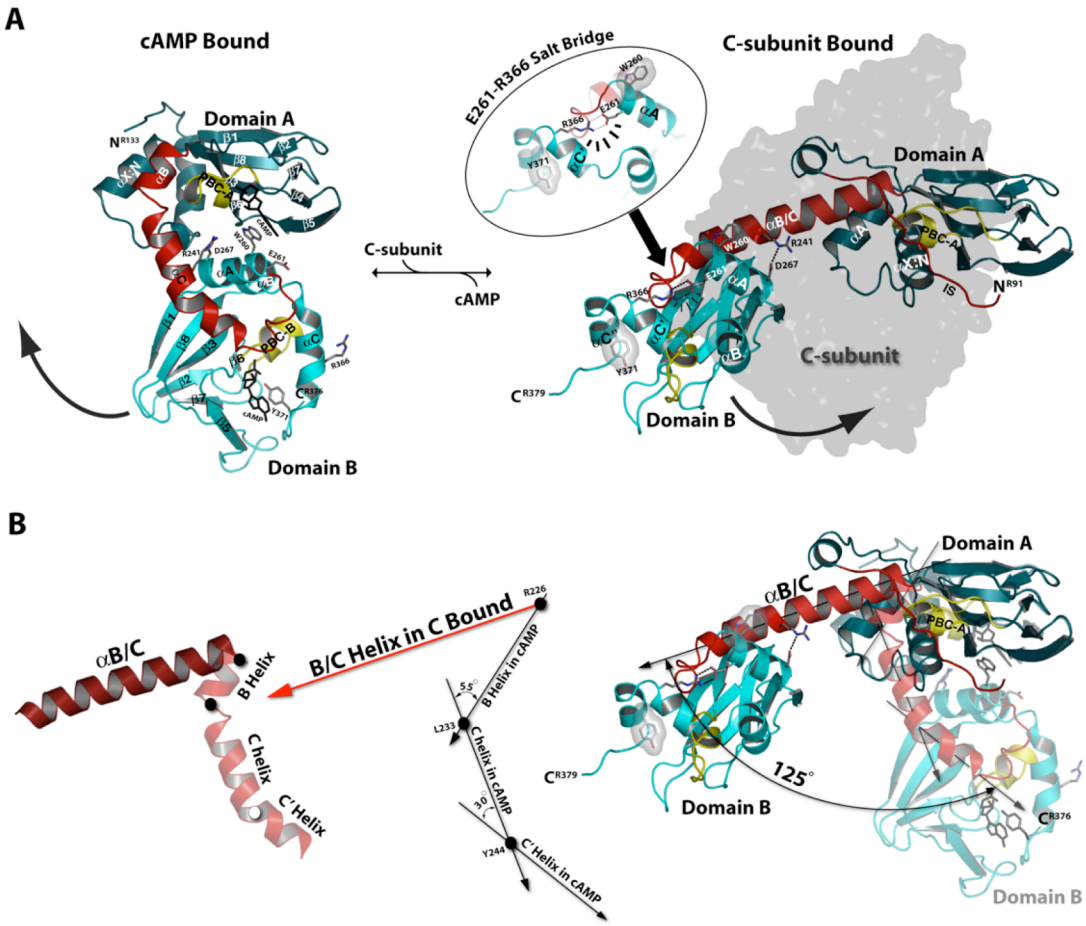

Figure 12. RIα Undergoes Dramatic Conformational Changes Upon Binding the Catalytic Subunit.

(A) The regulatory subunit bound to cAMP is shown on the left (PDB code 1RGS, in black) and bound to the C-subunit (in gray) on the right. The two hydrophobic capping residues important for cAMP-binding to the regulatory subunit, Trp260^{R} and Tyr371^{R}, are shown with a VDW surface. (B) Left, the global extension of the regulatory subunit is described by rotations at three pivot points (Arg226, Gly235, and Tyr244) located on the αB/C helix. Right, structural alignment of Domain A in the cAMP and catalytic subunit-bound conformations.

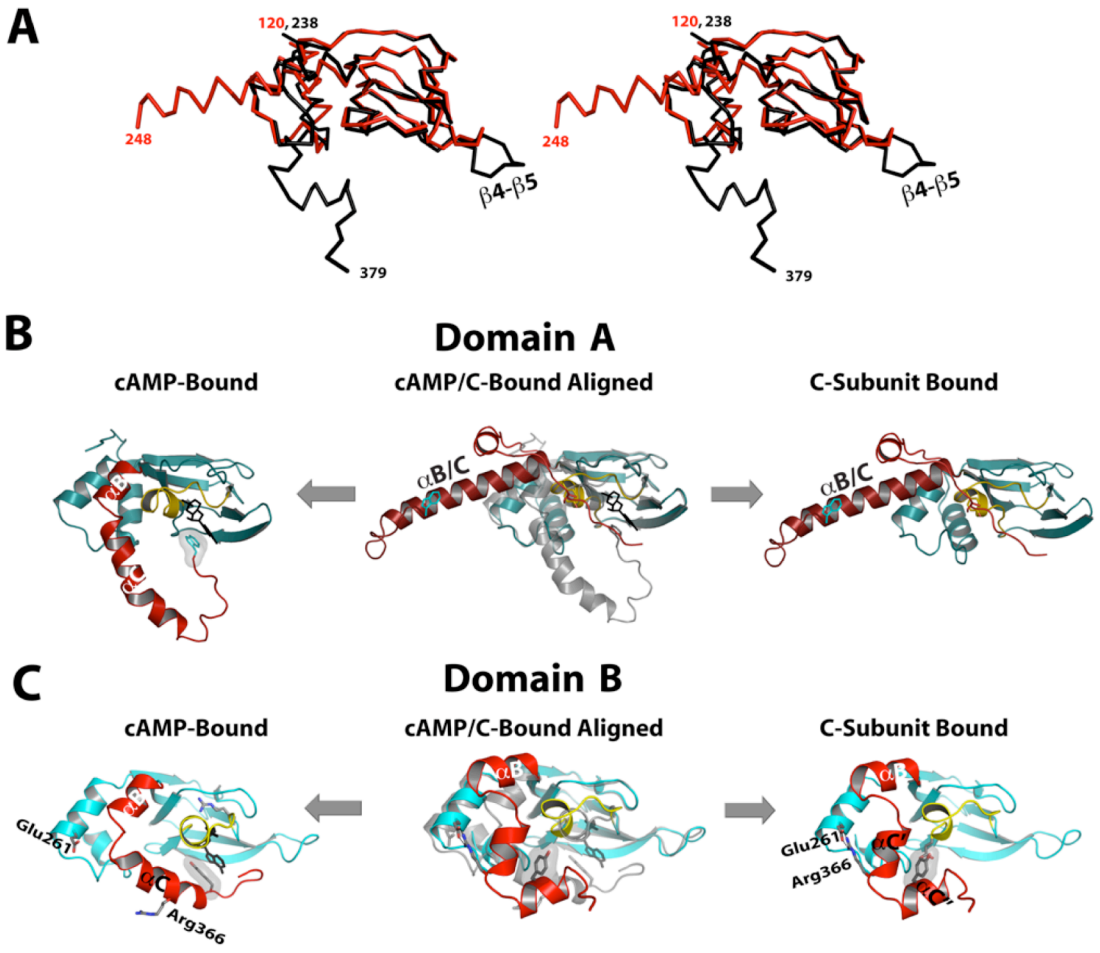

Figure 13. Conformational Changes in the Regulatory Subunit is a Result of Structural Rearrangements in the Helical Regions.

(A) Structural alignment of the regulatory subunit cAMP-binding domains in the holoenzyme conformation. Domain A is shown in red and Domain B in black. 92 equivalent C atoms from the ß-barrel region overlap with an r.m.s.d. of 1.1 Å, excluding a short insert between 4-5. (B, C) Comparisons between the two cAMP-binding domains in the cAMP and catalytic subunit-bound conformations. The cAMP-bound conformation is shown on the left and the holoenzyme conformation on the right. The two conformations are superimposed in the center. The αB/C helix is shown in red and the PBC in yellow. The cAMP bound conformation is shown in grey.

15). A major consequence of the conformational changes in the R-subunit, induced by binding of the catalytic subunit, is that both cAMP-binding sites are essentially destroyed because the phosphate binding pocket is separated from the adenine binding pocket.

Local changes in Domain A

Figure 16 shows the region where the helical motifs (the αB/C helix, phosphate binding cassette, and N3A motif) converge in the holoenzyme structure. For Domain A in the cAMP-bound state, the αB/C helix separates the surface formed between the phosphate binding cassette and N3A motif (Figure 16a, left). In the holoenzyme conformation, recruitment of the αB/C helix to the R/C interface, and the associated conformational changes, allow the remaining helices to reposition (Figure 16a, right). Essentially, the phosphate binding cassette and N3A motif move closer together to create a holoenzyme-specific hydrophobic surface in Domain A that then docks onto the hydrophobic surface on the C-subunit.

Local changes in Domain B.

The hydrophobic rearrangement associated with the helical regions in Domain B is analogous to Domain A, except that in Domain A the phosphate binding cassette and the extended αB/C helix is an integral part of the R/C interface (Figure 16b). In contrast to Domain A, the phosphate binding cassette in Domain B is solvent exposed due to the hydrophobic rearrangement and the docking of αB helix in Domain B to the C-subunit (Figure 7). The highly accessible cAMP binding site in Domain B observed in our structure explains kinetic studies showing Domain B as the fast association site for cAMP in holoenzyme (Ogreid and Doskeland, 1981a).

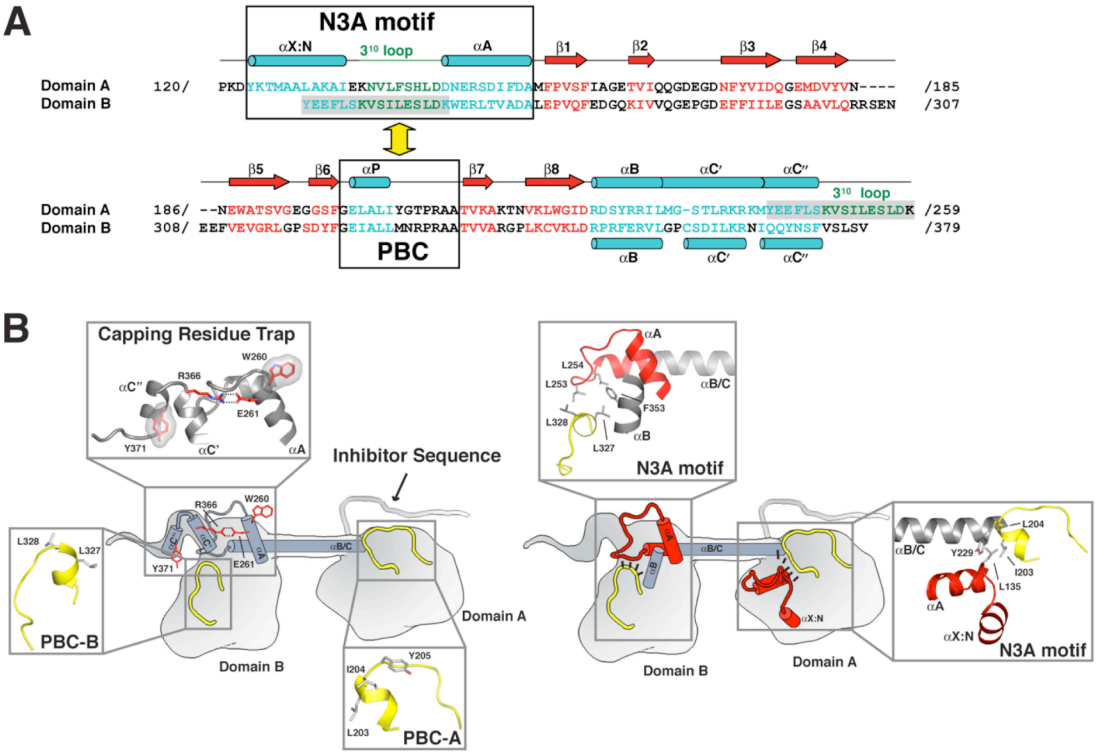

Figure 14. Schematic Diagram of the Structural Motifs in the Regulatory Subunit.

(A) Sequence alignment of Domains A and B. Residues in the grey boxes belong to Domain A, but are also aligned as part of the N3A motif of Domain B. (B) Cartoon schematic of the major structural elements of the regulatory subunit in the holoenzyme conformation.

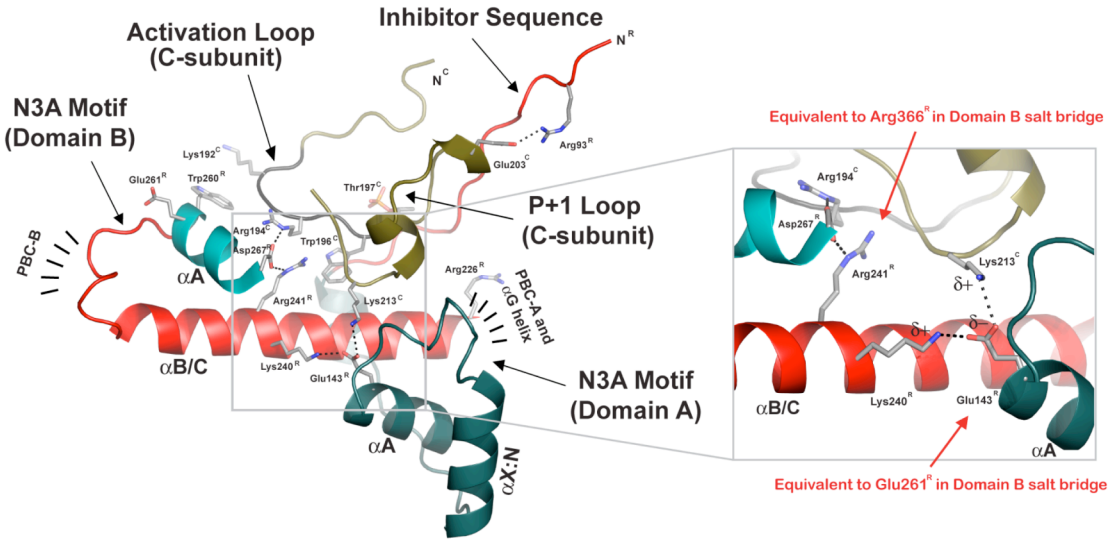

Figure 15. The global organization of the αB/C helix relative to the two N3A motifs in RIα and the activation loop and P+1 loop in the C-subunit.

Several electrostatic interactions in Domain A resemble those in Domain B as a consequence of forming the holoenzyme. First, Glu143^{R} in the A helix of Domain A is analogous to Glu261^{R} in Domain B. Previous mutational studies showed that Glu143^{R} was involved in the R/C interface (Gibson et al., 1997) and is now confirmed in the holoenzyme structure. Glu143^{R} forms key electrostatic interactions that help stabilize the holoenzyme conformation – one with the αB/C helix (Lys240^{R}) and the other with the C-subunit (Lys213^{c}). Second, Arg241^{R} in Domain A is analogous to Arg366^{R} in Domain B. In the holoenzyme, Arg241^{R} indirectly participates in the R/C interface through interaction of Asp267^{R} to Arg194^{c}. In the cAMP-bound state, Arg241^{R} contributes to the binding of cAMP by bringing the αB helix in contact with the phosphate binding cassette through binding with Glu200^{R}.

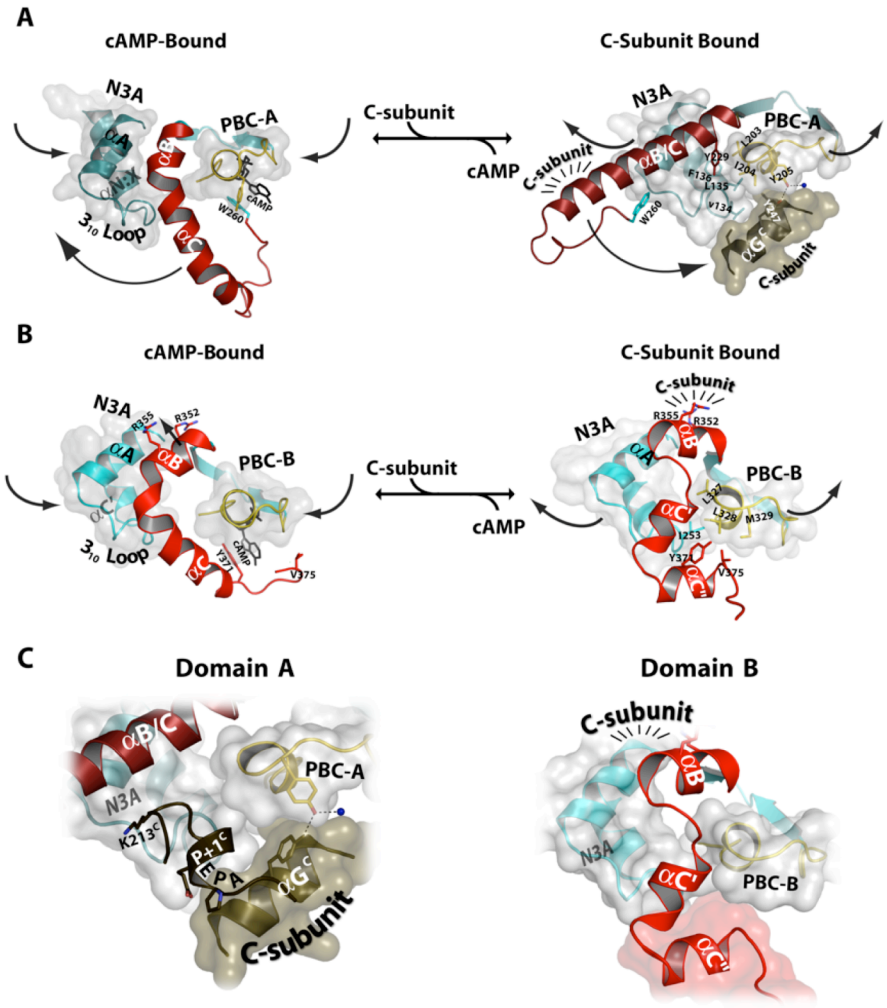

Figure 16. Binding of the Catalytic Subunit Reorganizes Two Regulatory Subunit Structural Motifs (the N3A motif and the Phosphate Binding Cassette) to Create a Contiguous Hydrophobic Interface.

(A) Comparison of the helical regions in Domain A between the cAMP (left) and catalytic subunit bound (right) conformations. Movement of the helical regions is mediated by hydrophobic rearrangement of the hinge residues in the phosphate binding cassette (Ile203^{R} and Leu204^{R}), the B helix (Tyr229^{R}), and the 3_{10} loop (Leu135^{R}). (B) Comparison of Domain B in the cAMP and catalytic subunit bound conformations, highlighting the C-terminal tail (red). In Domain B, the helical rearrangements are similar to Domain A where residues in the phosphate binding cassette (Leu327^{R} and Leu328^{R}), 3_{10} loop (Ile253^{R} and Leu254^{R}), and B helix (Phe353^{R}) come together. (C) Comparison between Domains A and B in the holoenzyme conformation. In Domain A, the N3A motif (residues 123-150) and PBC come together and serve as a docking surface for the P+1 loop (in black) and the G (in tan) of the catalytic subunit. In Domain B, a similar hydrophobic interface is formed between the N3A motif (residues 245-367) and PBC, however, the C-terminal tail (B, C', and C" helices) lies on top of the hydrophobic interface.

Comparison between Domains A and B show that the αB and αC helices do not extend in Domain B as they do in Domain A. Instead, they remain as distinct helices and form a novel helix-turn-helix motif that covers the hydrophobic surface (Figure 16c). This helix-turn-helix motif provides the hydrophobic lid (from $Tyr371^{R}$) for the phosphate binding cassette in the cAMP-bound state.

2.4.5 αB/αC helix flexibility is important for PKA activation by cAMP

In the cAMP bound conformation of the R-subunit, a glycine (G235) is located at the first pivot point in the αB/αC helix. To assess the importance of αB/αC helix flexibility towards cAMP-induced PKA activity, three mutations were made: G235A, G235L, and G235P. By mutating the glycine to either alanine or leucine we had hoped to lock the protein into the extended holoenzyme conformation. However, our results show that these mutations do not have any effect on cAMP sensitivity towards PKA activity compared to wild-type (Figure 17). We predicted that the G235P would reduce the flexibility and prevent the extension of the helix that is essential for binding to the C-subunit. We have shown that this mutant is a poor inhibitor of the catalytic subunit. Based on gel filtration, the G235P mutant and the catalytic subunit form a complex, however, thorough biochemical characterization of the binding interaction is necessary. Furthermore, previous work has shown that the apparent inhibitory constants (Ki_{app}) for a deletion mutant of RIα(94-235) containing only Domain A to this glycine residue is ~1000-fold higher than the deletion mutant containing both Domains A and B (Huang and Taylor, 1998). These findings suggest that the extension of the αB/C helix upon

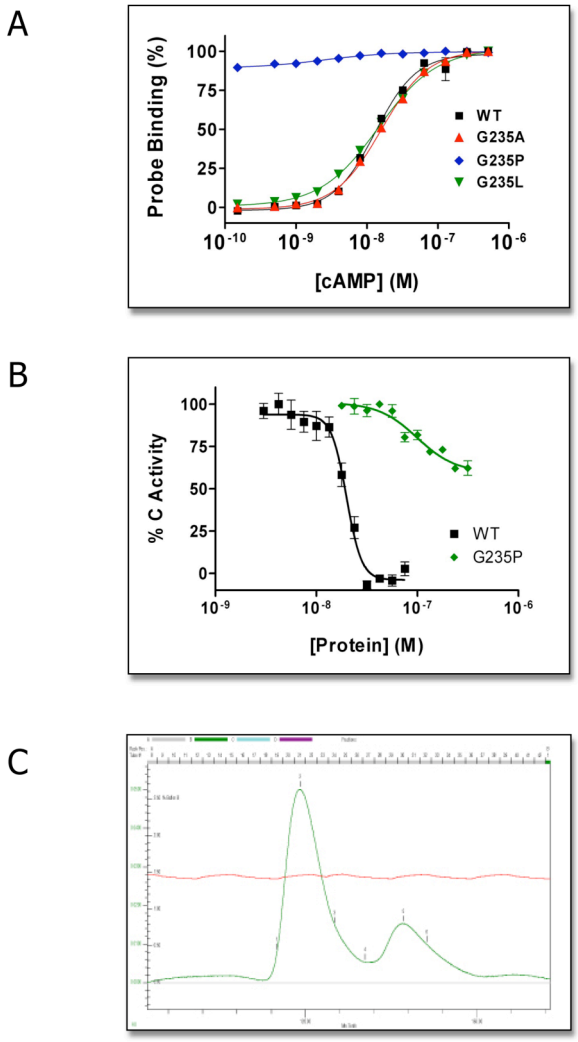

Figure 17. Effects of Gly235 mutants on inhibition and cAMP activation. (A) cAMP activation of Gly235 mutants (FP assay). (B) C-subunit inhibition with the RIα G235P mutant (Cook coupled assay). (C) Gel filtration purification of RIαG235P:C heterodimers. The first peak is solely C-subunit and the second peak is solely RIαG235P protein.

complex formation contributes to the high affinity interaction between the regulatory and catalytic subunits.

2.4.6 Residues Required for Stabilizing cAMP in the Regulatory Subunit are Trapped at a Remote Site in the Holoenzyme Structure

The extended conformation of RIα in the holoenzyme not only partitions the two cAMP-binding domains, but also separates many of the key residues that anchor cAMP in the phosphate binding cassette, effectively destroying both cAMP-binding sites. A common feature for cAMP-binding proteins is hydrophobic capping of the cAMP adenine ring (Berman et al., 2005). For CAP, HCN, and Domain B of RIα, the hydrophobic capping residue is located in the αC helix of the cAMP-binding domain. For Domain A of RIα, the capping residue is $Trp260^R$, located at the beginning of the αA helix of Domain B. Thus, for RIα both capping residues ($Trp260^R$ for Domain A and $Tyr371^R$ for Domain B) are in Domain B (Figure 12a).

In the holoenzyme structure, the capping residues are far removed from their respective phosphate binding cassettes. $Trp260^R$ moves over 30 Å and docks onto the C-subunit activation loop (Figure 11b). $Trp260^R$, the only residue from Domain B that binds directly to cAMP in Domain A, is important for communication between the two cAMP-binding domains (Canaves et al., 2000). As illustrated in Figure 16b, $Tyr371^R$ in the cAMP-bound state has a dual role – aromatic stacking with the adenine base and hydrogen bonding to the conserved $Glu324^R$ in the phosphate binding cassette, which binds to the 2'OH of the ribose ring of cAMP. Mutational studies confirm the importance of this residue for cAMP binding (Bubis et al., 1988a; Bubis et al., 1988b; Kapphahn and

Shabb, 1997). In contrast, in the holoenzyme conformation, Tyr371^R is 13 Å away from the phosphate binding cassette. Thus, binding of the catalytic subunit to RIα prohibits many interactions that are needed to stabilize the cAMP-bound structure.

2.4.7 The Glu261-Arg366 Salt Bridge Functions to Trap the Two cAMP Capping Residues.

The holoenzyme structure reveals for the first time a salt bridge formed between Glu261^R and Arg366^R. These two residues not only position the RIα C-terminal tail, but also sequester the two adenine capping residues (Trp260^R and Tyr371^R) away from their cAMP binding sites. In the cAMP-bound conformation, both of these highly conserved salt bridge residues are 15 Å apart where Arg366^R is exposed to solvent and Glu261^R is near the domain interface. It is only in the holoenzyme conformation that their true function can be appreciated. In effect, the salt bridge traps both hydrophobic residues far away from the cAMP-binding sites and forms a communication path that links the two R-subunit cAMP-binding domains. Our holoenzyme structure provides for the first time a molecular model to explain the ordered and highly cooperative pathway for the activation of the type I holoenzyme. The biochemical details for this model were first proposed based on kinetic arguments (Ogreid and Doskeland, 1981a, b) and then confirmed with mutants of the essential arginine residues in the cAMP-binding pocket (Arg209^R for Domain A and Arg333^R in Domain B) (Herberg et al., 1996b).

To test this model and the contribution of the electrostatic trapping of the capping residues, we engineered four RIα(91-379) mutants (W260A, Y371A, E261A, and R366A) and measured the effect of these mutations on PKA activation. For each mutant, the

inhibition of the C-subunit was not affected (Figure 18). In contrast, there were differences in cAMP-mediated activation of PKA, as measured by a catalytic coupled assay (Cook et al., 1982) and a fluorescence polarization binding assay (Saldanha et al., 2006). Holoenzyme complexes formed with mutants in RIα that contain a substitution of either Trp260^R or Tyr371^R with alanine were less sensitive to cAMP compared to the RIα(91-379) holoenzyme. RIα(91-379:W260A) requires 4.6-fold more cAMP while RIα(91-379:Y371A) requires 9-fold more cAMP (Figure 19a and 20). The difference for the W260A mutation can be attributed to the missing hydrophobic capping abilities of the aromatic side chain. The larger difference observed for the Y371A mutation is most likely due to the absence of both the aromatic cap and hydrogen bond, which together help stabilize cAMP in Domain B.

In contrast, holoenzyme complexes formed with mutants in RIα that contain a substitution of either Glu261^R or Arg366^R with alanine were more sensitive to cAMP activation. The EC_{50} decreases from 13.5 nM for RIα(91-379) to 4.7 nM and 6.6 nM for RIα(91-379:E261A) and RIα(91-379:R366A) mutants, respectively. The differences in EC_{50} values for these salt bridge deficient mutants are likely to be greater than 3-fold since 10 nM C-subunit was used in our assays. Nevertheless, these results conclusively show that disrupting the salt bridge makes the holoenzyme more sensitive to cAMP and shifts the equilibrium towards a “more activation prone state”. Not only are Glu261^R and Arg366^R conserved in all regulatory subunit isoforms, their homologous counterparts in Domain A, Glu143^R and Arg241^R respectively, provide equally important contributions to the molecular architecture of the holoenzyme (Figure 15).

The highly cooperative interaction between the two tandem cAMP-binding domains of RIα allows the enzyme to respond rapidly to the second messenger signal

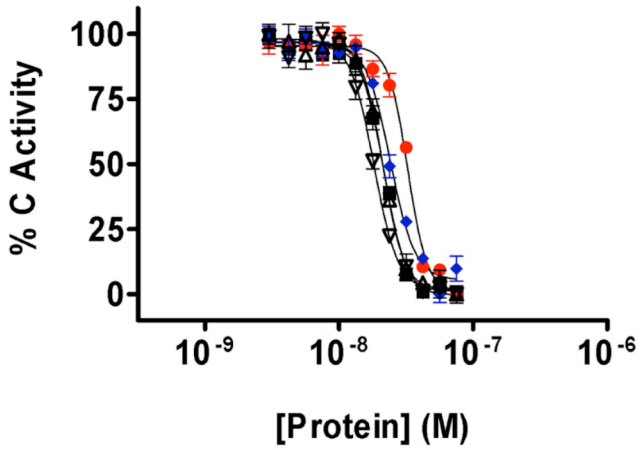

Protein	IC_{50} (nM)
RIα(91-379)	21.6 ± 0.01
RIα(91-379) E261A	32.5 ± 0.01
RIα(91-379) R366A	24.1 ± 0.01
RIα(91-379) W260A	21.3 ± 0.01
RIα(91-379) Y371A	18.2 ± 0.01

Figure 18. Association of mutant regulatory subunits with catalytic subunits measured by the catalytic Cook Coupled assay.

The table shows IC_{50} values of the four RI mutants (RI(91-379), black filled squares; RIα(91-379:E261A), red circles; RIα(91-379:R366A), blue diamonds; RIα(91-379:W260A), black open triangles; and RIα(91-379:Y371A), black open inverted triangles.

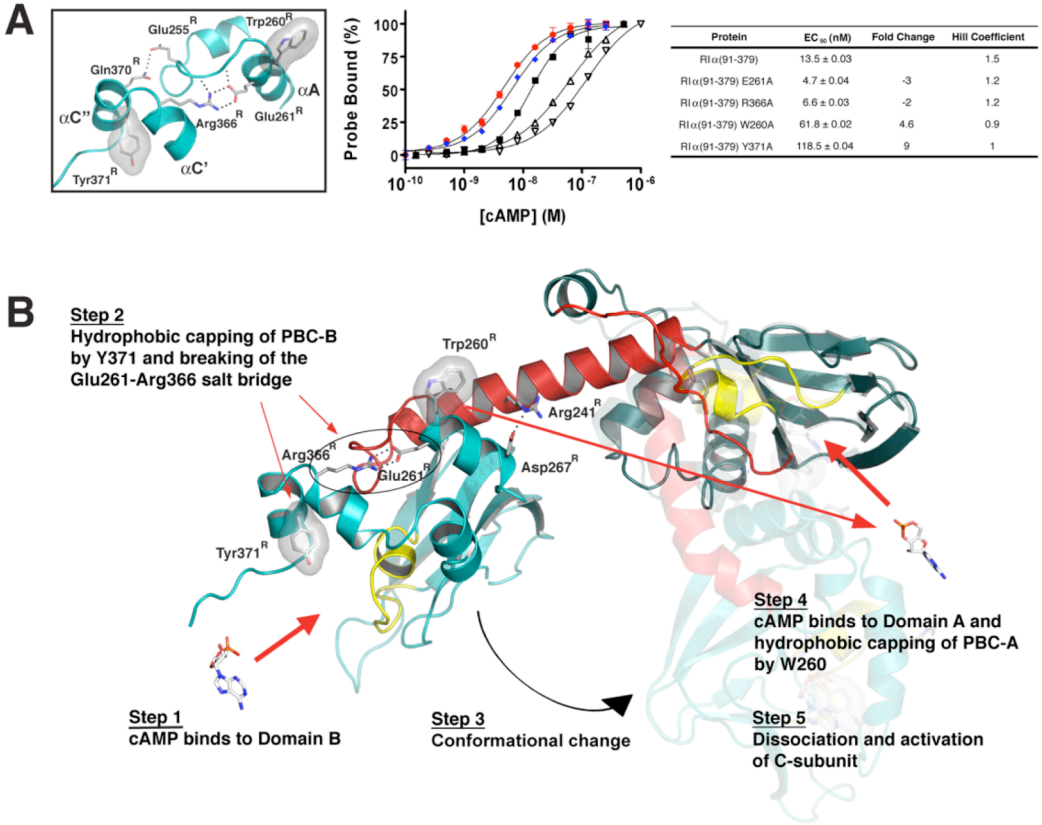

Protein	EC_{50} (nM)	Fold Change	Hill Coefficient
RIα(91-379)	13.5 ± 0.03		1.5
RIα(91-379) E261A	4.7 ± 0.04	-3	1.2
RIα(91-379) R366A	6.6 ± 0.03	-2	1.2
RIα(91-379) W260A	61.8 ± 0.02	4.6	0.9
RIα(91-379) Y371A	118.5 ± 0.04	9	1

Figure 19. A Novel RIα Electrostatic Interaction in the Holoenzyme Conformation Functions as a "Capping Residue Trap" Important for PKA Activation.

(A) *Left*, the salt bridge between Glu261^R and Arg366^R structurally couples the two hydrophobic capping residues for Domain A and Domain B, Trp260^R and Tyr371^R, respectively. *Middle*, the effect of RIα(91-379) (black), RIα(91-379:W260A) (open trianges), and RIα(91-379:Y371A) (open inverted triangles), RIα(91-379:E261A) (red circles), and RIα(91-379:R366A) (blue diamonds) on PKA activation by cAMP measured by the fluorescence polarization assay. Fold changes are given relative to RIα(91-379) data. (B) Stepwise model of PKA activation by cAMP.

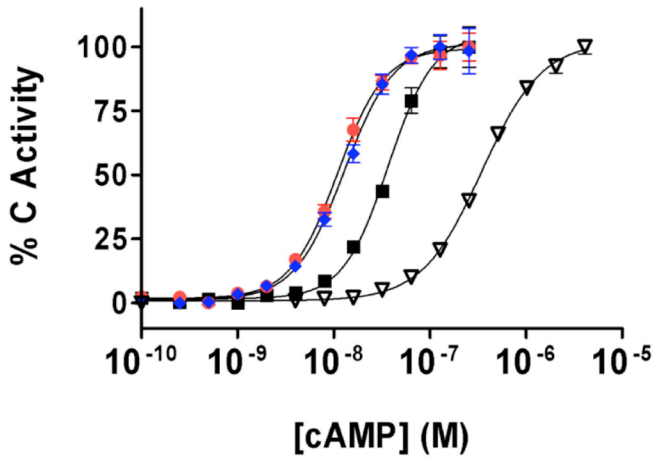

Protein	EC_{50} (nM)	Fold Change	Hill Coefficient
RIα(91-379)	36.8 ± 0.03		1.9
RIα(91-379) E261A	11.0 ± 0.02	-3	1.7
RIα(91-379) R366A	12.8 ± 0.03	-3	1.6
RIα(91-379) Y371A	347.1 ± 0.01	9.4	1.3

Figure 20. Activation of PKA with cAMP monitored by the catalytic Cook Coupled assay.

The table shows EC_{50} values for PKA activation with the four RIα mutants (RIα(91-379), black squares; RIα(91-379:E261A), red circles; RIα(91-379:R366A), blue diamonds; and RIα(91-379:Y371A), open triangles). Fold changes for the point mutants are given relative to RIα(91-379):C.

cAMP. Our data and that of others suggest that several factors contribute to this cooperative process. Comparison of the Hill coefficients in the cAMP activation data for both capping residue mutants relative to wild-type RIα suggest that these residues play an important role in the cooperative cAMP activation process. The Hill coefficients were reduced significantly from 1.5 for wild-type to 0.9, and 1 for W260A, and Y371A, respectively (Figure 19a). Mutations that remove the salt bridge between Glu261 and Arg366 also show reductions in the Hill coefficients (1.2 for both E261A and R366A), but the protein concentrations used in our assays may have limited our ability to determine true Hill coefficients since titration effects will also influence these values. Furthermore, previous studies show that Arg241^{R}, which mediates a salt bridge between Domain A (Arg241^{R}) and Domain B (Asp267^{R}) (Figure 12 and 15), not only disrupts high affinity cAMP binding, but also plays an important role in the cooperative coupling between the two domains (Symcox et al., 1994). In light of both our data and others, it is apparent that there is not just one residue that contributes to cooperativity, but that it involves a number of residues that all contribute to the activation process in a synergistic way.

2.4.8 Model of PKA Activation by cAMP

Previous biochemical data proposed an ordered and sequential pathway of cAMP binding to the Type Iα holoenzyme where cAMP must first bind to Domain B and then to Domain A (Herberg et al., 1996b). Our new structure and mutagenesis data together provides corroboration for this mechanism and allows us for the first time to propose a molecular explanation for the highly ordered pathway for activation by cAMP where Domain B serves as a “gatekeeper” for cAMP access to Domain A (Figure 19b).

- *Step1*. cAMP first binds to the phosphate binding cassette in Domain B. The phosphate binding cassette in Domain B is more accessible than in Domain A. The cAMP-binding site in Domain A is masked by the R/C interface so that Trp260^{R} and Arg241^{R}, key residues that stabilize cAMP binding, are not accessible. In fact, Trp260^{R}, the hydrophobic capping residue for Domain A, is not only 30 Å from the phosphate binding cassette in Domain A, but is also docked to the activation loop of the C-subunit (Figure 11b). Furthermore, the phosphate binding cassette in Domain A is partially occluded by the C-subunit at the site 2 interface (Figure 7 and 10). Specifically, Tyr247^{C} (in the αG helix of the C-subunit) hydrogen bonds to Tyr205^{R} and the two subunits are docked through a hydrophobic interface at this site. These structural details are consistent with studies that find Domain B to be the fast association site for cAMP in holoenzyme (Ogreid and Doskeland, 1981a).
- *Step 2*. We predict that recruitment of the C-terminal tail to stabilize cAMP in the phosphate binding cassette of Domain B will disrupt the Glu261^{R}-Arg366^{R} salt bridge. Both our mutational studies and those of others (Kapphahn and Shabb, 1997) show Tyr371^{R} to be a critical element that influences PKA activation by cAMP. Mutation of Tyr371^{R} to alanine results in 9-fold more cAMP needed to activate PKA compared to wild-type RIα, presumably due to removal of the hydrophobic and hydrogen bonding capabilities of this residue. In addition, single point mutations of either Glu261^{R} or Arg366^{R} that disrupt the salt-bridge require 3-fold less cAMP to activate PKA, suggesting that positioning of the C-terminal tail is destabilized in the absence of the salt bridge.

- *Step 3*. The R-subunit undergoes a large conformational change in response to uncoupling the Glu261^{R}-Arg366^{R} salt bridge. Breaking the salt bridge also releases Trp260^{R}, the capping residue for cAMP-binding in Domain A. Several observations support this idea. First, as seen in Figure 11c, the αB helix in Domain B interacts with the αH-αI loop of C. The movement of the C-terminal tail towards the phosphate binding cassette in Domain B weakens the interaction between the C-subunit and Domain B, thereby facilitating the conformational change. Second, in the holoenzyme complex, Trp260^{R} is buried in the R/C interface. Since the Glu261^{R}-Arg366^{R} interaction structurally couples the two hydrophobic capping residues, Trp260^{R} and Tyr371^{R}, docking of cAMP to Domain B breaks the salt bridge and pulls the Trp260^{R} away from the C-subunit activation loop. These motions collectively destabilize the extended αB/C helix and the concerted motions of Domain B bring Trp260^{R} towards the phosphate binding cassette in Domain A.
- *Step 4*. Binding of a second molecule of cAMP to the phosphate binding cassette in Domain A is stabilized by Trp260^{R}. Mutation of Trp260^{R} to alanine showed a 4.6-fold decrease in cAMP sensitivity for PKA activation. It is apparent in our holoenzyme structure that a second cAMP molecule can only bind to the phosphate binding cassette in Domain A if this domain is dislodged from the C-subunit. It remains to be established if the C-subunit dissociates from the psuedosubstrate site in the R-subunit before or after trapping cAMP in Domain A or if these these steps are coordinated.
- *Step 5*. In the final step, release of the C-subunit from the inhibitor site of the R-subunit leads to activation of PKA.

2.4. Conclusions

In this report, we describe the structure of the PKA catalytic subunit bound to a deletion mutant of RIα containing both cAMP-binding domains. The structure demonstrates the exceptional mobility of the cAMP-binding domains in RIα and confirms that there is a large movement of Domain B relative to Domain A as the R-subunit shuttles between its binding partners, namely the catalytic subunit and cAMP. The conversion of the globular conformation of the cAMP-bound structure into a dumbbell shaped holoenzyme complex, where the two cAMP-binding domains are separated, is mediated by extension of the αB/C helix of Domain A. The RIα*:C structure also shows that the αB and αC helices in Domain B are equally dynamic, but their conformations are very different from the αB/C helices in Domain A. When bound to the C-subunit, RIα utilizes a unique set of residues that stabilize the C-subunit bound conformation without directly participating in the R/C interaction. We show through mutagenesis that a conserved salt bridge plays a significant role in cAMP activation of PKA, most likely by trapping the two adenine capping residues in RIα away from their cAMP-binding sites. These hydrophobic capping residues also contribute to the cooperative activation of the enzyme through cAMP. Finally, these data provide for the first time a molecular explanation for the highly ordered pathway whereby binding of cAMP to Domain B leads to the eventual activation of kinase activity.

Chapter 2, in full, is a reprint of the material as it appears in Kim C*, Cheng CY*, Saldana A, and Taylor SS. “PKA-Iα Holoenzyme Structure Reveals Mechanism for

cAMP-dependent Activation." Cell. 2007. Sep 21:130(6):1032-43. I was the primary investigator and author of this paper. (* denotes co-authorship)

Chapter 3

Small Angle X-ray Scattering and Site-Directed Mutagenesis Uncovers a Dynamic RIα Domain B in PKA-RIα Complexes

---

3.1. Introduction

The PKA-Iα holoenzyme crystal structure described in Chapter 2 illuminated the detailed interactions between the C- and R-subunits, and elucidated a molecular mechanism for the ordered and cooperative activation of PKA by cAMP. Both the structure and mutational data highlight the role of Domain B as the gatekeeper domain for Domain A. cAMP first binds to Domain B, triggering a conformational change that leads to cAMP binding to Domain A, which then releases free catalytically active C-subunit. Mutation of the cAMP binding site in Domain B greatly diminishes the ability of PKA to respond to cAMP (Herberg et al., 1996a). Furthermore, deletion of Domain B requires 500-fold more cAMP to activate the holoenzyme even though it still binds to the

C-subunit with high affinity (Huang and Taylor, 1998). These data suggest that for RIα, Domain B initiates activation of PKA.

While crystal structures provide atomic resolution data of molecules, they do not capture the true dynamic nature of proteins as they exist in solution. In order to fully understand the intrinsic behavior of the RIα:C protein complex, we must also turn to solution techniques that will provide insights into the flexibility and mobility between domains (if any). The structural and solution data can be used in conjunction as a platform to understand the mechanism of RIα inhibition and activation and how it compares to the regulation of other PKA isoforms.

There are four R-subunit isoforms of PKA (RIα, RIβ, RIIα, and RIIβ). Each isoform shares the same domain organization, but differ in biological function and biochemical properties. (The biological differences between isoforms are discussed in detail in Chapter 1.3.2.) Previous small angle X-ray scattering data (SAXS) showed differences in the overall shape of holoenzymes formed with truncated RI- and RII-subunits (Vigil et al., 2004; Vigil et al., 2005, 2006a). These R-subunit constructs excluded the N-terminal dimerization domains so that we were only monitoring the effects of the heterodimers. The RIIα and RIIβ heterodimers form compact, globular particles, whereas the RIα heterodimer exhibits a more elongated shape. Although the source of the extended tail has not been elucidated, we hypothesize that it is due to extension of a highly dynamic Domain B in RIα. The purpose of this chapter is to address four main questions: 1) In the RIα P(r) function, is the shoulder due to Domain B? 2) Can SAXS be used as a method to monitor the dynamic properties of Domain B and are the dynamic properties of RIα altered when you introduce mutations in either Domain A or B? 3) Can we use SAXS to sense mutations in the catalytic subunit? 4)

Finally, can we interpret the SAXS differences observed between RI and RII? It is hoped that these studies will address how variations between R-subunit isoforms give rise to the unique and sophisticated mechanisms of PKA regulation in cells.

To test our hypothesis of a highly flexible Domain B in PKA-Iα and the effects of the R333K mutation (used in the crystal structure), we utilized a combination of site-directed mutagenesis, biochemical analysis of activation, and small angle X-ray scattering analysis to better understand the role of Domain B dynamics in the activation process of Type Iα PKA.

3.1.1. Small angle X-ray scattering

Small angle X-ray scattering (SAXS) is a solution technique that measures the intensity of scattered X-rays by atoms within a protein as a function of the scattering angle (Figure 21). The basic principle governing X-ray diffraction is the same between X-ray crystallography and SAXS. Incoming X-rays excite electrons in the sample, which in turn release secondary radiation at the same frequency. These secondary X-rays interfere both constructively and destructively, thereby generating characteristic intensity profiles at the detector. Only the intensity, not amplitude, is recorded at the detector as a function of the scattering angle. Each pair of scattering centers (or atoms) of the particle contributes to the overall scattering profile. Scattering due to long-distance pairs are reflected in the intensities at smaller angles, whereas scattering due to short-distance pairs are reflected at larger angles.

Advantages and Disadvantages of SAXS

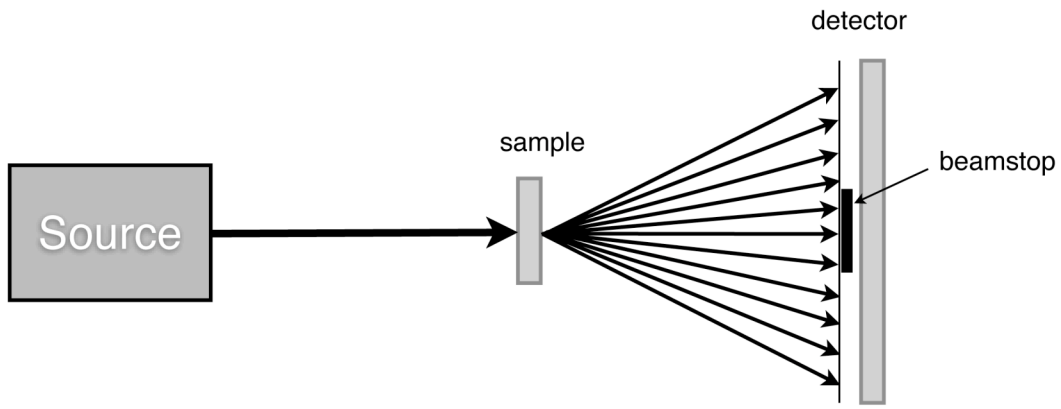

Figure 21. SAXS experimental setup.

Although both SAXS and X-ray crystallography rely on the diffraction of X-rays from electrons in the sample, the two techniques differ in many aspects. Firstly, SAXS measures the particle scattering in *solution*, thus the laborious task of finding crystal growth conditions (which is impossible in some cases) is unnecessary. Furthermore, solution conditions better mimic the physiological nature of proteins, thus eliminating conformational artifacts that may result from crystal packing. Thirdly, the atomic structure of the particles cannot be calculated from SAXS data as it can in crystallography. Structures can only be determined if both the phases and amplitudes of scattering vectors are known. In SAXS experiments, particles are tumbling isotropically in solution, thus only the vector lengths but not the directions (or phases) are inferred from the scattering profile. In crystallography, phases can be determined using strategies such as heavy-atom soaking, molecular replacement, or isomorphous replacement. As a result, the information content from SAXS is much lower than crystallography.

SAXS offers several advantages over other structural analysis methods such as crystallography, NMR spectroscopy, and cryoEM. First, a wide range of buffer conditions can be utilized (pH, temperature, salt, viscosity), including buffers that are physiologically relevant. Second, only a small amount of sample is sufficient for a typical experiment (50 μl at 2 mg/ml concentration). Third, SAXS is amenable to flexible or disordered systems. Proteins are dynamic and flexible species and in SAXS, these motions are averaged in the scattering profile. Fourth, a wide variety of particle sizes can be measured, ranging from small domains 50 amino acids in length to multi-domain proteins or even large protein complexes such as ribosomes (in contrast to nuclear magnetic resonance spectroscopy, which cannot measure proteins greater than ~50,000 Da). Lastly, SAXS can be used in conjunction with high-resolution techniques such as crystallography,

NMR or electron microscopy to build models that provide information regarding domain and subunit organization. SAXS is also fast compared to the other structural techniques.

There are several disadvantages to using SAXS. First and foremost, SAXS is extremely sensitive to small amounts of aggregation, which is severely accelearated by protein damage due to X-ray radiation. Second, the rotational averaging of particles in solution makes unique 3D structure determination impossible (i.e., the 1D scattering profile cannot uniquely determine a 3D structure), however recent advances in modeling techniques permit more robust insights into the particle shapes. Finally, this technique is technically demanding and expensive (compared to crystallography, NMR, cyroEM?).

Informational content of SAXS data

In a SAXS experiment, data are collected as an angular distribution of scattered X-rays from both the solvent and the sample. The intensity of scattering, *I*, is a function of scattering vector length, *q*, given by:

$$q = \frac{4\pi \sin\theta}{\lambda} \qquad \text{(equation 3.1)}$$

where 2θ is the scattering angle between the incident and scattered beam, and λ is the wavelength of radiation. With the assumption that the particles are identical and mono-disperse in solution, the small-angle scattering intensity profile is given by:

$$I(q)\left|\left\langle \int_V \rho(\vec{r}) - \rho_s e^{-i\vec{q}\bullet\vec{r}} d^3 r \right\rangle\right|^2 \qquad \text{(equation 3.2)}$$

where ρ and ρ_s are the scattering densities of the particle and solvent, respectively, and r is the position within a volume V. This treatment is a time- and ensemble-averaged technique that takes into account *all* conformations and orientations of the particles in solution. Thus, contrary to the single snapshot captured in X-ray crystallography, SAXS

data represent the conformational heterogeneity found in solution. Since this is a time-averaged technique, SAXS is not sensitive to the atomic details of a particle. Instead, it gives information about the *global* conformations of the molecule.

Parameters extracted from the scattering data relate to the size and shape of the particle including: the scattering at zero angle (I(0)), radius of gyration (R_g), molecular volume, molecular weight, the distribution of vector lengths between scattering centers in a particle (P(r)), and the maximum particle dimension (D_{max}). Each of these will be discussed in turn below.

Guinier fit analyses is a method that evaluates scattering curves, *I(q)*, as a function of q^2 at low q values to determine the forward scattered intensity, *I(0),* and R_g from simple slope and intercept analysis of the linear equation:

$$\ln I(q) = \ln I(0) - R_g^{\,2} q^2 / 3 \qquad \text{(equation 3.3)}$$

I(0) is simply the intensity of scattered X-rays at zero angle. In practice, I(0) cannot be measured directly since a beamstop is required to protect the detector from the direct and intense X-rays at zero angle. Nonetheless, *I(0)* is a robust parameter that can be calculated by extrapolating intensities at low angles given by equation 3.3. Analysis of the I(0) data as a function of concentration provides information regarding particle association or dissociation states and can detect possibilities of aggregation during sample collection. The forward scatter, *I(0)*, is directly proportional to the molecular weight times the concentration (in mg/ml). Experimentally, one can determine the I(0) by comparison to a known standard like lysozyme. This is typically accomplished by dissolving a known mass of lysozyme powder into water at five different concentrations. SAXS measurements are performed with each sample and the I(0) is extrapolated to

infinite dilution. Since I(0) is proportional to the molecular weight and concentration, the following relation is exploited to assess sample aggregation or oligomerization:

$$I(0)_{lys} / c_{lys} / MW^2{}_{lys} = I(0)_{sample} / c_{sample} / MW^2{}_{sample} \qquad \text{(equation 3.4)}$$

where $I(0)_{lys}$ and $I(0)_{sample}$ are the forward scatter, MW_{lys} and MW_{sample} are the molecular weights of lysozyme and sample respectively. The sample concentration (c_{sample}) is calculated from equation 3.4 and compared to the measured concentration by amino acid analysis. Since this analysis relies heavily on having an extremely accurate measured concentration, the Bradford assay or absorbance readings at A_{280} are not as reliable as quantitative amino acid analysis. (Note: It is also possible to determine sample concentration or MW using water as an absolute standard.)

The radius of gyration (R_g) is an indicator of the overall size of a particle and represents the root-mean squared distance of electrons from the center of gravity of the particle. R_g is sensitive to both size and shape of a molecule. The R_g value calculated by Guinier analysis is extremely robust and is simply the slope calculated from equation 3.3.

SAXS data are often analyzed in terms of an inverse Fourier transform of the intensity distribution *I(q)*. *I(q)* is measured in reciprocal space with units of $Å^{-1}$, and can be converted into a distance distribution function, P(r), providing structural information in real space with units of Å. This conversion is given by the relation:

$$P(r) = \frac{1}{2\pi^2} \int_0^\infty I(q) qr \sin(qr) dq \qquad \text{(equation 3.5)}$$

P(r) corresponds to the distribution of all scattering pair-distances, *r*, within the particle. This P(r) function provides information on general particle shape characteristics. In practice, calculation of the P(r) curves is implemented with the program GNOM and involves empirical evaluation of the maximum assumed linear dimensions of the particle,

D_{max}. The final choice of D_{max} is based on having positive intensities throughout the P(r) function (simply put: the r at which P(r) reaches zero). D_{max} is highly sensitive to the presence of aggregation in samples. Aggregation contributes to the scattering intensity at the low q region. Since D_{max} is most influenced by data at low q where the intensities are the greatest, determination of D_{max} is prone to error in samples containing even small amounts of aggregates.

To highlight the kinds of information gleaned from P(r) analysis, Figure 22 shows simulated P(r) functions of three differently shaped molecules. Panel A shows the P(r) function for a globular shaped protein (the C-subunit of PKA_C). This curve has a Gaussian shape with a single peak corresponding to the most frequent distribution of scattering centers; this peak identifies the average radius of the particle. Panel B of Figure 22 shows the P(r) function of a bi-lobal, dumbbell shaped particle. The curve has two peaks, the first of which corresponds to the most common set of scattering vectors corresponding to the average radius one of the two balls of the dumbbell, whereas the second peak corresponds to the scattering vectors between the centers of the two balls of the dumbbell. Lastly, panel C shows the P(r) function of a rod-shaped particle. Particles of this shape have a broad, sloping scattering distribution at high r vlaues since there is no localized globular center in the molecule.

From the P(r) function, R_g and I(0) values can also be calculated with the following relations:

$$R_g^{\ 2} = \frac{\int_0^{d_{\max}} P(r) r^2 dr}{2\int_0^{d_{\max}} P(r) dr} \qquad \text{(equation 3.6)}$$

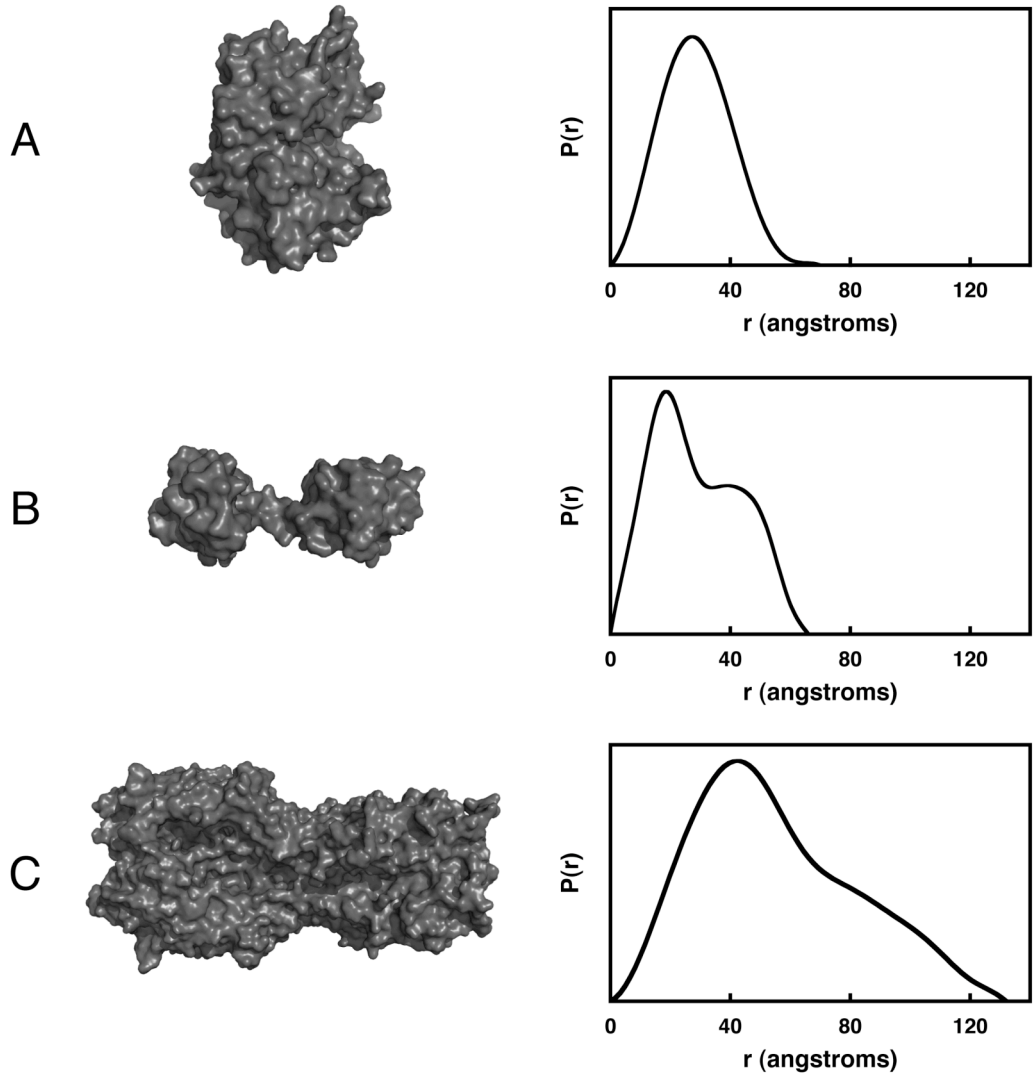

Figure 22. Simulated P(r) functions of particles with different shapes.

(A) Globular, spherical-shaped particle: PKA C-subunit, 1ATP.pdb. The P(r) function is symmetrical with a single peak. (B) Dumbbell-shaped particle: Calmodulin, 1CLL.pdb. The P(r) function has 2 peaks, the first peak corresponds to the center of mass of the smaller lobe, and the second peak corresponds to the center of mass of the overall particle. (C) Extended rod-like shaped particle: Hemagglutinin, 1HGF.pdb. The P(r) function exhibits a pronounced shoulder due to the extended particle shape.

$$I(0) = \int_0^{d_{\max}} p(r)dr \qquad \text{(equation 3.7)}$$

These results take the entire q envelope into account and should clearly agree with the values calculated by Guinier analysis that only uses the low q range, although a highly asymmetric shape will give larger R_g values than by Guinier.

If high-resolution structures are known, scattering profiles can be calculated from atomic coordinates in a pdb file with the program CRYSOL (Svergun, 1995). The resulting I(q) function can thus be compared to experimental results to distinguish if particle behavior in solution differs from the static structures determined by X-ray crystallography or high resolution electron microscopy. Deviations between calculated and experimentally determined scattering profiles can be attributed to different conformational states, particle flexibility, or oligomerization states in the crystal versus solution structures.

3.2. Experimental Methods

3.2.1. Protein preparation

The catalytic subunit was expressed and purified in *E. coli* as described previously (Gangal et al., 1998). All RIα proteins were also expressed in *E. coli* BL21 (DE3) cells (Novagen) and purified as described previously (Su et al., 1995a; Wu et al., 2004).

Holoenzymes of RIα mutants (RIα(91-379), RIα(91-244), RIα(91-379:R209K), and RIα(91-379:R333K)) were formed by mixing with wild-type C-subunit in a 1:1.2 molar ratio and dialyzed overnight at 4°C in 10 mM MOPS (pH 7.0), 50mM NaCl, 2mM $MgCl_2$, 2mM DTT, and 0.5mM ATP. Each holoenzyme complex was separated from

excess C-subunit by gel filtration chromatography as described (Wu et al., 2004). Care was taken to concentrate samples immediately prior to SAXS data collection since these complexes were extremely prone to aggregation at concentrations higher than 5 mg/ml.

3.2.2. SAXS Data collection

Small angle X-ray scattering measurements were collected at the University of Utah with an Anton Paar SAXSess instrument with line collimation and an image plate detector. Protein samples were concentrated to 2-5 mg/ml and filtered (0.22 μm) immediately prior to data collection. Scattering data for protein samples and their respective solvent blanks were collected in a 1-mm quartz capillary with the use of a 10-mm slit. Data for protein samples were collected for 60 min while buffer samples were collected for 30 minutes, both at 12 °C. Data for beam profiles used for desmearing calculations were collected for 30 min at 12 °C.

3.2.3. Data analysis

Solvent subtractions and data reduction to I(q) versus q (where $q = (4\pi \sin \theta)/\lambda$, where 2θ is the scattering angle and λ is the wavelength of the radiation (1.54 Å)) were done with the program SAXSquant1D (Anton-Paar, Austria), while desmearing calculations were done with the program GNOM (Svergun, 1992). Radius of gyration (R_g) and zero angle scattering (I(0)) parameters were calculated with both GNOM and by Guinier analysis with the program PRIMUS (Konarev, 2003). Inverse Fourier transform calculations of I(Q) to yield P(r) functions, I(0), R_g, and the maxium dimension (D_{max}) was

performed using a q-range of 0.013 to 0.17 1/Å. CRYSOL was used to calculate theoretical scattering intensity from pdb coordinates. Ab initio shape restoration modeling was done with DAMMIN (Svergun, 1999). Figures were made in PyMOL (DeLano Scientific LLC, San Carlos, CA, USA).

3.3. Results

SAXS data were collected for seven PKA-Iα protein complexes formed with a combination of four RIα mutants (RIα_{AB}, RIα_{AB}R333K, RIα_{AB}R209K, and RIα_{A}) and two C-subunit proteins (wt and K285P). To study the contribution of just the two cAMP binding domains on PKA-Iα dynamics, we used a construct that lacked the N-terminal dimerization domain and linker region, RIα(91-379). The inhibitor sequence region (residues 91-100) was necessary to form a high affinity complex with the C-subunit. The SAXS intensity plots of *I(q) versus q*, the Guinier plots, and the associated distance distribution P(r) functions are shown in Figures 23-26. Guinier plots for all samples are linear at the low q range, indicative of a monodisperse solution where non-specific aggregation was absent during data acquisition. These results together signify that each sample contained monodisperse particles so these data are suitable for structural analysis. The intensity curves were fit and inverse Fourier transforms were performed to generate P(r) functions.

3.3.1. RIα heterodimers

To assess the general shape characteristics of the RIα heterodimers containing both Domains A and B, we measured the SAXS profiles of RIα(91-379) and wild-type C-subunit complexes (Figure 23). The P(r) functions for $RI\alpha_{AB}$:C show very similar profiles to previous data, where there is a single peak (maxima at 35 Å) and a long extended tail at the high q range. The maximum dimension (122 Å) and R_g values (34.7 +/- 0.2 and 38.9 +/- 0.3 Å, from Guinier and GNOM analysis, respectively) are also consistent with previous data.

3.3.2. Effect of deleting Domain B

To assess the contribution of Domain B to the overall shape of the heterodimer, we measured the X-ray scattering of a complex formed with RIα containing only one of the two cAMP binding domains (residues 91-244, subsequently called $RI\alpha_A$). This protein is the smallest fragment of RIα that still binds to both cAMP and C-subunit with high affinity. The resulting P(r) function resembles a spherical, globular particle with a symmetrical Gaussian curve with no indication of a broad shoulder at the high r region (Figure 24). The maximum dimension measured by SAXS is 70 Å, consistent with the maximum dimensions determined from the crystal structure solved with the same constructs (Kim et al., 2005). Thus, not only does Domain B contribute to the overall size of the complex, but it also contributes to the broad shoulder observed in the P(r) function.

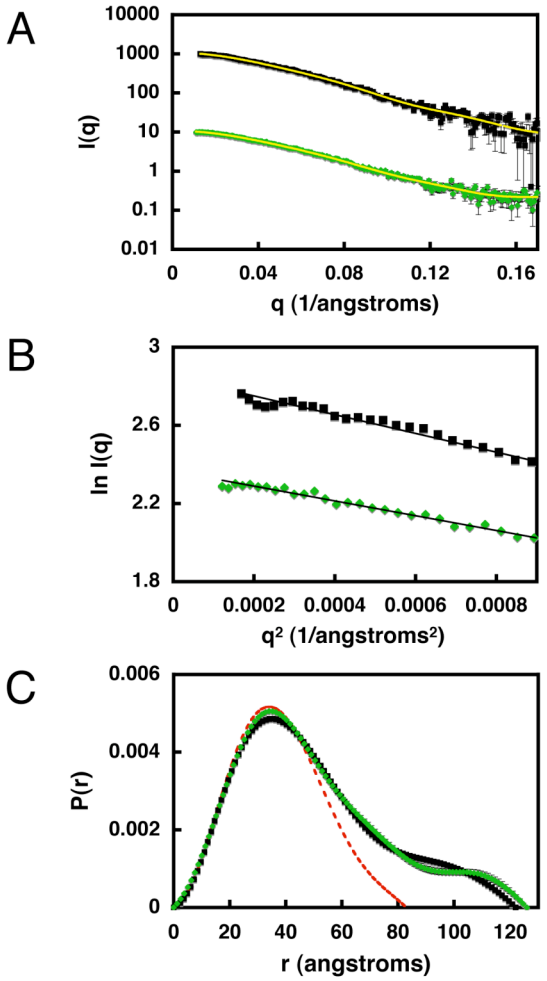

Figure 23. SAXS profiles of RIα(91-379) heterdimers.

(A) I(q) versus q plots. (B) Gunier plots. (C) P(r) curves calculated from X-ray scattering data. RIα_{AB}:C heterodimers are in black and RIα_{AB}:C(K285P) heterodimers are in green. The red dotted line in panel C is the P(r) function calculated from coordinates of the RIα_{AB}R333K:C crystal structure. The intensities for (A) and (B) are in arbitrary units.

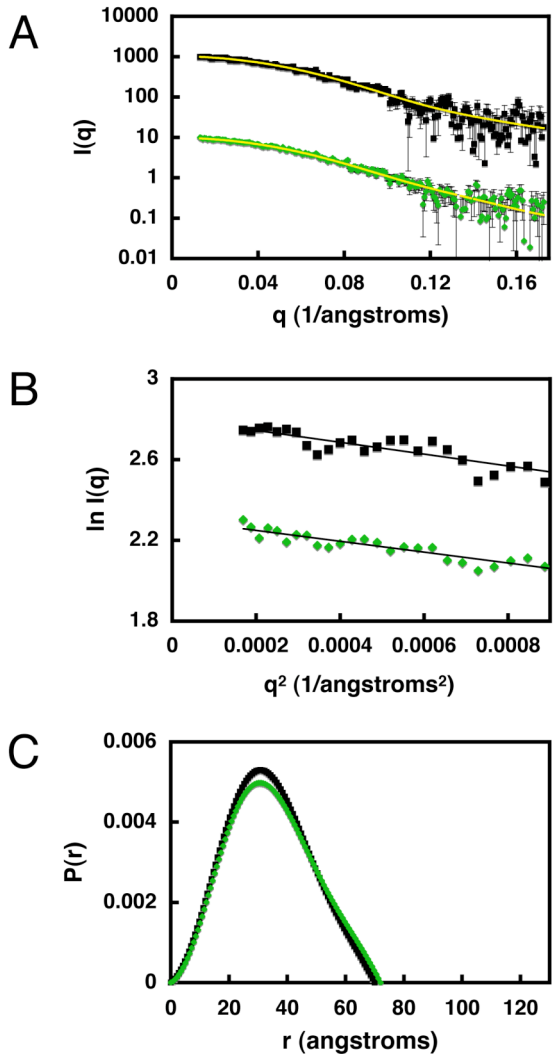

Figure 24. SAXS profiles of RIα(91-244) heterodimers.

(A) I(q) versus q plots. (B) Gunier plots. (C) P(r) functions. The RIα_A:C heterodimer is shown in black while the RIα_A:C(K285P) heterodimer is shown in green. The heterodimer formed with RIα_A shows a very compact shape and no differences are observed with the C(K285P) mutant.

3.3.3. Effect of R333K on RIα heterodimer

The PKA RIα:C structure solved in Chapter 2 was obtained by using a mutant regulatory subunit, R333K. Arg333 is a residue essential for high affinity cAMP binding to the B-domain (the corresponding residue in the A-domain is Arg209). While attempting to crystallize the PKA-Iα holoenzyme complex, parallel crystallization trials were set up for three RIα deletion mutants ($RI\alpha_{AB}$, $RI\alpha_{AB}$R209K, and $RI\alpha_{AB}$R333K, where $RI\alpha_{AB}$ refers to the RIα residues 91-379) in complex with the C-subunit. Only the holoenzyme formed with $RI\alpha_{AB}$R333K produced well-diffracting crystals. In this study, we want to determine the effects of the R333K mutation, if any, on the global architecture of the RIα:C complex in solution.

In contrast to the extended P(r) curve observed with the wild-type $RI\alpha_{AB}$ heterodimer, the P(r) function for the $RI\alpha_{AB}$R333K heterodimer exhibits a Gaussian distribution typical of a globular, spherical particle (Figure 25). GNOM analysis reveals a P(r) function with a peak maximum at 34.9 Å, that goes to zero at the maximum dimension, D_{max}, of 83 Å, and a computed R_g value of 25.7 ± 0.4 Å (28.3 +/- 0.9 Å from Guinier analysis). Clearly, the extended tail at the high r region in the $RI\alpha_{AB}$:C heterodimer data is not observed for $RI\alpha_{AB}$R333K. PKA heterodimers formed with the mutant $RI\alpha_{AB}$R333K resemble the more compact structures observed with the RII heterodimers (Vigil et al., 2005). Compared to $RI\alpha_{AB}$ heterodimers without the R333K mutation, the D_{max} is smaller (39 Å) and the R_g is smaller as well (7.1 Å).

The crystal structure of the RIα:C complex was solved using the R333K mutant. We hypothesized that this mutation somehow trapped the R-subunit into a compact structure with favorable crystal packing, but which is unlike the structure of the wild-type

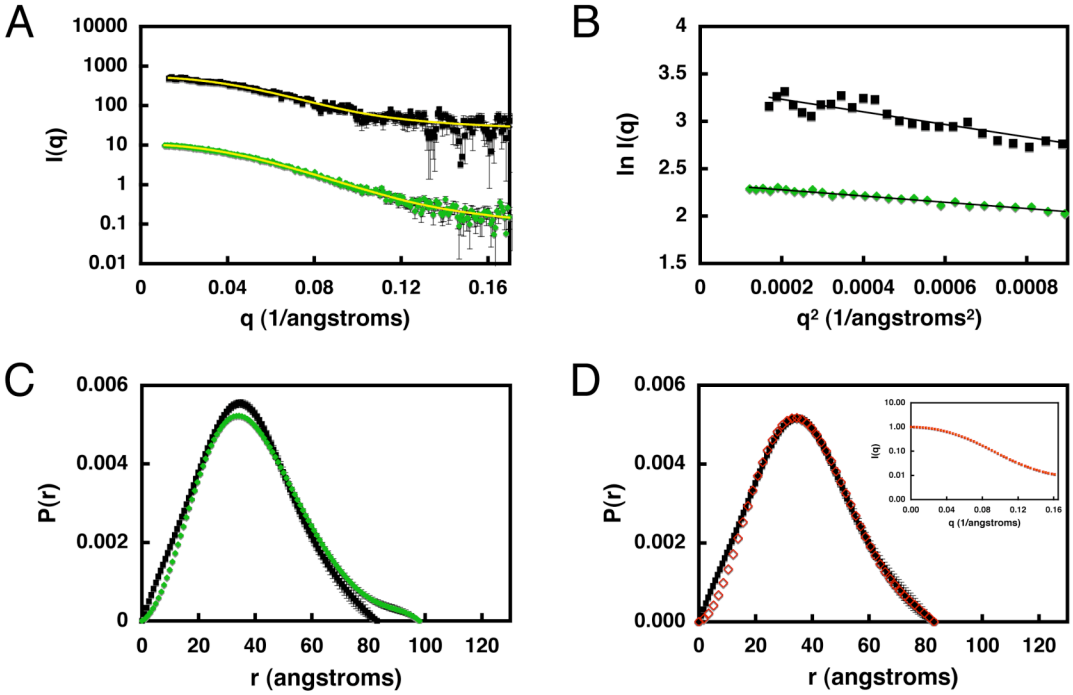

Figure 25. SAXS profiles of R333K heterodimers.

(A) I(q) versus q plots. (B) Gunier plots. (C) P(r) curves calculated from X-ray scattering data. (D) Calculated scattering intensity from RIα_{AB}R333K:C heterodimer crystal structure (1QCS.pdb). P(r) functions of the experimental (black) and calculated (red) data for the RIα_{AB}R333K heterodimer are comparable. Inset, calcluated scattering intensity from coordinates from 1QCS.pdb with the program CRYSOL. RIα_{AB}R333K:C heterodimers are in black and RIα_{AB}R333K:C(K285P) heterodimers are in green. The intensities for (A) and (B) are in arbitrary units.

complex found in solution. To investigate this hypothesis, we used the program CRYSOL (Svergun et al., 1995) to calculate the theoretical scattering intensities from atomic coordinates of the RIα_{AB}R333K:C structure (2QCS.pdb). We then generated a P(r) function based on the theoretical scattering data for comparison. Figure 25d shows the relationship between the experimental and calculated P(r) functions. As predicted, the experimental and calculated P(r) curves overlap without any hint of the extended tail we see for the wild-type complex. Both the D_{max} and R_g values are in agreement between experimental and calculated results. In contrast, these calculated intensity profiles compared to the experimental wild-type complexes clearly show a discrepancy at long vector lengths (Figure 23 and 25) suggesting that the conformation observed in the crystal structure is distinct from what occurs naturally in solution. Instead, the complex between RIα_{AB}R333K and C-subunit represents one out of many possible conformational states that are present in solution. We propose the R333K mutation somehow pushes the equilibrium state of RIα into its most extended conformation, an asymmetric dumbbell shape, where Domain B extends away from Domain A and the C subunit. This conformation makes it less able to compete for the compact cAMP-bound conformation, thus stabilizing the holoenzyme conformation. This extended conformation is most likely stabilized by contacts on the αH-αI loop of the C-subunit.

3.3.4. Effect of R209K on RIα heterodimers

The R333K mutation impairs cAMP binding to Domain B; the corresponding mutation for Domain A is R209K. To test whether this mutation also affects the dynamics of the R- and C-subunit interaction, we measured the X-ray scattering of heterodimers

formed with R209K. Unlike the R333K mutation, the P(r) function for R209K clearly shows no difference in the overall shape compared to the wild-type heterodimer, but its maximum dimensions are smaller than wild-type (Figure 26). The P(r) function has a maximum peak at 34.7 Å, a maximum dimension of 105 Å and an R_g value of 34.6 ± 0.4 Å (33.5 +/- 0.9 Å from Guinier analysis). Clearly, the compaction of $RI\alpha_{AB}$:C is specific only to the mutation in Domain B.

3.3.5. Effect of K285P mutation on RIα heterodimers

The PKA-Iα holoenzyme structure (see Chapter 2) defined a novel interaction site between Domain B of RIα and a short S-shaped loop (αH-αI loop) of the C-subunit (Figure 27). In PKA-Iα, Domain B docks onto the C-subunit through side chain interactions in the $Asp276^C$:$Arg352^R$ and $Thr278^C$:$Arg355^R$ pairs and backbone interactions with $Lys285^C$ to both $Arg355^R$ and $Leu357^R$. A similar configuration is seen in the PKA-IIα holoenzyme structure. Again, Domain B of RIIα is docked onto the αH-αI loop of the C-subunit through several hydrogen pairs. Each of the three residues in both RIα and RIIα that dock to this loop is conserved in all R-subunit isoforms (Figure 28). Unfortunately, crystal structures of the PKA-Iβ or PKA-IIβ complexes containing both Domains A and B have not been solved, but we hypothesize that their B-domains interact with the C-subunit in a similar fashion seen with the PKA-Iα and PKA-IIα complexes.

To assess the effect of the K285P mutation in the C subunit on RIαAB complex formation, we measured and compared the X-ray scattering profiles of complexes between wild-type and K285P C-subunits. Although the K285P mutant plays a pivotal

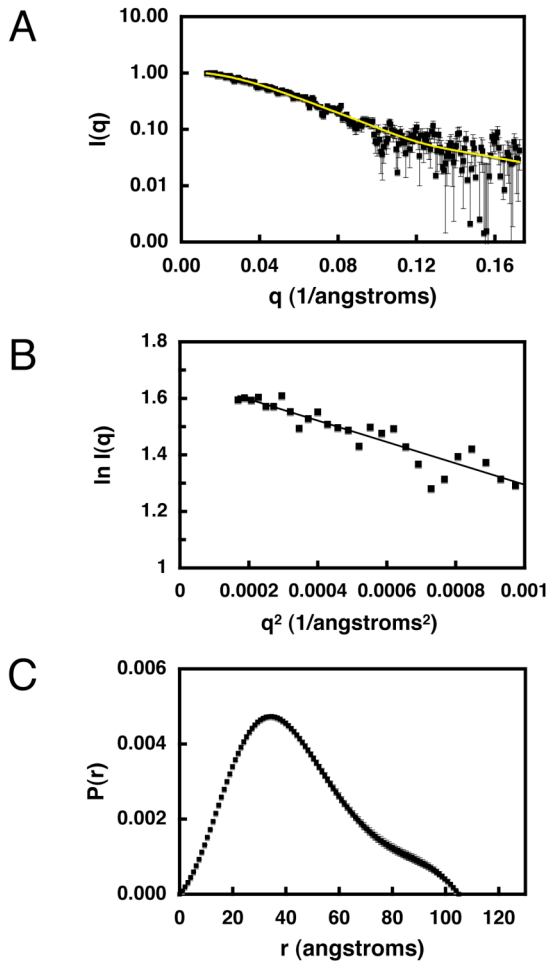

Figure 26. SAXS profiles of R209K heterdimers.

(A) I(q) versus q plots. (B) Gunier plots. (C) P(r) curves calculated from X-ray scattering data.

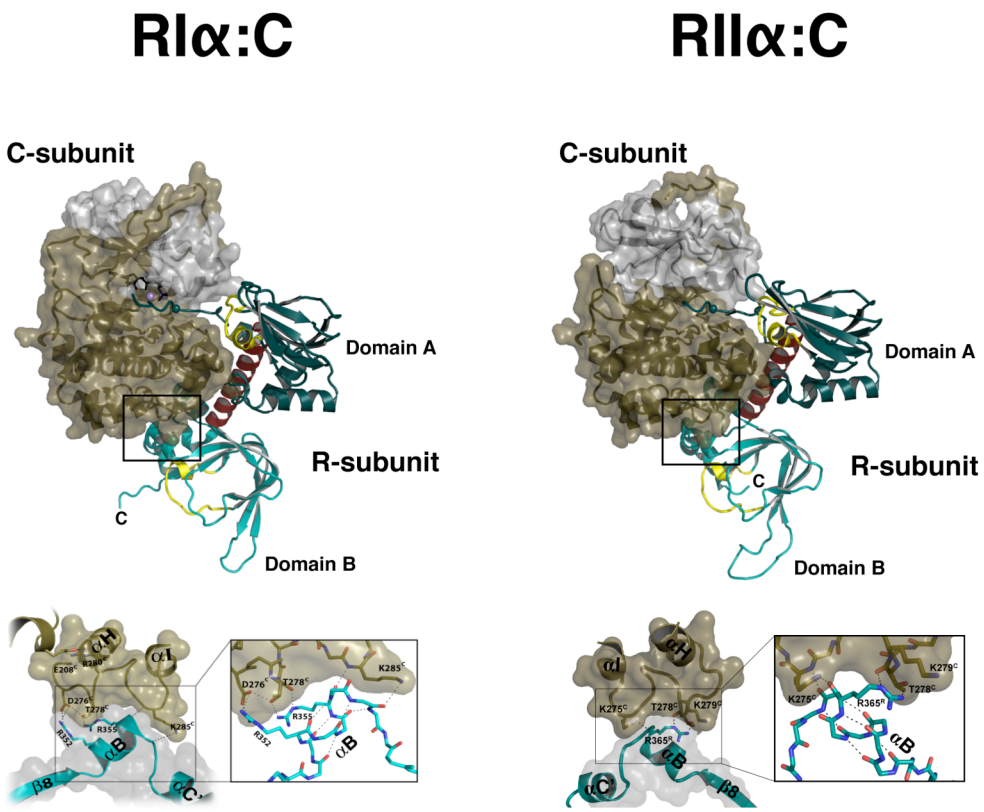

Figure 27. Comparison of R-subunit Domain B interactions in PKA-Iα and PKA-IIα Structures.

Left, PKA-Iα structure, 2QCS.pdb Right, PKA-IIα structure,2QVS.pdb Top, overall structural arrangement between the R- and C-subunits. The R-subunit is shown in cartoon rendering with Domain A in dark teal, Domain B in light teal, the connecting αB/C helix in red, and the phosphate binding cassette in yellow. The C-subunit is shown in surface rendering with the small lobe in white and the large lobe in brown. Boxed region indicates the interaction of the R-subunit Domain B and the αH-αI loop of PKA_C. Bottom, detailed illustration of the interaction between Domain B and the αH-αI loop of $PKA_{C,}$ with specific residues highlighted. Note that perspectives between PKA-Iα and PKA-IIα in the bottom panels are flipped 180°.

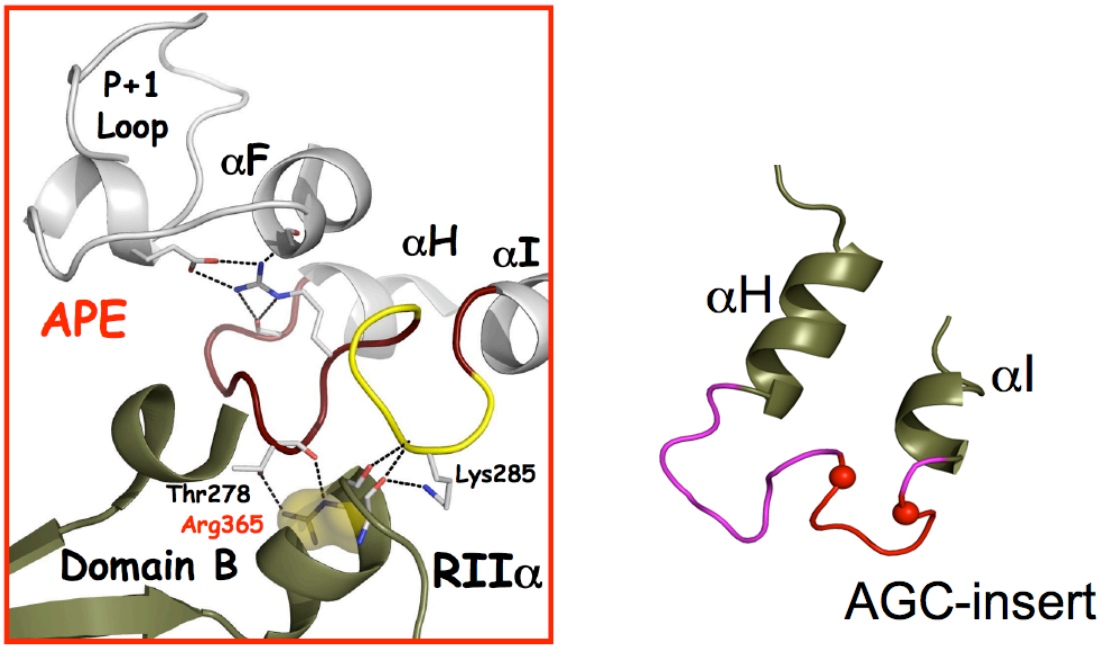

Figure 28. AGC insert.

The αH-αI Helix (right) contains a unique AGC insert (in red between the two balls) and serves as a docking site for Domain B of the RII subunits (left).

role in RIIβ complex formation through interactions with Domain B, we postulated that this mutation would not affect the overall shape characteristics of the RIα heterodimers given the dynamic nature of Domain B in PKA-Iα (Yang et al., 2009). Indeed, the P(r) functions of both RIα_{AB}:C and RIα_{AB}:C(K285P) complexes show very similar profiles where a single peak is followed by a long extended tail at the high r region (Figure 23). The maximum dimension of each complex was roughly the same (122 and 126 Å for wild-type and K285P C-subunits, respectively). Furthermore, the R_g values were similar for both proteins (38.9 Å and 39.2 Å for wild-type and K285P, respectively; Table 2).

We predicted that the X-ray scattering of heterodimers formed with the RIα_A protein and the K285P mutant would be identical since the absence of Domain B makes the interaction site with residue 285 in the C subunit irrelevant. Indeed, the P(r) functions are indistinguishable (Figure 24) for the RIα_A complexes formed with wild-type and K285P mutant of C. The D_{max} (70 Å) and R_g (25.7 ± 0.2 Å) values clearly discriminate the size and shape characteristics between the RIα_{AB} and RIα_A heterodimers.

For the R333K heterodimer, we investigated whether the compact nature of the complex would be disrupted by interfering with the interaction between Domain B and the large lobe of the C-subunit. To do this, we utilized the K285P mutant in hopes of disrupting the interaction at this site. Indeed, the RIα_{AB}R333K:C(K285P) double mutant complex no longer exhibits the compact symmetric P(r) curve observed with RIα_{AB}R333K:C complex. Figure 25c illustrates that the P(r) function shows an extended tail at the high r region like the wild-type heterodimer, but not quite to the same extent. These differences are further supported by differences observed with the D_{max} and R_g parameters, where the double mutant complex D_{max} is 105 Å (compared to 83 Å for RIα_{AB}R333K:C and 122 Å for RIα_{AB}:C) and the R_g is 32.5 ± 0.4 Å (compared to 28.4 for

RIα_{AB}R333K:C and 38.9 Å for RIα_{AB}:C). Table 2 summarizes of all the SAXS measurements.

3.3.6. Biochemical analysis of PKA-Iα heterodimers

Surface plasmon resonance was used to measure the binding constants between R- and C-subunit proteins. C-subunits were immobilized to CM5 chips by amine coupling. The active site Lys72 was protected during the coupling process with 1 mM ATP and 2 mM $MgCl_2$. The K285P mutant resulted in a modest 5-fold difference in binding affinities between the RIα and C-subunits, where the K_D for the wild-type C-subunit complex was 0.9 nM and the K295P complexes was 4.9 nM (Table 3). In contrast, the K285P mutation made large differences in the dissociation constants for the RIIβ heterodimers, where the K_D for wild-type C-subunit complex was 2.9 nM and K295P complex was 111 nM. The difference between the binding constants is solely attributed to differences in the dissociation rate.

We also used a P^{32} assay to measure the ability of RIα to inhibit both wild-type and mutant C-subunits. There was no statistically significant difference in IC_{50} values between wild-type and K285P C-subunits (Figure 29).

3.4. Discussion

Previous SAXS studies suggested that the RIα subunit is quite dynamic when bound to the C-subunit, where Domain B is loosely tethered to the C-subunit by a highly dynamic αC helix that connects the two cAMP binding do(Gullingsrud et al., 2006; Vigil et al., 2004). This earlier SAXS work was completed before the RIα_{AB}R333K:C

Table 2. Comparison of R_g and D_{max} of PKA-Iα heterodimers.

R-subunit	C-subunit	R_g (Å)[a]	R_g (Å)[b]	I(0)[b]	D_{max} (Å)[b]
$RI\alpha_{AB}$	C	34.7 +/- 0.2	38.9 +/- 0.3	3.4 +/- 0.02	122
$RI\alpha_{AB}$	C (K285P)	34.0 +/- 0.2	39.2 +/- 0.4	3.5 +/- 0.03	126
$RI\alpha_{A}$	C	26.5 +/- 0.7	25.7 +/- 0.2	2.47 +/- 0.02	70
$RI\alpha_{A}$	C (K285P)	27.3 +/- 0.6	26.4 +/- 0.2	2.41 +/- 0.02	72
$RI\alpha_{AB}$R333K (exp)	C	28.3 +/- 0.9	28.4 +/- 0.4	0.134 +/- 0.002	83
$RI\alpha_{AB}$R333K (calc)	C	N/A	28.8 +/- 0.008	N/A	83
$RI\alpha_{AB}$R333K	C (K285P)	32.6 +/- 0.6	32.5 +/- 0.4	2.94 +/- 0.04	105
$RI\alpha_{AB}$R209K	C	33.5 +/- 0.9	34.6 +/- 0.4	3.08 +/- 0.05	105

[a] Derived using Guinier approximation
[b] Calculated using the program GNOM

Table 3. Association and dissociation rates of PKA-Iα and PKA-IIβ complexes (BIACORE).

R-subunit	C-subunit	k_a ($M^{-1}s^{-1}$)	k_d (s^{-1})	K_D (nM)
RIα(91-379)	C	91.9×10^4	8.44×10^{-4}	0.9
RIα(91-379)	C (K285P)	90.6×10^4	44.3×10^{-4}	4.9
RIIβ(108-416)	C	11×10^4	3.16×10^{-4}	2.9
RIIβ(108-416)	C (K285P)	11×10^4	123×10^{-4}	111

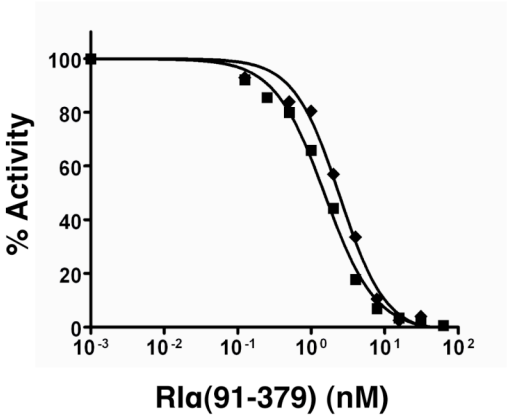

Protein Complex	IC_{50}
RIa(91-379):C	4.32
RIa(91-379):C(K285P)	2.62

Figure 29. Inhibition of C-subunit with RIα mutants.

The Cook coupled assay was performed with ATP^{32}, monitoring the downstream results of Kemtide phosphorylation. No difference is observed between complexes formed with wild-type and K285P C-subunit. Data for heterodimers formed with wild-type C-subunit is shown in diamonds and with K285P C-subunit is shown in squares.

heterodimer crystal structure was solved (Kim et al., 2007). The crystal structure revealed a contact point between the αB helix in Domain B (through residues Arg352^{R}, Arg355^{R}, and Gly357^{R}) and the αH-αI loop region of the C-subunit (through residues Asp276^{C}, Thr278^{C}, and Lys285^{C}). The R-subunit αB helix precisely complements the surface formed by the αH-αI loop (Figure 27, left) and Lys285^{C} in this loop operates as a helix cap where the C-terminal end of αB helix props up against the side chain of Lys285^{C}. A similar configuration was observed in the crystal structure of the RIIα:C heterodimer complex highlighting the functional significance of the αH-αI loop (Figure 27, right) (Wu et al., 2007). Intriguingly, bioinformatics analysis pinpointed a short segment within the αH-αI loop (Gly282-Gly286) to be an AGC kinase-specific insert, suggesting that the C- and R-subunits have co-evolved to accommodate each other at this binding interface. Crystal structures are oftentimes plagued by artificial conformations induced by favorable crystal packing. Other times, the single snapshots observed in crystal structures are not representative of the full range of conformational states proteins can occupy in solution. In this study, we collected biochemical and solution small-angle X-ray scattering data for PKA-Iα complexes and compared these results to the crystal structure (Kim et al., 2007).

In this study, we probed the contribution of the RIα Domain B towards the equilibrium dissociation constants, inhibition of the C-subunit, and overall shape of the RIα:C-subunit complexes. We utilized a C-subunit mutation, K285P, located on the αH-αI loop that contributes to the major contact site with Domain B on the R-subunit. K285P had only modest effects on both the binding affinity (0.9 nM for wild-type and 4.9 nM for K285P) and RIα inhibition (IC_{50} was 4.32 nM for wild-typ and 2.62 nM for K285P).

Additionally, our SAXS data show that the K285P mutant did not affect the general shape characteristics or particle dimensions for complexes formed with both RIα_{AB} and RIα_{A}. These results suggest that K285P is not critical for RIα:C complex formation.

K285P only made a difference in the P(r) function with the RIα_{AB}R333K mutant. The RIα_{AB}R333K:C heterodimer assumes the most compact shape of all the RIα complexes, presumably why crystallization of this complex (and not the wild-type) was successful. SAXS analysis of the RIα_{AB}R333K:C(K285P) complex shows a P(r) function with a slightly extended tail at the high r region, but not to the large extent that we observe for the RIα_{AB}:C complex. In other words, although the K285P mutation does disrupt the interaction between Domain B and the C-subunit to some extent, it does not fully represent the large dynamic range of the wild-type heterodimer, suggesting that the average conformational state of Domain B in the RIα_{AB}R333K:C(K295P) complex is intermediate between the fully compact form observed in the RIα_{AB}R333K:C crystal structure and the extended wild-type heterodimer. The crystal structure highlights two additional ion pairs at this site: Asp276^{C}:Arg352^{R} and Thr278^{C}:Arg355^{R} (Figure 27). It is possible that these two interactions compensate for the dissolution of the Lys285^{C}: Arg355^{R}/Leu357^{R} interactions, thereby allowing for transient stabilization of Domain B against the C-subunit. The shoulder observed in the wild-type heterodimer P(r) function is most likely the result of Domain B movement away from the C-subunit. Given that the first peak at 34.3 Å dominates the curve and the tail is only a small portion of curve, the complex is most likely a heterogeneous composition of conformational states where a small fraction of the population has Domain B detached from the C-subunit. This hypothesis is also consistent with hydrogen-deuterium exchange mass spectrometry data where only 1 amide is protected in the αH-αI loop of the RIα_{AB}:C complex (Anand et

al., 2007b). Furthermore, the affinity between RIα_A and the C-subunit is 5-10 nM, compared to 0.4 nM for the RIα_{AB}:C complex. Although Domain B in RIα is unnecessary for high affinity binding with the C-subunit, it *is* essential for the cAMP-dependent activation and release of the C-subunit. Blocking cAMP access to Domain B increases the activation constant from 25 nM to 1500 μM (Herberg et al., 1996a). Collectively, these data are in agreement with the notion that Domain B is dispensable for RIα:C complex formation. Instead, the role of Domain B is to initiate activation of the RIα:C complex in response to cAMP.

Proteins are in continuous motion, constantly sampling an ensemble of different conformations. In the case of RIα, Domain B seems to explore a large conformational space. Although the precise domain motion is not clear, we speculate that the flexibility stems from some portion of the αB/αC helix that connects the two cAMP binding domains (Figure 30). Analysis of various crystal structures demonstrates the full range of motions RIα can adopt. When RIα is bound to the C-subunit, the αB/αC helix is extended into one contiguous helix. When RIα is bound to cAMP, this same region is divided into three distinct helices separated by 2 kinks or bends at Gly235^R and Tyr244^R. There is a 40 Å difference in the maximum dimension between the most compact heterodimer (RIα_{AB}R333K:C) and the most extended (RIα:C), most likely due to unhinging motions at the Gly235^R position. Just C-terminal to Gly235^R is a helical region between residues 226 and 235 that forms a particularly hydrophobic interface with the C-subunit. Leu 233^R and Met234^R from the R-subunit creates a hydrophobic cluster that secure the R- and C-subunits together. Biochemical studies show mutation of these residues unfastens the hydrophobic zipper making it easier to activate the holoenzyme (unpublished). Therefore, this region is firmly anchored to the C-subunit. Thus, we

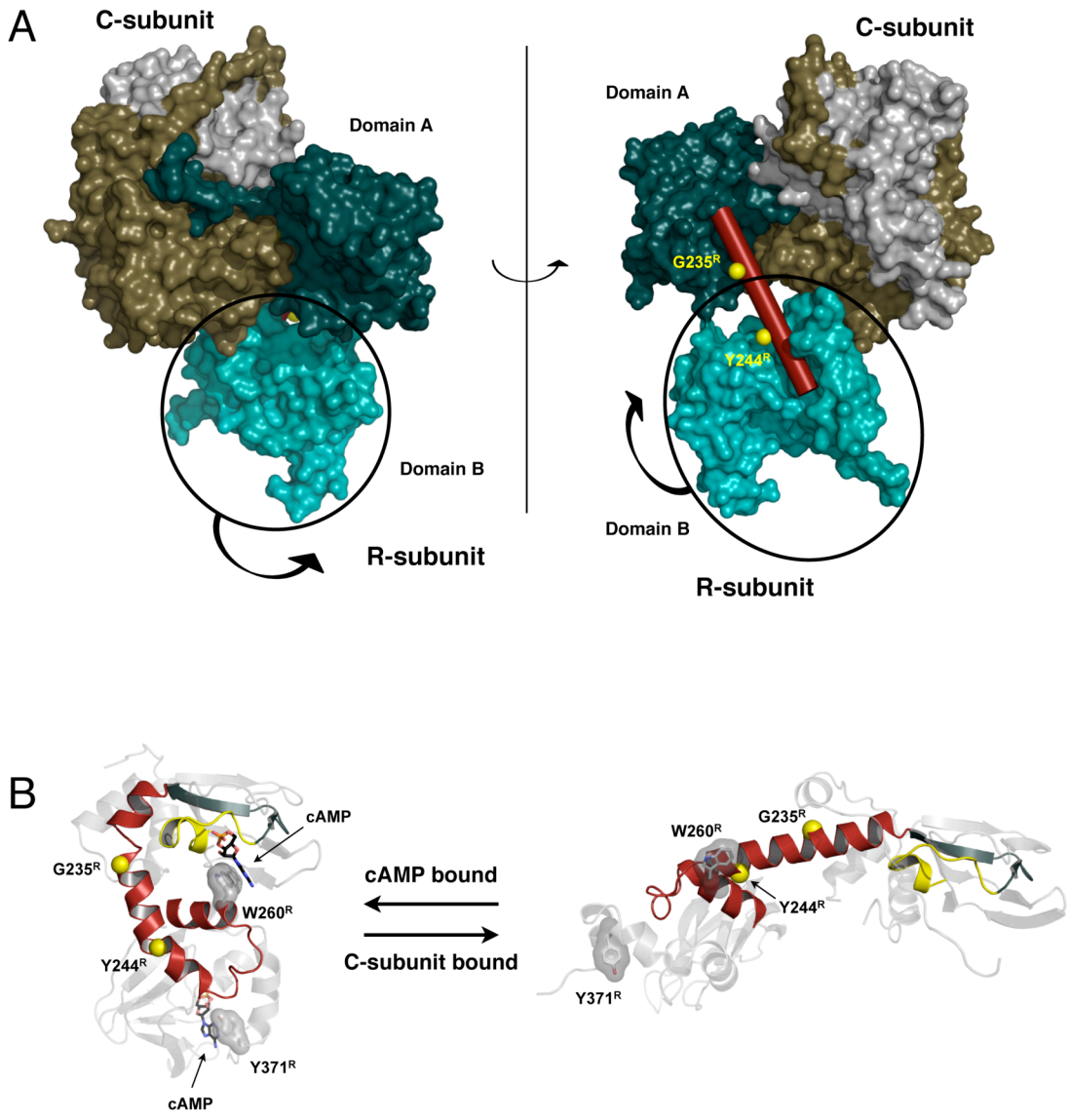

Figure 30. Model of Domain B motion of PKA-Iα.

(A) The small lobe of the C-subunit is shown in white and the large lobe in brown. The R-subunit Domain A is in dark teal, Domain B in light teal, and the connecting αB/C helix is shown as a red cylinder. The two hinge points are highlighted with yellow spheres. (B) Conformational change of R-subunit upon binding cAMP (left) and C-subunit. The αB/C helix is highlighted in red, PBC in yellow, hydrophobic capping residues in surface rendering, and the Gly235 and Tyr244 hinge-points are depicted as yellow spheres.

believe the motions observed in our SAXS data stem from hinge regions either at Gly235^R or Tyr244^R.

To test this theory, we artificially introduced kinks at the Gly235 hinge point of the RIα crystal structure and computed their scattering intensities and corresponding P(r) functions (Figure 31). Movement of Domain B resulted in larger R_g values and particle dimensions, compatible with the dimensions derived from experimental data. Even though the extended tail of these modeled P(r) functions is present in each curve, they are not as pronounced as the experimental data. It is likely that RIα adopts a mixture of these states.

From our data and others, it is unmistakable that the role of Domain B differs between RI and RII-subunits. The activation of RIα:C is a stepwise process where cAMP must bind to Domain B before Domain A. For RIIβ, cAMP activation is not sequential and cAMP binding to either domain is sufficient. For RIIβ, we also observed large differences in the binding constants with the K285P mutant, where the K_D was 10-fold weaker between K285P and RIIβ proteins; the difference in binding constants was indistinguishable for RIα. Previous studies also demonstrated that the K285P mutation reduced the ability of RIIβ to inhibit the C-subunit, and was sufficient to completely abolish BCY1 (the yeast homolog of RII subunits) inhibition of the C-subunit (Yang et al., 2009). Third, based on data from hydrogen/deuterium exchange-mass spectroscopy experiments, the αH-αI loop is well-protected in the RIIβ complex (Anand et al., 2007b; Zawadzki and Taylor, 2004), whereas minimal protection is seen in the RIα complex(Hamuro et al., 2004). Lastly, SAXS analysis shows a P(r) function that resembles a compact particle, corroborating the view that Domain B forms a tight

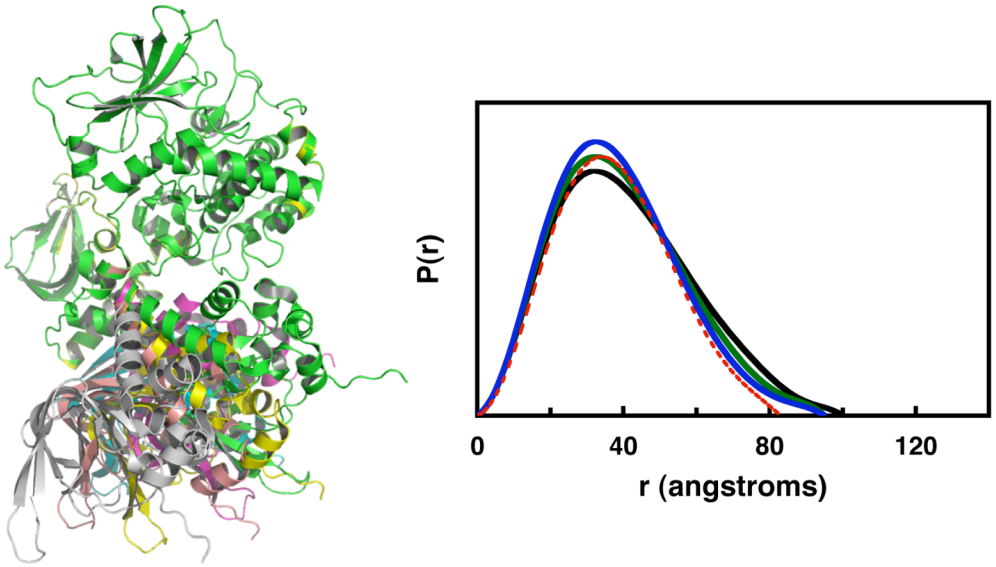

Figure 31. Simulations of Domain B motion of PKA-Iα.

Left, modeled movement of Domain B at the Gly235 hinge point. Right, simulated P(r) curves for 3 of the models (solid curves). The dotted red line shows the calculated scattering data from the RIα_{AB}R333K:C crystal structure.

interaction with the C-subunit. Taken together, these data suggest opposing roles of Domain B in RIIβ and RIα. For RIIβ, not only does Domain B interact tightly with the C-subunit, it is also necessary for inhibition of the C-subunit. In contrast, for RIα, Domain B is highly mobile and its interaction with the C-subunit αH-αI S-loop is not necessary for inhibition, but Domain B *is* essential for cAMP-dependent activation.

3.5. Conclusions

In this study, we utilized SAXS and mutational analysis to investigate the dynamic behavior of the RIα:C complex in solution. In particular, we show that the RIα:C complex forms an extended particle whose P(r) function exhibits a broad shoulder at long vector lengths. This shoulder is a result of the RIα Domain B since no shoulder is observed for the $RI\alpha_A$:C complex. A R333K mutation introduced in the cAMP binding domain altered the dynamic properties of Domain B in which RIα heterodimer collapsed into its most compact conformation. The P(r) function of the R333K heterodimer no longer contains the extended shoulder observed with the wild-type heterodimers. SAXS analysis of a double mutant complex, $RI\alpha_{AB}$R333K:C(K285P), displayed a shoulder at the high r region in the P(r) curve, suggesting that the interaction site between RIα Domain B and C-subunit may have been partially disrupted. These results together suggest that Domain B in the RIα:C complex is in an equilibrium state of motion not locked in one position against the C-subunit. These observations are in contrast to the RII heterodimers where Domain B interaction with the C-subunit is critical for both inhibition and complex formation. The structural and functional differences between RI

and RII-subunits described here contribute to the broad functional diversity of PKA isoforms.

Chapter 4

Dissecting the Regulatory Subunit Inhibitor Sequences as Binding Motifs for the Catalytic Subunit

---

4.1 Introduction

The regulatory subunits are modular, dynamic proteins, with well-defined domains capable of binding multiple proteins at a time. There are four isoforms of regulatory subunits (RIα, RIβ, RIIα, and RIIβ) that differ in biological function and biochemical properties. Despite these differences, each regulatory subunit is comprised of 4 main segments: an N-terminal dimerization/docking domain, a flexible linker, an inhibitor site, and two cAMP binding domains. Each individual element, in turn, plays a unique role in the function and regulation of PKA. At the N-terminus is a dimerization/docking domain that binds to a class of scaffolding proteins called A Kinase Anchoring Proteins (AKAPs) responsible for targeting the regulatory subunits to unique cellular compartments. A variable and flexible linker follows and accounts for differences in the overall shapes of the four isoforms (Vigil et al., 2006a). For RIα, this region has been proposed to bind Grb2 (Tortora et al., 1997), Rsk (Chaturvedi et al., 2006), and 14-3-3 (unpublished). The inhibitor sequence is situated next to the linker region and is also

highly variable among isoforms. For all isoforms, this region contains the canonical PKA substrate recognition motif R-R-X-S/T-ψ that binds to the active site cleft of the C-subunit. The most important distinction between all isoforms is a phosphorylatable serine at the P-site for RII subunits, but not for RI subunits where they have either an alanine or glycine at this site. This makes the RII subunits both inhibitors and substrates of the C-subunit, providing them an additional level of PKA regulation by being sensitive to ATP. At the C-terminus lie two tandem cAMP binding domains that serve as sensors for cAMP.

The RIα:C structure described in Chapter 2 outlined how components in the inhibitor site and the two cAMP binding domains bind and interact with the C-subunit. Domain A plays a large role in providing essential elements needed to achieve high affinity interactions with the C-subunit. A large surface area is enclosed within the interface between Domain A and C-subunit. Moreover, constructs containing the inhibitor sequence to the end of Domain A (residues 91-244) bind to the C-subunit with high affinity (K_D = 5 nM) in the presence of Mg_2ATP. Domain B is highly dynamic (as described in Chapter 3) and its main role is to limit cAMP access to Domain A, thereby functioning as a portal for PKA activation. Domain B is certainly dispensable in terms of providing high affinity between the R- and C-subunits, but does provide a small amount of binding energy to increase the K_D from 0.2 nM to 5 nM for full-length and a RIα construct that lacks Domain B, respectively.

The inhibitor sequences are substrate-like in themselves because they contain the PKA recognition sequence R-R-X-P_{site}-ψ. The crystal structure of RIα:C illustrates for the first time how the inhibitor sequence becomes ordered by binding in the active site groove of the C-subunit. The basic residues in the RIα consensus site complement the

acidic residues in the C-subunit active site. Four arginine residues preceding the P-site (the phosphorylatable position) each interact with glutamate residues on the C-subunit. Furthermore, the P+1 residue, Ile100, is part of a hydrophobic core at the C-subunit interface (Figure 9). A sequence alignment of the inhibitor sequences from all R-subunit isoforms shows considerable variability in this region (Figure 32 and 33). First, RII subunits only contain 2 out of the four arginines present in RIα. Second, RII-subunits contain a serine at the P-site. Third, the RII-subunits contain a cysteine residue at the P+2 site that can potentially form a disulfide bond with the reactive cysteine, Cys199, in the C-subunit. In contrast, RI subunits always contain a serine at the P+2 site. Moreover, there are extensive differences in the preceding linker region. RIα contains a proline-rich region N-terminal to the P-site. RII subunits, on the other hand, contain a hydrophobic-rich region in the same area. Potentially, the RII subunits could utilize the hydrophobic patch of the C-subunit like PKI but different for RI subunits.

cAMP activation of PKA is a classic example of allosteric regulation where binding of cAMP to the R-subunit C-terminal domains, far removed from the C-subunit active site, triggers dissociation of the the R:C complex. In this chapter, we aim to characterize the contribution of the inhibitor sequences to the overall allosteric regulation of PKA activation. Undoubtedly, the primary role of this segment is to block substrate access to the C-subunit active site cleft since the chief function of the regulatory subunits is to *regulate* C-subunit activity. A question that remains is whether this segment alone can still bind the C-subunit with high affinity. It is possible that this segment is simply tethered to Domain A not to convey additional affinity, but to provide a latch to release the inhibitor site in response to cAMP. The focus of this chapter is to take a reductionist approach to assess whether the inhibitor sequences could function independently to bind

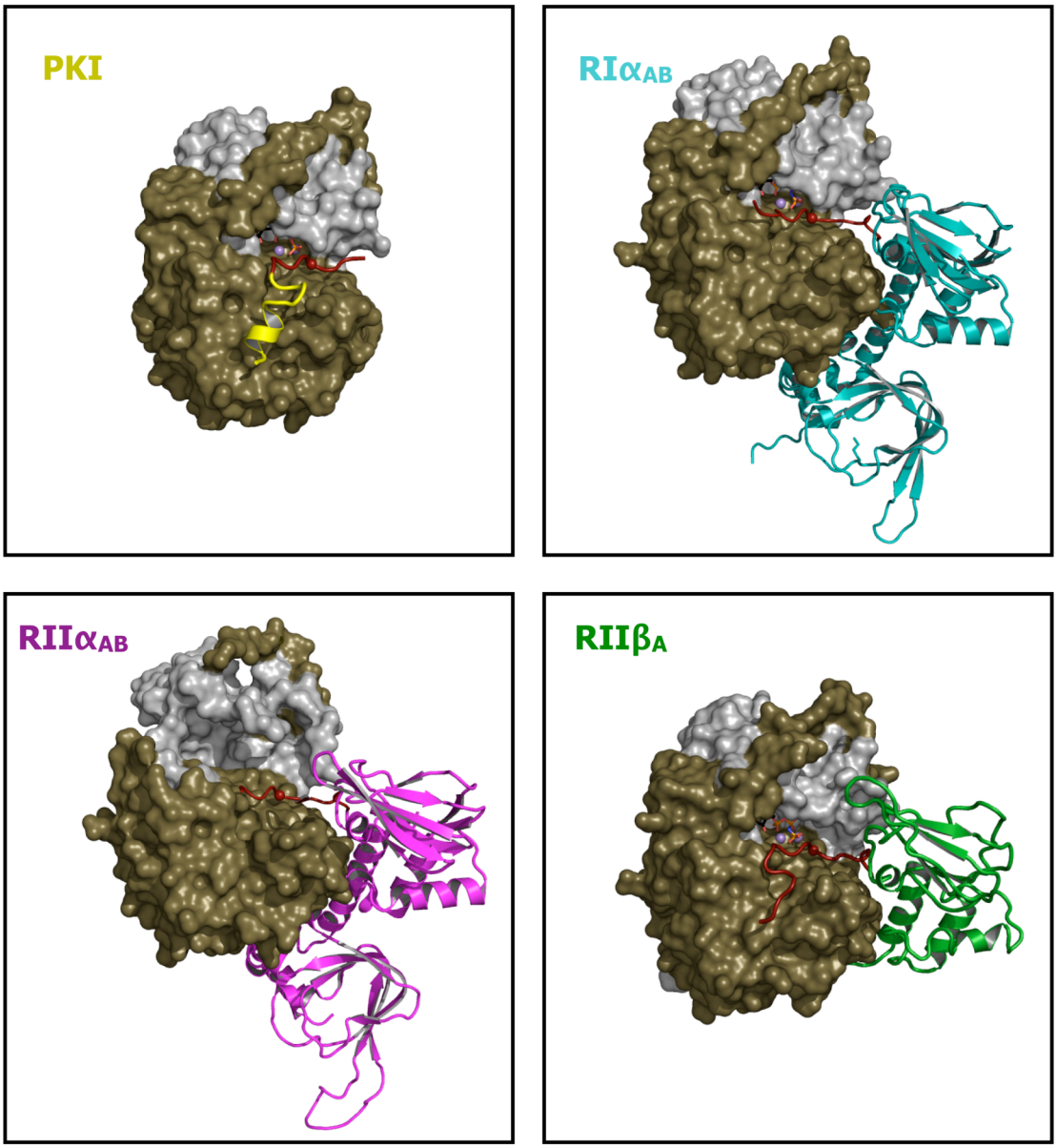

Figure 32. Crystal structures of C-subunit complexes to date.

Inhibitor sequences are colored in red and the P-site is indicated with a sphere.

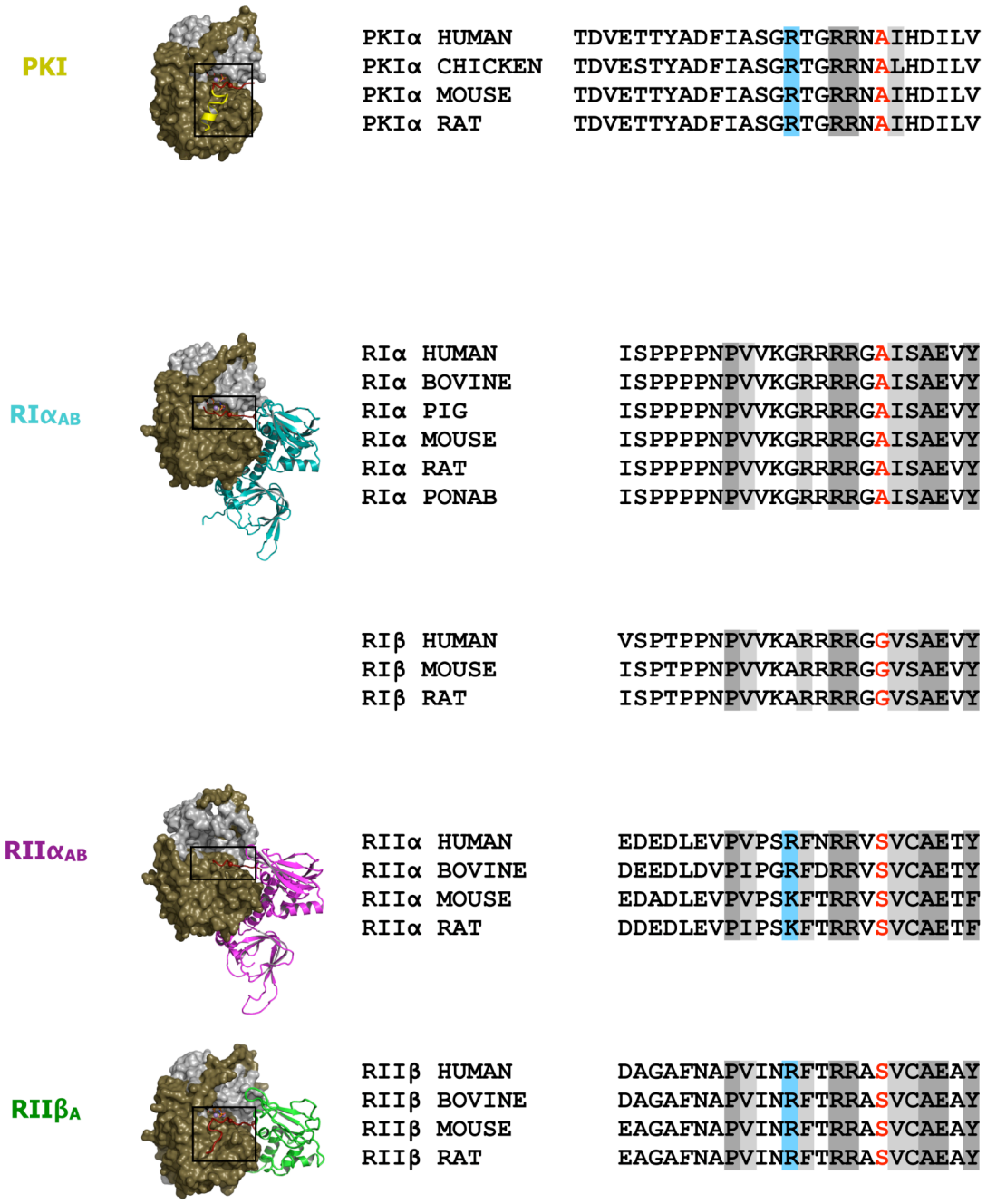

Figure 33. Sequence alignment of R-subunit inhibitor sequences.

Sequences marked in grey are conserved amino acids in all proteins, the gradation indicating the level of conservation. Sequences in blue are common to only the indicated proteins. The crystal structure of the RIβ:C complex has not been solved.

the C-subunits. Specifically, we addressed three main questions. 1) Is the short inhibitor segment sufficient to inhibit the C-subunit with high affinity? If so, what is the minimum sequence required for high affinity binding to the C-subunit? 2) Is there a dependence on nucleotide binding? 3) Finally, do the inhibitor sequences function similarly between all R-subunit isoforms given their sequence diversity? This study paves the way for not only understanding the mechanistic role of another R-subunit module, but also to begin thinking about utilizing these peptide sequences to potentially create a class of highly specific inhibitors for PKA.

4.2 Experimental Methods

4.2.1. Protein Preparation

The catalytic subunit was expressed and purified in *E. coli* as described previously (Gangal et al., 1998).

Synthetic peptides for biochemical and structural analysis were purchased from GenScript (Piscataway, NJ). The sequences were as follows:

RIα	CGRRRRGAISAEVY
RIIα_{short}	CRFNRRVSVAAETY
RIIα_{long}	CEDLEVPVPSRFNRRVSVAAETY
RIIβ_{short}	CRFTRRASVAAEAY
RIIβ_{long}	CGAFNAPVINRFTRRASVAAEAY

Peptides were dissolved in 10 mM Tris (pH 8.5) and 20 mM DTT. The peptides were centrifuged for 10 minutes at 13K RPM and the supernatant was 0.2 μm filtered to remove trace amounts of insoluble material.

4.2.2. Peptide Array

Synthetic peptide arrays were generated with the MultiPep Flexible Parallel Peptide Synthesizer (Intavis Bioanalytical Instruments, Germany). The peptides are covalently coupled to cellulose membrane supports at the N-terminus. Peptide blots were overlaid with C-subunit alone or with AMP-PNP and Mg^{2+}.

Newly synthesized membranes were first soaked in 100% ethanol for 5 minutes then washed extensively with water. Membranes were washed with 1x TTBS for 10 minutes then blocked with 5% milk in 1x TTBS for 20 minutes at room temperature. 2 μM C-subunit in 5% milk (TTBS) was added and incubated overnight at 4°C on a platform rotator. For high affinity interactions, a 2-hour incubation at room temperature is sufficient. After overlaying with C-subunit, the membranes were washed 3 times with 1x TTBS (no milk) at room temperature, 5 minutes for each wash. The blots were next incubated with α-PKA_C (BD Transduction Laboratories, CA) in 5% milk (TTBS) at 1:1000 dilution for 1 hour at room temperature, then washed three times with TTBS (no milk) at room temperature. Membranes were then probed with α-mouse (BD Biosciences, Franklin Lakes, NJ) for 1 hour at room temperature, and then washed three times with TTBS (no milk) at room temperature. Membranes were then placed on a dry surface and SuperSignal West Pico Chemiluminescent Substrate for detection of HRP (Thermo Scientific Product #34090) was added to cover the blot entirely. The membranes were

then transferred between two transparencies then exposed to film. When no signal was detected, SuperSignal West Femto Maximum Sensitivity Substrate (Thermo Scientific Prod #34095) was used to increase signal sensitivity at both 1:100 and 1:10 dilutions. The schematic is depicted in Figure 34.

Incubation steps with protein and antibodies were done in plastic bags sealed on all sides, just large enough to accommodate blots for maximum signal.

Peptide blots were also overlaid with 1 mM AMP-PNP and 1 mM $MgCl_2$ to assess the effect of nucleotide on peptide binding to the C-subunit.

4.2.3. Peptide Blot Regeneration

For low affinity interactions, membranes were sufficiently regenerated with Restore™ PLUS Western Blot Stripping Buffer (Thermo Scientific, Rockford, IL). Blots were incubated with the stripping buffer for 30 minutes at 37°C. Membranes were probed with primary and secondary antibodies to ensure efficacy of the regeneration method.

When the above procedure failed to strip bound proteins, a more stringent wash was necessary. Membranes were first washed with water (three 10-minute washes), then with dimethylformamide (three 10-minute washes), and finally with water again (two 10-minute washes). Next, membranes were incubated in 8 M urea, 350 mM sodium dodecyl sulfate, and 14 mM beta mercaptoethanol for 30 minutes (three 10-minute washes), followed by 50% ethanol and 10% acetic acid for 30 minutes (three 10-minute washes). Membranes were then washed two times with methanol and allowed to air dry.

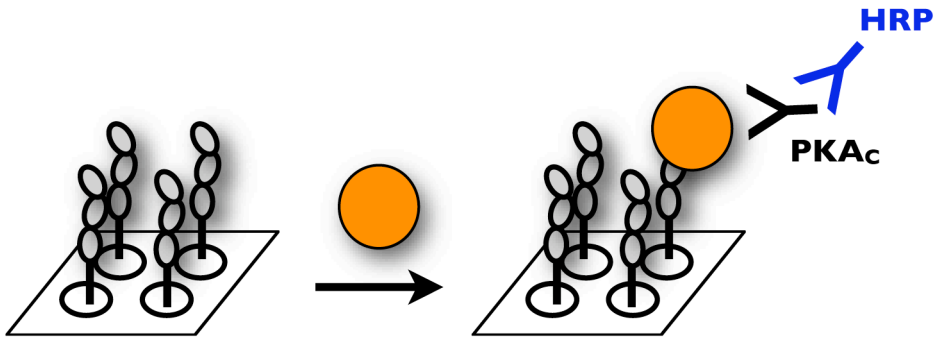

Figure 34. Schematic of Peptide Array.

Each peptide is covalently linked to membrane supports at the N-terminus. The membranes are overlaid with C-subunit (orange spheres), and binding was visualized with antibody detection methods.

4.2.4. Crystallography

The C-subunit was dialyzed into 50 mM bicine (pH 8.0), 150 mM ammonium acetate, and 10 mM DTT and concentrated to 10 mg/ml (determined by the Bradford assay). A complex between PKA_C, RIIα peptide, AMP-PNP, and $MgCl^{2+}$ was obtained by mixing the components in a 1:5:10:10 molar ratio. The protein mixture was incubated on ice for 2 hours and filtered with 0.2 μm centrifugal devices (Life Sciences). Crystallization trials were setup on CrystalClear Duo sitting drop plates (Douglas Instruments) using the Oryx8 Protein Crystallization Robot (Douglas Instruments, UK). The following commercial HT crystal screens were used to determine initial crystallization conditions: PACT, JCSG, Proplex, Structure Screen I&II, Clear Strategy I, and Clear Strategy II (Molecular Dimensions), Crystal Screen HT (Hampton Research, HR2-130) and Wizard™ Screens I & II (Jena Bioscience, Germany). Screens were done with 0.5 μl drops, testing both 40% and 60% protein concentrations and 4°C and 22.5°C temperatures.

4.3 Results

4.3.1. RI peptides

To test the ability of RI inhibitor sequences to bind the C-subunit, an array of peptides corresponding to various lengths of RIα and RIβ were synthesized on membrane supports. Sequence alignment of the inhibitor segments reveals several conserved residues C-terminal to the P-site (Figure 33): alanine, glutamate, and tyrosine/phenylalanine (P+3, P+4, and P+6 residues, respectively). In summary, all four

R-subunit isoforms fall into the sequence scheme: R-R-X-S/T-ψ-S/C-A-E-X-ψ, (P-site is underlined for reference). To date, sequence analysis efforts has been focused on the R-R-X-S/T-ψ motif, but not the flanking sequences. Thus, we set out to test the contribution of residues flanking both sides of the P-site in their ability to bind the C-subunit.

In one set of RIα peptides, each included the sequence –RRGAISA, containing 3 residues C-terminal to the P-site (subsequently referred to as P+3 peptides). In the second set, all peptides included the sequence –RRGAISAEVY containing 6 residues C-terminal to the P-site (subsequently referred to as P+6 peptides). Each ensuing peptide added an additional amino acid to the N-terminus on the array. The same was done for RIβ where in the P+3 set, all peptides included the sequence –RRGGVSA, while in the P+6 set, all peptides included the sequence – RRGGVSAEVY. Each of these blots was probed for their ability to bind free C-subunit both in the absence and presence of AMPPNP and Mg^{2+} (Figure 35).

In the absence of nucleotide, binding was not detected between the C-subunit and any of the RIα or RIβ peptides. Addition of residues C-terminal to the P-site had no effect on binding to the C-subunit. Upon addition of nucleotide, we detected weak binding between the C-subunit and both RIα and RIβ P+6 peptides, but not P+3 peptides. The smallest RIα peptide that bound to the C-subunit was RRRRGAISAEVY and the smallest RIβ peptide was RRRRGGVSAEV. Slightly stronger binding was also detected starting with the longer sequences PPPNPVVKGRRRRGAISAEVY for RIα and TPPNPVVKARRRRGGVSAEVY for RIβ.

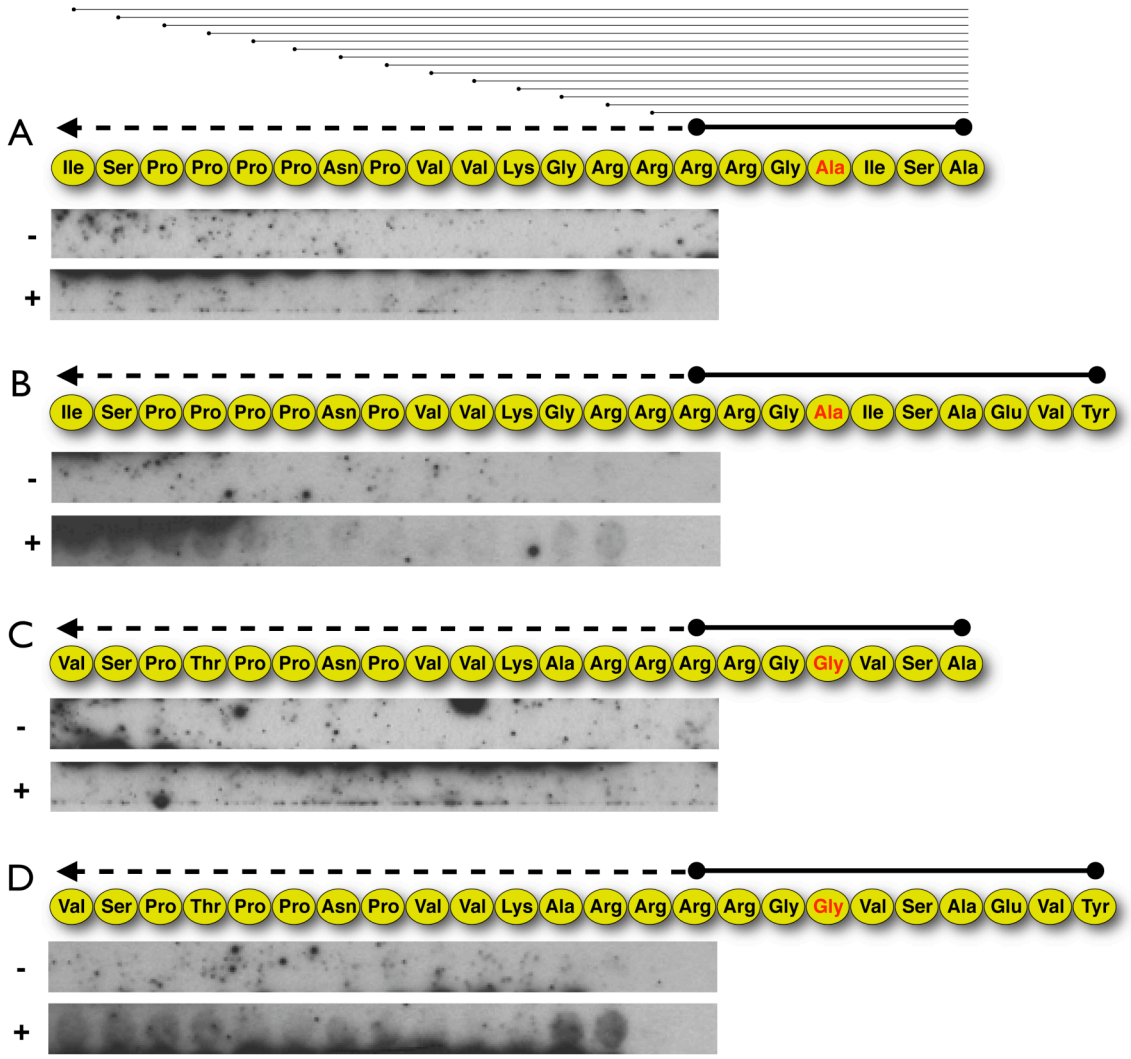

Figure 35. Peptide blots of RIα and RIβ inhibitor sequences.

Each spot corresponds to a sequence beginning with the amino acid above the spot to the C-terminus of that particular sequence. Each blot was overlaid with free C-subunit (-) and with C-subunit, AMPPNP, and Mg^{2+} (+). RIα inhibitor sequences with residues to the P+3 position (A), and to the P+6 position (B). RIβ inhibitor sequences with residues to the P+3 position (C) and to the P+6 position (D). In (A) and (C), the blot without AMPPNP was exposed for 2 minutes and the blot with AMPPNP and Mg^{2+} was exposed for 5 seconds. In (B) and (D), the blots were exposed for 30 seconds. The amino acid in red designates the P-site.

4.3.2. RIIα peptides

The same strategy was utilized to assess the capacity of RIIα peptides to bind the C-subunit. An array of peptides corresponding to various lengths of RIIα was synthesized on membrane supports. In the P+3 set, all peptides included the sequence – RRVSVCA. In the P+6 set, all peptides included the mouse sequence –RRVSVCAETF and the human sequence –RRVSVCAETY. Each subsequent peptide added additional amino acids to the N-terminus. We overlaid each array with C-subunit and examined them for binding in the presence and absence of AMPPNP and Mg^{2+} (Figure 36)

In the absence of AMPPNP/Mg^{2+}, binding was not detected between the C-subunit and any of the RIIα P+3 peptides except for the longest 21 amino acid peptide. Surprisingly, binding *was* detected between the C-subunit and the RIIα P+6 peptides from both mouse and human sequences. The three C-terminal residues (Glu-Thr-Phe/Tyr) unmistakably enhanced the affinity of these peptides for the C-subunit. Sequence alignment signifies conservation of the Glu and Phe/Tyr residues across all R-subunit isoforms, suggesting that these residues may play an important functional role and our array data substantiates this idea. The shortest peptide that bound C-subunit alone consisted of a fragment from the P-6 residue (a lysine in the mouse sequence and an arginine in the human sequence) to the P+6 residue.

In contrast, the presence of nucleotide made a dramatic difference, where all peptides from both P+3 and P+6 groups bound to the C-subunit. For the P+3 peptides, the two shortest peptides bound weakly, whereas sequences as short as FTRRVSVCA bound strongly. The equivalent P+6 mouse sequences shared the same pattern. For the P+6 peptides with human sequences, the three shortest peptides bound weakly, whereas sequences as short as RFNRRVSVCAETY bound strongly.

Figure 36. Peptide blots of RIIα inhibitor sequences.

Each spot corresponds to a sequence beginning with the amino acid above the spot to the C-terminus of that particular sequence. Each blot was overlaid with free C-subunit (-) and with C-subunit + AMPPNP + Mg^{2+} (+). (A) Mouse sequence to P+3 position. The blot without AMPPNP was exposed for 2 minutes and the blot with AMPPNP and Mg^{2+} was exposed for 5 seconds. (B) Mouse sequence to P+6 position. Both blots were exposed for 30 seconds. (C) Human sequence to P+6 position. Both blots were exposed for 30 seconds. The asterisk marks amino acids that are different between mouse and human sequences. The amino acid in red designates the P-site.

In an effort to determine which amino acids are essential for binding to the C-subunit, we generated a peptide array that substituted each amino acid in the RIIα peptide with one of the other 19 possible amino acids. We started with a parent peptide corresponding to the 13 amino acid human sequence RFNRRVSVCAETY, with 6 residues before and after the P-site. This peptide was the shortest segment that bound the C-subunit in the absence of nucleotide. We monitored the effect of nucleotide on the interaction with the C-subunit (Figure 37). The interaction of peptides with C-subunit is noticeably more sensitive to amino acid substitutions in the absence rather than in the presence of nucleotide and Mg^{2+}. We first discuss data for overlays with free C-subunit.

In the absence of AMPPNP and Mg^{2+}, alanine substitutions indicate only 4 positions are tolerant of substitution compared to the wild-type sequence: Asn (P-4), Val (P-1), Ala (P+3), and Thr (P+5). Eight out of the nine sensitive positions are conserved across all R-subunit isoforms. All the arginine residues (P-6, P-3, and P-2) are irreplaceable. The phenylalanine at P-5 is tolerable to only conserved changes to aromatic and non-polar residues. The P-site serine accommodates a handful of amino acids (Arg, Asn, Asp, Gly, His, Pro, and Trp), which surprisingly does not include the more conservative mutations to cysteine or threonine. The P+1 site is typically a hydrophobic residue, but our peptide array clearly shows that the C-subunit can still bind to RIIα peptides with a variety of polar amino acids at this position. Both the P+4 glutamate and P+6 tyrosine residues were exceedingly sensitive to substitution. Other aromatic residues could effectively replace the P+6 tyrosine, suggesting that the hydrophobic interaction is important. Long non-polar residues such as histidine, methionine, and tryptophan could replace the P+4 glutamate. The sensitivity of these two residues is consistent with our truncation analysis where peptides with residues to

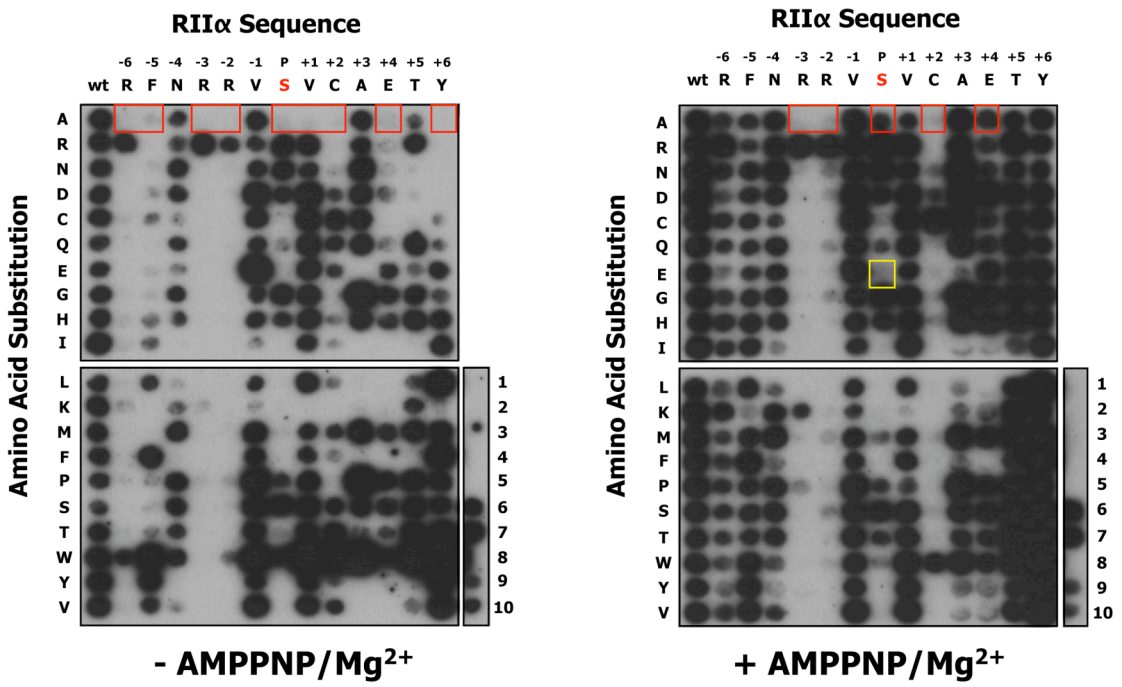

Controls

1 P_{15}
2 A_{15}
3 LRRASLG (Kemptide)
4 RRRRGAISAEVY (RIα)
5 RRRRGGVSAEVY (RIβ)
6 RFTRRASVCAEAY (RIIα)
7 PVINRFTRRASVCEAY (RIIβ)
8 FIASGRTGRRNAIHD (PKI)
9 TYADFIASGRTGRRNAIHD (PKI)
10 RLERRWSWCWDWW

Figure 37. Amino acid substitution of RIIα peptides.

RIIα peptides were synthesized on a solid membrane support. Peptides were overlaid with C-subunit, then detected with α-PKA_C. Blots were overlaid with (right) and without (left) AMPPNP and Mg^{2+}. Side boxes are control lanes. Both blots were exposed for 30 seconds. Red boxes indicate amino acids that were sensitive to alanine substitution. The yellow box highlights the phosphorylation mimic.

the P+6 position, but not the P+3 position, bound to free C-subunits.

Alanine substitutions abolished binding to the C-subunit for fewer residues in the presence than in the absence of AMPPNP and Mg^{2+} (three and eight positions, respectively). In the presence of nucleotide, the three amino acids sensitive to C-subunit binding were Arg (P-3), Arg (P-2), and Cys (P+2). The only mutations tolerated were a conserved lysine mutation at the P-3 arginine and a tryptophan mutation at the P+2 cysteine. In addition, although alanine substitution for both the P-site serine and the P+4 glutamate did not abolish C-subunit interactions, they did exhibit reduced affinity. Moreover, not all amino acids were tolerated at these two positions. All of the other positions were not sensitive to substitutions. In general, AMPPNP and Mg^{2+} clearly diminished the sensitivity of individual amino acid replacements towards interaction with the C-subunit.

4.3.3. RIIβ peptides

We next assessed which residues in the RIIβ inhibitor sequence were essential for binding to the C-subunit. Overall, RIIβ peptides exhibited a similar pattern of binding as the RIIα peptides (Figure 38). In the absence of nucleotide, binding was not detected between the C-subunit and the P+3 peptides, whereas binding was detected for most of the P+6 peptides. The shortest peptide that bound to the C-subunit was FTRRA<u>S</u>VCAEAY, which is one amino acid shorter than observed for RIIα. In the presence of AMPPNP/Mg^{2+}, all P+3 and P+6 peptides bound to the C-subunit. Again, spots corresponding to the two shortest peptides show weaker binding, and all of the longer peptides show strong binding.

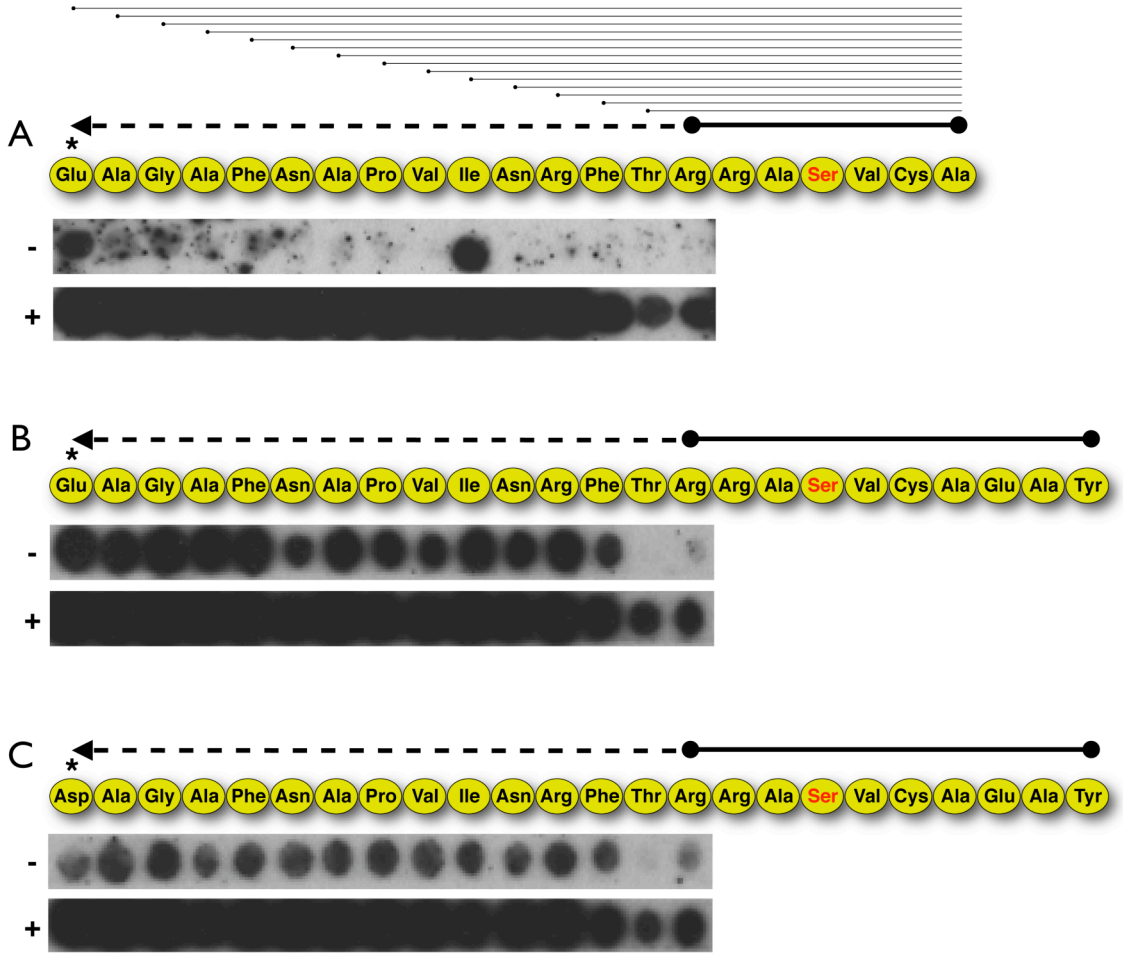

Figure 38. Peptide blots of RIIβ inhibitor sequences.

Each spot corresponds to a sequence beginning with the amino acid above the spot to the C-terminus of that particular sequence. Each blot was overlaid with free C-subunit (-) and with C-subunit + AMPPNP + Mg^{2+} (+). (A) Mouse sequence to P+3 position. The blot without AMPPNP was exposed for 2 minutes and the blot with AMPPNP and Mg^{2+} was exposed for 5 seconds. (B) Mouse sequence to P+6 position. Both blots were exposed for 30 seconds. (C) Human sequence to P+6 position. Both blots were exposed for 30 seconds. The asterisk marks amino acids that are different between mouse and human sequences. The amino acid in red designates the P-site.

In an effort to determine which amino acids are essential for binding to the C-subunit, we generated a peptide array that substituted each amino acid in the RIIβ peptide to one of the other 19 possible amino acids. We started with the parent peptide corresponding to the 13 amino acid human sequence RFTRRA<u>S</u>VCAEAY containing 6 residues before and after the P-site. The RIIα and RIIβ human sequences differ by only three residues (P-4, P-1, and P+5) and we wanted to assess whether these differences would change the overall amino acid footprint. We monitored the effect of nucleotide and magnesium on the interaction of these peptides with the C-subunit (Figure 39). In the absence of AMPPNP and Mg^{2+}, alanine mutagenesis affected 7 of the 13 positions. All of these positions were identical to the RIIα array. The only difference observed between the arrays was that alanine substitution of positions Arg (P-6) and Tyr (P+6) affected RIIα, but not RIIβ peptides binding to the C-subunit. In the presence of AMPPNP and Mg^{2+}, fewer peptides were sensitive to mutation (like the RIIα peptides) and only four residues exhibited discernible reduction in binding to the C-subunit: Arg (P-3), Arg (P-2), Cys (P+2), and Glu (P+4). Of these residues, only the glutamate differed from RIIα and appears to play a larger role in RIIβ binding to C-subunit.

4.3.4. Effect of phosphorylation site mimics

As stated in section 4.3.1, RII subunits are inhibitors as well as substrates for the C-subunit because of a serine at the P-site. However, the effect of phosphorylation on RII binding and inhibition has not been well studied. Glutamate mutations are often times used to mimic the negative environment of a phosphate group. Here, we monitored the effect of glutamate on C-subunit binding to our RII inhibitor sequence peptides. Figures

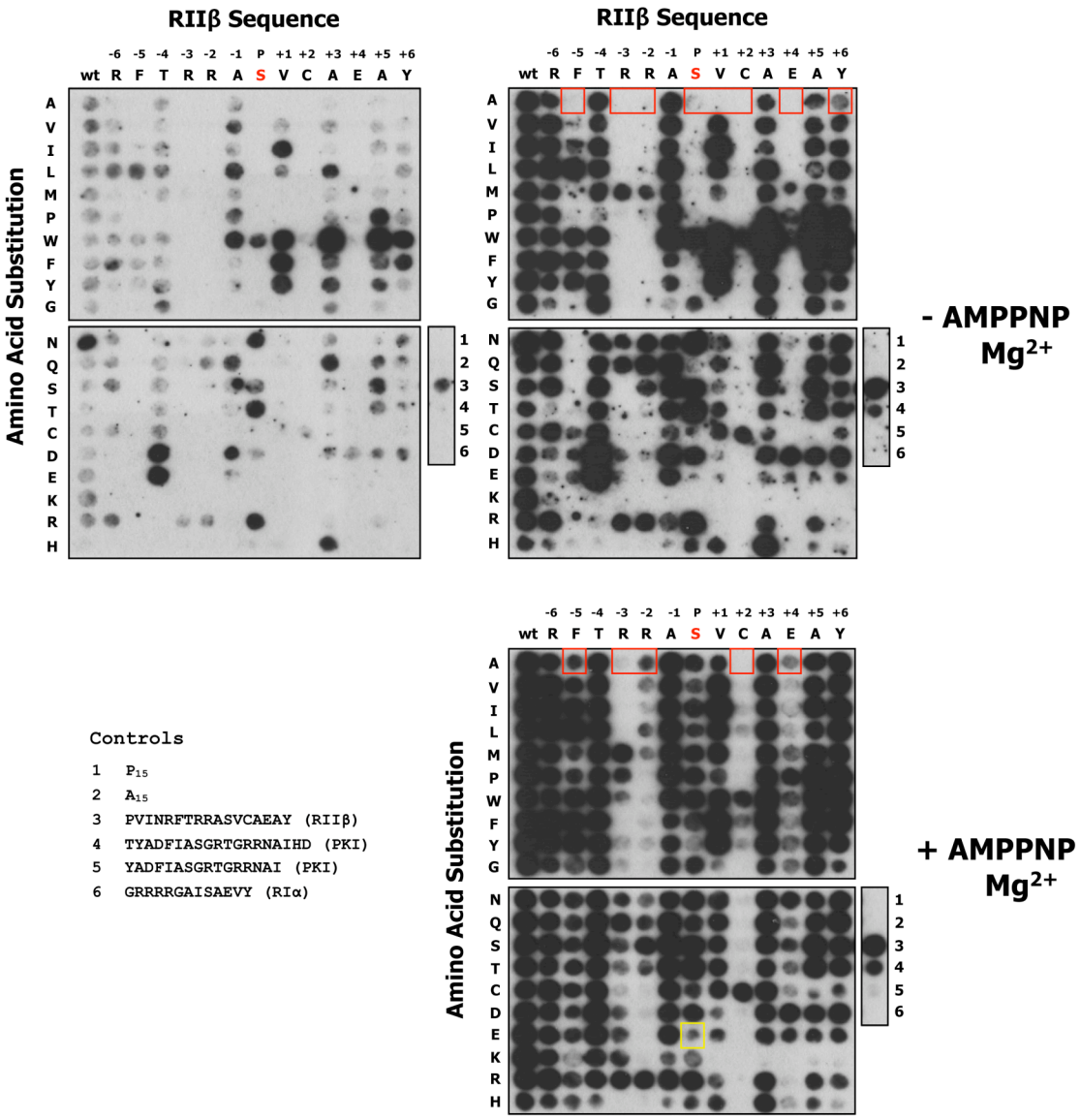

Figure 39. Amino acid substitution of RIIβ peptides.

RIIβ peptides were synthesized on a solid membrane support. Peptides were overlaid with C-subunit, then detected with α-PKA$_C$. Top panels were overlaid without AMPPNP. Different exposures are presented for comparison (left 30 seconds, right 10 minutes). The bottom panel was overlaid with AMPPNP (5 seconds). Red boxes indicate amino acids that were sensitive to alanine substitution. The yellow box highlights the phosphorylation mimic.

37, 39, and 40 highlight the effect of alanine and glutamate mutations at the P-site. For both RIIα and RIIβ, binding to the C-subunit is largely diminished with both mutants. Second, we mutated the RIα P-site from alanine to serine and observed increased apparent binding to the C-subunit (Figure 40).

4.3.5. PKI

PKI is another endogenous PKA protein inhibitor that is widely expressed in cells. It is a 76 amino acid protein that contains the PKA consensus sequence and a nuclear export signal. To assess the minimal component for high affinity binding to the C-subunit, we performed the same truncation analysis for PKI as we did for the R-subunit inhibitor sequences with P+3 and P+6 peptides. In addition, we generated arrays starting with peptides N-terminal to the P-site and added individual residues to the C-terminus to assess the contribution of the amino terminus (Figure 41).

Overall, the truncation peptide arrays demonstrated that binding between the C-subunit and PKI peptides occurred regardless of AMPPNP and Mg^{2+}. Furthermore, addition of the P+4, P+5, and P+6 residues did not affect C-subunit binding as they did for the RIIα and RIIβ peptides.

Although PKI peptides bound irrespective of AMPPNP and Mg^{2+}, the specific length of peptide that permitted C-subunit binding differed. In the absence of nucleotide, the shortest peptide that bound the C-subunit was an 18-mer consisting of 14 amino acids preceding the P-site and 3 amino acids following (very faint spots were also detected with slightly shorter sequences). In the presence of nucleotide the shortest peptide that bound the C-subunit was a 16-mer consisting of 12 amino acids preceding

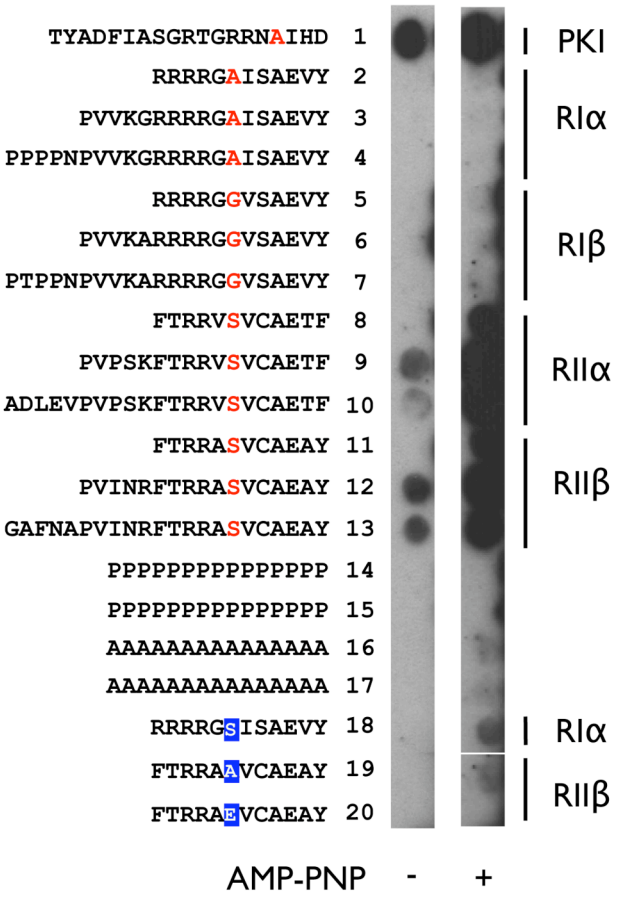

Figure 40. Summary of inhibitor sequence peptides and mutation of phosphorylation sites.

Each blot was overlaid with free C-subunit (-) and with C-subunit + AMPPNP + Mg^{2+} (+). The P-site is designated in red. Mutations from wild-type sequences are designated in blue. Both blots were exposed for 10 seconds. Mutation of RIα P-site from alanine to serine increased binding to the C-subunit (compare lanes 2 and 18). Mutation of RIIβ P-site from serine to either alanine or glutamate drastically decreased binding to the C-subunit (compare lanes 11, 19, and 20).

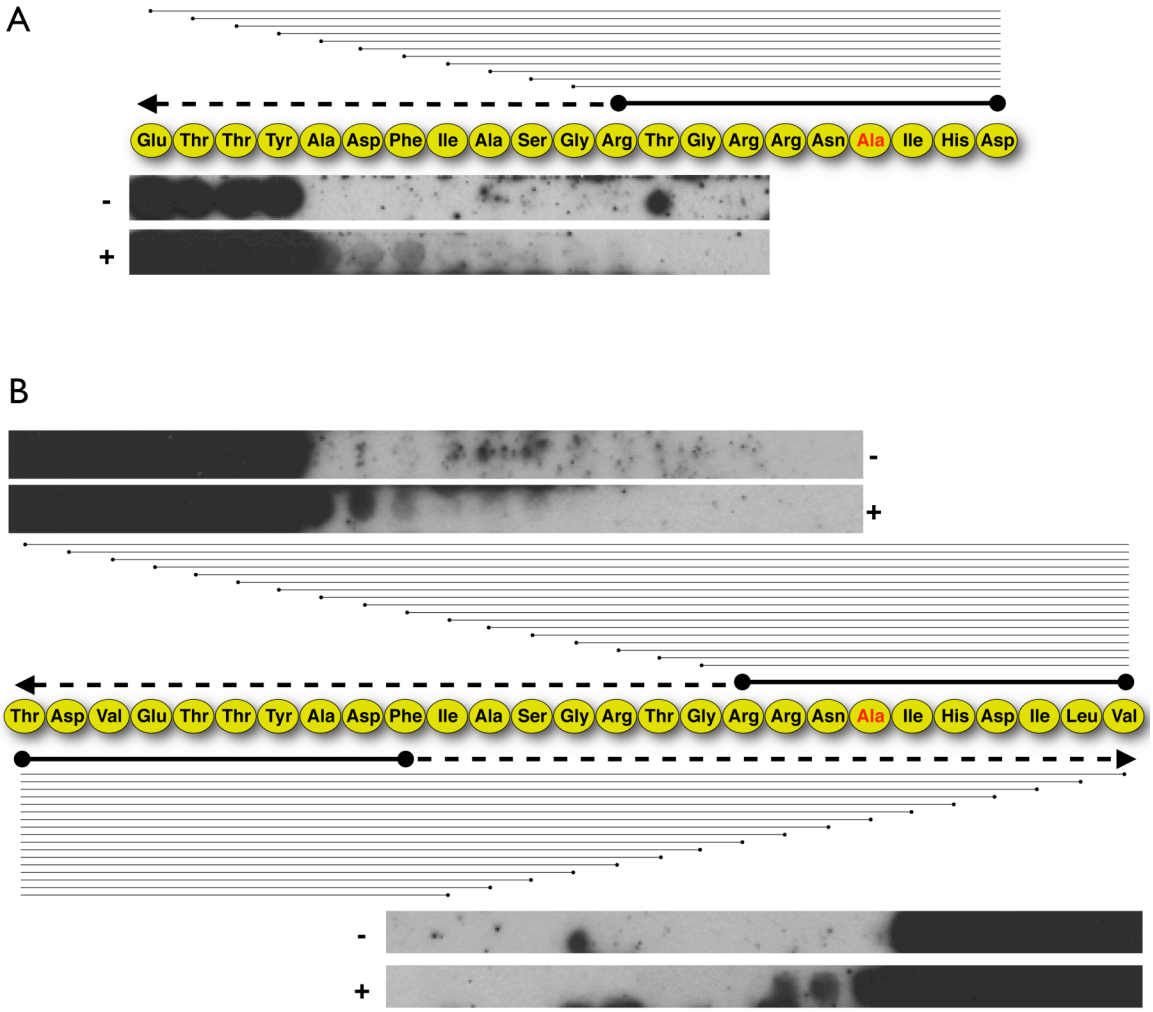

Figure 41. Peptide blots of PKI.

Each spot corresponds to a sequence beginning with the amino acid above the spot to the C-terminus of that particular sequence. Each blot was overlaid with free C-subunit (-) and with C-subunit + AMPPNP + Mg^{2+} (+). (A) Sequences to P+3 position. The blot without AMPPNP was exposed for 2 minutes and the blot with AMPPNP and Mg^{2+} was exposed for 5 seconds. (B) Sequences to P+6 position. Both blots were exposed for 30 seconds. The amino acid in red designates the P-site.

the P-site and 3 amino acids following. For comparison to RII, binding between the C-subunit was detected with peptides containing the 6 amino acids preceding the P-site. These results suggest that the binding affinity of PKI and C-subunit arises from a different source than the RII peptides. Since the arrays detected binding at a distal N-terminal site from the P-site, we generated an array that started with the first 10 residues of PKI, and adding single amino acids to the C-terminus. In the absence of nucleotide, peptides did not bind the C-subunit until a 22-mer ending with Ile (P+1), and in the presence of nucleotide, peptides did not bind until the 19-mer ending with Arg (P-4). Taken together, these results suggest that high affinity interaction between PKI and the C-subunit requires both the N-terminal helix and the inhibitor site.

To assess the contribution of each residue in PKI towards binding to C-subunit, we generated an array that replaced each amino acid in PKI with one of the other 19 naturally occurring amino acids. We used a parent peptide 19 amino acids long, corresponding to residues 6-25 (Figure 42). In the absence of nucleotide, alterations to many of the N-terminal amino acids were detrimental to C-subunit interaction, including the hydrophobic residues Tyr2, Phe5, Ile6, and the polar residues Ser8, Arg10, Gly12, Arg13, and Arg14. In the presence of nucleotide, more amino acid substitutions are tolerated overall. However, all of the same residues observed to affect C-subunit binding without nucleotide are also detrimental in the presence of nucleotide except Ile6 and Gly12.

4.3.6. Co-crystallization of RII Inhibitor Peptides and C-subunit

In an effort to understand how RIIα and RIIβ peptides interact with the C-subunit,

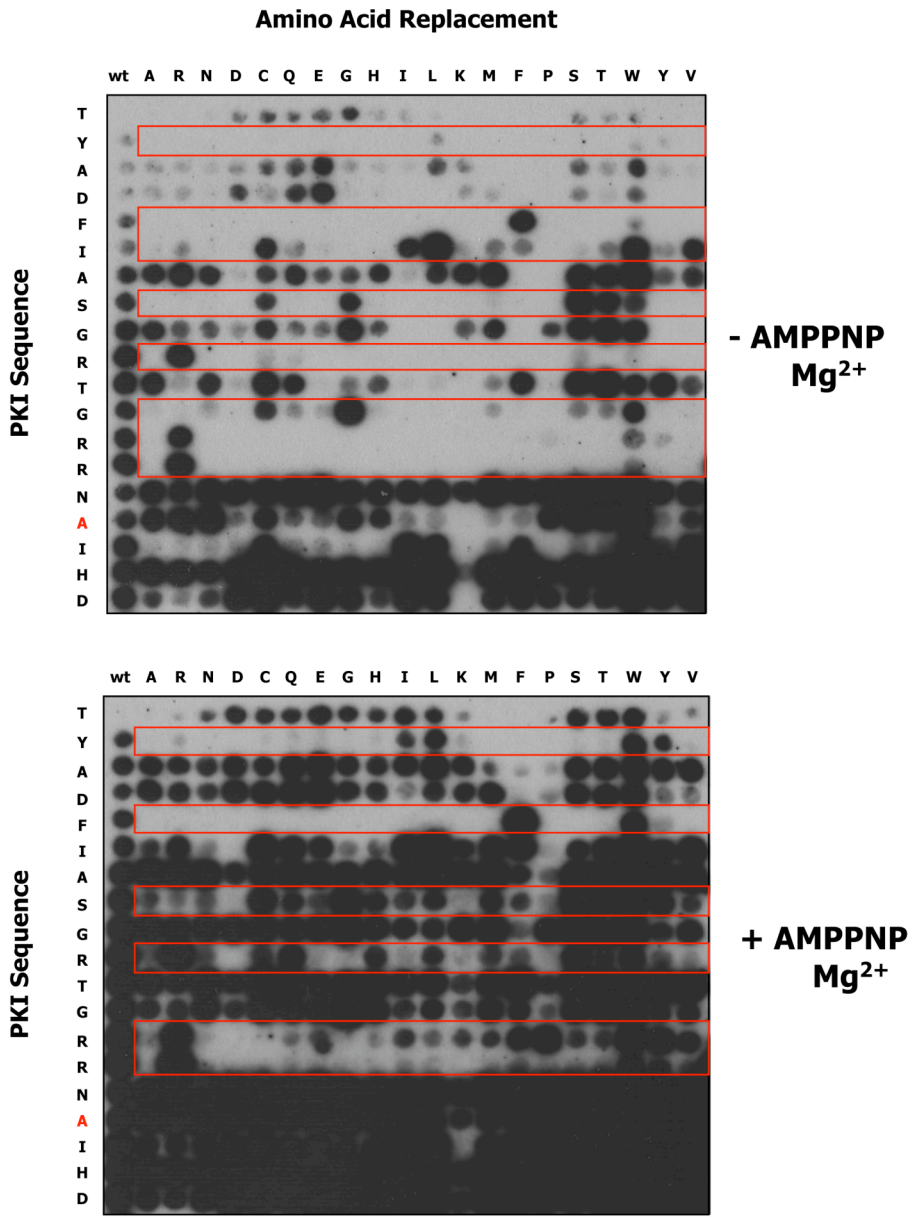

Figure 42. Amino acid substitution of PKI peptides.

PKI peptides are synthesized on a solid membrane support. Peptides are overlaid with C-subunit, then detected with α-PKA$_C$. Both blots were exposed for 10 seconds

we attempted to co-crystallize a long and short version of each isoform. The short peptide for RIIα and RIIβ corresponds to the shortest 13 amino acid segment that bound to C-subunit in the absence of AMPPNP and Mg^{2+}. The longest peptide is a 22 amino acid segment. Crystals have been obtained for each of the 4 complexes In the presence of ATPγS (Figure 43), but have not been tested for diffraction. Ongoing efforts are being made to solve the structure of these PKA:peptide complexes.

4.4 Discussion

The regulatory subunits are modular and dynamic proteins that mediate the allosteric regulation of PKA activation through its effector molecule cAMP. Binding of cAMP to the R-subunits leads to a conformational change that liberates C-subunit inhibition. Extensive biochemical and structural studies have focused on how different isoforms bind to and inhibit the C-subunit (Figure 32) as well as the mechanism by which holoenzymes are activated by cAMP. For RIα, this process is sequential where cAMP must first bind to Domain B before a second molecule can bind to Domain A and release the inhibition. For the RII subunits, cAMP can bind to either Domain A or Domain B to release the inhibition. Clearly, the allosteric mechanism that controls PKA activation through cAMP is distinct between the RI and RII subunits. What is not apparent is if and how the inhibitor sequences contribute to the allosteric process of PKA activation. Since the mechanism of activation differs between isoforms, we hypothesized that the RI and RII inhibitor sequences play distinct roles.

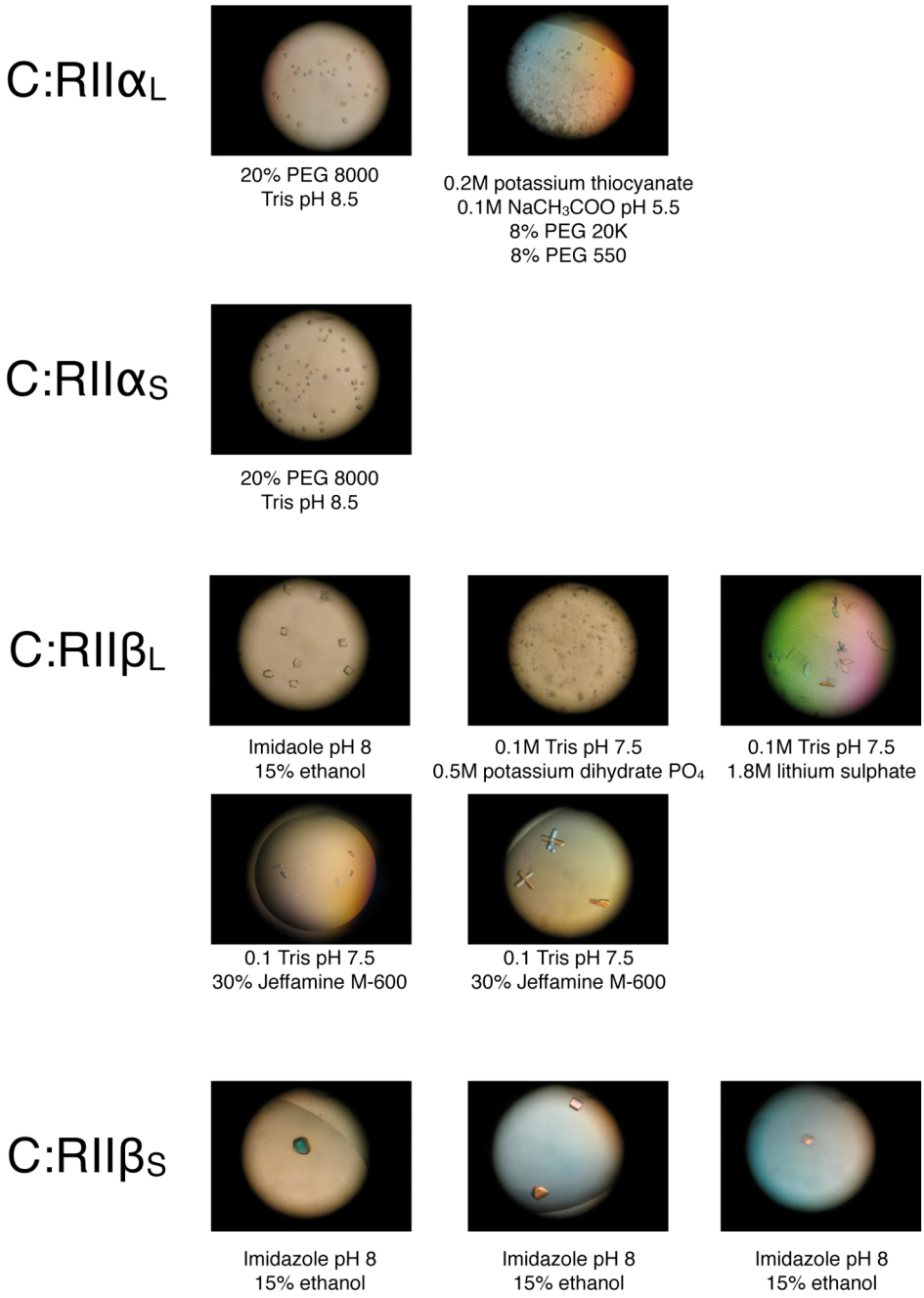

Figure 43. Co-crystallization of R-subunit inhibitor peptides, C-subunit, and ATPγS.

L designates long and S designates short.

4.4.1. Binding determinants for RII inhibitor sequences

In the arrays of inhibitor sequences, we uncovered RII, but not RI, peptides that bound with apparent high affinity to the C-subunit. Given the poor affinities between substrates and kinases, we were surprised to detect binding of any inhibitor sequences to the catalytic subunit. Moreover, we discovered RII peptides that can bind to C-subunits in the absence of nucleotide. In the absence of nucleotide for both RIIα and RIIβ peptides, we observed that residues flanking both sides of the P-site were essential for peptide binding. First, peptide binding to the C-subunit was not detected for sequences that lack the P+3 to P+6 residues, nor was peptide binding to the C-subunit detected until the P-6 residue (6 residues N-terminal to the P-site) was added (Figure 44). Thus, these two ends function as clamps to lock the peptide onto the large lobe of the C-subunit. In the absence of nucleotide, the small lobe is probably not engaged, as shown in the RIIα:C crystal structure (Figure 32), and relies solely on interactions with the large lobe. In the presence of nucleotide, these clamps were dispensable for binding to the C-subunit presumably because the small lobe was utilized to supply additional binding energy necessary for the high affinity interactions. The peptides bound to C-subunit regardless of whether the P+4, P+5, and P+6 residues were present. In addition, although the N-terminal clamp was not crucial for binding, it did enhance the interaction between C-subunit and the inhibitor peptides.

Without crystal structures of the RII peptides bound to the C-subunit, the precise molecular features that govern the interactions are not known. However, the amino acid substitution arrays offer a glimpse of which residues may be important. Although there are slight differences between the RIIα and RIIβ arrays, the general pattern of amino acids necessary for binding to the C-subunit in the absence of nucleotide emerges as

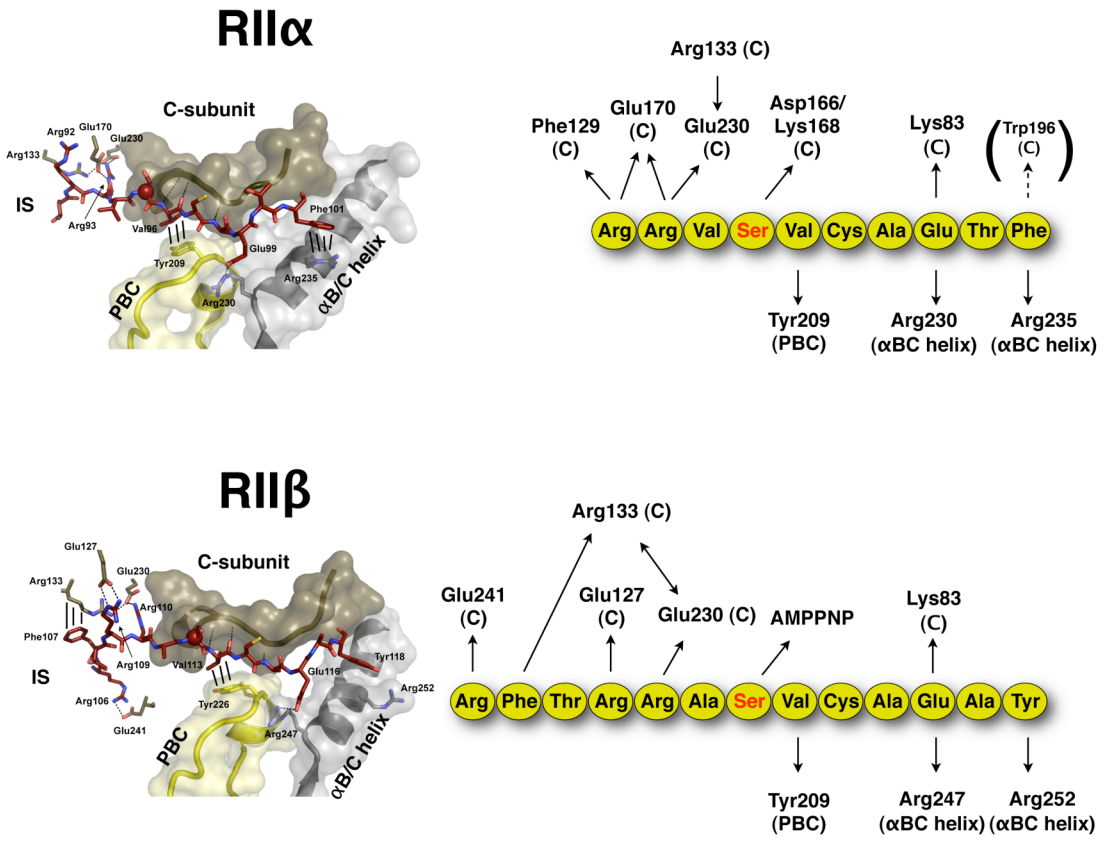

Figure 44. Detailed interactions of RIIα:C and RIIβ:C inhibitor sequences.

The C-subunit peptide positioning loop is depicted in brown. The R-subunit inhibitor sequence is depicted in red, the PBC in yellow, the αB/C helix in grey. Side chain interactions are outlined in the cartoon figure to the right. The backbone atoms from the P+1 and P+3 R-subunit residues are anchored to the C-subunit P+1 loop, shown in dashed lines. Trp196 does not interact with the P+6 residue in the R-subunit, but is in close proximity such that for the RII peptides alone (without the cAMP binding domains), the two residues may form a hydrophobic stack.

the following: (R)-φ-x-R-R-x-Z-φ-C-x-E-x-φ, where the first arginine is only important for RIIα, φ is any hydrophobic residue, and Z is Trp, Asn, Ser, Thr, Asp, Arg, or His.

Although efforts are still underway to co-crystallize the RII peptides and the C-subunit, the structures of two PKA:RII complexes ($RII\alpha_{AB}$:C and $RII\beta_A$:C:AMPPPNP:Mg^{2+}) can be utilized for initial analysis to see how the inhibitor peptides interact with the C-subunit. The interactions between the C-subunit and RIIα inhibitor sequence are mapped in Figure 44. The RIIα:C structure was solved in the absence of AMPPNP and Mg^2 and can be used to guide analysis of the peptide array data performed under the same condition. Indeed, interactions observed between the inhibitor site and C-subunit corroborates with the mutational data from the peptide array. Alanine mutagenesis affected Arg (P-3), Arg (P-2), Ser (P), Val (P+1), Cys (P+2), and Glu (P+4). (Unfortunately, density for P-6 to P-4 residues was not observed.) The P-3, P-2, P, and P+4 sites all form interactions with the C-subunit, explaining why substitution at these sites is detrimental to C-subunit binding. The structure does not explain why the P+6 residue was sensitive to amino acid substitution. Certainly, the peptide array data was done in the context of inhibitor sequences alone, which may very well bind differently to the C-subunit when the cAMP-binding domains are omitted. Presumably, the plasticity of short peptides would permit different conformations (whether it be side chain rotations or backbone flexibility) to accommodate features within the C-subunit active site cleft to achieve a high affinity interaction. For example, in the RIIα:C structure, Trp196 in the C-subunit is within 4 Å of the P+6 tyrosine in the R-subunit. Binding of the inhibitor sequence peptide to the C-subunit could allow the P+6 tyrosine to form a hydrophobic stack with Trp196, explaining why only substitution of other hydrophobic residues at this site are tolerated in the peptide array data.

For RIIβ, a crystal structure was solved with a construct containing only one of the two cAMP binding domains co-crystallized with C-subunit, AMPPNP, and Mg^{2+}. Like RIIα, the peptide array data support interactions observed in the crystal structure, except for the P-6 arginine and P+2 cysteine. The P-6 arginine interacts with Glu241 in the C-subunit, but the peptide array data shows that this site is not sensitive to substitution. Upon closer examination, the B-factor for this arginine in the crystal structure is rather high, making it plausible that this interaction is transient.

4.4.2. Comparison between RI and RII peptides

The next question is why do the RII but not RI inhibitor sequence peptides bind? The RI human sequence is **G/A**-R-R-R-R-G-**A/G**-**I/V**-S-A-E-V-Y. The RIα and RIβ sequences differ by only three residues at this site (marked in bold, where the first residue in the pair corresponds to RIα and the second corresponds to RIβ). Although the RI sequence closely follows the rule governing high affinity binding of RII peptides in the absence of nucleotide, they are not identical. The P-5, P, and P+2 residues do not follow the consensus sequence. First, RI contains an arginine at the P-5 site. In RII peptides, any hydrophobic residue is acceptable. In the context of the 13 residue peptide, the array data shows that this position is not amenable to arginine (Figures 37 and 39). Second, RI peptides contain either an alanine or glycine, whereas RII peptides contain a serine. The RIIα and RIIβ arrays show that the P-site serine is a critical determinant for binding the C-subunit. To assess whether placing a serine at the RIα inhibitor P-site would promote binding to C-subunit, we generated an array where the RIα alanine was mutated to serine. Indeed, enhanced binding was observed although not to the extent of

the RII peptides (Figure 40, lanes 2 and 18). Third, the RI subunits contain a serine at the P+2 site, whereas RII subunits contain a cysteine. Mutation of this cysteine for both RIIα and RIIβ resulted in decreased binding to the C-subunit. The RII peptide arrays were probed without DTT, so it is possible that the P+2 cysteine forms a disulfide bond with the reactive cysteine in the C-subunit. Individually, each of the three positions (P-5, P, and P+2) may not significantly increase the affinity of RI peptides to the C-subunit, but together may synergistically function to largely enhance binding to the C-subunit.

In the presence of nucleotide, only 4 positions were critical for high affinity binding to the C-subunit: Arg P-3, Arg P-2, Cys P+2, and Glu P+4. The RI inhibitor sequence contains all of these residues except the P+2 cysteine, suggesting that this is an important determinant for peptide binding. Of course, this observation is based solely on single amino acid changes within the peptide. It does not rule out the notion that the flanking residues together contribute to the affinity.

4.4.3. Binding determinants of PKI

In an effort to characterize how another endogenous protein binds to the active site cleft and to test our peptide array method, we investigated how the protein kinase inhibitor (PKI) achieves its specificity with the C-subunit. The binding constant between these proteins is 5 nM. Truncation analysis indicates that the driving force behind the high affinity interaction stems from elements between residues Tyr8 and Ile23 in the absence of AMPPNP/Mg^{2+} and Asp10 and Arg20 in the presence of AMPPNP/Mg^{2+}. In the absence of nucleotide, amino acid analysis indicates that the hydrophobic residues (Tyr8, Phe11, Ile12, and Ile23) and arginines (residues 16, 19, and 20) cannot be

substituted. The interaction between PKA and PKI has been extensively studied, and our results are consistent with those findings (Scott et al., 1985; Scott et al., 1986). This agreement supports utilization of peptide arrays to characterize peptide:protein interactions.

4.4.4. Proposed mechanism for allosteric regulation

We have critically analyzed the differences between RI and RII inhibitor sequence peptides to determine why RI but not RII inhibitor sequences bind to C-subunits. Furthermore, we established that RII inhibitor sequences could bind to C-subunits irrespective of whether nucleotide is present. We know that RI subunits cannot bind to C-subunits without ATP and Mg^{2+}, whereas RII-subunits do not have this dependency. Our results show that this difference stems (at least partly so) from the inhibitor sequence itself and that this is one way in which RI- and RII-subunits have evolved to develop independent modes of allosteric regulation.

The role of RI-subunits is simply to inhibit the C-subunit and to release this inhibition once cAMP is around. As previously discussed, the model of PKA-RIα activation is that cAMP first binds to Domain B, then Domain A before the C-subunit is released. Mutational data suggests that much of the affinity between the two subunits is concealed in the hydrophobic cluster at the beginning of the RIα αB/C helix (Huang and Taylor, 1998) and the hydrophobic interface between the C-subunit αG helix and the R-subunit cAMP-binding site in Domain A. Binding of cAMP to Domain B permits a conformational switch that releases the αB/C helix (and elements that stabilize cAMP in Domain A discussed in Chapter 2) and frees the cAMP-binding site in Domain A. Since

the inhibitor sequence only binds weakly to the C-subunit, once cAMP binds to Domain A, the two proteins most likely dissociate. We propose that the inhibitor sequence does not convey additional affinity between the C- and R-subunits, but is only tethered to Domain A and would be released once cAMP binds to Domain A.

The RII-subunits are also substrates as well as inhibitors of PKA, so they must be able to bind the catalytic subunits in the absence of nucleotide. Thus, not only are the RII-subunits regulated by cAMP, they are also regulated by ATP. In the absence and presence of nucleotide, our data shows that the inhibitor sequence itself can bind to the C-subunit, suggesting that the ability of RII-subunits binding to apo C-subunit stems from (or at least partly so) the inhibitor sequence. For both RIIα and RIIβ, the N-terminal end clamps to the C-subunit, while the C-terminal end clamps to both C- and R-subunits through side chain and main chain interactions (Figure 44). For RIIα and RIIβ, the C-terminal clamp comes from Glu (P+4) and Phe/Tyr (P+6) interactions with arginine from the R-subunit PBC and αB/C helix. In RIIα, Glu99 hydrogen bonds with Arg230 and Phe101 stacks with Arg235. In RIIβ, Glu116 forms a hydrogen bond with Arg247 and Tyr118 stacks with Arg252. Previous mutational studies show that mutation of the P+4 glutamate severely decreases the ability of RII subunits to inhibit the C-subunits (Gibson et al., 1997). The peptide array shows that these two residues are also important in the context of free inhibitor sequences binding to the C-subunit. The structures show that the inhibitor sequence is intimately linked to the PBC and the αB/C helix, the binding cAMP would provide enough energetic pull to strip the inhibitor sequence from the C-subunit.

Nature may have evolved RII inhibitor sequences to bind more tightly than RI inhibitor sequences to give them distinct modes of allosteric regulation, but we can also use this information as a foundation for designing peptide inhibitors specific to PKA.

Many efforts towards generating kinase-specific inhibitors have been focused on ATP analogs. Since most kinases bind to ATP, it has been a challenge to achieve distinct specificities. Given the unique nature of PKA where its inhibitor also serves as a substrate, we can hijack the inhibitor sequences that nature evolved to generate peptides highly specific for the C-subunit. Moreover, we have found peptides that bind to the catalytic subunit in the absence of nucleotide, which for PKA, has not been done before. This is beneficial for therapeutic development since it reduces the number of requirements needed for high affinity interactions. We are continuing our efforts to crystallize the RII inhibitor peptides with the C-subunit to determine the precise molecular map of how these peptides dock onto the catalytic subunit. Furthermore, we aim to quantify how tightly these peptides actually bind to the C-subunit. We hope that the structure and biochemical data will help guide us in the development of more potent peptide inhibitors.

4.5 Conclusions

Peptide array analysis was utilized to determine whether the short R-subunit inhibition sequences are sufficient to bind the catalytic subunit with high affinity. Only peptides corresponding to RII isoforms (but not RI) demonstrated detectable binding in the presence and in the absence of AMPPNP and Mg^{2+}. Specifically, the shortest peptide that bound to C-subunit in the absence of nucleotide and Mg^{2+} corresponds to a 13-mer that spans 6 residues before and after the P-site. The overall rule that governs high affinity binding between a peptide and C-subunit was determined to be R-φ-x-R-R-x-<u>Z</u>-φ-C-x-E-x-φ, where Z is Trp, Asn, Ser, Thr, Asp, Arg, or His. This study not only

gives a better understanding of the allosteric regulation of PKA, but also paves the way of potentially generating PKA-specific peptide inhibitors.

Chapter 5

Biochemical and Structural Characterization of Phospholamban-PKA Complex: Implications Towards Heart Disease

---

5.1. Introduction

cAMP dependent kinase (PKA) is a serine/threonine protein kinase that phosphorylates a wealth of intracellular substrates as a consequence of external signaling responses. PKA is comprised of two catalytic and two regulatory subunits. Binding of cAMP to each of the regulatory subunits dissociates the tetramer, permitting free active C-subunits to phosphorylate its downstream protein substrates. While Chapters 2-4 focused on understanding the allosteric mechanism by which RIα senses cAMP and releases the C-subunit, this chapter focuses on an example of how an actual substrate interacts with the catalytic subunit and how this information provides insights into heart disease.

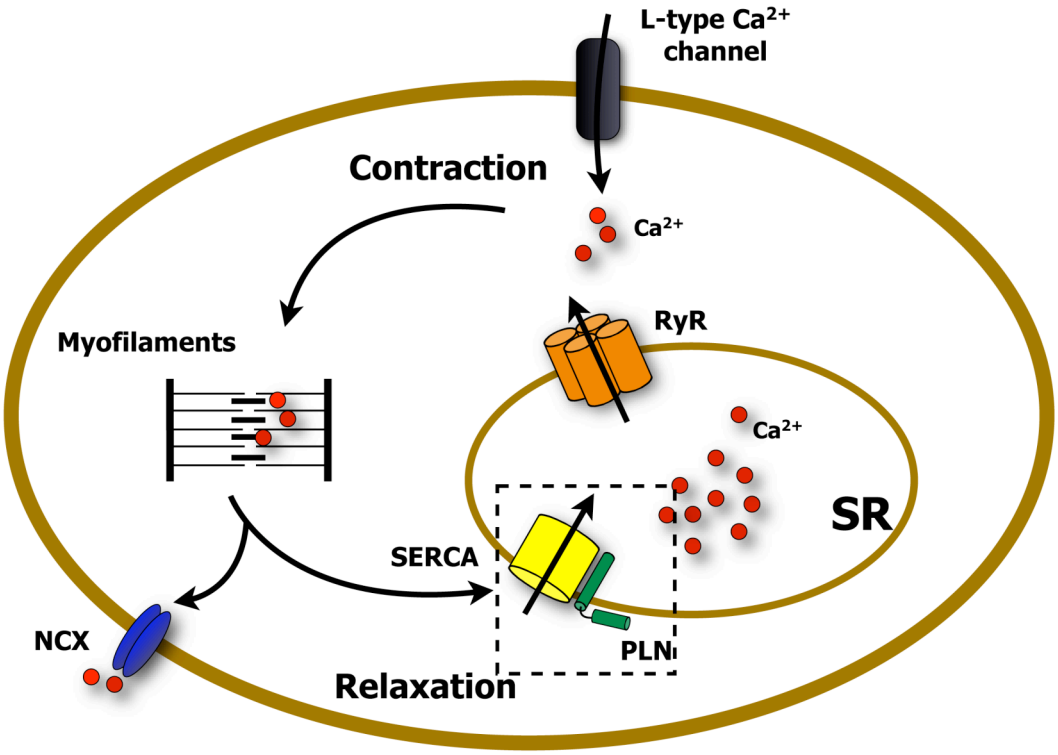

Figure 45. Calcium cycling in cardiac myocytes regulates cellular contraction and relaxation.

One of PKA's numerous substrates is a small 52 amino acid protein, phospholamban (PLN). Phospholamban is a single transmembrane protein that spans the sarcoplasmic reticulum membrane and helps orchestrate the cycling of Ca^{2+} in cardiac myocytes. This Ca^{2+} cycling process, in turn, regulates the contraction and relaxation of cytoplasmic myofilaments, or muscle cells (Figure 45). Contraction occurs when cytoplasmic Ca^{2+} binds to myofilaments, while relaxation occurs when the Ca^{2+} is released from the myofilaments and transported into the sarcoplasmic reticulum via the Ca^{2+}-ATPase or sarco(endo)plasmic reticulum calcium pump (SERCA). SERCA facilitates Ca^{2+} movement into the SR by switching between two conformations, one with high affinity for Ca^{2+} and a second with low affinity for Ca^{2+} (Stokes and Wagenknecht, 2000). SERCA, in turn, is regulated by phospholamban.

Unphosphorylated phospholamban binds to and inhibits SERCA function. Upon phosphorylation of phospholamban by either PKA (at serine 16) or CamKII (at serine 17), SERCA inhibition is relieved and cytoplasmic Ca^{2+} is transported into the sarcoplasmic reticulum (Figure 46) (Simmerman et al., 1986; Tada and Katz, 1982; Tada et al., 1975). This process is reversible through the action of cardiac SR-associated type 1 protein phosphatase (MacDougall et al., 1991). Studies have shown that phospholamban phosphorylation at only one of the two sites is sufficient to relieve SERCA inhibition and that phosphorylation of both sites does not further enhance SERCA function. *In vivo* studies show distinct phenotypes are induced between serine16 and serine17 phosphorylation, suggesting that the phosphorylation mechanisms are mutually exclusive (Mattiazzi et al., 2004; Mattiazzi et al., 2006; Vittone et al., 2008). Thus, phosphorylation of phospholamban by PKA signifies a major driving force for Ca^{2+} translocation.

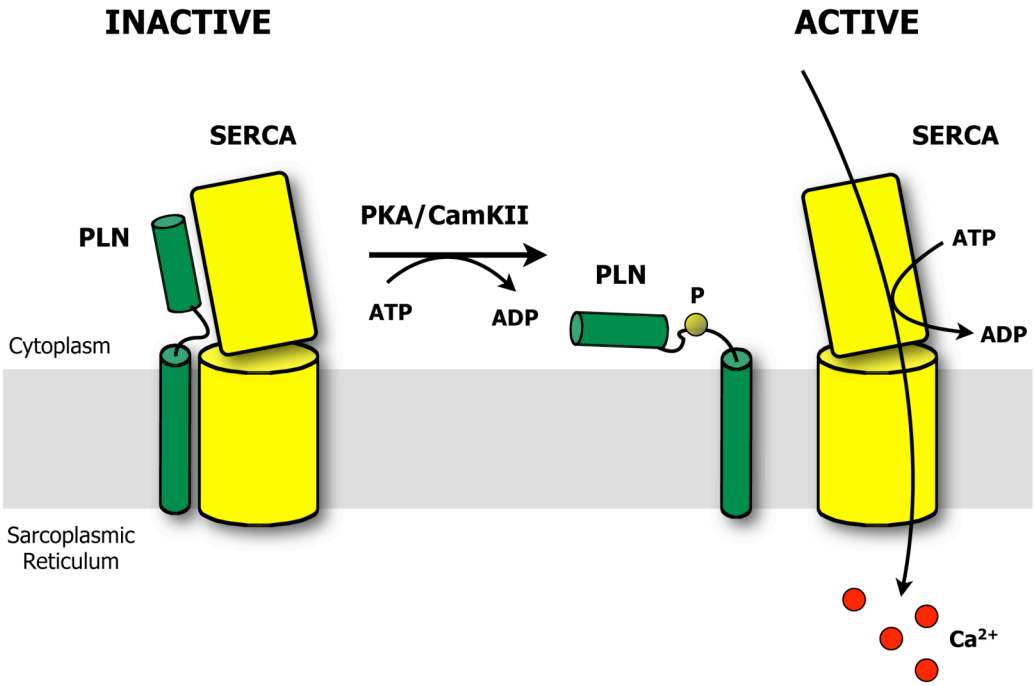

Figure 46. Activation of SERCA.

SERCA activity is inhibited when bound to unphosphorylated phospholamban. Phosphorylation of phospholamban by either PKA or CamKII releases the inhibition and Ca^{2+} is readily transported into the sarcoplasmic reticulum.

The solid-state NMR structure of the dephosphorylated form of phospholamban reveals a simple domain structure of two alpha helices: an N-terminal cytoplasmic amphipathic Domain Ia (residues 1-19), a linker region Domain Ib (residues 20-31), and a C-terminal single transmembrane Domain II (residues 32-52) (Figure 47) (Mascioni et al., 2002; Traaseth et al., 2007). The two phosphorylation sites are located within Domain Ia. Upon phospholamban phosphorylation by PKA, a portion of Domain Ia containing the phospho-serine unfolds, perturbing the structure and dynamics in this region (Mascioni et al., 2002; Mortishire-Smith et al., 1995; Oxenoid et al., 2007; Traaseth et al., 2006). Although the mechanism by which phosphorylated phospholamban releases SERCA inhibition is poorly understood, it is thought that the conformational change induced by phospholamban phosphorylation results in one of two scenarios: 1) phosphorylation of phospholamban results in complete detachment with SERCA, promoting the high Ca^{2+}-affinity conformation; 2) phosphorylation of phospholamban results in detachment of only the cytoplasmic domain from SERCA. Although no structural information is available for the phospholamban:SERCA interaction to distinguish between the two models mutational studies have mapped interaction sites at both Domain I and II (Tada and Toyofuku, 1996).

The regulatory role of phospholamban is crucial for normal cardiac function. Rabbits expressing high levels of phospholamban show significant morbidity and early death; reduced expression levels to 30% resulted in normal hearts, but show diminished levels of SR Ca^{2+} uptake (Pattison et al., 2008). Furthermore, recent studies directly link hereditary dilated cardiomyopathy to several phospholamban mutations: Arg9Cys (Schmitt et al., 2003), deletion of Arg14 (ΔR14) (DeWitt et al., 2006; Haghighi et al., 2006), and premature stop codon at Leu39 (Haghighi et al., 2003). Leu39 is located in

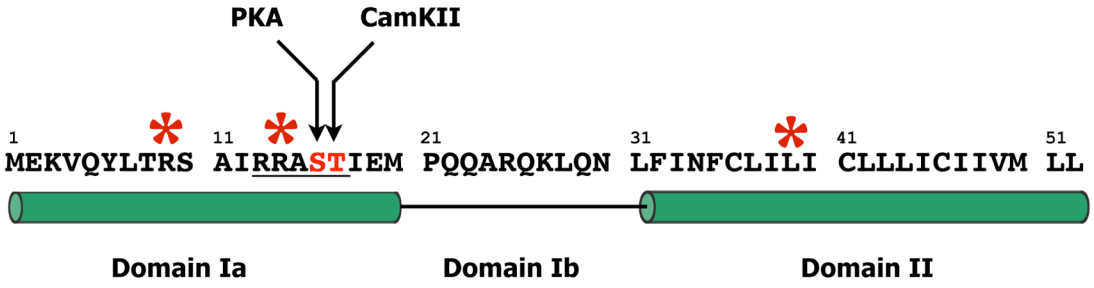

Figure 47. Phospholamban domain organization.

Phospholamban is comprised of an N-terminal cytoplasmic region (domain I) and a C-terminal single transmembrane region (domain II). Asterisks indicate single point mutations associated with inherited dilated cardiomyopathy.

the transmembrane domain of phospholamban. Premature chain termination at Leu39 would presumably prevent proper insertion of phospholamban in the SR membrane and block effective inhibition of SERCA. Transgenic mice expressing both the R9C and ΔR14 recapitulated human cardiomyopathies where they had similar histopathologic abnormalities, dramatic increases in heart size, and premature death. Over-expression of ΔR14 in HEK293 cells led to SERCA superinhibition. While R9C did not affect SERCA activity, it could not be phosphorylated by PKA and even appeared to prevent phosphorylation of wild-type phospholamban proteins.

The biochemical explanation by which these phospholamban mutants lead to detrimental phenotypes is not well understood. This chapter describes our use of structural and biochemical techniques to 1) understand the molecular details that govern phospholamban interaction with the C-subunit of PKA and 2) elucidate the molecular basis of why PKA phosphorylation is diminished in the R9C and ΔR14 mutations that give rise to dilated cardiomyopathies.

5.2. Experimental Methods

5.2.1. Materials

An E203Q C-subunit mutant for fluorescence polarization assays was generated by Quikchange mutagenesis (Stragene) using the following oligos:

E203Q-F: 5' GG ACC TTG TGT GGG ACC CCT **C**AG TAC TTG GCC 3'

E203Q-R: 5' GGC CAA GTA CT**G** AGG GGT CCC ACA CAA GGT CC 3'

The mutant was expressed in *e.coli* BL21 cells and purified in the same manner as wild-type C-subunit (Gangal et al., 1998). Protein yields for both mutants were similar to that of the wild-type protein.

The phospholamban peptide used in crystallographic studies corresponded to the N-terminal 19 amino acids with the sequence MEKVQYLTRSAIRRASTIE. The peptide was synthesized by Larry Masterson at the University of Minnesota, purified by HPLC, and verified by mass spectrometry.

N-terminally labeled 5-FAM phospholamban peptides (residues 1-19) were purchased from GeneScript Co. (Piscatway, NJ) at 98.7% purity for fluorescence polarization assays. Since the C-subunit phosphorylation site was located on the cytoplasmic domain of phospholamban, we thought it was sufficient to use the first 19 residues in our binding assays. The sequences of each peptide are as follows:

fPLN: 5-FAM MEKVQYLTRSAIRRASTIE

fPLN-R9C: 5-FAM MEKVQYLTCSAIRRASTIE

fPLN-ΔR14: 5-FAM MEKVQYLTRSAIRASTIE

0.5 mg of each peptide was initially dissolved in 40% DMSO. Since some precipitates remained, the solution was centrifuged at 13,000 RPM. The soluble fraction was removed and filtered through 0.22 μM spin columns. The concentration of each peptide was determined by measuring A_{485} (ε=68000 $M^{-1}cm^{-1}$).

5.2.2. Peptide array

An array of phospholamban peptides was synthesized with the MultiPep Flexible Parallel Peptide Synthesizer (Intavis Bioanalytical Instruments, Germany). The array

consisted of peptides corresponding to residues 1-19 of phospholamban, with N-terminal covalent attachments to the membrane support. Each membrane was probed for binding to the C-subunit in the presence and absence of AMPPNP/Mg^{2+} and binding was identified by antibody detection methods, as described in Figure 48a.

Membranes were first washed with ethanol, water, 1x TTBS (each for 10 minutes), then blocked with 5% milk (in TTBS) for 20 minutes. The membranes were then incubated with C-subunit in 5% milk overnight at 4°C. The overlays were washed with TTBS (3x, 5 minutes each) and incubated with α-PKA_C (BD Transduction Laboratories, CA) for one hour at room temperature. The blots were again washed with TTBS (3x, 5 minutes each) then incubated with α-mouse (BD Biosciences, Franklin Lakes, NJ) for one hour at room temperature. The membranes were then placed on a dry surface and probed with SuperSignal West Pico Chemiluminescent Substrate for detection of HRP (Thermo Scientific Product #34090). When no signal was detected, SuperSignal West Femto Maximum Sensitivity Substrate (Thermo Scientific Prod #34095) was used to increase signal sensitivity at both 1:100 dilution and 1:10 dilution.

To assess the effect of nucleotide on substrate-enzyme binding, 1 mM AMP-PNP and 1 mM $MgCl_2$ were added to the C-subunit overlays then probed in the same fashion.

5.2.3. Crystallography

The catalytic subunit was expressed and purified in *E. coli* as described previously (Gangal et al., 1998). The major peak fraction (peak 2) was dialyzed into 50 mM bicine (pH 8.0), 150 mM ammonium acetate, and 10 mM DTT at 4°C overnight then concentrated to 23.8 mg/ml.

The PKA C-subunit:phospholamban complex was obtained by combining a 1:10:10:10 molar ratio mixture of C-subunit (7 mg/ml), PLN, $MgCl_2$, and AMP-PNP. The protein mixture was incubated on ice for 2 hours then filtered with 0.2 μm centrifugal devices (Life Sciences). Crystallization trials were setup on CrystalClear Duo sitting drop plates (Douglas Instruments) using the Oryx8 Protein Crystallization Robot (Douglas Instruments, UK). Commercial HT crystal screens were used to determine initial crystallization conditions (PACT, JCSG, Proplex, Structure Screen I&II, Clear Strategy I, and Clear Strategy II (Molecular Dimensions)). Screens were done with 0.5 μl drops, testing both 50% and 70% protein concentrations and 4°C and 22.5°C temperatures.

Initial crystal hits were optimized using the Oryx8 robot. The final condition was 4.3 mg/ml C-subunit, 0.09 M sodium malonate (pH 7.0), 15.5% PEG 3350, which produced 0.2 – 0.3 μm sized tetragonal crystals at 22.5°C. Crystals were harvested, transferred to mother liquor consisting of 15% glycerol, and flash-frozen in liquid nitrogen. Diffraction data were collected to 2.8 Å at The Advanced Light Source (Lawrence Berkeley National Laboratory, Berkeley, CA) on beamline 2.2.1.

5.2.4. Data processing and refinement

Diffraction data were integrated and scaled with HKL2000 (Otwinowski, 1997). The space group was unambiguously determined to be P61. Initial phases were generated by molecular replacement using the program molrep (Vagin, 1997) and the coordinates of the PKA C-subunit:IP20 complex (PDB code 1ATP) (Knighton et al., 1991c) as a search model. The PKI peptide was removed from the PDB file to prevent biases in the model. Two molecules were found in the asymmetric unit (RFZ=13.6,

RFZ=26.5 for molecule 1 and RFZ=8.8, TFZ=38.7 for molecule 2) corresponding to a solvent content of 52%. All ambiguous main chains and side chains were removed and manually rebuilt using Coot (Emsley and Cowtan, 2004), followed by iterative cycles of structure refinement using REFMAC in the CCP4 suite (1994; Murshudov et al., 1997). Upon inspection of the F_o-F_c maps, electron density in the N-terminal lobe for one of the two molecules did not match with the model so residues 32-89 were removed. Both peptide and nucleotide appeared to be absent in this molecule so we thought it could be the apo form of the C-subunit. We aligned the large lobes of the apo structure (PDB code 1J3H) (Akamine et al., 2003) and our second molecule to obtain a rough estimate of the small lobe position. Coot was utilized in subsequent model building and REFMAC for refinement. The phospholamban peptide was not manually built until all atoms in the C-subunit were satisfactorily refined. TLS refinement (Winn et al., 2001) was implemented for each lobe. Simulated annealing via the program Phenix (Adams et al., 2004; Adams et al., 2002) was used in the final stages of refinement because geometric restraints were too loose with REFMAC. The final R and R_{free} values were 21.6% and 28.7%, respectively, with excellent geometry. The final model contained C-subunit residues 16-350 bound to AMP-PNP, two Mg^{2+} ions, and phospholamban residues 5-15 in the first molecule and the apo form of C-subunit with residues 13-350. Water molecules were manually incorporated. All figures were made using PyMol (DeLano Scientific).

5.2.5. Fluorescence polarization

Fluorescence polarization (FP) was first described in 1926 (Perrin, 1926) but not utilized for quantification of biological systems until 40 years later (Dandliker and Feigen,

1961). The basic principle behind FP is the ability of fluorophores to absorb polarized light. When plane-polarized light excites a solution of fluorescent molecules, the molecules parallel to the plane are excited. The extent to which fluorescent molecules rotate during its excitation lifetime determines its anisotropy, or polarization. Thus, molecules that remain stationary during the excitation period will continue to be excited, while highly mobile molecules will rotate and cease to be excited by the plane-polarized light. Consequently, fluorescence polarization can be used to measure the apparent molecular weight of proteins since larger proteins rotate more slowly than smaller ones. The rotational rate of a molecule is described by the rotational correlation time θ, given by:

$$\theta = \frac{\eta V}{RT} \qquad \text{(Equation 5.1)}$$

where η is the viscosity, V is the molecular volume, R is the gas constant, and T is the termperature (in Kelvin). FP can therefore be used to monitor the interaction between two proteins since binding of a fluorescence molecule to another molecule increases its volume (or molecular weight) and consequently changes its rotational correlation time. In a FP experiment, the observed polarization value is a weighted average between free and bound fluorescent molecules, and thus a direct measure of fraction bound. FP is advantageous because it does not require the use of radiolabeled ligands, requires small amounts of material, is not time-consuming, and amenable to high throughput format.

Fluorescence polarization was utilized to quantify phospholamban:C-subunit interactions in the presence and absence of AMPPNP/Mg^{2+}. Three phospholamban mutants (PLN_{1-19}, $PLN_{1-19}\Delta R14$, and $PLN_{1-19}R9C$) and two C-subunits (wild-type and E203Q) were analyzed. All C-subunits were dialyzed into 20 mM H_2PO_4, 150 mM KCl, 5

mM DTT, (pH 6.5). Each fluorescence polarization reaction consisted of 45 μl of a C-subunit dilution and 5 μl of assay mix, solution A or solution B. Solution A consisted of 5 mM DTT and 500 nM fluorescent peptide and solution B consisted of 1 mM AMPPNP, 10 mM $MgCl_2$, 5 mM DTT, and 500 nM fluorescent peptide. 2 fold C-subunit dilutions were made in 20 mM H_2PO_4, 150 mM KCl, 5 mM DTT, (pH 6.5), ranging from 0.5 nM to 500 nM and each mixed with either solution A or solution B. Reactions were incubated for 45 minutes at room temperature in black bottom Costar 96-well half area plates (Corning). Non-specific binding was determined in the presence of 10 μM unlabeled phospholamban peptides. Fluorescence polarization readings were taken on a GenesisPro plate reader (Tecan, NC) with 485 nm excitation (20 nm bandpass) and 535 nm emission (20 nm bandpass) filters. The gain optimization was automated, 10 readings were taken and averaged per well, and the G-factor was set to 1.0062496. Fluorescence polarization (FP) measurements were based on:

$$FP = \frac{I_{\parallel} - I_{\perp}}{I_{\parallel} + I_{\perp}} \qquad \text{(Equation 5.2)}$$

where $I_{\parallel}$ is the intensity parallel to the excitation plane and $I_{\perp}$ is the intensity perpendicular to the excitation plane. The polarization unit, P, is a dimensionless parameter independent from the intensity of emitted light and concentration of fluorophore. Polarization measurements are given in mP, or one-thousandth of P. mP readings were corrected for non-specific binding and converted to anisotropy measurements by the relation:

$$r = \frac{2P}{3 - P} \qquad \text{(Equation 5.3)}$$

where r is the anisotropy measurement and P is the polarization measurement. Saturation binding curves were fit using a 1:1 binding model with Prism4 software (GraphPad Software, Inc., San Diego, CA). Each protein was tested in triplicate.

5.3. Results

5.3.1. Peptide Array identifies phospholamban residues important for C-subunit recognition

PKA substrates contain the consensus R-R-X-S/T-φ motif, where φ is any hydrophobic residue. Peptide array analysis of the phospholamban peptide indicates that substitution of amino acids flanking the PKA consensus motif with acidic residues (aspartate or glutamate) and lysine decreased the apparent binding for the C-subunit (Figure 48b, purple boxes). To complement the basic nature of PKA substrates, the active site cleft of the C-subunit is predominantly acidic. These opposing charges presumably draw the two proteins together to help promote phosphoryl transfer from ATP to the substrate serine or theronine. In the peptide array, not only are basic residues needed near the phosphoryl transfer site, charged residues surrounding the consensus sequence are not tolerated.

To assess which amino acids are critical for phopholamban:C-subunit complex formation, phospholamban peptides 19 amino acids in length were synthesized on a cellulose membrane support. A grid of peptides was generated such that each position in phospholamban was mutated to each of the other 19 possible naturally occurring amino acids. The membrane was probed for binding to C-subunit in the presence and absence of AMP-PNP and Mg^{2+} by antibody detection methods (Figure 48a). Figure 48b shows

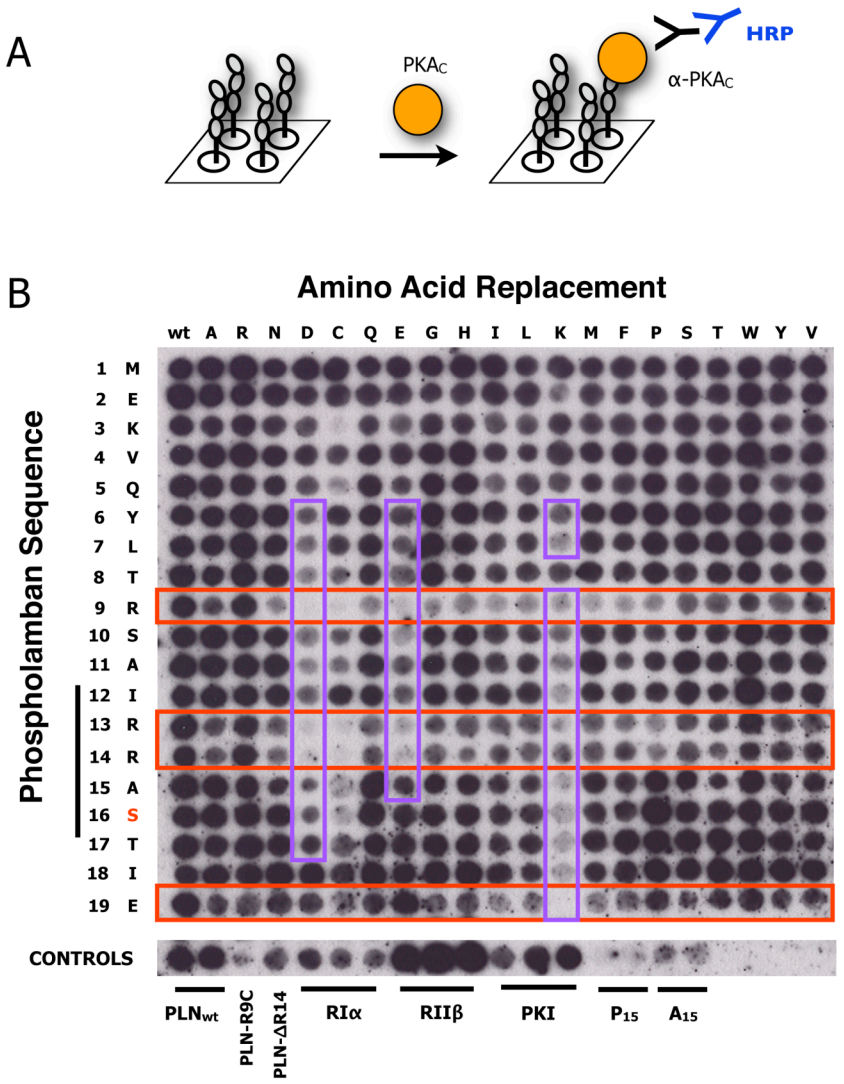

Figure 48. Peptide array of phospholamban peptides.

(A) Schematic of peptide array. Phospholamban peptides are synthesized on a solid membrane support. Peptides are overlaid with PKA_c, then detected with α-PKA_c. (B) Amino acid substitution of phospholamban peptides overlaid with PKA_c. Arg9, Arg13, Arg14, and Glu19 have low tolerances for substitution with the other amino acids.

that Arg9, Arg13, Arg14, and Glu19 have low tolerances for substitution with other amino acids compared to the wild-type sequence, suggesting that these residues are important for binding to the C-subunit. Peptides with cysteine substitution appeared to affect binding, but empirical data suggests peptides containing cysteines do not behave consistently in the arrays.

5.3.2. Structural Overview of the PKA C-subunit:PLN:AMPPNP Complex

The structure of phospholamban$_{1-19}$, AMP-PNP, and Mg^{2+} bound to C-subunit was solved to 2.8 Å resolution using the C-subunit:IP20:ATP:Mg^{2+} structure (1ATP) as a molecular replacement probe. The complex crystallized in the P61 space group with a tetragonal morphology containing 52.0% solvent content and 2 molecules in the asymmetric unit (asu) (Table 4). Only one of the two molecules in the asu contained a phospholamban peptide bound to the C-subunit (Figure 49). (The C-subunit molecules with and without peptide are subsequently called molecules 1 and 2, respectively.) Backbone structural alignment of molecule 1 in the PLN:C-subunit complex with the C-subunit from either RIα:C-subunit or PKI:C-subunit (Kim et al., 2007; Knighton et al., 1991b) complexes match precisely. The small lobe is collapsed against the large lobe, with the peptide between the domains, typical of the PKA closed conformation. Despite the presence of phospholamban peptide, AMP-PNP, and two Mg^{2+} ions in molecule 1, electron density for several regions typically ordered in closed conformation C-subunits was not observed. These include the N-terminus (residues 1-16), the glycine rich loop (residues 52-54), and the C-terminal tail (residues 339-342) (see Figure 4 for reference). NMR dynamics analysis was done on the same phospholamban peptide bound to the C-

Table 4. Data and refinement statistics for the phospholamban$_{1-19}$:C-subunit:AMPPNP:Mg^{2+} complex.

Beamline	ALS bl2.2.2
Space Group	P61
Cell Dimensions (Å)	a=b=92.2, c=192.2
Number of crystals	1
Wavelength (Å)	1.0
Mosaicity (°)	0.8-1.4
Total No. reflections	264629
Average redundancy	10.5
Unique reflections	25304
Resolution range for refinement (Å)	39.1 to 2.8
Rsym[a] (%)	8.4 (48)
Completeness (%)	99.5
$\langle I \rangle / \langle \alpha \rangle$	38.8 (5.1)
Total reflections used	26095
No. molecules per asu	2
Number of protein atoms	5210
Number of water molecules	21
RMSD bond lengths (Å)	0.006
RMSD bond angles (°)	0.951
R_{work}[ll]	21.6
R_{free}	28.7
Wilson B factor (Å^2)	51.6

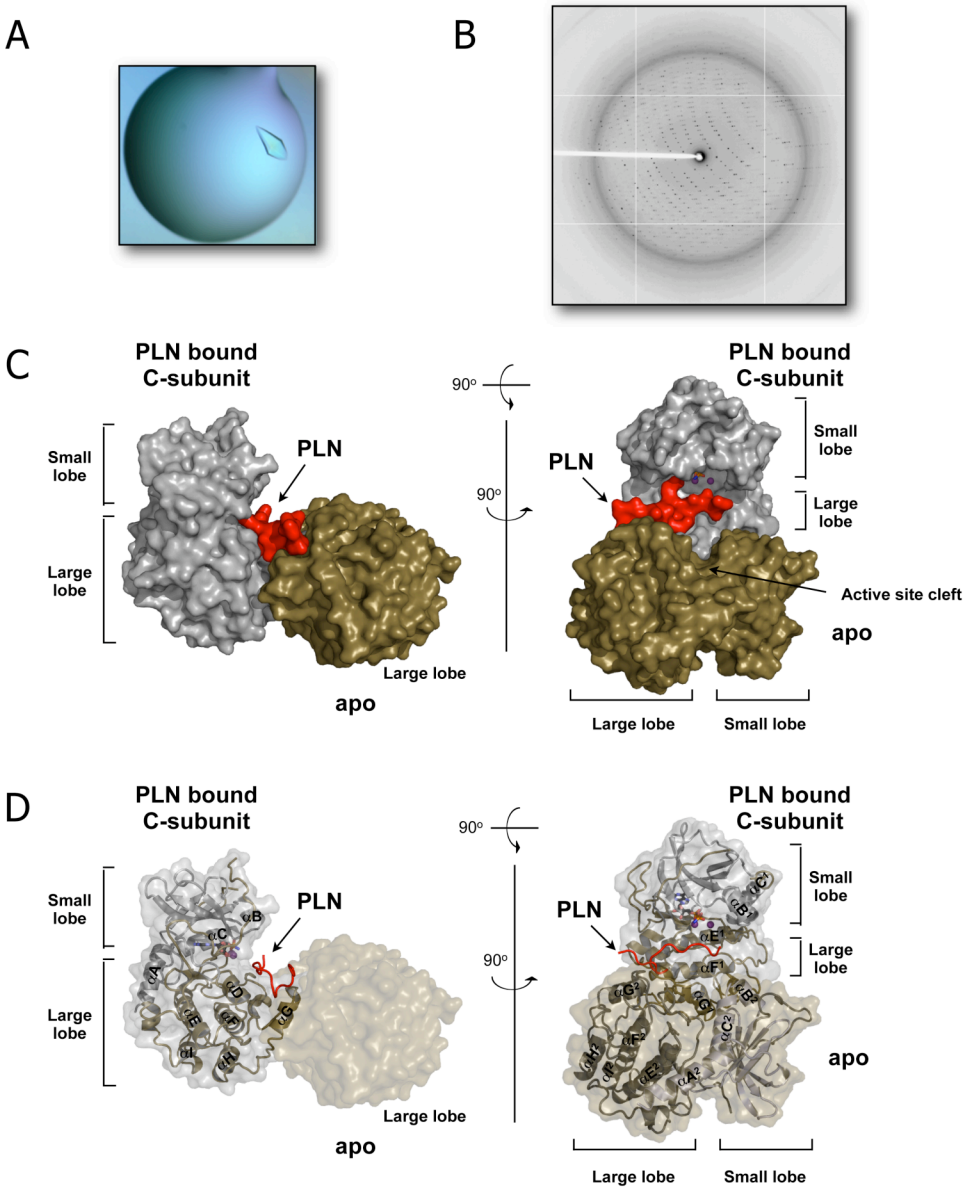

Figure 49. Structure of PKA C-subunit bound to Phospholamban$_{1\text{-}19}$.

(A) Tetragonal crystals diffracted to 2.8 A. (B) Diffraction image collected at the Advanced Light Source (Lawrence Livermore National Laboratory). (C) Structural overview of the C-subunit:phospholamban complex. Two C-subunit molecules were found in the asu: one bound to phospholamban (white) and the second was the apo form (tan). Phospholamban is in red, AMP-PMP in sticks, and Mg^{2+} in purple. (D) Cartoon rendering of the overall complex. Superscripts in the right panel denote helix labels for molecule 1 (PLN bound) and molecule 2 (apo).

subunit. These results also indicated a highly dynamic glycine rice loop and C-terminal tail (Larry Masterson, data not shown), corroborating with our crystallographic observations that these regions are indeed dynamic.

In contrast, molecule 2 is in an open apo conformation, consistent with a previous apo structure of the C-subunit (Akamine et al., 2003). In this conformation, the N-terminal small lobe is displaced away from the large lobe. Intriguingly, the phospholamban peptide is sandwiched between the two C-subunit molecules (Figure 49c). While most of the phospholamban peptide sits on the large lobe of molecule 1, molecule 2 is packed orthogonally to molecule 1 and binds to the N-terminal region of phospholamban. The non-polar residues from both phospholamban (Tyr6 and Thr8) and molecule 2 (Ile210, Leu211, Ile244, Val251, and Tyr247) are buried at the protein:protein interface. The remainder of molecule 2 is packed entirely against the large lobe of molecule 1, such that the αG helix of molecule 1 is located in the active site cleft of molecule 2 (Figure 49d).

The structure of free unphosphorylated phospholamban contains an N-terminal helix (residues 1-19), a flexible linker region containing the PKA phosphorylation site (P-site, serine 16), and a C-terminal single transmembrane region (residues 32-52) (Mascioni et al., 2002; Traaseth et al., 2007). In our structure of the phospholamban:C-subunit complex, phospholamban looses most of its helical structure to accommodate interactions within the active site of molecule 1 and against the large lobe of molecule 2. Figure 50 (left) illustrates how the surface of phospholamban precisely complements the groove of the C-subunit active site. There is a slight semblance of a helix where the carbonyl of Thr8 forms a hydrogen bond with the backbone nitrogen of Ile12, four residues apart like a conventional α-helix. However, no other backbone residues within

phospholamban form hydrogen bonds. Instead, the backbone hydrogen bond creates a single twist in the backbone. The relevance of this twist will be discussed below. Out of the 19 amino acids in the peptide, electron density was observed for only residues 5-15, presumably because the N- and C-terminal ends are dynamic.

5.3.3. Detailed interactions at the active site cleft

Although electron density for many of the phospholamban side chains were not ordered in the crystal structure, those that were ordered formed ionic interactions with the C-subunit. Within the R-R-X-S-φ consensus sequence, the two arginine residues ($Arg13^P$ and $Arg14^P$) form hydrogen bonds with $Glu127^C$ and $Glu230^C$, respectively, in the same manner as other structures of PKA:inhibitor complexes (RIα, RIIα, RIIβ, and PKI). Also within the C-subunit active site are two backbone interactions ($Arg14^P$:$Lys168^C$ and $Thr17^P$:$Gly200^C$) that anchor phospholamban to the C-subunit large lobe. These interactions together define the molecular features that make up the R-R-X-S-φ consensus sequence. The P-site serine is also perfectly positioned to accept the γ-PO_4 from AMPPNP (Figure 50, center), similar to that observed in the RIIβ:C-subunit:AMPPNP crystal structure (Brown, Submitted). Although the PLN:PKA:AMPPNP structure is not a transition-state mimic (Madhusudan et al., 2002), it shows the conformation of how the substrate aligns with the γ-phosphate prior to phosphate transfer.

We analyzed our peptide arrays to determine which interactions observed in the crystal structure are actually important for phosopholamban:C-subunit complex formation (Figure 48). Substitution of either $Arg13^P$ or $Arg14^P$ in phospholamban to any of the other

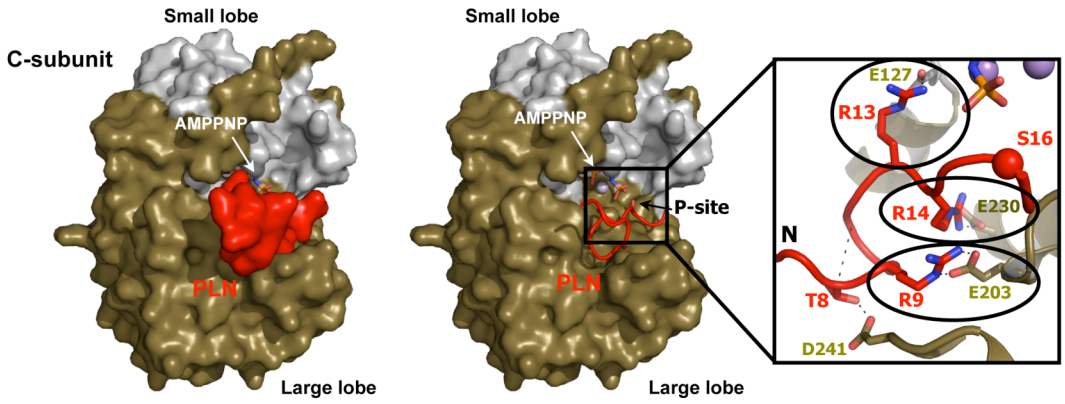

Figure 50. Hydrogen bond interactions between C-subunit and phospholamban.

C-subunit small lobe is shown in white and the large lobe in tan. Phospholamban is shown in red. Left, phospholamban is illustrated with surface rendering. Center, phospholamban is illustrated in cartoon. Serine 16 (P-site) is positioned to accept γ-PO_4 from AMPPNP. Right, detailed ionic interactions between phopholamban and the C-subunit. The lone dashed line is a hydrogen bond interaction between backbone atoms of Thr8 and Ile12.

amino acids decreases the binding to the C-subunit. Both the ionic and hydrophobic properties of arginine are essential for peptide docking since lysine substitution did not preserve the apparent binding affinity. In fact, based on the array, the apparent binding affinity between the C-subunit and phospholamban is only slightly reduced upon replacement of Arg13^{P} and Arg14^{P} with hydrophobic residues, namely tryptophan and tyrosine. In light of the phospholamban:C-subunit structure, Arg13 forms hydrophobic stacking with the neighboring amino acids Phe129^{C} and Glu127^{C}, therefore justifying why this site can tolerate other hydrophobic residues.

In contrast to structures of PKA:inhibitor complexes, there are two unique ion pairs that anchor the phospholamban peptide to the large lobe of the C-subunit: Thr7^{P}-Asp241^{C}, Arg9^{P}-Glu203^{C} (Figure 50). The α-helical kink in phospholamban described in section 5.3.2 could be responsible for positioning Arg9 within hydrogen bond distance to Glu203 in the C-subunit. It is also possible that crystal packing from the second C-subunit molecule influences the conformation observed in the structure. As described above, molecule 2 packs against the N-terminal end of phospholamban. Whether the dimerization of the C-subunit is physiologically relevant is unclear. But based on our peptide array data, (Figure 48) the two salt bridges appear to be important for phospholamban binding to the C-subunit. Mutation of Thr7^{P} to aspartate or glutamate and substitution of Arg9 with any amino acids diminishes the ability of the C-subunit to bind phospholamban. These data suggests that both the Thr7^{P}-Asp241^{C} and Arg9^{P}-Glu203^{C} ionic interactions play an important role in peptide recognition.

5.3.4. Biochemical analysis of Glu203 on phospholamban binding

To investigate the contribution of the Glu203^{C}-Arg9^{P} salt bridge towards phospholamban and C-subunit interaction, a Glu203Gln (E203Q^{C}) mutant was engineered and binding constants were measured by fluorescence polarization. Fluorescence polarization has been used to measure the affinity between fluorescently labeled IP20 (PKI, residues 5-20) and C-subunit (Saldanha et al., 2006). Here, conjugation of the probe at the N-terminus significantly improved the K_D compared with conjugation at the C-terminus. Thus, we used this rationale and purchased phospholamban peptides with N-terminal 5-FAM conjugations.

Mutatation of glutamate to glutamine is the most conserved change that removes the charge moiety, but preserves the length of the side chain. FP measurements indicate a three-fold lower affinity between 5-FAM phospholamban and wild-type compared with E203Q^{C} in the absence of nucleotide, where the K_D was 131.3 ± 18.3 μM and 519.3 ± 93.4 μM for wild-type and E203Q^{C}, respectively (Figure 51). These results imply that the charge interaction provided by Glu203 plays a significant role in PKA substrate recognition.

Upon addition of AMP-PNP, the K_D for wild-type C-subunit and phospholamban decreased from 131.3 ± 18.3 μM to 31.7 ± 3.6 μM. AMP-PNP had no affect on binding between E203Q^{C} and the phospholamban peptide (K_D = 566.2 ± 67.2 μM).

5.3.5. Effect of phospholamban peptide length on C-subunit complex formation

To determine the minimum component of phospholamban needed to bind to the C-subunit, we synthesized an array of peptides containing varying lengths of

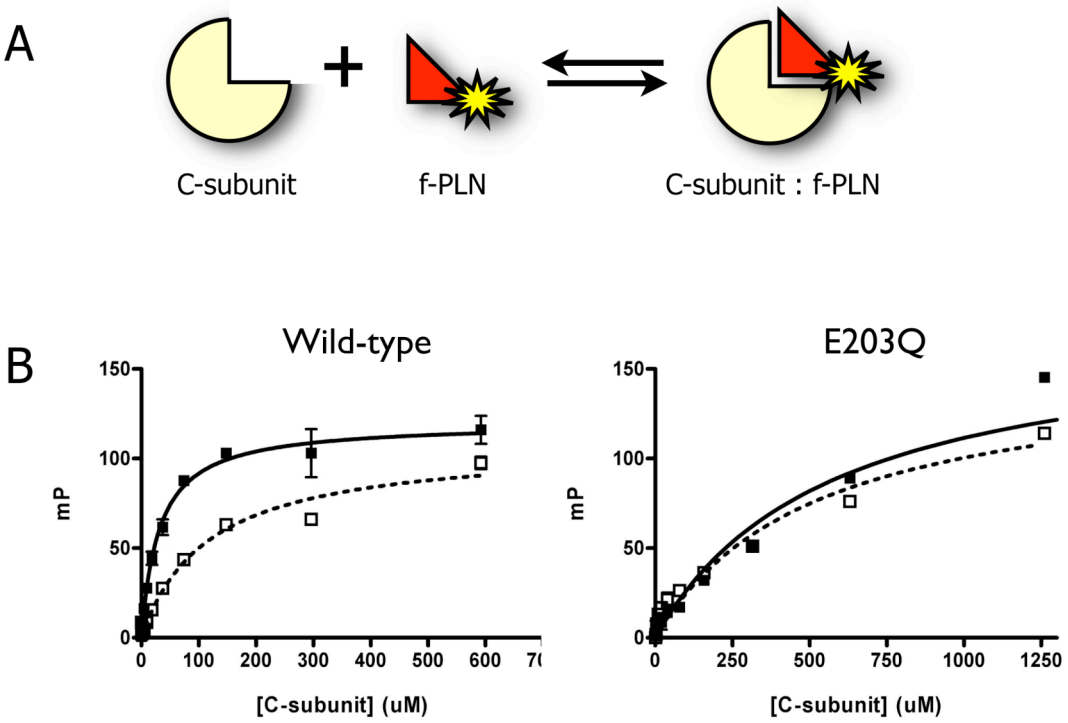

C

	WT	E203Q
- AMPPNP/$MgCl_2$	131.3 ± 18.3 µM	519.3 ± 93.4 µM
+ AMPPNP/$MgCl_2$	31.7 ± 3.6 µM	566.2 ± 67.2 µM

Figure 51. Effect of AMP-PNP on f-PLN binding to wild-type and E203Q C-subunit.

(A) Schematic of fluorescence polarization (FP) assay. Binding of 5-FAM phospholamban to C-subunit was measured by change in FP between bound and unbound probe. (B) Effect of AMP-PNP and E203Q PKA_C binding to 5-FAM phospholamban peptides. FP assays were performed with (solid) and without (dashed) AMP-PNP. (C) Calculated K_D values.

phospholamban. The shortest sequence was RRA<u>S</u>TIE, from which we added 1 amino acid at a time to the C-terminus (the P-site serine is underlined for reference). We also tested the effect of AMPPNP/Mg^{2+} on C-subunit binding (Figure 52). In the absence of nucleotide, no apparent binding was observed between phospholamban and C-subunit. The peptide array method appears to be insensitive to affinities in the 100 μM range, since our FP analysis measured the K_D to be 131.3 μM for the 1-19 peptide. In contrast, in the presence of nucleotide, we detected binding of phospholamban peptides to the C-subunit. The smallest peptide that bound the C-subunit corresponded to the 11 amino acid peptide containing Arg9. Addition of two more residues (Leu7 and Thr8) dramatically increased the apparent binding affinity. These data further support the notion that Arg9 plays an important role in substrate:enzyme recognition. The addition of Leu7 and Thr8 may help stabilize the backbone twist to bring Arg9 near its interacting partner $E203^C$ (Figure 50, right). Whether this backbone twist is physiologically relevant is unclear because it is possible that crystal packing of molecule 2 against the N-terminus of phospholamban may induce this helical twist (Figure 49).

5.3.6. Effect of phospholamban ΔR14 and R9C mutations on C-subunit interactions

Phospholamban mutations ΔR14 and R9C are correlated with dilated cardiomyopathy. We utilized fluorescence polarization to assess the effect of these mutations on the binding affinity for the C-subunit (Figure 53). In the presence of AMPPNP for both mutants, we measured a significant difference in the binding affinity from wild-type phospholamban. The K_D was 31.7 ± 3.6 μM for wild-type, 273.2 ± 76.8 μM

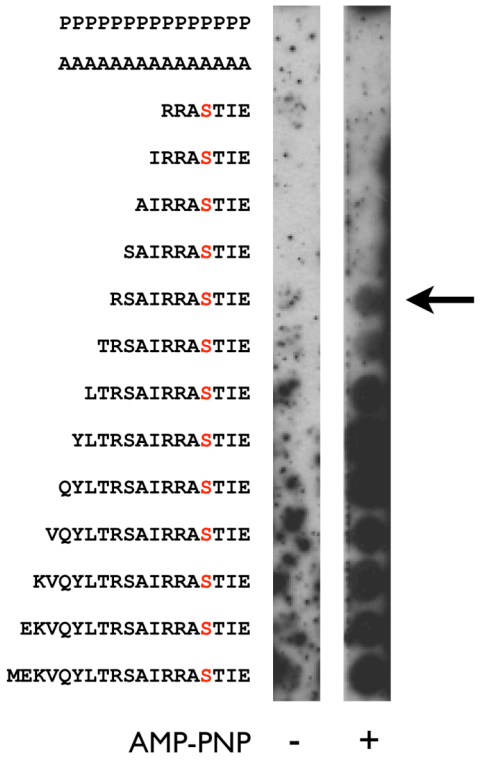

Figure 52. Effect of phospholamban peptide length and AMP-PNP on binding to the C-subunit.

Synthetic phospholamban peptides were generated on a membrane support and probed for C-subunit binding. The minimum peptide that bound to C-subunit is designated with an arrow. The C-subunit phosphorylation site is highlighted in red. The blot without AMPPNP was exposed for 2 minutes and the blot with AMPPNP was exposed for 5 seconds.

for ΔR14, and 464.5 ± 200.3 μM for R9C. In the absence of AMPPNP, the K_D was 131.3 ± 18.3 μM for wild-type and 388.5 ± 43.7 μM for ΔR14. Unfortunately, the concentration of protein needed in our assay reached the solubility limit of C-subunit and an accurate top point could not be obtained. Suffice to say, the binding constants we measured are the upper limits of what the K_Ds actually are. R9C did not show specific binding to the C-subunit in the absence of AMPPNP.

5.4. Discussion

5.4.1. AMPPNP traps phospholamban within the C-subunit active site

Although a number of structures have been solved with the PKA C-subunit bound to its endogenous protein inhibitors (RIα (Kim et al., 2007), RIIα (Wu et al., 2007), RIIβ (Brown, Submitted), and Protein Kinase Inhibitor, PKI (Knighton et al., 1991b)), there are no structures of the C-subunit bound to non-regulatory subunit substrates. Here, we report the first structure of a C-subunit complex with an endogenous substrate, phospholamban. Presumably, crystallization of enzyme:substrate complexes has been elusive because of the intrinsic low affinity between substrates and their respective enzymes. In the past, other enzymes have been co-crystallized with low affinity peptide substrates by utilizing non-hydrolyzable ATP analogs such as AMPPNP or ATP-γS to trap substrates in a transition-like state. For PKA, co-crystallization of RIIβ (which is both an inhibitor and substrate of PKA since it has a serine at the P-site) and the C-subunit in the presence of AMPPNP was successful (Brown, Submitted). AMPPNP essentially trapped RIIβ into the active site cleft of the C-subunit. We presumed that AMPPNP would also trap phospholamban in a complex with the C-subunit by increasing the apparent

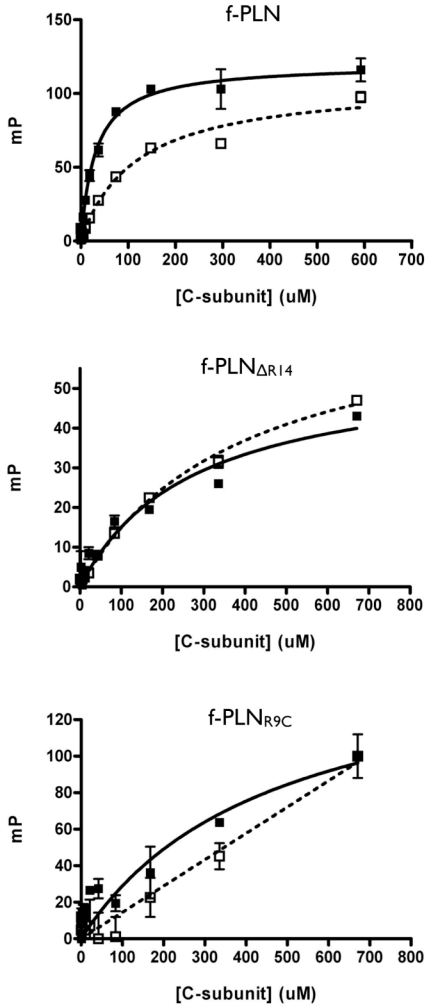

	WT	f-PLN$_{\Delta R14}$	f-PLN$_{R9C}$
- AMPPNP/$MgCl_2$	131.3 ± 18.3 μM	388.5 ± 43.7 μM	N/A
+ AMPPNP/$MgCl_2$	31.7 ± 3.6 μM	273.2 ± 76.8 μM	464.5 ± 200.3 μM

Figure 53. Effect of phospholamban mutations ΔR14 and R9C on binding to wild-type C-subunit.

Saturation binding curves were measured by fluorescence polarization using 5-FAM labeled PLN, PLN$_{\Delta R14}$, and PLN$_{R9C}$ peptides. FP assays were performed with (solid) and without (dashed) AMP-PNP. (C) Calculated K_D values.

affinity of the two proteins. We confirmed this hypothesis by measuring the equilibrium dissociation constants of phospholamban in the presence and absence of AMPPNP. Indeed, our fluorescence polarization data shows a four-fold increase in binding affinity between phospholamban and C-subunit in the presence of nucleotide (K_D = 31.7 ± 3.6 μM) than in the absence of nucleotide (K_D = 131.3 ± 18.3 μM) (Figure 51). We pursued crystallization of the ternary complex and successfully solved the structure of the C-subunit bound to phospholamban and AMPPNP to 2.8 Å resolution.

5.4.2. Comparison of the PLN:C-subunit complex with other PKA structures

To date, four protein complexes with PKA C-subunit have been crystallized: RIα, RIIα, RIIβ, and PKI. The C-subunit adopts a closed conformation in all but the RIIα complex since the nucleotide was omitted in the crystallization process. In each of these structures, the inhibitor sequence binds to the active site cleft in a similar fashion, where the two consensus arginines interact with the same respective glutamate partners in the phospholamban:C-subunit complex (Figure 44 and 50).

In phospholamban, a third arginine (Arg9 at the P-7 position) makes a contact with Glu203 in the C-subunit. None of the inhibitor proteins contain a P-7 arginine. However upon closer examination, each inhibitor possess an arginine residue N-terminal to the consensus sequence, although from different positions in sequence relative to the P-site. In RIα, this arginine is located at the P-4 position. In both PKI and RIIβ, this arginine is located at the P-6 position. In all cases, this N-terminal arginine interacts with Glu203 in the C-subunit (Figure 54). Clearly, the arginine-glutamate pair is structurally

conserved across many protein:PKA interactions and could not have been predicted by sequence alignment alone (Figure 55).

To evaluate the contribution of the $Arg9^P$:$E203^C$ salt bridge in substrate recognition, we engineered a $E203Q^C$ C-subunit mutation and tested its ability to bind phospholamban. Indeed, the K_D increased from 31.7 μM to 566.2 μM for wild-type and $E203Q^C$, respectively. Furthermore, our peptide array analysis indicates that phospholamban mutagenesis of $Arg9^P$ to any of the other amino acids decreases the apparent binding to the C-subunit (Figure 38). Lastly, phospholamban truncation experiments show that removing the first 7 residues slightly decreases binding to the C-subunit, while removing the entire sequence from the N-terminus to $Arg9^P$ completely abolishes binding to the C-subunit (Figure 52). The phospholamban:C-subunit structure reveals a twist in the phospholamban backbone between residues 7 and 9, stabilized by backbone hydrogen bonds. As discussed in section 5.3.2, this twist may help position $Arg9^P$ to come in contact with $Glu203^C$. Taken together, the peptide array analysis, site-directed mutagenesis, and fluorescence polarization measurements show that the $Arg9^P$:$Glu203^C$ interaction significantly contributes to the affinity between phospholamban and C-subunit. In the case of PKI, previous studies showed that Glu203 also plays a major role in maintaining high affinity between the C-subunit and PKI. Mutation of this residue to either alanine or glutamine significantly compromised the ability of PKI to inhibit PKA (Baude et al., 1994). Thus, the presence of an N-terminal arginine appears to be an additional determinant for PKA substrate recognition.

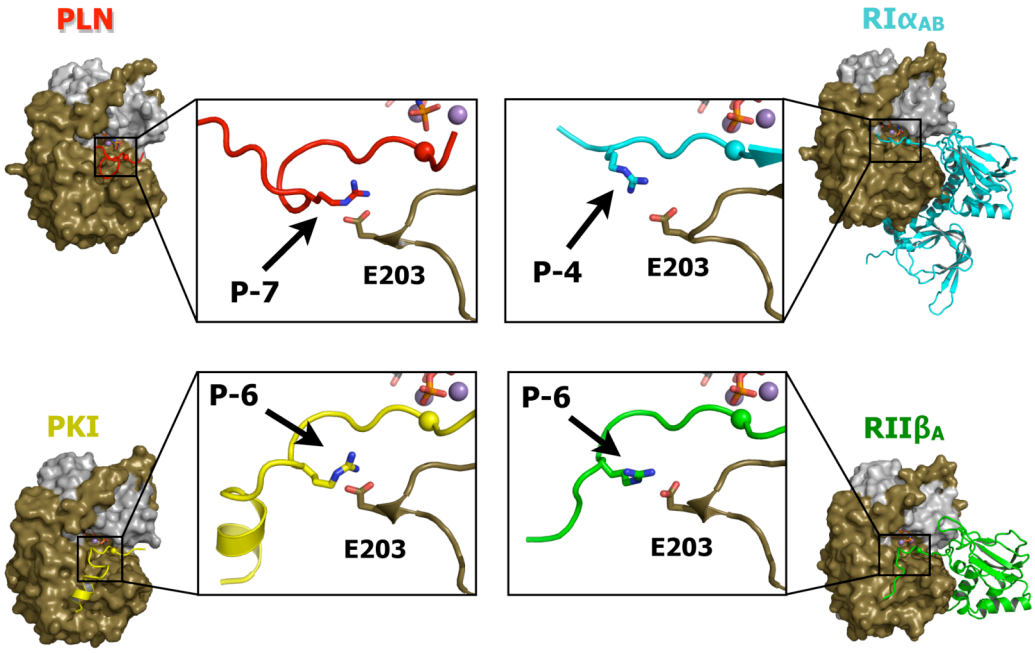

Figure 54. N-terminal Arginine and Glu203^C Interaction is Conserved.

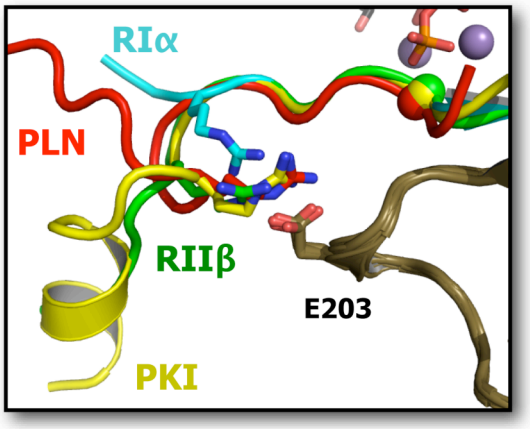


```
                        P-7 P-6 P-4   P-site
PLN     MEKVQYLTRSAIRRASTIE
PKI     TYADFIASGRTGRRNAIHD
RIα     PPPPNPVVKGRRRRGAISA
RIIβ    GAFNAPVINRFTRRASVCA
```

Figure 55. Role of Glu203 in C-subunit Substrate/Inhibitor Recognition.

Top, structural alignment of PLN, PKI, RIα, and RIIβ Arginine-Glutamate ion pair. Bottom, sequence alignment of substrate and inhibitor sequences at the consensus PKA phosphorylation site.

5.4.3. Redefining PKA substrate classification

In light of the role of N-terminal arginine residues in phospholamban, we analyzed PKA substrate sequences of 241 proteins. We discovered that 99 out of 241 substrates (or 41%) contain an arginine at the P-8, P-7, P-6, P-5, or P-4 positions (Figures 56 and 57). Whether or not these arginine residues form hydrogen bonds with the C-subunit E203 is unknown. The proteins probably fold in a variety of ways to dock onto the C-subunit large lobe. Regardless, these observations demonstrate that sequence alignment alone could not have predicted the importance of this region. It would be of interest to compare how substrates with and without N-terminal arginines bind to the C-subunit as well compare the phosphorylation kinetics. These sequence alignments, our structural observations, and biochemical analysis suggests that an alternative PKA substrate binding motif should be R-X_y-R-R-X-S/T-φ, where y is 0-4 residues.

5.4.4. Physiological relevance of Glu203-Arg9 ion pair

Not only does our study point to how important the arginine residues are for C-subunit interaction, it also gives us a sense of why two point mutations of PLN, R9C and ΔR14, are correlated with inherited dilated cardiomyopathy in humans. Transgenic mice containing the phospholamban R9C mutation show increased heart chamber size, increased systolic and diastolic diameters, and early onset of death. The precise biochemical mechanism of these point mutations on impaired myocytes was not well understood. In light of our biochemical and structural analysis (Figures 48 and 50), we conclude that the R9 position is extremely important for phospholamban binding to the

Protein	Sequence
vitamin D receptor	SRHTPSFSGDSSSSCSDHCI
Estrogen receptor alpha	QCTIDKNRRKSCQACRLRKC
Acetylcholine receptor protein,	DWQNDLKLRRSSSVGYISKA
Acetylcholine receptor protein,	TPEKPQPRRRSSFGIMIKAE
Beta-ARK-1	LSKVPLVQRGSANGL
Cytokine recpetor common beta chain	GPYLGPPHSRSLPDILGQPE
MAP3K3	QPPEPRSRHLSVSSQNPGRS
Presenilin 1	EGDPEAQRRVSKNSKYNAES
Lipase hormone sensitive	SGRLTESMRRSVSEAALAQP
	AFPDGFHPRRSSQGVLHMPL
	FPDGFHPRRSSQGVLHMPLY
	SEPIAEPMRRSVSEAALAQP
	AFPEGFHPRRSSQGATQMPL
	FPEGFHPRRSSQGATQMPLY
Raf1	VQQFGYQRRASDDGKLTDPS
tau	GTPGSRSRTPSLPTPPTREP
Glia maturation factor	YKYQHDDGRVSYPLCFIFSS
Aurora kinase A	SVHAPSSRRTTLCGTLDYLP
Aurora-C	SVHTPSLRRKTMCGTLDYLP
	PSLRRKTMCGTLDYLPPEMI
Orphan nuclear receptor NR4A1	GMVKEVVRTDSLKGRRGRLP
	SLKGRRGRLPSKPKQPPDAS
GTPase activating protein	GTANAALRRESQGSLNSSAS
	VPSSATGKRQTCDIEGLVEL
GTPase activating protein	PDAQTAAKRASRIYNT
Perilipin	WSMEPVVRRLSTQFTAANEL
	KAKPSLLRRVSTLANTLSRH
	AAMQVVSRRQSEVRVPWLHN
PCTAIRE1	DRMKKIKRQLSMTLRGGRGI
	RMRNHPPRKISTEDINKRLS
	ISTEDINKRLSLPADIRLPE
cAMP-dependent protein kinase type	PVPSRFNRRVSVCAETYNPD
cAMP-dependent protein kinase type	PVINRFTRRASVCAEAYNPD
Phosphodiesterase 5A	SVPGTPTRKISASEFDRPLR
CPI-17	GGLQKRHARVTVKYDRRELQ
ATP-binding cassette 1	QLSGGMQRKLSVALAFVGGS
	NYSGGNKRKLSTAMALIGGP
S-protein	RGHNQNSRRPSRATWLSLFS
NF-ATc1	RHSPSTSPRASVTEESWLGA
	PASPCNKRKYSLNGRQPPYS
	TPSPHGSPRVSVTDDSWLGN
HAND1	LGGRLGRRKGSGPKKERRRT
	GSGPKKERRRTESINSAFAE
	GPKKERRRTESINSAFAELR
Fos	PSCAAAHRKGSSSNEPSSDS
HMG14	GAAKEEPKRRSARLSAKPPA
	EEPKRRSARLSAKPPAKVEA
Rho guanine nucleotide exchange	LPKRKPERKPSDEEFASRKS
	SDEEFASRKSTAALEEDAQI
Transforming protein RhoA	ALQARRGKKKSGCLVL
Lipocortin I (annexinI)	LYEAGERRGTDVNVFNTIL
Beta-2 adrenergic receptor	GRTGHGLRRSSKFCLKEHKA
	AFQELLCLRRSSLKAYGNGY
	FQELLCLRRSSLKAYGNGYS
Connexin 32	RRSNPPSRKGSGFGHRLSPE
Neutrophil cytosol factor 1	SIHQRSRKRLSQDAYRRNSV
	RLSQDAYRRNSVRFLQQRRR
	PLEERRQTQRSKPQPAVPPR
	KPQPAVPPRPSADLILNRCS
STK24	WGLALNKRRATLPHPGGSTN
Synapsin-1	MNYLRRRLSDSNFMANLPN
	MNYLRRRLSDSNFMANLPN
GSK-3 alpha	PGGSGRARTSSFAEPGGGGG
Rap1GAP	VPGKSPTRKKSGPFGSRRSS
	KSGPFGSRRSSAIGIENIQE

Protein	Sequence
Ras related protein 1A	PVEKKKPKKKSCLLL
Nuclear factor NF-kappa-B p105 subunit	ASVFVQLRRKSDLETSEPKPF
Solute carrier family,member 2	FFKVPETKGKSFEEIAAEFQK
	EEIAAEFQKKSGSAHRPKAAV
	IAAEFQKKSGSAHRPKAAVEM
Octamer binding transcription factor 1	GLSRRRKKRTSIETNIRVALE
Cyclic-AMP-dependent transcription factor	TLKFGPARNDSVIVADQTPTP
GluR-4	SEAIRNKARLSITGSVGENGR
Integrin alpha 4	SILQEENRRDSWSYINSKSND
CTP synthase	GGTMRLGKRRTLFQTKNSVMR
Desmoplakin	SGSRSGSRRGSFDATGNSSYS
NPR-A	SLERHLRSAGSRLTLSGRGSN
TAL-1 protein	TTNNRVKRRPSPYEMEITDGP
C/EBP beta	REANNIAVRKSRDKAKMRNLE
Tryptophan 5-hydroxylase 1	IESRKSKRRNSEFEIFVDCDI
Wilm tumor protein	CDFKDCERRFSRSDQLKRHQR
	FQCKTCQRKFSRSDHLKTHTR
CETN2	QEFLRIMKKTSLY
Merlin	DFKDTDMKRLSMEIEKEKEVEY
CAD	SMRGAGGRRLSSFVTKGYRTR
APC	SSAMPKKKKPSRLKGDNEKHS
Moesin	NMRLGRDKYKTLRQIRQGNTK
Phospholamban	YLTRSAIRRASTIEMPQQARQ
Drp1	DVPVPVARKLSAREQRDCEVI
Tumor necrosis factor receptor superfamily	TPPPEGEKLHSDSGISVDSQS
Nitric-oxide synthase, brain	ERKSYKVRFNSVSSYSDSQKS
Aquaporin 0	YDFLLFPRLKSISERLSVLKG
	FLLFPRLKSISERLSVLKGAK
CAPN2	TKMDGNWRRGSTAGGCRNYPN
HLA-A1	VVAAVMWRRKSSDRKGGSYTQ
CD91	YATLYMGGHGSRHSLASTDEK
	LYMGGHGSRHSLASTDEKREL
Phospholemman precursor	PDEEEGTFRSSIRRLSTRRR
Melanocortin 4 receptor	YALRSQELRKTFKEIICCYPL
	CYPLGGLCDLSSRY
	YPLGGLCDLSSRY
PTBP1	PDIAVGTKRGSDELFSTCVTN
MHC class II transactivator	HVVQELPGRLSFLGTRLTPPD
	PSLAASLLRLSLYNNCICDVG
Tyrosine-protein phosphatase, non-receptor	KHVRLQERRGSNVALMLDVRS
Prostaglandin E2 receptor, EP4 subtype	RMHRQFMRRTSLGTEQHHAAA
	PRLSDHRRRSFRRIAGAEIQ
Alpha adducin	FNMMEQKKRVSMILQSPAFCE
	PALREKSKKYSDVEVPASVTG
	DSGTCSPLRHSFQKQQREKTR
	KWTKEDGHRTSTSAVPNLFVP
Beta adducin	FNLMEQKKRVTMILQSPSFRE
	SKKKKKFRTPSFLKKSKKKEK
	KKSKKKEKVES
HDAC8	DSLAKIPKRASMVHSLIEAYA
Cut like 1	EKKAYMKRRHSSVSDSQPCEP
CFTR	FDQFSAERRNSILTETLHRFS
	TGEFGEKRKNSILNPINSIRK
	DSDEPLERRLSLVPDSEQGEA
	EQGEAILPRISVISTGPTLQA
	GPTLQARRRQSVLNLMTHSVN
	RKTTASTRKVSLAPQANLTEL
	TELDIYSRRLSQETGLEISEE
Aquaporin 2	WEERREVRRRQSVELHSPQSLP
Histone H2B.a/g/h/k/l	AKSAPAPKKGSKKAVTKAQKK
	QKKDGKKRKRSRKESYSVYVY
	GKKKKRSRKESYSVYVYKVLK
A-kinase anchoring protein.	MRSLSPFRRHSWGPGKNAASD
	SELSVSPKRNSISRTHKDKGP

Figure 56. Alignment of PKA substrate phosphorylation sites.

The P-site is highlighted in grey and arginines from P-8 to P-4 positions are highlighted in red.

Protein	Sequence
GluR-1	AIRTSTLPRNSGAGASSGGSG
UNC84B	SRRSQKLTRYSQGDDDGSSSS
	RKKSSNMKRLSPAPQLGPSSD
	GTGGSESSRASGLVGRKATED
Histone H2A.c/d/i/n/p	KAKAKAKTRSSRAGLQFPVGR
Troponin I, cardiac muscle	RPAPAPIRRRSSNYRAYATEP
	PAPAPIRRRSSNYRAYATEPH
Arachidonate 5 lipoxygenase	MVECSLERQLSLEQEVQQGNI
	YVYGMKGRKSSGFPKSVKSRE
CD243	DSRSSLIRKRSTRRSVRGSQA
	RGSQAQDRKLSTKEALDESIP
Tyr-3-hydroxylase	MVRGQGAPGPSLTGSPWPGTA
	RSPRFIGRRQSLIEDARKERE
	LENPGLGRKLSDFGQETSYIE
PLC gamma 1	QLFHGKAREGSFESRYQQPFE
6-phosphofructokinase, liver type	SGELEHVTRRTLSMDKGF
Fibrinogen alpha chain	TSGSTTTTRRSCSKTVTKTVI
Thimet oligopeptidase 1	LNSKVGMDYRSCILRPGGSED
Protamine Z	ARRRRSRRASRPVRRR
	ARRRRSRRASRPVRRRRPRR
ATP-citrate synthase	TSTPAPSRTASFSESRADEVA
Erythrocyte membrane protein band 4.2	EGALLNKRRGSVPILRQWLTG
PMCA1	EGLEKPESRSSIHNFMTHPEF
Erythrocyte band 7 integral membrane	MAEKRHTRDSEAQRLPDSFK
Chorionic gonadotrophin beta subunit	VCNYRDVRFESIRLPGCPRGV
	LSCQCALCRRSTTDCGGPKDH
	SCQCALCRRSTTDCGGPKDHP
Cytochrome P450 2B2	GERWKALRRFSLATMRDFGMG
	RRRVTSATRRSYVSSSEMVVG
	GRRLGPGTRLSLARMPPPLPA
Vimentin	MSTRSVSSSSYRRMF
	FGGSGTSSRPSSNRSYVTTST
	TYSLGSALRPSTSRSLYSSSP
	GSALRPSTSRSLYSSSPGGAY
Thyroid hormone receptor alpha	RWLDGKRKRKSSQCLVKSSMS
	WLDGKRKRKSSQCLVKSSMSG
Serine/threonine-protein kinase Sgk1	NWDDLINKKITPPFNPNVSGP
CD42C	RARARAARLSLTDPLVAERA
HSP27	RVPFSLLRGPSWDPFRDWYPH
Brain sodium channel 2	GKCQKEAKRSSADKGVALSLD
PIN1	KLPPGWEKRMSRSSGRVYYFN
Phosducin	DSKERMSRKMSIQEYELIHQD
	DSKERFSRKMSVQEYELIHKD
Ras-related protein Rap-1b	TPVPGKARKKSSCQLL
REL	ITVKMQLRRPSDQEVSEPMDF
Ryanodine receptor 2	SDLTIRGRLLSLVEKVTYLKK
	MALYNRTRRISQTSQVSVDAA
Glucosamine--fructose-6-phosphate	PGQAVGTRRGSPLLIGVRSEH
	LYRTARTQIGSKFTRWGSQGE
DPDE4	TFPGHSQRRESFLYRSDSDYD
VASP	GPSEHIERRVSNAGGPPAPPA
	AIAGAKLRKVSKQEEASGGPT
	NAMLARRRKATQVGEKTPKDE
Voltage-dependent L-type calcium	GDIVPSSRKSTPPSSAIDIDA
	TDRSAPIRSASQAEEEPSVEP
	EPVKKSQHRSSSSAPHHNHRS
	PVKKSQHRSSSSAPHHNHRSG
Dematin	WKRNELKKKASLF
GABA(A) receptor B1	PSKGRHRRRASQLKVKIPDLT
Centrin 1	EEFLRIMKKTSLY
Potassium voltage-gated channel	RESCASVRRASSADDIEAMRA
	LPQEGPTRRLSLPGQLGALTS

Protein	Sequence
GluR-6	DGATMTFFKKSKISTYDKMWA
	MWAFMSSRRQSVLVKSNEEGI
PPP1R14D	IPRSRRPSRLTVKYDRGQLQR
NIPP1	EFNTAHNKRISTLTIEEGNLD
	IQRPKRKRKNSRVTFSEDDEI
Nitric-oxide synthase, endothelial	VSSWRKKRKESSNTDSAGALG
TBXA2R	QPRLSTRPRRSLTLWPSLEYS
Calcium/calmodulin-dependent protein	HISPRAWRRPTIESHHVAISD
Rhodopsin kinase	ANSAFIAARGSFDGSSSQPSR
Phosphodiesterase 3B	YGSCKIFRRPSLPCISREQMI
GRK7	NTAYLQARKPSDCDSKELQRR
	DSKELQRRRRSLALPGLQGCA
LASP1	GEGMEPERRDSQDGSSYRRPL
SOX9	PKGEPDLKKESEEDKFPVCIR
	DYKYQPRRKSVKNGQAEAEE
MYOM1	AEKARLKSPLSTLDWTVIVTE
hnRPD	EGHSNSSPRHSEAATAQREEW
G alpha 13	QQDILLARRPTKGIHEYDFEI
NFE2L1	LPPPSALKKGSKEKQADFLDK
Sodium bicarbonate cotransporter	DEKKKKKKKGSLDSDNDDSDC
ETV5	REGPPYQRRGSLQLWQFLVTL
Nopp140	RRKKGEKRASSPFRRVREEEI
MLCK	DVKLVASSHISKTSLSVDPSR
Serotonin acetylase	PESPSCQRRHTLPASEFRCLT
	IRGHPFLRRNSGC
Protein phosphatase 1, regulatory	SPQPSRRGSDSSEDIYLDTPS
Synapsin II	MMNFLARRLSDSSFIANLPN
FGF2	NYNTYRSRKYTSWYVALKRTG
Cullin 5	IQIMKMRKKISNAQLQTELVE
14-3-3 zeta/delta	YKNVVGARRSSWRVVSSIEQK
Neurabin II protein	PRASPRGVRLSLPRASSLNEN
	GVRLSLPRASSLNENVDHSAL
GFPT2	PGEAVATRRGSPLLIGVRSKY
HRH1	KFTWKRLRSHSRQYVSGLHMN
PLC beta 3	QKILDRKRHNSISEAKMRDKH
Src	KPKDASQRRRSLEPAENVHGA
BAD	GAVEIRSRHSSYPAGTEDDEG
B-Raf	SPGPQARERKSSSSSEDRNRMK
hnRPA1	ASSSQRGRSGSGNFGGGRGGG
CREB	KREILSRRPSYRKILNDLSS
Cyclin D1	LAMNYLDRFLSLEPVKKSRLQ
	ALCATDVKFISNPPSMVAAGS
	LSYYRLTRFLSRVIKCDPDCL
Tyrosine-protein phosphatase, non-	ARDFVRLRRLSTKYRTEKIYP
	QIDKKLERNLSFEIKKVPLQE

Figure 57. Alignment of PKA substrate phosphorylation sites.

The P-site is highlighted in grey and arginines from P-8 to P-4 positions are highlighted in red.

C-subunit. The equilibrium dissociation constant measurements with a fluorescently labeled R9C peptide showed drastic increase in K_D values in the presence of nucleotide (31.7 ± 3.6 μM and 464.5 ± 200.3 μM for wild-type phospholamban and R9C, respectively). Moreover, no specific binding was observed in the absence of nucleotide. Certainly, the change in affinity between the two proteins could explain why substrate phosphorylation is defective. A thorough measurement of kinetic rates would explain whether this process is most affected by the binding or release of the mutant. In addition, the R9C could very well be forming dimers through the cysteine, effectively weakening the ability of phospholamban to interact with the C-subunit.

For the ΔR14 deletion, we also observed a decrease in binding affinity between the mutant and C-subunit. The K_D was 7-fold larger for mutant than wild-type in the presence of nucleotide (31.7 ± 3.5 μM and 224.0 ± 63.5 μM for wild-type and ΔR14, respectively). In the absence of nucleotide, although the K_D for both wild-type and mutant were larger than in the presence of nucleotide, the K_D was still 3.5-fold larger for the mutant than wild-type (131.3 ± 18.3 μM and 453.4 ± 44.3 μM for wild-type and ΔR14, respectively). The deletion of R14 removes an essential hydrogen bond between the P-2 arginine in RIα and a glutamate in C-subunit and shifts the register of the P-7 arginine. Our peptide array analysis shows that both these positions are important for binding to the C-subunit and mutation of either residue diminishes, but not completely abolishes binding to the C-subunit. Removal of both these elements together could easily disrupt the entire phospholamban:C-subunit interaction, thereby rendering a low affinity substrate, as we observed from the fluorescence polarization assays.

5.5. Conclusions

Phospholamban is a key regulator of Ca^{2+} cycling in the sarcoplasmic reticulum that is essential for cardiac function. PLN function is regulated by PKA phosphorylation and breakdown of this process leads to detrimental heart defects. This chapter investigated the structural properties of the phospholamban:C-subunit interaction and identified the critical determinants for high affinity binding between the two proteins. Peptide array analysis shows that the three most critical residues in PLN that affect PKA binding are Arg9, Arg 13, and Arg 14. The crystal structure of the PLN:C-subunit complex highlights the conformational change within phospholamban that occurs to accommodate interactions with the C-subunit. Phospholamban converts from a helical structure to an unstructured fragment. In addition, the structure highlights how each of the arginine residues identified in the peptide array analysis participates in a hydrogen bond with an adjacent residue in the C-subunit active site cleft. Fluorescent polarization measurements show that the $Arg9^{P}$:$Glu203^{C}$ ion pair plays a significant role in peptide binding and demonstrates the ability of AMPPNP to increase the affinity between phospholamban and the C-subunit. Our combined biochemical and structural analysis offers a rationalization of how the phospholamban mutations R9C and ΔArg14 are inert to PKA phosphorylation, which explains how these mutations lead to inherited dilated cardiohypertrophy.

Chapter 6

cAMP Analog Specificity of PKA Isoforms

6.1. Introduction

There are four isoforms of regulatory subunits, and each are functionally non-redundant. Moreover, various studies support the notion that the balance of PKA RI and RII protein levels plays a major role in the growth and differentiation of cells. Loss of this balance has a potential to promote cancer formation and progressions. In fact, the expression of RI proteins in cancer cells is significantly higher than RII proteins (Cheadle et al., 2008; Meoli et al., 2008; Miller, 2002). Moreover, cancer cells that expressed more RIα displayed enhanced growth rates (Cho-Chung, 1990; McDaid et al., 1999). Targeting RIα with anti-sense oligonucleotides for both cancer cell lines and animal models show reduction in cell as well as tumor growth, providing a potential target for cancer therapies (Nesterova and Cho-Chung, 2005; Tortora et al., 1991).

In contrast to cancers, PKA mRNA and protein levels are reduced in patients with Systemic Lupus Erythematosus (SLE). SLE is an autoimmune disease of unknown origin that afflicts mostly women of child-bearing age. It is characterized by deviant T lymphocyte effector function that targets and eliminates a host's own antigens (Dayal

and Kammer, 1996). Patients afflicted with this disease often have central nervous system problems and have in increased chances of both kidney failure and heart disease. In SLE T-cells, RIα, RIβ, and RIIβ protein and mRNA levels are drastically reduced. Furthermore, protein phosphorylation by the Type-Iα and Type-IIβ in SLE T-cells are also reduced (80% and 40%, respectively) (Kammer et al., 1994; Khan et al., 2001). Again, as observed with cancers, a change in the overall balance between RI and RII subunits results in deleterious heath defects. In addition, cDNA sequence analysis of SLE patients revealed a number of mutations in RIα transcripts including deletions, transitions, and transversions (Laxminarayana and Kammer, 2000; Laxminarayana et al., 2002). These patients exhibit a high prevalence of PKA activity that persists over time (Kammer, 1999). Several of these mutations are in the cAMP binding domains, which could lead to inefficient regulation of PKA by cAMP. Other mutations cause premature truncation of transcripts, which may lead to ineffective binding (and therefore inhibition) of the C-subunit.

Clearly, the aberrant change in Type I and/or Type II isoform levels are correlated with detrimental health defects. In light of these data, we sought to assess whether a class of cAMP analogs can be generated to specifically target one PKA isoform over another. Binding affinities between R-subunits and cAMP derivatives with different chemical groups at the phosphate and adenine ring have been exhaustively catalogued. Binding affinity measurements of these analogs for each of the two cAMP binding sites have also been comprehensibly studied. (Dostmann et al., 1990a; Dostmann, 1987; Dostmann et al., 1990b; Ogreid and Doskeland, 1982; Øgreid and Døskeland, 1982) However, these data did not provide insights into how well the analogs activated the PKA holoenzymes.

Previous work screened a library of 21 commercially available cAMP analogs for isoform specific PKA activation between RIα and RIIβ (Figure 58) (Simon Brown, unpublished). A fluorescence polarization assay was designed to measure the dissociation of C-subunits in the presence of varying concentrations of cAMP derivatives (Saldanha et al., 2006). A general isoform-specific activation scheme emerged from this work where cAMP analogs with substituents placed at the C8 position showed preferential activation of RIα holoenzymes, whereas substitutions placed at the N6 position showed preferential activation of RIIβ holoenzymes. 8-(4-chlorophenylthio)-cAMP (8-CPT) activated the RIα subunit with the most selectivity over RIIβ, as well as to the same level that cAMP activated RIα holoenyzmes. The EC_{50} was 33 nM for RIα, which was 4.5-fold lower than for RIIβ. HE-33 (a compound with a dipropyl group at the N6 position) activated the RIIβ subunit with the most selectivity over RIα (the EC_{50} was 45 nM for RIIβ, which was 9.2 fold lower than for RIα). Furthermore, the EC_{50} for HE-33 activation was only 2.5-fold higher than the EC_{50} for cAMP activation of RIIβ holoenzymes (18 nM).

The work outlined in this chapter was to take a structural approach to understand why cAMP molecules with N6 substituents preferentially activate RIIβ holoenzymes and why C8 substituents preferentially activate RIα holoenzymes. We co-crystallized both RIα and RIIβ subunits with HE-33 and are still currently undergoing efforts to co-crystallize 8-CPT with RIα. It is hoped that this study will pave the way for future development of isoform selective cAMP analogs.

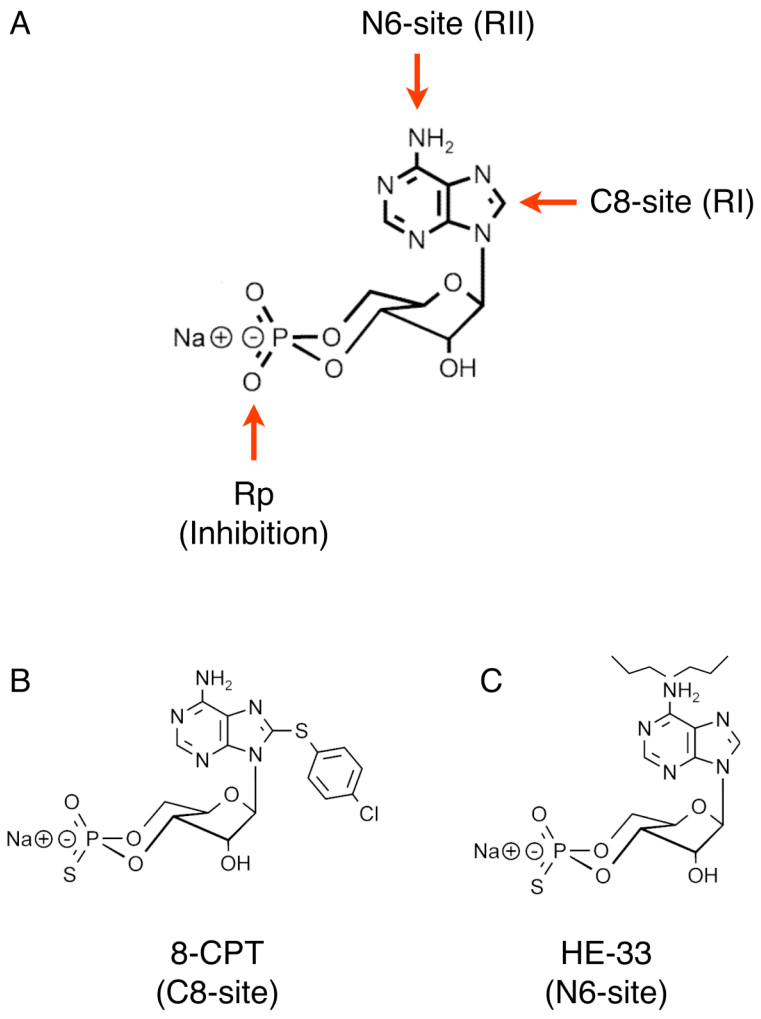

Figure 58. Summary of cAMP analog substitutions.

cAMP analogs selectively activated RIα or RIIβ holoenzymes depending on whether chemical groups were placed at the N6 or C8 positions. Substitutions on N6 specifically activate RIIβ subunits, while substitutions on C8 specifically activate RIIα subunits. 8-CPT was the most selective analog for RIα (B), while HE-33 was the most selective analog for RIIβ (C).

6.2. Experimental Methods

6.2.1. Protein preparation

RIα was expressed in *E.coli* BL21 using 1 L of Overnight Express, Instant TB media (Novagen). Briefly, one colony from a freshly transformed plate was used to inoculated 50 mls of LB and grown overnight at 37°C. On the following day, 5 mls of the starter culture was transferred to each 500 mls of Overnight Express media, then grown at 25°C for 24 hours. The protein was purified as previously described (Su et al., 1995a; Wu et al., 2004).

6.2.2. HE-33 Crystallization, Data Processing, and Refinement

HE-33 was generously provided by Howard Cottom (University of California, San Diego Moores Cancer Center). 100 mM stocks of HE-33 were made with 100% DMSO and stored at -20°C. Purified RIα was dialyzed into 50 mM MES (pH 5.8), 200 mM NaCl, 2 mM EDTA, 2 mM EGTA, 2 mM TCEP-HCl, and 10% glycerol and concentrated to 11 mg/ml. RIα was incubated with 10x HE-33 on ice for 2 hours and spin filtered prior to use.

All crystallization trials were setup with the Oryx8 Protein Crystallization Robot (Douglas Instruments, UK). RIα(91-379) bound to HE-33 was crystallized by hanging drop at 25°C in 6.3% PEG 3350, 0.074 M sodium malonate (pH 7.0) after 3 weeks of growth. Crystals were harvested, transferred to mother liquor containing 20% glycerol, and flash-frozen in liquid nitrogen. X-ray diffraction data was collected at The Advanced Light Source beamline 8.2.1 (Lawrence Berkeley National Laboratory, Berkeley, CA).

Diffraction data were integrated and scaled with HKL2000 (Otwinowski, 1997). The space group was unambiguously determined to be P6522. Initial phases were generated by molecular replacement using the program phaser (Storoni et al., 2004) and the coordinates for the RIα:Sp-cAMP$_2$ complex (PDB code 1NE6) (Wu et al., 2004) as a search model. The two Sp-cAMP molecules were removed from the PDB file to prevent model bias. One molecule was found in the asymmetric unit (RFZ=9.0, RFZ=37.8) corresponding to a solvent content of 63.5%. All ambiguous main chains and side chains manually rebuilt using Coot (Emsley and Cowtan, 2004), followed by iterative cycles of structure refinement using REFMAC in the CCP4 suite (1994; Murshudov et al., 1997). TLS refinement (Winn et al., 2001) was implemented for each lobe. Simulated annealing via the program Phenix (Adams et al., 2004; Adams et al., 2002) was used in the final stages of refinement because geometric restraints were too loose with REFMAC. The final R and R_{free} values were 21.6% and 28.7%, respectively, with excellent geometry. The final model contained R-subunit residues 107-372 bound to two HE-33 molecules. All figures were made using PyMol (DeLano Scientific).

6.2.3. 8-CPT Crystallization

8-(4-chlorophenylthio)-cAMP (8-CPT) was purchased from Biolog Life Science Institute (Bremen, Germany). 100 mM stocks of 8-CPT were made with 100% DMSO and stored in -20°C. Purified RIα was dialyzed into 4L of 50 mM MES (pH 6.0), 200 mM NaCl, 2 mM EDTA, 2 mM EGTA, 10 mM DTT, and 10% glycerol and concentrated to 14.2 mg/ml. RIα was incubated with 10x 8-CPT on ice for 2 hours and spin filtered prior to use.

The RIα(91-379):8-CPT complex was screened with using commercial 96-well HT PACT (Molecular Dimension), JCSG (Molecular Dimensions), Crystal Screen HT (Hampton Research, HR2-130) reagents. Crystallization trials were done using 1 μl drops in CrystalClear Duo plates (Douglas Instruments, UK), with final protein concentrations of 5.7 and 8.5 mg/ml at 22.5°C. Crystals were observed in the following conditions after 1 week:

PACT E10	0.02 M Sodium/potassium phosphate, 20% w/v PEG 3350
JCSG E3	0.2 M Sodium chloride, 0.1 M HEPES pH 7.5, 10% v/v 2-propanol
JCSG F6	0.1 M Bicine pH 9.0, 10% v/v MPD
JCSG D8	0.1 M Tris pH 8.0, 40% v/v MPD
Hampton G10	0.05 M Cadmium sulfate hydrate, 0.1 Hepes pH 7.5, 1 M sodium acetate trihydrate
Hampton H10	0.1 M Sodium chloride, 0.1 M Bicine pH 9.0, 20% v/v PEG monomethyl ether 550

The JCSG E3 condition was repeated and optimized in hanging drop EasyXtal Tool plates (QIAGEN), yielding 0.2 μM three-dimensional hexagonally shaped crystals. Unfortunately, these crystals did not diffract. Subsequently, additives were screened in attempts to manipulate crystal quality for this condition. Each drop consisted of 90% of 7 mg/ml sample, 0.2 M NaCl, 0.1 M Hepes (pH 7.4), 6% isopropanol and 10% of each additive (Additive Screen HT, Hampton Research). Of these, 9 conditions produced crystals with either different morphologies (needles and rods) or the same hexagonal shapes.

The Hampton G10 condition was repeated and optimized in hanging drop EasyXtal Tool plates (QIAGEN) at 22.5°C, yielding only two three-dimensional 0.8 μM long rod-shaped crystals after 3 months (Figure 59). Crystals were harvested, transferred to mother liquor containing 20% glycerol as a cryoprotectant, and flash-frozen in liquid nitrogen. The two crystals diffracted to 3.7Å and 7Å on a MarResearch Imaging Plate-345 detector system mounted on a Rigaku RU-200 rotating unit (UCSD home source).

6.3. Results

6.3.1. Progress RIα_{AB}:8-CPT Co-Crystallization

Crystallization of RIα bound to 8-CPT has proven to be difficult. However, after months of optimization and additive screens, we were able to obtain two crystals that diffracted to 4 Å at the UCSD home source (Figure 59). These crystals will be taken to a synchotron source in efforts to improve the resolution range. We are also currently trying to reproduce these results, as well as improve crystallization conditions to generate crystals with higher quality diffraction.

6.3.2. Crystal structure of RIα bound to HE-33

The crystal structure of RIα bound to 2 molecules of HE-33 was solved to 3.0 Å resolution using the RIα:Sp-cAMP$_2$ structure (PDB: 1NE6) as a molecular replacement probe. The complex crystallized in the P6$_5$22 space group with one molecule in the

A

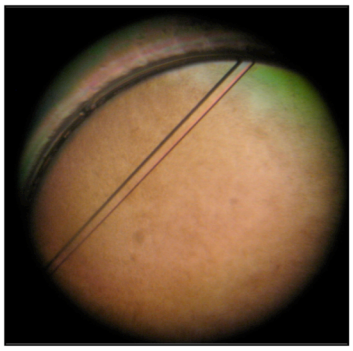

B

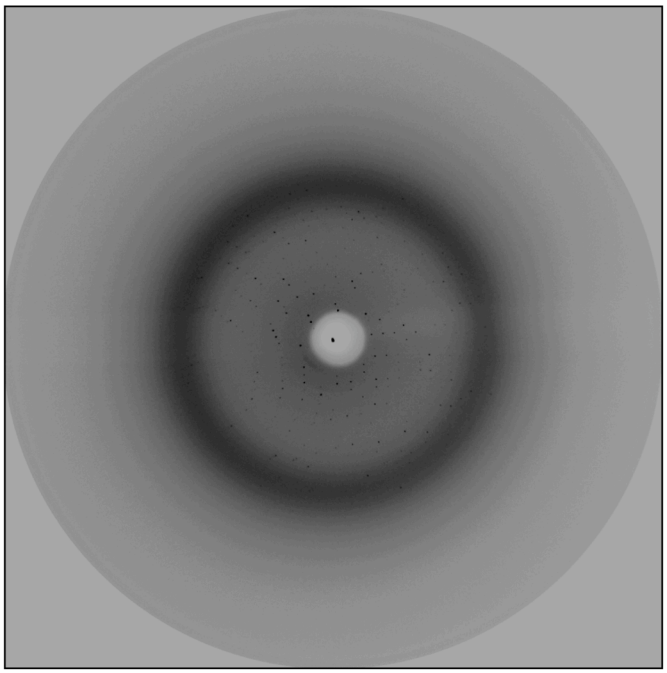

Figure 59. Co-crystallization of RIα and 8-CPT.

(A) The only diffracting crystals obtained were from a condition with cadmium sulfate hydrate, hepes (pH 7.5), and sodium acetate trihydrate. (B) Image of the diffraction pattern with the UCSD home X-ray source.

Table 5. Crystallographic data reduction and refinement statistics for the RIα:HE-33_2 complex.

Beamline	ALS bl 8.2.1
Space Group	$P6_522$
Cell Dimensions (Å)	a=b=89.8, c=185.1
Number of crystals	1
Wavelength (Å)	1.0
Mosaicity (^{o})	0.85
Resolution range for refinement (Å)	50-3
Total No. reflections	90832
Average redundancy	9.3 (9.3)
Unique reflections	9430 (901)
Rsym[a] (%)	7.4 (41.7)
Completeness (%)	99.7 (99.8)
<I>/<α>	42.5 (4.4)
Total reflections used	9850
No. molecules per asu	1
Number of protein atoms	2018
RMSD bond lengths (Å)	0.01
RMSD bond angles (^{o})	1.418
R_{work}[ll]	21.8
R_{free}	28.6
Wilson B factor (Å^2)	84.84

asymmetric unit (Table 5). The overall R-subunit conformation observed in the HE-33 complex is similar to previous cyclic nucleotide conformations where the protein forms a compact globular structure (Figure 60). The two domains come together at a common interface, connected by a kinked αB/C helix that connects the two modules (Figure 61). The two molecules of HE-33 fit into the nucleotide binding pocket in a similar fashion as cAMP. Both of the two hydrophobic capping residues (Trp260 for Domain A and Tyr371 for Domain B, also discussed in chapter 2) stack against the adenine ring of the nucleotide derivative. The differences in the structure arise from localized movements of both side chains and backbones in the cAMP binding pocket to accommodate the bulky substituent of the nucleotide.

Figure 62 shows a surface rendering of the cAMP binding pockets in Domain A. When RIα is bound to cAMP, the nucleotide binding pocket is just large enough to accommodate cAMP. When RIα is bound to HE-33, the pocket opens up near the N6 position to provide room for the dipropyl chemical group. The precise movements are relegated to changes in the side chain and backbone positions of β-strands 4 and 5 (Figure 62b). In Domain B, the nucleotide binding pocket is again opened up upon binding of HE-33 with respect to the pocket when RIα is bound to cAMP (Figure 63). In fact, electron density was not observed in two regions surround HE-33 in Domain B, suggesting that these regions are dynamic in solution (Figure 61). These regions are the loop that connects β-strands 4 and 5 in Domain B (residues 303-310) and C-terminal tail residues 373-379. The absence of β4-β5 loop and C-terminal tail creates additional space around HE-33 dipropyl groups.

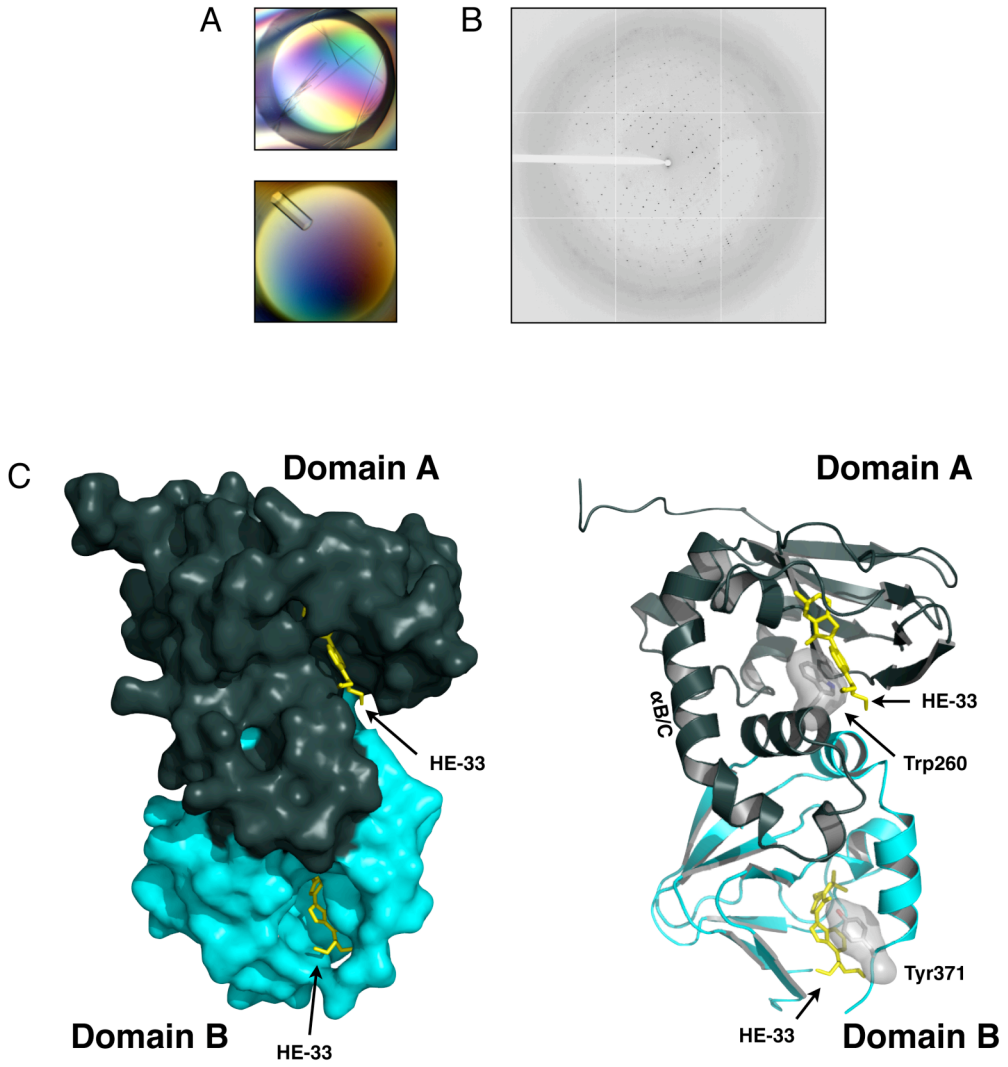

Figure 60. Structural overview of HE-33 bound to RIα.

(A) Protein crystals of the complex. The top panel shows the initial hit, while the bottom panel are crystals obtained after optimization. (B) Sample diffraction pattern. (C) Left, surface rendering of the complex, with HE-33 in yellow sticks, RIα Domain A in dark teal, and Domain B in cyan. Right, ribbon diagram of the complex. The hydrophobic capping residues are highlighted in grey (Trp260 for Domain A and Tyr 371 for Domain B).

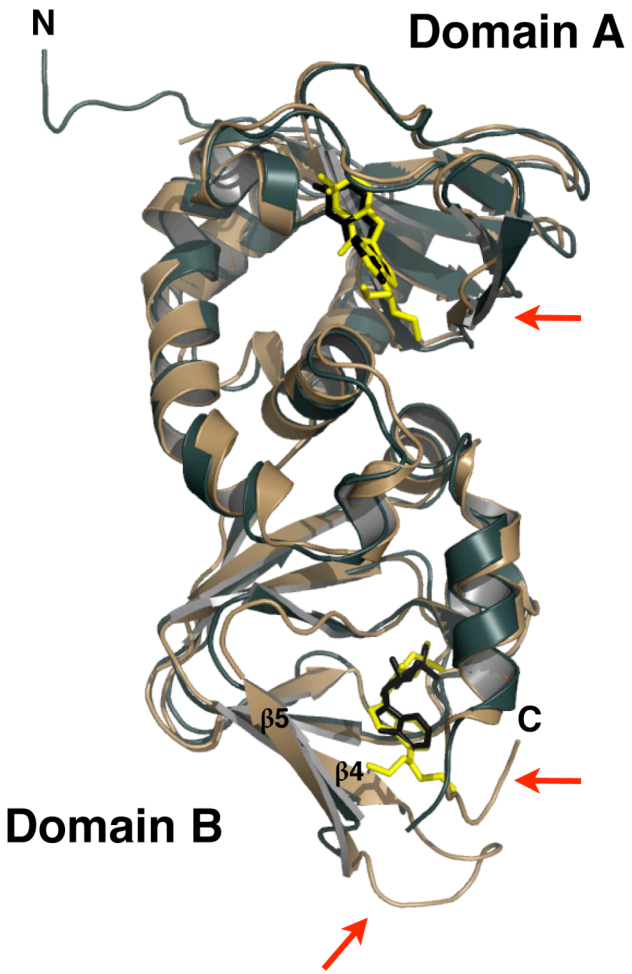

Figure 61. Structural alignment of RIα bound to cAMP and HE-33.

The cAMP bound conformation is shown in tan, while the HE-33 conformational is shown in dark green. cAMP is in black and HE-33 is in yellow sticks. The red arrows indicate backbone regions that are significantly different between the two structures.

6.4. Discussion

The balance between RI and RII-subunits plays a critical role in cell growth and differentiation. Shifts in the relative expression and activity levels of these isoforms are correlated with several cancers and autoimmune disease (SLE). Thus, it is of interest to develop classes of small molecules that could preferentially activate one isoform over another in order combat irregular activation of Type I or Type II PKA holoenzymes. One strategy is to utilize cAMP as a parent molecule and synthesize variants that contain chemical groups at different positions. A library of 21 cAMP analogs was tested for activation of RIα and RIIβ holoenzymes. This work demonstrated the prevalence of N6 substitutions on cAMP to activate RII-subunits at lower concentrations than RI-subunits, while C8 substitutions on cAMP activated RI-subunits at lower concentrations than RII-subunits (Simon Brown, unpublished). The purpose of this study was to use a structural approach to determine why particular classes of cAMP derivatives change the activation potency between RI and RII subunits.

The HE-33 compound was the most selective for RIIβ-subunits, where 9.2-fold less HE-33 was needed to activate RIIβ over RIα holoenzymes. On the contrary, 8-CPT was the most selective compound for RIα. We obtained crystals of RIα bound to 8-CPT, but they only diffracted to 4 Å. We are still in the process of optimizing conditions to improve the diffracting resolution of these crystals. However, we report here the co-crystallization of RIα with the cAMP analog, HE-33 (which contains an N6 dipropyl substitution), and compare it with a previously solved structure of RIIβ co-crystallized with HE-33, as well as their cAMP bound counterparts.

The structures of RIα and RIIβ bound to cAMP show significant differences in their cAMP binding sites. In Domain A, RIIβ has is a large pocket near the N6 position of cAMP that is absent in RIα (Figure 62a). In Domain B, both pockets from RIα and RIIβ are equally accessible (Figure 63a). Our structures of both RIα and RIIβ bound to HE-33, demonstrate quite different properties. The structure of RIIβ bound to HE-33 shows that the space that was present near the N6 position in the cAMP conformation is now occupied by the N6 alkyl substituent. The dipropyl groups are enveloped in a hydrophobic environment provided by many residues (Ile199, Val201, Val210, Gln377, and the hydrophobic capping residue, Arg381) (Figure 62b). Conversely, although HE-33 still binds to Domain A in RIα, the nucleotide binding site becomes more opened, where β-strands 4 and 5 are pushed away relative to the conformation observed in the cAMP bound structure. Furthermore, it lacks the tight network of hydrophobic interactions around the N6 substituent observed for RIIβ. The hydrophobic capping residue, Trp260, stacks against the adenine ring, as was observed in the cAMP bound conformation. However, hydrophobic residues in β4 and β5 are almost 5 Å from the nucleotide.

In Domain B, the nucleotide pocket is somewhat exposed for both HE-33 bound to RIα and RIIβ. In each case, the hydrophobic residue still caps the adenine ring of HE-33 (Figure 63b). A couple residues provide a hydrophobic environment around the N6 substituents, but not to the extent as observed in Domain A. Furthermore, the B-factors for the compound in Domain B for both RIα and RIIβ are fairly high, suggesting that the binding of HE-33 is not stable (data not shown).

The model of PKA activation by cAMP differs between the RI and RII-subunits. In RIα holoenzymes, the activation is a cooperative and ordered pathway where cAMP must first bind to Domain B before Domain A is accessible, and it is this binding of cAMP

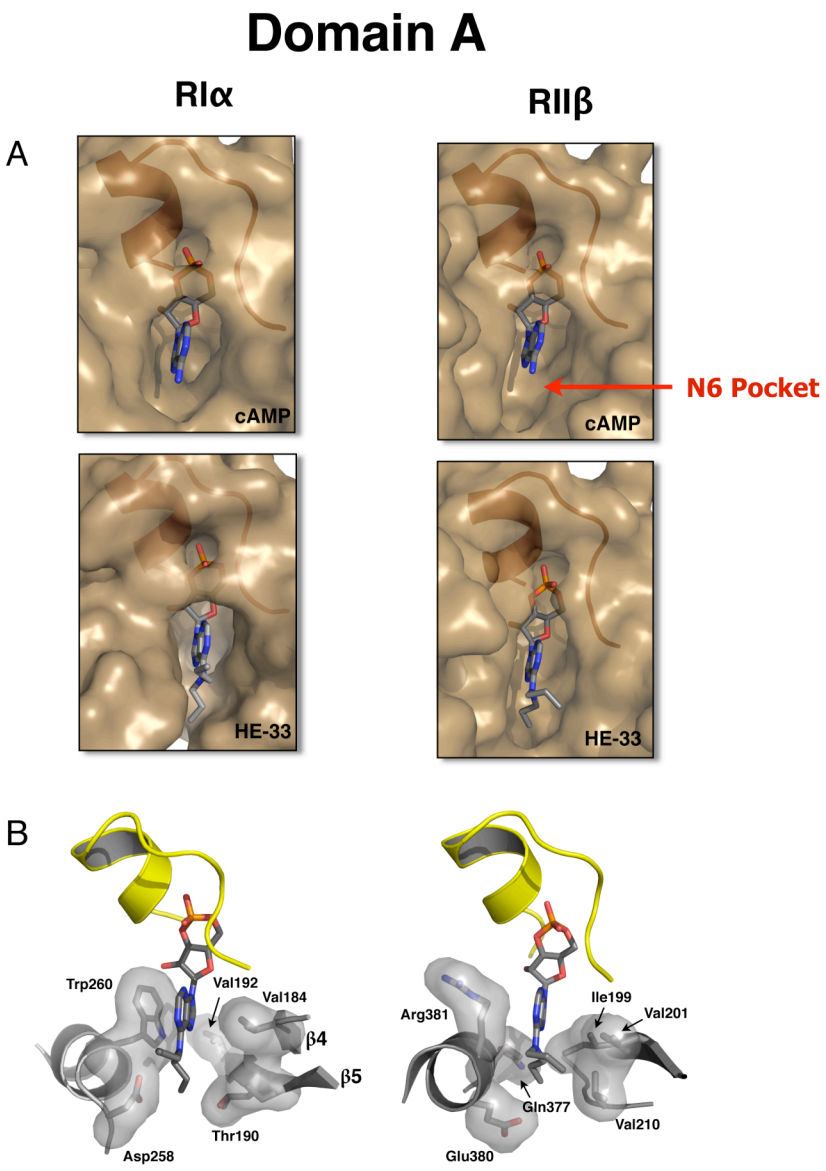

Figure 62. Structural comparison of Domain A nucleotide binding pockets between RIα and RIIβ.

(A) Top panels show the nucleotide binding pocket in the presence of cAMP for RIα and RIIβ. RIIβ has a pocket next to the N6 position of cAMP, whereas RIα does not. Bottom panels show the nucleotide binding pocket in the presence of HE-33 for RIα and RIIβ. The dipropyl groups of HE-33 fit into the N6 pocket, whereas amino acids are displaced in RIα to accommodate the substituents. The phosphate binding cassette is shown in red ribbons for reference. (B) Specific interactions around HE-33 compound for RIα (left) and RIIβ (right).

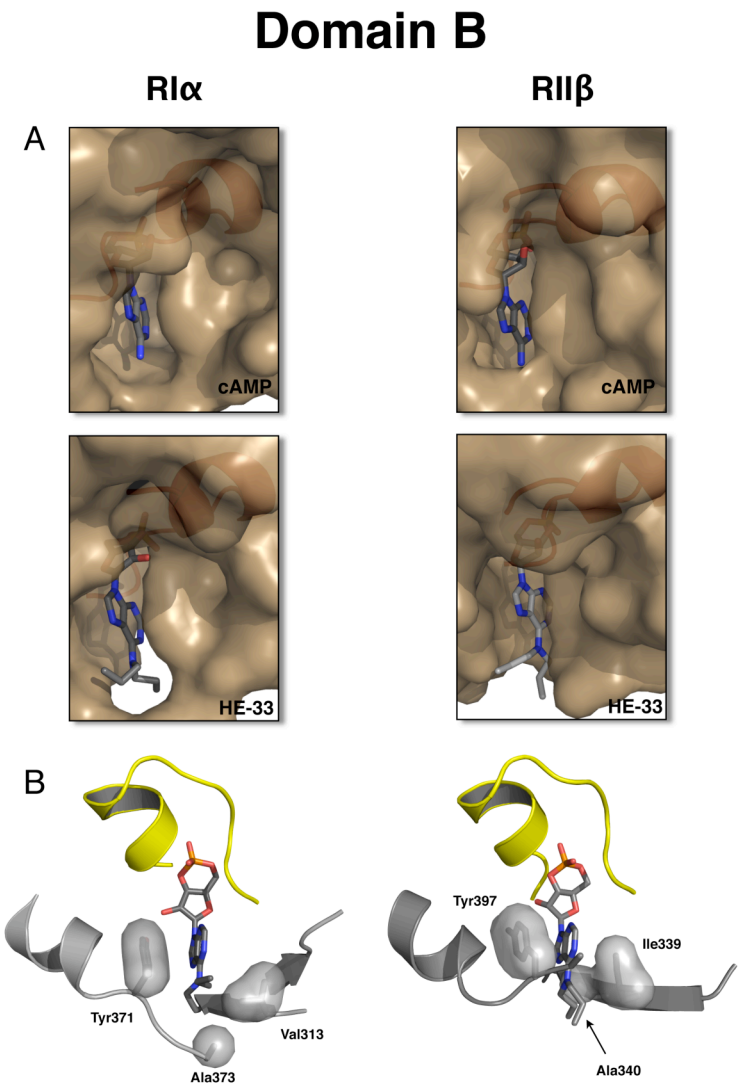

Figure 63. Structural comparison of Domain B nucleotide binding pockets between RIα and RIIβ.

(A) Top panels show the nucleotide binding pocket in the presence of cAMP for RIα and RIIβ. Bottom panels show the nucleotide binding pocket in the presence of HE-33 for RIα and RIIβ. The phosphate binding cassette is shown as a red ribbon for reference. (B) Specific interactions around HE-33 compound for RIα (left) and RIIβ (right. Note that the orientation shown in (B) is flipped 180 degrees from (A).

to Domain A that releases the C-subunit. In constrast, RIIβ holoenzymes do not follow the sequential pathway. Instead, binding of cAMP to either Domain A or Domain B activates PKA. In light of these biochemical models of cAMP-induced PKA activation, our structural analysis of HE-33 interactions with both RIα and RIIβ may explain how selectivity of N6 analogues for RIIβ is achieved. Clearly, HE-33 is able to bind both free RIα and RIIβ proteins. However, in RIα, Domain B surrounding HE-33 is not well ordered, suggesting that the compound does not strongly associate with RIα relative to cAMP at this site. In the context of the activation process, if HE-33 only weakly associates with Domain B, the ordered and cooperative activation pathway may be impaired (or at least retarded) such that Domain A is not as readily accessible to facilitate C-subunit dissociation and activation. This could explain why there is a 10-fold increase in EC_{50} for HE-33 relative to cAMP. For RIIβ, our structural analysis shows that HE-33 forms well-ordered interactions in Domain A, stabilized by hydrophobic interactions. The space around the N6 pocket also provides extra room for bulky N6 substituents, thereby reducing the potential for steric clashes. Since activation of RIIβ holoenzymes does not require ordered cAMP-binding events, the binding of N6-cAMP derivatives in Domain A would be sufficient to activate the RIIβ isoforms, explaining why analogs with N6 substituents may preferentially activate RII holoenzymes.

Intriguingly, the HE-33 compound was also tested in an autoimmune animal model where it was administered to MRL/lpr mice exhibiting human SLE-like symptoms. These mice typically have mortality rates of 50% at 18-20 weeks. Upon oral administration of HE-33, the mean survival time of mice doubled compared with control mice that received water (unpublished). In light of our work, HE-33 could potentially be working through RIIβ holoenzymes. Since protein and activity levels of RIα are

drastically diminished compared to RIIβ, the HE-33 compound could facilitate RII activation to compensate for the deficient RI-dependent protein phosphorylation.

Our studies provide the first steps towards the development of isoform-specific cAMP analogs for drug therapies. With these studies, future work can be done to optimize the chemical substituents for even greater selectivity of PKA isoforms.

6.5. Conclusions

The structures of RIα and RIIβ bound to cAMP show significant differences in the cAMP binding sites. In Domain A, RIIβ has is a large pocket near the N6 position of cAMP that is absent in RIα. We solved the structure of both RIα and RIIβ bound to HE-33, the most RIIβ selective analog. The structure of RIIβ:HE-33_2 shows that the space near the N6 position is now occupied by the N6 alkyl substituent, surrounded in a hydrophobic environment. Conversely, RIα lacks this hydrophobic shell and binding of HE-33 results in a more open pocket. In Domain B, both RIα and RIIβ display opened pockets. In light of the different biochemical mechanisms of cAMP-induced activation between RI and RII subunits, these structural studies explain why selectivity of N6 analogues for RIIβ is achieved.

Chapter 7

Conclusions

Protein Kinase A holoenzyme is one of the major receptors for the second messenger, cAMP, where an extracellular stimuli is converted to a protein kinase signaling response. Cyclic adenosine monophosphate (cAMP) signaling through cAMP-dependent protein kinase (PKA) is a ubiquitous mammalian signaling pathway conserved from bacteria to man and is involved in a broad range of biological functions such as metabolism (Krebs and Beavo, 1979), memory (Arnsten et al., 2005), and cell growth (Chen et al., 1998). While the PKA catalytic (C) subunit has served as a prototype for the protein kinase superfamily, the regulatory (R) subunit defines the mechanism whereby the second messenger, cAMP, translates an extracellular signal into an intracellular biological response. Misregulation of this process is associated with a number of diseases including cancer (Taimi et al., 2001), dilated cardiomyopathy (Antos et al., 2001), and systemic lupus erythematosusm (Kammer et al., 1994; Kammer et al., 2004).

A major goal of this dissertation is to understand the molecular features that govern cAMP-induced activation of PKA in order to develop therapeutic agents that combat disease. Three approaches have been used to achieve this goal: 1) to solve the

crystal structure of the R:C heterodimer complex; 2) to elucidate the molecular rules that govern substrate recognition; and 3) to understand the molecular basis for isoform-specific activation of PKA by cAMP analogs.

Prior to this work, a crystal structure of a complex between the C-subunit and a RIα fragment containing only one of two cAMP binding domains was solved. This structure showed how the C-subunit was inhibited by the regulatory subunit and hinted at a conformational rearrangement of Domain B. However, since Domain B was absent in the structure, we could not fully understand the nature of this conformational change, nor could we explain the mechanism of cAMP-induced activation. The allosteric regulation of PKA-Iα is an ordered and cooperative process where cAMP must first bind to Domain B before the Domain A site becomes accessible. Without a structure of a complex containing both cAMP binding domains, we could not explain the molecular features that govern the activation process.

We report here the structure of a complex between the PKA catalytic subunit and a mutant RIα regulatory subunit, RIα(91-379:R333K) containing both cAMP-binding domains. This structure defines the large lobe of the catalytic subunit as a docking scaffold including a novel docking site in Domain B of RIα. A dramatic conformational change occurs in RIα upon binding to catalytic subunit, where the two cAMP-binding domains uncouple and wrap around the large lobe of the catalytic subunit. Prior to this structure, we had no concept of how dramatic the conformational change could be when associated with the C-subunit. The large mobility of the cAMP-binding domains uncovers the concerted mechanism required to bind and inhibit the catalytic subunit. The structure also reveals a holoenzyme-specific salt bridge between two conserved residues, Glu261 and Arg366, that tethers the two adenine capping residues far from their cAMP binding

sites. Both Glu261 and Arg366 are exposed to solvent in the cAMP bound conformation. Mutagenesis of this salt bridge confirms its importance for PKA activation. Our new structural insights combined with mutagenesis studies provides for the first time a molecular mechanism for the ordered and cooperative activation of PKA by cAMP.

The use of small angle X-ray scattering (SAXS) allowed us to investigate the role of RIα heterodimers in a solution-based technique to complement our crystallographic studies. More specifically, we were interested in investigating the dynamic nature of Domain B in RIα when bound to the C-subunit. SAXS analysis allowed us to characterize the RIα:C heterodimers under physiological conditions as well as test the effect of the R333K mutation that was used in our crystallization efforts. We showed that wild-type heterodimer displayed a more extended conformation while heterodimers with the R333K mutation produced a compact conformation, explaining how the mutation could have facilitated the crystallization of the RIα_{AB}R333K:C complex. Mutation of a C-subunit residue (K285P) at the RIα Domain B/C-subunit interface produced a P(r) function that was intermediate to the compact RIα_{AB}R333K:C and extended RIα_{AB}:C heterodimer. The SAXS data suggest that Domain B in wild-type RIα is highly dynamic, and most likely adopts an ensemble of conformations in solution.

The R:C structure outlined how the different components of the R-subunits bind and interact with the C-subunit. We also took a reductionist approach and assessed whether the inhibitor sequences alone could bind the C-subunits. Peptide array analysis was initiated to determine whether these short sequences are sufficient to bind the catalytic subunit with high affinity. Surprisingly, only peptides corresponding to RII isoforms demonstrated detectable binding in the presence and absence of ATP and Mg^{2+}. The shortest peptide corresponds to a 13-mer that spans 6 residues before and

after the P-site, or the position that is phosphorylated in substrates. The differences in apparent binding affinities of the inhibitor sites across the regulatory isoforms suggests that the Type I and Type II isoforms utilize different modes of cAMP-induced activation.

To date, all the structural information available for PKA are with endogenous protein inhibitors. No structures are currently available of a PKA:substrate complex (and very few of enzyme:substrates complexes in general), presumably due to the low affinities that substrates naturally have for their enzyme counterparts. Our present understanding of how proteins dock to PKA is based entirely on protein inhibitors, so we were interested in solving a structure of PKA bound to an endogenous substrate, phospholamban. Phospholamban plays a crucial role in regulating Ca^{2+} in cardiac myocytes. Mutations in phospholamban (R9C, ΔR14, and $L39_{stop}$) are correlated with inherited cardiomyopathies and the goal of this study was to take a structural and biochemical approach towards understanding the molecular basis for these defects. A crystal structure was solved of a phospholamban:C-subunit complex in the presence of a non-hydrolyzable ATP analog, AMPPNP. The structure identified an interaction between $R9^P$ from phospholamban and $E203^C$ from the C-subunit. Biochemical and mutational analysis shows that this interaction plays a key role in peptide docking to the C-subunit. $E203^C$ also forms interaction with arginine residues for RIα, RIIβ, and PKI and sequence alignment alone could not have predicted this interaction. Analysis of other PKA substrate sequences shows that over 40% contain an arginine N-terminal to the R-R-X-S/T-φ consensus site, suggesting that an alternative PKA substrate binding motif should be R-X_y-R-R-X-S/T-φ, where y is 0-4. For phospholamban, this N-terminal arginine is R9, and mutation of this residue is detrimental to binding to the C-subunit (and most likely phospholamban phosphorylation) explaining why the R9C mutation could lead to heart

disease in humans. The deletion of R14 removes both the P-2 and shifts the register of the P-7 arginine. Our peptide array analysis shows that both these positions are important for binding to the C-subunit and mutation of either residue diminishes, but does not completely abolish, binding to the C-subunit. Removal of both these elements together could easily disrupt the entire phospholamban:C-subunit interaction, therefore preventing turnover of PKA-dependent phosphorylation of phospholamban proteins and resulting in the downstream phenotypes observed in patients with dilated cardiomyopathies.

Lastly, we aimed to define the structural determinants of cAMP analogs to target specific PKA isoforms. A library of 21 cAMP analogues was screened for isoform specific PKA activation (RIα and RIIβ) using a fluorescence polarization assay designed to measure dissociated C-subunits. cAMP analogues with substituents placed at the C8 position showed preferential activation of RIα holoenzymes, whereas substitutions placed at the N6 position showed preferential activation of RIIβ holoenzymes. The structures of RIα and RIIβ bound to cAMP show significant differences in the cAMP binding sites. In Domain A, RIIβ has is a large pocket near the N6 position of cAMP that is absent in RIα. We solved the structure of both RIα and RIIβ bound to HE-33, the most RIIβ selective analog. The structure of RIIβ bound to HE-33 shows that the space near the N6 position is now occupied by the N6 alkyl substituent, surrounded in a hydrophobic environment. Conversely, RIα lacks this hydrophobic shell and binding of HE-33 results in a more open pocket. These structural differences may explain the selectivity of N6 analogues for RIIβ.

It is hoped that these studies will address how variations between R-subunit isoforms give rise to the unique and sophisticated mechanisms of PKA regulation in cells and provide a platform for designing isoform-specific inhibitors to combat disease.

7.1. Future Work

With the structure of the PKA C-subunit bound to RIα_{AB}, we hope to pave the way for development of small molecule inhibitors specific for PKA. In the case of RIα, the mechanism of cAMP-induced activation is a stepwise process where cAMP must first bind to Domain B before Domain A is accessible. Previously, cAMP derivatives have been developed in the context of cAMP bound structures of free R-subunits. However, the PKA-Iα structure clearly shows that the cAMP binding pocket in Domain B is completely different and that previous work was biased since it was based on an inaccurate cAMP binding pocket. Future studies need to target this new cAMP binding pocket in order to trap the PKA-Iα holoenzyme in an inhibited state.

The majority of efforts in kinase drug development have been focused on ATP analogs. However, given the large number of kinases in the genome, it is difficult to generate an ATP-based small molecule specific for one kinase. Based on our studies, we defined the inhibitor sequences of RII subunits as individual moieties that can independently bind to the C-subunit. This new development can pave the way for developing a new class of high affinity peptide inhibitors specific for the catalytic subunit of PKA. We have already identified the amino acids required for binding to the C-subunit. An immediate direction is to quantify the binding affinities of these peptides for the C-

subunit. These peptides can easily be optimized and tested to bind PKA with high affinity.

REFERENCES

(1994). The CCP4 suite: programs for protein crystallography. Acta crystallographica *50*, 760-763.

Adams, J.A., McGlone, M.L., Gibson, R., and Taylor, S.S. (1995). Phosphorylation modulates catalytic function and regulation in the cAMP-dependent protein kinase. Biochemistry *34*, 2447-2454.

Adams, P.D., Gopal, K., Grosse-Kunstleve, R.W., Hung, L.W., Ioerger, T.R., McCoy, A.J., Moriarty, N.W., Pai, R.K., Read, R.J., Romo, T.D.*, et al.* (2004). Recent developments in the PHENIX software for automated crystallographic structure determination. Journal of synchrotron radiation *11*, 53-55.

Adams, P.D., Grosse-Kunstleve, R.W., Hung, L.W., Ioerger, T.R., McCoy, A.J., Moriarty, N.W., Read, R.J., Sacchettini, J.C., Sauter, N.K., and Terwilliger, T.C. (2002). PHENIX: building new software for automated crystallographic structure determination. Acta crystallographica *58*, 1948-1954.

Akamine, P., Madhusudan, Wu, J., Xuong, N.H., Ten Eyck, L.F., and Taylor, S.S. (2003). Dynamic features of cAMP-dependent protein kinase revealed by apoenzyme crystal structure. Journal of molecular biology *327*, 159-171.

Anand, G., Taylor, S.S., and Johnson, D.A. (2007a). Cyclic-AMP and Pseudosubstrate Effects on Type-I A-Kinase Regulatory and Catalytic Subunit Binding Kinetics. Biochemistry *46*, 9283-9291.

Anand, G.S., Hotchko, M., Brown, S.H., Ten Eyck, L.F., Komives, E.A., and Taylor, S.S. (2007b). R-subunit isoform specificity in protein kinase A: distinct features of protein interfaces in PKA types I and II by amide H/2H exchange mass spectrometry. Journal of molecular biology *374*, 487-499.

Anand, G.S., Law, D., Mandell, J.G., Snead, A.N., Tsigelny, I., Taylor, S.S., Ten Eyck, L.F., and Komives, E.A. (2003). Identification of the protein kinase A regulatory RIalpha-catalytic subunit interface by amide H/2H exchange and protein docking. Proc Natl Acad Sci U S A *100*, 13264-13269.

Antos, C.L., Frey, N., Marx, S.O., Reiken, S., Gaburjakova, M., Richardson, J.A., Marks, A.R., and Olson, E.N. (2001). Dilated cardiomyopathy and sudden death resulting from constitutive activation of protein kinase a. Circulation research *89*, 997-1004.

Arnsten, A.F., Ramos, B.P., Birnbaum, S.G., and Taylor, J.R. (2005). Protein kinase A as a therapeutic target for memory disorders: rationale and challenges. Trends in molecular medicine *11*, 121-128.

Banky, P., Huang, L.J., and Taylor, S.S. (1998). Dimerization/docking domain of the type Ialpha regulatory subunit of cAMP-dependent protein kinase. Requirements for dimerization and docking are distinct but overlapping. The Journal of biological chemistry *273*, 35048-35055.

Banky, P., Newlon, M.G., Roy, M., Garrod, S., Taylor, S.S., and Jennings, P.A. (2000). Isoform-specific differences between the type Ialpha and IIalpha cyclic AMP-dependent protein kinase anchoring domains revealed by solution NMR. The Journal of biological chemistry *275*, 35146-35152.

Banky, P., Roy, M., Newlon, M.G., Morikis, D., Haste, N.M., Taylor, S.S., and Jennings, P.A. (2003). Related protein-protein interaction modules present drastically different surface topographies despite a conserved helical platform. Journal of molecular biology *330*, 1117-1129.

Baude, E.J., Dignam, S.S., Olsen, S.R., Reimann, E.M., and Uhler, M.D. (1994). Glutamic acid 203 of the cAMP-dependent protein kinase catalytic subunit participates in the inhibition by two isoforms of the protein kinase inhibitor. The Journal of biological chemistry *269*, 2316-2323.

Berman, H.M., Ten Eyck, L.F., Goodsell, D.S., Haste, N.M., Kornev, A., and Taylor, S.S. (2005). The cAMP binding domain: an ancient signaling module. Proc Natl Acad Sci U S A *102*, 45-50.

Bertherat, J., Horvath, A., Groussin, L., Grabar, S., Boikos, S., Cazabat, L., Libe, R., Rene-Corail, F., Stergiopoulos, S., Bourdeau, I.*, et al.* (2009). Mutations in regulatory subunit type 1A of cyclic AMP-dependent protein kinase (PRKAR1A): phenotype analysis in 353 patients and 80 different genotypes. The Journal of clinical endocrinology and metabolism.

Brandon, E.P., Idzerda, R.L., and McKnight, G.S. (1997). PKA isoforms, neural pathways, and behaviour: making the connection. Curr Opin Neurobiol *7*, 397-403.

Brown, S.H.J., Wu, J., Kim, C., Alberto, K., and Taylor, S.S. (Submitted). Protein Kinase A RIIb Holoenzyme: Trapping a Transition-like State with
AMP-PNP.

Bubis, J., Neitzel, J.J., Saraswat, L.D., and Taylor, S.S. (1988a). A point mutation abolishes binding of cAMP to site A in the regulatory subunit of cAMP-dependent protein kinase. J Biol Chem *263*, 9668-9673.

Bubis, J., Saraswat, L.D., and Taylor, S.S. (1988b). Tyrosine-371 contributes to the positive cooperativity between the two cAMP binding sites in the regulatory subunit of cAMP-dependent protein kinase I. Biochemistry *27*, 1570-1576.

Canaves, J.M., Leon, D.A., and Taylor, S.S. (2000). Consequences of cAMP-binding site mutations on the structural stability of the type I regulatory subunit of cAMP-dependent protein kinase. Biochemistry *39*, 15022-15031.

Carr, S.A., Biemann, K., Shoji, S., Parmalee, D.C., and Titani, K. (1982). n-Tetradecanoyl in the NH2 Terminal Blocking Group of the Catalytic Subunit of the Cyclic AMP-Dependent Protein Kinase from Bovine Cardiac Muscle. Proc Natl Acad Sci USA *79*, 6128-6131.

Chaturvedi, D., Poppleton, H.M., Stringfield, T., Barbier, A., and Patel, T.B. (2006). Subcellular localization and biological actions of activated RSK1 are determined by its interactions with subunits of cyclic AMP-dependent protein kinase. Molecular and cellular biology *26*, 4586-4600.

Cheadle, C., Nesterova, M., Watkins, T., Barnes, K.C., Hall, J.C., Rosen, A., Becker, K.G., and Cho-Chung, Y.S. (2008). Regulatory subunits of PKA define an axis of cellular proliferation/differentiation in ovarian cancer cells. BMC medical genomics *1*, 43.

Chen, T.C., Hinton, D.R., Zidovetzki, R., and Hofman, F.M. (1998). Up-regulation of the cAMP/PKA pathway inhibits proliferation, induces differentiation, and leads to apoptosis in malignant gliomas. Laboratory investigation; a journal of technical methods and pathology *78*, 165-174.

Cheng, X., Phelps, C., and Taylor, S.S. (2001). Differential binding of cAMP-dependent protein kinase regulatory subunit isoforms Ialpha and IIbeta to the catalytic subunit. J Biol Chem *276*, 4102-4108.

Cho-Chung, Y.S. (1990). Role of cyclic AMP receptor proteins in growth, differentiation, and suppression of malignancy: new approaches to therapy. Cancer research *50*, 7093-7100.

Coghlan, V.M., Langeberg, L.K., Fernandez, A., Lamb, N.J., and Scott, J.D. (1994). Cloning and characterization of AKAP 95, a nuclear protein that associates with the regulatory subunit of type II cAMP-dependent protein kinase. The Journal of biological chemistry *269*, 7658-7665.

Cook, P.F., Neville, M.E., Jr., Vrana, K.E., Hartl, F.T., and Roskoski, R., Jr. (1982). Adenosine cyclic 3',5'-monophosphate dependent protein kinase: kinetic mechanism for the bovine skeletal muscle catalytic subunit. Biochemistry *21*, 5794-5799.

Corbin, J.D., Keely, S.L., and Park, C.R. (1975). The distribution and dissociation of cyclic adenosine 3':5'-monophosphate-dependent protein kinases in adipose, cardiac, and other tissues. The Journal of biological chemistry *250*, 218-225.

Cowtan, K. (1994). 'dm': An automated procedure for phase improvement by density modification. Joint CCP4 and ESF-EACBM Newsletter on Protein Crystallography *31*, 34-38.

Cummings, D.E., Brandon, E.P., Planas, J.V., Motamed, K., Idzerda, R.L., and McKnight, G.S. (1996). Genetically lean mice result from targeted disruption of the RII beta subunit of protein kinase A [see comments]. Nature *382*, 622-626.

Dandliker, W.B., and Feigen, G.A. (1961). Quantification of the antigen-antibody reaction by the polarization of fluorescence. Biochemical and biophysical research communications *5*, 299-304.

Dayal, A.K., and Kammer, G.M. (1996). The T cell enigma in lupus. Arthritis and rheumatism *39*, 23-33.

De Bondt, H.L., Rosenblatt, J., Jancarik, J., Jones, H.D., Morgan, D.O., and Kim, S.H. (1993). Crystal structure of cyclin-dependent kinase 2. Nature *363*, 595-602.

de Rooij, J., Zwartkruis, F.J., Verheijen, M.H., Cool, R.H., Nijman, S.M., Wittinghofer, A., and Bos, J.L. (1998). Epac is a Rap1 guanine-nucleotide-exchange factor directly activated by cyclic AMP. Nature *396*, 474-477.

Demaille, J.G., Peters, K.A., and Fischer, E.H. (1977). Isolation and properties of the rabbit skeletal muscle protein inhibitor of adenosine 3',5'-monophosphate dependent protein kinases. Biochemistry *16*, 3080-3086.

Deminoff, S.J., Howard, S.C., Hester, A., Warner, S., and Herman, P.K. (2006). Using substrate-binding variants of the cAMP-dependent protein kinase to identify novel targets and a kinase domain important for substrate interactions in Saccharomyces cerevisiae. Genetics *173*, 1909-1917.

DeWitt, M.M., MacLeod, H.M., Soliven, B., and McNally, E.M. (2006). Phospholamban R14 deletion results in late-onset, mild, hereditary dilated cardiomyopathy. Journal of the American College of Cardiology *48*, 1396-1398.

DiFrancesco, D., and Tortora, P. (1991). Direct activation of cardiac pacemaker channels by intracellular cyclic AMP. Nature *351*, 145-147.

Diller, T.C., Madhusudan, Xuong, N.H., and Taylor, S.S. (2001). Molecular basis for regulatory subunit diversity in cAMP-dependent protein kinase: crystal structure of the type II beta regulatory subunit. Structure *9*, 73-82.

Dostmann, W., Taylor, S.S., Genieser, H.-G., Jastorff, B., Døskeland, S.O., and Øgreid, D. (1990a). Analogs of Adenosine Cyclic-3',5'-phosphorothioates: Probing the Cyclic Nucleotide Binding Sites of cAMP-dependent Protein Kinases I and II. J Biol Chem *265*, 10484-10491.

Dostmann, W.R.G. (1987). Adenosine-3',5'-cyclic-phosphorothioate (cAMPS): Methods for synthesis and biological properties of new types of derivatives. Dissertation Thesis *Bremen, FRG*.

Dostmann, W.R.G., Taylor, S.S., Genieser, H.-G., Jastorff, B., Døskeland, S.O., and Øgreid, D. (1990b). Probing the Cyclic Nucleotide Binding Sites of cAMP-dependent Protein Kinases I and II with Analogs of Adenosine 3',5'-Cyclic Phosphorothioates. J Biol Chem *265*, 10484-10491.

Emsley, P., and Cowtan, K. (2004). Coot: model-building tools for molecular graphics. Acta crystallographica *60*, 2126-2132.

Fischer, E.H., and Krebs, E.G. (1955). Conversion of Phosphorylase b to Phosphorylase a in Muscle Extracts. J Biol Chem *216*, 121-132.

Gangal, M., Cox, S., Lew, J., Clifford, T., Garrod, S.M., Aschbaher, M., Taylor, S.S., and Johnson, D.A. (1998). Backbone flexibility of five sites on the catalytic subunit of cAMP-dependent protein kinase in the open and closed conformations. Biochemistry *37*, 13728-13735.

Gauss, R., Seifert, R., and Kaupp, U.B. (1998). Molecular identification of a hyperpolarization-activated channel in sea urchin sperm. Nature *393*, 583-587.

Gibson, R.M., Ji-Buechler, Y., and Taylor, S.S. (1997). Identification of Electrostatic Interaction Sites Between the Rergulatory and Catalytic Subunits of Cyclic AMP-Dependent Protein Kinase. Protein Science *6*, 1825-1834.

Gould, C.M., Kannan, N., Taylor, S.S., and Newton, A.C. (2009). The chaperones Hsp90 and Cdc37 mediate the maturation and stabilization of protein kinase C through a conserved PXXP motif in the C-terminal tail. The Journal of biological chemistry *284*, 4921-4935.

Groussin, L., Horvath, A., Jullian, E., Boikos, S., Rene-Corail, F., Lefebvre, H., Cephise-Velayoudom, F.L., Vantyghem, M.C., Chanson, P., Conte-Devolx, B.*, et al.* (2006). A PRKAR1A mutation associated with primary pigmented nodular adrenocortical disease in 12 kindreds. The Journal of clinical endocrinology and metabolism *91*, 1943-1949.

Gullingsrud, J., Kim, C., Taylor, S.S., and McCammon, J.A. (2006). Dynamic binding of PKA regulatory subunit RI alpha. Structure *14*, 141-149.

Haghighi, K., Kolokathis, F., Gramolini, A.O., Waggoner, J.R., Pater, L., Lynch, R.A., Fan, G.C., Tsiapras, D., Parekh, R.R., Dorn, G.W., 2nd*, et al.* (2006). A mutation in the human phospholamban gene, deleting arginine 14, results in lethal, hereditary cardiomyopathy. Proceedings of the National Academy of Sciences of the United States of America *103*, 1388-1393.

Haghighi, K., Kolokathis, F., Pater, L., Lynch, R.A., Asahi, M., Gramolini, A.O., Fan, G.C., Tsiapras, D., Hahn, H.S., Adamopoulos, S.*, et al.* (2003). Human phospholamban null results in lethal dilated cardiomyopathy revealing a critical difference between mouse and human. The Journal of clinical investigation *111*, 869-876.

Hamuro, Y., Anand, G.S., Kim, J.S., Juliano, C., Stranz, D.D., Taylor, S.S., and Woods, V.L., Jr. (2004). Mapping intersubunit interactions of the regulatory subunit (RIalpha) in the type I holoenzyme of protein kinase A by amide hydrogen/deuterium exchange mass spectrometry (DXMS). J Mol Biol *340*, 1185-1196.

Hanks, S.K., and Hunter, T. (1995). Protein kinases 6. The eukaryotic kinase superfamily: kinase (catalytic) domain structure and classification. FASEB J *8*.

Hanks, S.K., Quinn, A.M., and Hunter, T. (1988). The protein kinase family: conserved features and deduced phylogeny of the catalytic domains. Science (New York, NY *241*, 42-52.

Herberg, F.W., and Taylor, S.S. (1993). Physiological inhibitors of the catalytic subunit of cAMP-dependent protein kinase: effect of MgATP on protein-protein interactions. Biochemistry *32*, 14015-14022.

Herberg, F.W., Taylor, S.S., and Dostmann, W.R. (1996a). Active Site Mutations Define the Pathway for Cooperative Activation of cAMP-dependent Protein Kinase. Biochemistry *35*, 2934-2942.

Herberg, F.W., Taylor, S.S., and Dostmann, W.R. (1996b). Active site mutations define the pathway for the cooperative activation of cAMP-dependent protein kinase. Biochemistry *35*, 2934-2942.

Horvath, A., Bossis, I., Giatzakis, C., Levine, E., Weinberg, F., Meoli, E., Robinson-White, A., Siegel, J., Soni, P., Groussin, L.*, et al.* (2008). Large deletions of the PRKAR1A gene in Carney complex. Clin Cancer Res *14*, 388-395.

Huang, L.J., and Taylor, S.S. (1998). Dissecting cAMP Binding Domain A in the RIa Subunit of cAMP-dependent Protein Kinase: Distinct subsites for recognition of cAMP and the catalytic subunit. J Biol Chem *273*, 26739-26746.

Hubbard, S.R. (1997). Crystal structure of the activated insulin receptor tyrosine kinase in complex with peptide substrate and ATP analog. EMBO J *16*, 5572-5581.

Hubbard, S.R., Wei, L., Ellis, L., and Hendrickson, W.A. (1994). Crystal structure of the tyrosine kinase domain of the human insulin receptor. Nature *372*, 746-754.

Hulme, J.T., Lin, T.W., Westenbroek, R.E., Scheuer, T., and Catterall, W.A. (2003). Beta-adrenergic regulation requires direct anchoring of PKA to cardiac CaV1.2 channels via a leucine zipper interaction with A kinase-anchoring protein 15. Proceedings of the National Academy of Sciences of the United States of America *100*, 13093-13098.

Iyer, G.H., Garrod, S., Woods, V.L., Jr., and Taylor, S.S. (2005). Catalytic independent functions of a protein kinase as revealed by a kinase-dead mutant: study of the Lys72His mutant of cAMP-dependent kinase. Journal of molecular biology *351*, 1110-1122.

Jeffrey, P.D., Russo, A.A., Polyak, K., Gibbs, E., Hurwitz, J., Massague, J., and Pavletich, N.P. (1995). Mechanism of CDK activation revealed by the structure of a cyclinA-CDK2 complex. Nature *376*, 313-320.

Jiang, T., and Qiu, Y. (2003). Interaction between Src and a C-terminal proline-rich motif of Akt is required for Akt activation. The Journal of biological chemistry *278*, 15789-15793.

Johnson, D.A., Akamine, P., Radzio-Andzelm, E., Madhusudan, M., and Taylor, S.S. (2001). Dynamics of cAMP-dependent protein kinase. Chem Rev *101*, 2243-2270.

Johnson, L., Noble, M., and Owen, D. (1996). Active and Inaactive protein Kinases: Structural Basis for Regulation. Cell *85*, 149-158.

Kammer, G.M. (1999). High prevalence of T cell type I protein kinase A deficiency in systemic lupus erythematosus. Arthritis and rheumatism *42*, 1458-1465.

Kammer, G.M., Khan, I.U., and Malemud, C.J. (1994). Deficient type I protein kinase A isozyme activity in systemic lupus erythematosus T lymphocytes. The Journal of clinical investigation *94*, 422-430.

Kammer, G.M., Laxminarayana, D., and Khan, I.U. (2004). Mechanisms of deficient type I protein kinase A activity in lupus T lymphocytes. International reviews of immunology *23*, 225-244.

Kannan, N., Haste, N., Taylor, S.S., and Neuwald, A.F. (2007a). The hallmark of AGC kinase functional divergence is its C-terminal tail, a cis-acting regulatory module. Proc Natl Acad Sci U S A *104*, 1272-1277.

Kannan, N., Wu, J., Anand, G.S., Yooseph, S., Neuwald, A.F., Venter, J.C., and Taylor, S.S. (2007b). Evolution of allostery in the cyclic nucleotide binding module. Genome biology *8*, R264.

Kapphahn, M.A., and Shabb, J.B. (1997). Contribution of the carboxyl-terminal regional of the cAMP-dependent protein kinase type I alpha regulatory subunit to cyclic nucleotide interactions. Arch Biochem Biophys *348*, 347-356.

Kawasaki, H., Springett, G.M., Mochizuki, N., Toki, S., Nakaya, M., Matsuda, M., Housman, D.E., and Graybiel, A.M. (1998). A family of cAMP-binding proteins that directly activate Rap1. Science (New York, NY *282*, 2275-2279.

Khan, I.U., Laxminarayana, D., and Kammer, G.M. (2001). Protein kinase A RI beta subunit deficiency in lupus T lymphocytes: bypassing a block in RI beta translation reconstitutes protein kinase A activity and augments IL-2 production. J Immunol *166*, 7600-7605.

Kim, C., Cheng, C.Y., Saldanha, S.A., and Taylor, S.S. (2007). PKA-I holoenzyme structure reveals a mechanism for cAMP-dependent activation. Cell *130*, 1032-1043.

Kim, C., Xuong, N.H., and Taylor, S.S. (2005). Crystal structure of a complex between the catalytic and regulatory (RIalpha) subunits of PKA. Science *307*, 690-696.

Kinderman, F.S., Kim, C., von Daake, S., Ma, Y., Pham, B.Q., Spraggon, G., Xuong, N.H., Jennings, P.A., and Taylor, S.S. (2006). A Dynamic Mechanism for AKAP Binding to RII Isoforms of cAMP-Dependent Protein Kinase. Mol Cell *24*, 397-408.

Kinzel, V., Konig, N., Pipkorn, R., Bossemeyer, D., and Lehmann, W.D. (2000). The amino terminus of PKA catalytic subunit-a site for introduction of postranslational heterogeeities by deamidation: D-Asp2 and D-isoAsp2 containing isozymes. Protein Science *11*, 2269-2277.

Knighton, D.R., Xuong, N.H., Taylor, S.S., and Sowadski, J.M. (1991a). Crystallization studies of cAMP-dependent protein kinase. Cocrystals of the catalytic subunit with a 20 amino acid residue peptide inhibitor and MgATP diffract to 3.0 A resolution. J Mol Biol *220*, 217-220.

Knighton, D.R., Zheng, J., Ten Eyck, L.F., Ashford, V.A., Xuong, N.-h., Taylor, S.S., and Sowadski, J.M. (1991b). Crystal Structure of the Catalytic Subunit of cAMP-dependent Protein Kinase. Science *253*, 407-414.

Knighton, D.R., Zheng, J., Ten Eyck, L.F., Xuong, N.H., Taylor, S.S., and Sowadski, J.M. (1991c). Structure of a Peptide Inhibitor Bound to the Catalytic Subunit of Cyclic Adenosine Monophosphate-Dependent Protein Kinase. Science (New York, NY *253*, 414-420.

Knighton, D.R., Zheng, J.H., Ten Eyck, L.F., Ashford, V.A., Xuong, N.H., Taylor, S.S., and Sowadski, J.M. (1991d). Crystal structure of the catalytic subunit of cyclic adenosine monophosphate-dependent protein kinase. Science *253*, 407-414.

Konarev, P.V., Volkov, V.V., Sokolova, A.V., Koch, M.H., and Svergun, D.I. (2003). PRIMUS: a Windows PC-based system for small-angle scattering data analysis. J Appl Cryst *36*, 1277-1282.

Krebs, E.G., and Beavo, J.A. (1979). Phosphorylation-dephosphorylation of enzymes. Annual review of biochemistry *48*, 923-959.

Laskowski, R.A., MacArthur, M.W., Moss, D.S., and Thornton, J.M. (1993). PROCHECK: a program to checkk the stereochemical quality of protein structures. J Appl Cryst *26*, 283-291.

Laxminarayana, D., and Kammer, G.M. (2000). mRNA mutations of type I protein kinase A regulatory subunit alpha in T lymphocytes of a subject with systemic lupus erythematosus. International immunology *12*, 1521-1529.

Laxminarayana, D., Khan, I.U., and Kammer, G. (2002). Transcript mutations of the alpha regulatory subunit of protein kinase A and up-regulation of the RNA-editing gene transcript in lupus T lymphocytes. Lancet *360*, 842-849.

MacDougall, L.K., Jones, L.R., and Cohen, P. (1991). Identification of the major protein phosphatases in mammalian cardiac muscle which dephosphorylate phospholamban. European journal of biochemistry / FEBS *196*, 725-734.

Madhusudan, Akamine, P., Xuong, N.H., and Taylor, S.S. (2002). Crystal structure of a transition state mimic of the catalytic subunit of cAMP-dependent protein kinase. Nat Struct Biol *9*, 273-277.

Mascioni, A., Karim, C., Zamoon, J., Thomas, D.D., and Veglia, G. (2002). Solid-state NMR and rigid body molecular dynamics to determine domain orientations of monomeric phospholamban. Journal of the American Chemical Society *124*, 9392-9393.

Mattiazzi, A., Mundina-Weilenmann, C., Vittone, L., and Said, M. (2004). Phosphorylation of phospholamban in ischemia-reperfusion injury: functional role of Thr17 residue. Molecular and cellular biochemistry *263*, 131-136.

Mattiazzi, A., Mundina-Weilenmann, C., Vittone, L., Said, M., and Kranias, E.G. (2006). The importance of the Thr17 residue of phospholamban as a phosphorylation site under physiological and pathological conditions. Brazilian journal of medical and biological research = Revista brasileira de pesquisas medicas e biologicas / Sociedade Brasileira de Biofisica [et al *39*, 563-572.

McDaid, H.M., Cairns, M.T., Atkinson, R.J., McAleer, S., Harkin, D.P., Gilmore, P., and Johnston, P.G. (1999). Increased expression of the RIalpha subunit of the cAMP-dependent protein kinase A is associated with advanced stage ovarian cancer. British journal of cancer *79*, 933-939.

Meoli, E., Bossis, I., Cazabat, L., Mavrakis, M., Horvath, A., Stergiopoulos, S., Shiferaw, M.L., Fumey, G., Perlemoine, K., Muchow, M.*, et al.* (2008). Protein kinase A effects of an expressed PRKAR1A mutation associated with aggressive tumors. Cancer research *68*, 3133-3141.

Miller, W.R. (2002). Regulatory subunits of PKA and breast cancer. Annals of the New York Academy of Sciences *968*, 37-48.

Mortishire-Smith, R.J., Pitzenberger, S.M., Burke, C.J., Middaugh, C.R., Garsky, V.M., and Johnson, R.G. (1995). Solution structure of the cytoplasmic domain of phopholamban: phosphorylation leads to a local perturbation in secondary structure. Biochemistry *34*, 7603-7613.

Murshudov, G.N., Vagin, A.A., and Dodson, E.J. (1997). Refinement of macromolecular structures by the maximum-likelihood method. Acta crystallographica *53*, 240-255.

Nakamura, T., and Gold, G.H. (1987). A cyclic nucleotide-gated conductance in olfactory receptor cilia. Nature *325*, 442-444.

Nesterova, M.V., and Cho-Chung, Y.S. (2005). Chemoprevention with protein kinase A RIalpha antisense in DMBA-mammary carcinogenesis. Annals of the New York Academy of Sciences *1058*, 255-264.

Newhall, K.J., Criniti, A.R., Cheah, C.S., Smith, K.C., Kafer, K.E., Burkart, A.D., and McKnight, G.S. (2006). Dynamic anchoring of PKA is essential during oocyte maturation. Curr Biol *16*, 321-327.

Newlon, M.G., Roy, M., Morikis, D., Carr, D.W., Westphal, R., Scott, J.D., and Jennings, P.A. (2001). A novel mechanism of PKA anchoring revealed by solution structures of anchoring complexes. Embo J *20*, 1651-1662.

Nolen, B., Taylor, S., and Ghosh, G. (2004). Regulation of protein kinases; controlling activity through activation segment conformation. Mol Cell *15*, 661-675.

Ogreid, D., and Doskeland, S.O. (1981a). The kinetics of association of cyclic AMP to the two types of binding sites associated with protein kinase II from bovine myocardium. FEBS Lett *129*, 287-292.

Ogreid, D., and Doskeland, S.O. (1981b). The kinetics of the interaction between cyclic AMP and the regulatory moiety of protein kinase II. Evidence for interaction between the binding sites for cyclic AMP. FEBS Lett *129*, 282-286.

Ogreid, D., and Doskeland, S.O. (1982). Activation of protein kinase isoenzymes under near physiological conditions. Evidence that both types (A and B) of cAMP binding sites are involved in the activation of protein kinase by cAMP and 8-N3-cAMP. FEBS Lett *150*, 161-166.

Øgreid, D., and Døskeland, S.O. (1982). Activation of Protein Kinase Isoenzymes Under Near Physiological Conditions: Evidence that both types (A and B) of cAMP binding sites are involved in the activation of protein kinase by cAMP and 8-N3-cAMP. FEBS Letters *150*, 161-166.

Otwinowski, Z.a.M., W. (1997). Processing of X-ray Diffraction Data Collected in Oscillation Mode. Methods in Enzymology *276:Macromolecular Crystallography, part A*, 307-326.

Owen, D.J., Noble, M.E., Garman, E.F., Papageorgiou, A.C., and Johnson, L.N. (1995). Two structures of the catalytic domain of phosphorylase kinase: an active protein kinase complexed with substrate analogue and product. Structure *3*, 467-482.

Oxenoid, K., Rice, A.J., and Chou, J.J. (2007). Comparing the structure and dynamics of phospholamban pentamer in its unphosphorylated and pseudo-phosphorylated states. Protein Sci *16*, 1977-1983.

Pattison, J.S., Waggoner, J.R., James, J., Martin, L., Gulick, J., Osinska, H., Klevitsky, R., Kranias, E.G., and Robbins, J. (2008). Phospholamban overexpression in transgenic rabbits. Transgenic research *17*, 157-170.

Pepperkok, R., Hotz-Wagenblatt, A., Konig, N., Girod, A., Bossemeyer, D., and Kinzel, V. (2000). Intracellular distribution of mammalian protein kinase A catalytic subunit altered by conserved Asn2 deamidation. J Cell Biol *148*, 715-726.

Perrin, F. (1926). Polarization de la lumiere de fluorescence: Vie moyenne de molecules dans l'etat excite. J Phys Radium *7*, 390.

Reimann, E.M., Walsh, D.A., and Krebs, E.G. (1971). Purification and properties of rabbit skeletal muscle adenosine 3',5'-monophosphate-dependent protein kinases. The Journal of biological chemistry *246*, 1986-1995.

Robinson, M.L., Wallert, M.A., Reinitz, C.A., and Shabb, J.B. (1996). Association of the type I regulatory subunit of cAMP-dependent protein kinase with cardiac myocyte sarcolemma. Archives of biochemistry and biophysics *330*, 181-187.

Roesler, W.J., Vandenbark, G.R., and Hanson, R.W. (1988). Cyclic AMP and the induction of eukaryotic gene transcription. The Journal of biological chemistry *263*, 9063-9066.

Russo, A.A., Jeffrey, P.D., and Pavletich, N.P. (1996). Structural basis of cyclin-dependent kinase activation by phosphorylation. Nat Struct Biol *3*, 696-700.

Saldanha, S.A., Kaler, G., Cottam, H.B., Abagyan, R., and Taylor, S.S. (2006). Assay principle for modulators of protein-protein interactions and its application to non-ATP-competitive ligands targeting protein kinase A. Anal Chem *78*, 8265-8272.

Sastri, M., Barraclough, D.M., Carmichael, P.T., and Taylor, S.S. (2005). A-kinase-interacting protein localizes protein kinase A in the nucleus. Proceedings of the National Academy of Sciences of the United States of America *102*, 349-354.

Schmitt, J.P., Kamisago, M., Asahi, M., Li, G.H., Ahmad, F., Mende, U., Kranias, E.G., MacLennan, D.H., Seidman, J.G., and Seidman, C.E. (2003). Dilated cardiomyopathy and heart failure caused by a mutation in phospholamban. Science (New York, NY *299*, 1410-1413.

Scott, J.D., Fischer, E.H., Demaille, J.G., and Krebs, E.G. (1985). Identification of an inhibitory region of the heat-stable protein inhibitor of the cAMP-dependent protein kinase. Proceedings of the National Academy of Sciences of the United States of America *82*, 4379-4383.

Scott, J.D., Glaccum, M.B., Fischer, E.H., and Krebs, E.G. (1986). Primary-structure requirements for inhibition by the heat-stable inhibitor of the cAMP-dependent protein kinase. Proceedings of the National Academy of Sciences of the United States of America *83*, 1613-1616.

Shoji, S., Parmelee, D.C., Wade, R.D., Kumar, S., Ericsson, L.H., Walsh, K.A., Neurath, H., Long, G.L., Demaille, J.G., Fischer, E.H.*, et al.* (1981). Complete Amino Acid

Sequence of the Catalytic Subunit of Bovine Cardiac Muscle Cyclic AMP-Dependent Protein Kinase. Proc Natl Acad Sci USA *78*, 848-851.

Sicheri, F., Moarefi, I., and Kuriyan, J. (1997). Crystal structure of the Src family tyrosine kinase Hck. Nature *385*, 602-609.

Simmerman, H.K., Collins, J.H., Theibert, J.L., Wegener, A.D., and Jones, L.R. (1986). Sequence analysis of phospholamban. Identification of phosphorylation sites and two major structural domains. The Journal of biological chemistry *261*, 13333-13341.

Steinberg, R.A., Cauthron, R.D., Symcox, M.M., and Shuntoh, H. (1993). Autoactivation of catalytic (C alpha) subunit of cyclic AMP-dependent protein kinase by phosphorylation of threonine 197. Mol Cell Biol *13*, 2332-2341.

Stokes, D.L., and Wagenknecht, T. (2000). Calcium transport across the sarcoplasmic reticulum: structure and function of Ca2+-ATPase and the ryanodine receptor. European journal of biochemistry / FEBS *267*, 5274-5279.

Storoni, L.C., McCoy, A.J., and Read, R.J. (2004). Likelihood-enhanced fast rotation functions. Acta Crystallogr D Biol Crystallogr *60*, 432-438.

Su, Y., Dostmann, W.R., Herberg, F.W., Durick, K., Xuong, N.H., Ten Eyck, L., Taylor, S.S., and Varughese, K.I. (1995a). Regulatory subunit of protein kinase A: structure of deletion mutant with cAMP binding domains. Science *269*, 807-813.

Su, Y., Dostmann, W.R.G., Herberg, F.W., Durick, K., Xuong, N.H., Ten Eyck, L.F., Taylor, S.S., and Varughese, K.I. (1995b). Regulatory (RIa) Subunit of Protein Kinase A: Structure of Deletion Mutant with cAMP Binding Domains. Science (New York, NY *269*, 807-819.

Sutherland, E.W., Jr., and Wosilait, W.D. (1955). Inactivation and activation of liver phosphorylase. Nature *175*, 169-170.

Svergun, D. (1992). Determination of the Regularization Parameter in Indirect-Transform Methods Using Perceptual Criteria. J Appl Cryst *25*, 495-503.

Svergun, D., Barberato, C., and Koch, M. (1995). CRYSOL - a Program to Evaluate X-ray Solution Scattering of Biological macromolecules from Atomic Coordinates. J Appl Cryst *28*, 768-773.

Svergun, D., Barberato, C., and Koch, M.H. (1995). CRYSOL - a Program to Evaluate X-ray Solution Scattering of Biological Macromolecules from Atomic Coordinates. J Appl Cryst *28*, 768-773.

Svergun, D.I. (1999). Restoring Low Resolution Structure of Biological Macromolecules from solution Scattering Using Simulated Annealing. Biophysical Journal *76*, 2879-2886.

Symcox, M.M., Cauthron, R.D., Ogreid, D., and Steinberg, R.A. (1994). Arg-242 is necessary for allosteric coupling of cyclic AMP-binding sites A and B of RI subunit of cyclic AMP-dependent protein kinase. J Biol Chem *269*, 23025-23031.

Tada, M., and Katz, A.M. (1982). Phosphorylation of the sarcoplasmic reticulum and sarcolemma. Annual review of physiology *44*, 401-423.

Tada, M., Kirchberger, M.A., and Katz, A.M. (1975). Phosphorylation of a 22,000-dalton component of the cardiac sarcoplasmic reticulum by adenosine 3':5'-monophosphate-dependent protein kinase. The Journal of biological chemistry *250*, 2640-2647.

Tada, M., and Toyofuku, T. (1996). SR Ca(2+)-ATPase/phospholamban in cardiomyocyte function. Journal of cardiac failure *2*, S77-85.

Taimi, M., Breitman, T.R., and Takahashi, N. (2001). Cyclic AMP-dependent protein kinase isoenzymes in human myeloid leukemia (HL60) and breast tumor (MCF-7) cells. Archives of biochemistry and biophysics *392*, 137-144.

Tortora, G., Damiano, V., Bianco, C., Baldassarre, G., Bianco, A.R., Lanfrancone, L., Pelicci, P.G., and Ciardiello, F. (1997). The RIalpha subunit of protein kinase A (PKA) binds to Grb2 and allows PKA interaction with the activated EGF-receptor. Oncogene *14*, 923-928.

Tortora, G., Yokozaki, H., Pepe, S., Clair, T., and Cho-Chung, Y.S. (1991). Differentiation of HL-60 leukemia by type I regulatory subunit antisense oligodeoxynucleotide of cAMP-dependent protein kinase. Proceedings of the National Academy of Sciences of the United States of America *88*, 2011-2015.

Traaseth, N.J., Thomas, D.D., and Veglia, G. (2006). Effects of Ser16 phosphorylation on the allosteric transitions of phospholamban/Ca(2+)-ATPase complex. Journal of molecular biology *358*, 1041-1050.

Traaseth, N.J., Verardi, R., Torgersen, K.D., Karim, C.B., Thomas, D.D., and Veglia, G. (2007). Spectroscopic validation of the pentameric structure of phospholamban. Proceedings of the National Academy of Sciences of the United States of America *104*, 14676-14681.

Vagin, A., Teplyakov, A. (1997). MOLREP: an Automated Program for Molecular Replacement. Journal of Applied Crystallography *30*, 1022-1025.

Vigil, D., Blumenthal, D.K., Heller, W.T., Brown, S., Canaves, J.M., Taylor, S.S., and Trewhella, J. (2004). Conformational Differences Among Solution Structures of the Type Ialpha, IIalpha and IIbeta Protein Kinase A Regulatory Subunit Homodimers: Role of the Linker Regions. J Mol Biol *337*, 1183-1194.

Vigil, D., Blumenthal, D.K., Taylor, S.S., and Trewhella, J. (2005). The conformationally dynamic C helix of the RIalpha subunit of protein kinase A mediates isoform-specific

domain reorganization upon C subunit binding. The Journal of biological chemistry *280*, 35521-35527.

Vigil, D., Blumenthal, D.K., Taylor, S.S., and Trewhella, J. (2006a). Solution scattering reveals large differences in the global structures of type II protein kinase A isoforms. Journal of molecular biology *357*, 880-889.

Vigil, D., Lin, J.H., Sotriffer, C.A., Pennypacker, J.K., McCammon, J.A., and Taylor, S.S. (2006b). A simple electrostatic switch important in the activation of type I protein kinase A by cyclic AMP. Protein Sci *15*, 113-121.

Vittone, L., Mundina-Weilenmann, C., and Mattiazzi, A. (2008). Phospholamban phosphorylation by CaMKII under pathophysiological conditions. Front Biosci *13*, 5988-6005.

Walsh, D.A., Perkins, J.P., and Krebs, E.G. (1968). An Adenosine 3',5'-Mono-Phosphate-Dependent Protein Kinase from Rabbit Skeletal Muscle. J Biol Chem *243*, 3763-3765.

Wen, W., Harootunian, A.T., Adams, S.R., Feramisco, J., Tsien, R.Y., Meinkoth, J.L., and Taylor, S.S. (1994). Heat-stable Inhibitors of cAMP-dependent Protein Kinase Carry a Nuclear Export Signal. J Biol Chem *269*, 32214-32220.

Wen, W., Meinkoth, J.L., Tsien, R.Y., and Taylor, S.S. (1995). Identification of a signal for rapid export of proteins from the nucleus. Cell *82*, 463-473.

Whitehouse, S., and Walsh, D.A. (1983). Inhibitor protein of the cAMP-dependent protein kinase: characteristics and purification. Methods Enzymol *99*, 80-93.

Winn, M.D., Isupov, M.N., and Murshudov, G.N. (2001). Use of TLS parameters to model anisotropic displacements in macromolecular refinement. Acta Crystallogr D Biol Crystallogr *57*, 122-133.

Wong, W., and Scott, J.D. (2004). AKAP signalling complexes: focal points in space and time. Nature reviews *5*, 959-970.

Wu, J., Brown, S.H., von Daake, S., and Taylor, S.S. (2007). PKA type IIalpha holoenzyme reveals a combinatorial strategy for isoform diversity. Science (New York, NY *318*, 274-279.

Wu, J., Jones, J.M., Nguyen-Huu, X., Ten Eyck, L.F., and Taylor, S.S. (2004). Crystal structures of RIalpha subunit of cyclic adenosine 5'-monophosphate (cAMP)-dependent protein kinase complexed with (Rp)-adenosine 3',5'-cyclic monophosphothioate and (Sp)-adenosine 3',5'-cyclic monophosphothioate, the phosphothioate analogues of cAMP. Biochemistry *43*, 6620-6629.

Xu, R.M., Carmel, G., Sweet, R.M., Kuret, J., and Cheng, X. (1995). Crystal structure of casein kinase-1, a phosphate-directed protein kinase. Embo J *14*, 1015-1023.

Xu, W., Doshi, A., Lei, M., Eck, M.J., and Harrison, S.C. (1999). Crystal structures of c-Src reveal features of its autoinhibitory mechanism. Mol Cell *3*, 629-638.

Yang, J., Kennedy, E.J., Wu, J., Deal, M.S., Pennypacker, J., Ghosh, G., and Taylor, S.S. (2009). Contribution of Non-catalytic Core Residues to Activity and Regulation in Protein Kinase A. The Journal of biological chemistry *284*, 6241-6248.

Yonemoto, W., McGlone, M.L., Grant, B., and Taylor, S.S. (1997). Autophosphorylation of the catalytic subunit of cAMP-dependent protein kinase in Escherichia coli. Protein Eng *10*, 915-925.

Zawadzki, K.M., and Taylor, S.S. (2004). cAMP-dependent protein kinase regulatory subunit type IIbeta: active site mutations define an isoform-specific network for allosteric signaling by cAMP. J Biol Chem *279*, 7029-7036.